DOCTORAATSPROEFSCHRIFT

2012 | Faculteit Wetenschappen

4*H*-Cyclopenta[2,1-*b*:3,4-*b*']dithiophene Donors and Quinoxaline Acceptors with Broadened Absorption Patterns toward Light Harvesting Materials for Organic Photovoltaics

Proefschrift voorgelegd tot het behalen van de graad van
Doctor in de Wetenschappen, Chemie, te verdedigen door:

Lidia MARIN

Promotor: prof. dr. Wouter Maes
Copromotoren: prof. dr. Dirk Vanderzande
dr. Laurence Lutsen

D/2012/2451/23

universiteit hasselt

Chairman	Prof. dr. Jean Manca, UHasselt
Promoter	Prof. dr. Wouter Maes, UHasselt
Copromoters	Prof. dr. Dirk Vanderzande, UHasselt
	Dr. Laurence Lutsen, IMEC/IMOMEC
Members of the jury	Dr. Agnès Rivaton,
	Université Blaise-Pascal, Clermont-Ferrand
	Dr. Nikolay Radychev,
	Carl von Ossietzky Universität Oldenburg
	Prof. dr. Wim Dehaen, KU Leuven
	Prof. dr. Peter Adriaensens, UHasselt
	Prof. dr. Thomas Junkers, UHasselt

Table of Contents

General Introduction

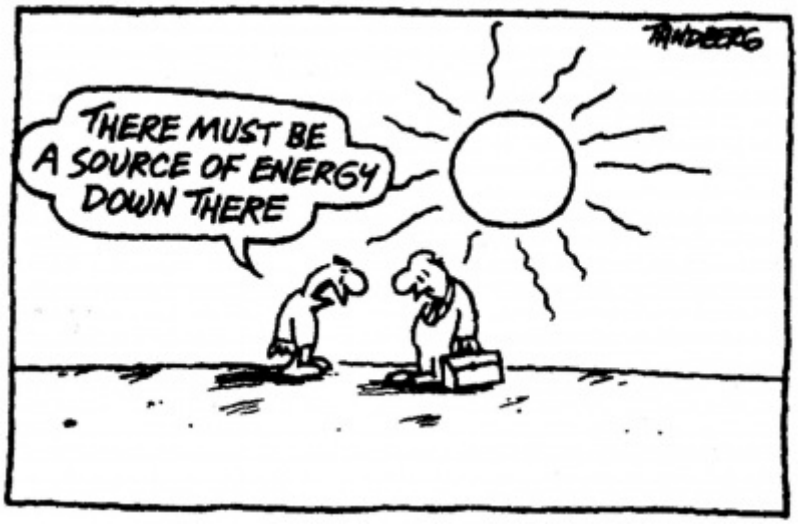

Current Energy Concerns

With world energy consumption close to 18 terawatt hours (TWh) in 2011[1] and an estimated increase of 1 gigawatt hours (GWh) each day, the global energy demand is very likely to approach 50 TWh by 2050.[2] At this moment, almost 90% of the consumed energy is coming from fossil fuels, *i.e.* oil, coal and natural gas, while the remaining 10% is retrieved from nuclear and renewable sources. A direct consequence of the extensive fossil fuel usage is the formation of large amounts of greenhouse gases, of which CO_2 is the most important. At this moment, the level of CO_2 present in the atmosphere is at its highest level in the history of mankind. In order to minimize the global warming effect (while it is still possible) the generation of clean (carbon free) energy, coming from **renewable sources**, *e.g.* solar, wind, water, biomass or geothermal, has to gradually take over and people's addiction to fossil fuels has to be reduced. One could even think of a "green revolution" in the energy production sector. Nuclear energy, due to its highly toxic residues which necessitate special transportation, treatment and storage, is less and less regarded as a clean and safe alternative. When talking about renewable sources, solar energy (the irradiant light and heat coming from the sun) can be regarded as the sole direct source, all others deriving their energy from the sun through secondary processes.[3] The amount of energy that the Earth's surface receives from the sun in one hour already exceeds the yearly global

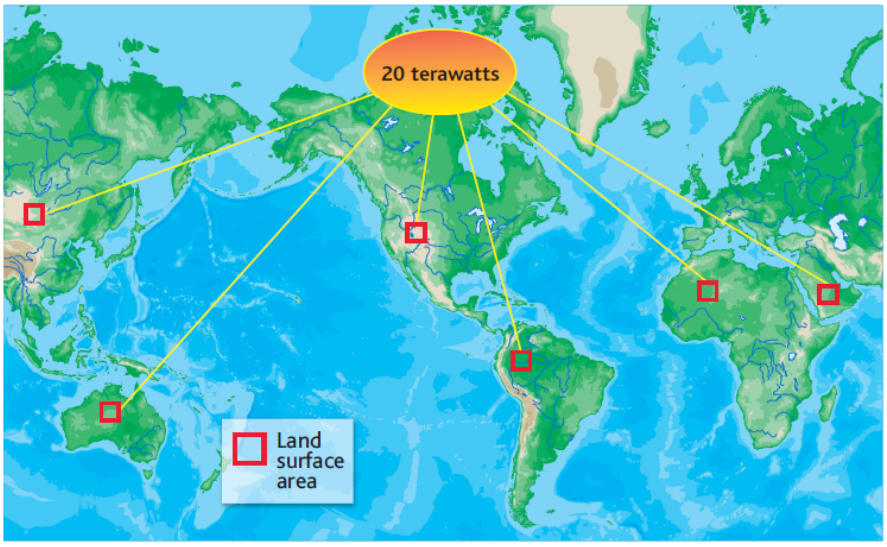

Figure 1. The land surface area needed to generate 20 TWh with 10% efficient solar cells.[2]

energy consumption. Installing solar panels with a moderate 10% energy conversion efficiency on less than 1% of the Earth's surface would suffice for generating 20 TWh of electricity (Figure 1). It is therefore wise to develop efficient technologies able to harvest and convert this enormous energy source into electricity.

Photovoltaics

The photovoltaic effect - the creation of a voltage or an electric current in a material upon exposure to light (from the Greek φῶς (phōs)) was first observed by A. E. Becquerel in 1839. The generation of energy upon solar irradiation of a (semi)conducting material is the basic working principle of a solar cell (SC). The photovoltaic technology has continuously evolved and developed toward architectures (affording lighter and cheaper modules) with improved efficiencies and stabilities. First and second generation SCs were made out of mono- or polycrystalline silicon (Si) and thin films of amorphous or crystalline silicon, CIGS (Copper Indium Gallium Selenide) or CdTe (Cadmium Telluride) deposited on glass substrates and/or ceramics, respectively. The development of thin film technology led to lower production costs and afforded lighter modules. The third generation photovoltaics (PVs), generally represented by multijunction (tandem) architectures, were developed with the goal to harvest more light and in consequence increase the power conversion efficiency to 30-60%.

As shown in Figure 2, the nature of the light harvesting material can be of inorganic (Si, CIGS, CdTe, etc.) or organic origin. Inorganic solar cells (the most mature technology) have been commercialized over the last 20 years and are most suitable for roof-top installation. As a result, they dominate the PV market at this moment. The fast growing branch of organic photovoltaics (**OPV**s) begins to gradually catch-up. The main advantage of organic materials is that they have very high absorption coefficients (~ 1000 times larger than silicon)[4] and active layers in the order of hundreds of nanometers are generally sufficient for efficient light harvesting. Dye sensitized solar cells (DSSCs), organic photovoltaics, as well as hybrid organic-inorganic PVs use small molecules[5] or conjugated polymers as the light harvesting materials. These are the most recent technologies that have emerged and have recorded fast progress in terms of efficiencies, stabilities and price effectiveness compared with their inorganic

counterparts. Since they are light-weight and flexible, organic solar cells (OSCs) can easily be integrated in portable devices such as solar bags, soft-sided structures (tents, sun shelters), lanterns and even smart textiles. Previous year, by completing the installation of the largest organic semi-transparent building integrated photovoltaic (BIPV) curtain wall, Konarka has achieved a major milestone and has proven that the technology of flexible modules can also go big.[6]

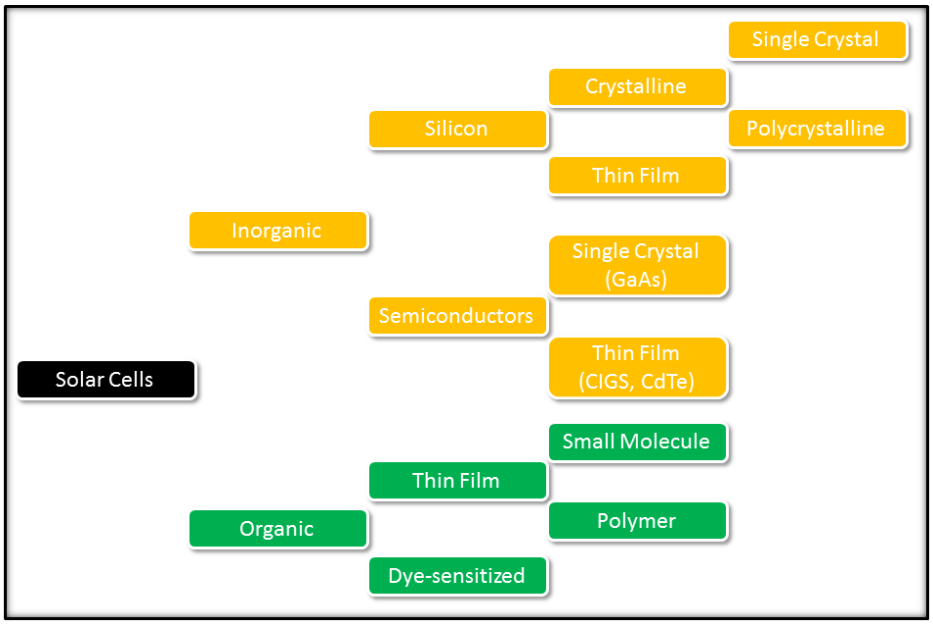

Figure 2. Overview of solar cell technologies.

The research community is nowadays putting considerable effort on improving solar cell performances and their efficiencies are steadily increasing every year. An overview with the best solar cell efficiencies obtained (at a laboratory scale) in all branches of the photovoltaic industry is displayed in Figure 3.

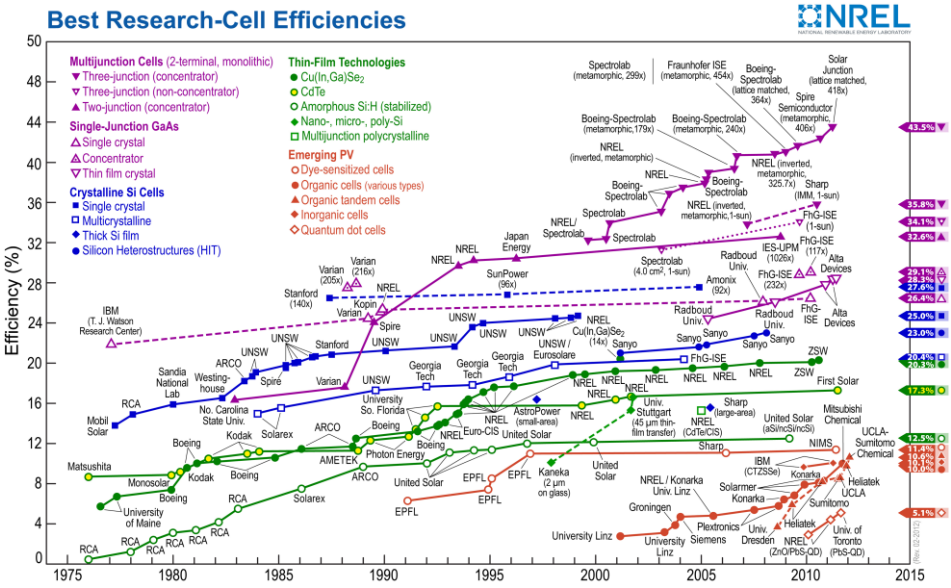

Figure 3. Highest certified solar cell efficiencies obtained at a laboratory scale (source: NREL).[7]

Organic Photovoltaics

Already in the beginning of the 20th century, small aromatic molecules such as anthracene[8] and various common dyes were found to be photoconductive. Toward the end of the century, the first (planar) heterojunction SC was reported by Tang. The device was made by sandwiching a donor and an acceptor molecule (a copper phthalocyanine (CuPc) and a perylene derivative, respectively) between two electrodes (Figure 4).[9] In the mid-nineties, by using the same **bilayer architecture**, Sariciftci was the first to combine a donor polymer, *i.e.* poly[2-methoxy-5-(2'-ethylhexyloxy)-*p*-phenylene vinylene] (**MEH-PPV**), and a small molecule fullerene acceptor, *i.e.* buckminsterfullerene (C_{60}). Although it showed quite low power conversion efficiency (0.04%), the system proved that photoinduced electron transfer from the donor to the acceptor and charge separation were taking place.[10] The relatively low efficiency arose mainly from the poor charge separation. Since the average exciton diffusion length (*vide infra*) is between 6 to 10 nm, this process occurs only within the first nanometers of the donor-acceptor interface. At this point it was envisaged that increasing the interface area between the donor and the acceptor could lead to increased charge transfer. The concept of a **bulk heterojunction** (BHJ) solar cell was born (Figure 4).

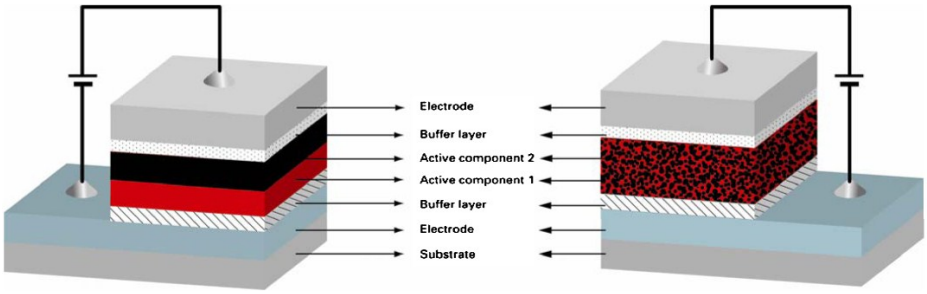

Figure 4. Schematic representation of bilayer (left) and bulk heterojunction (right) solar cells.[11]

One of the main advantages of organic materials (conjugated polymers or small molecules) over inorganic semiconductors is their low production cost. Processing of these materials requires less energy consumption during device fabrication since they can, in most cases, be processed from solution. The high temperatures required for vacuum deposition can thus be very elegantly and efficiently bypassed.

In BHJ organic solar cells, the active layer is obtained by processing a mixture of a donor and an acceptor material from solution. For deposition on rigid substrates (*e.g.* glass) and depending on the surface of the active area to be coated, a series of solution processing techniques (*e.g.* coating and doctor blading) can be used. While spin coating is mostly suitable for small substrates, larger surfaces, for which the risk of getting inhomogeneous films increases, are preferably coated by doctor blading. The biggest disadvantage of spin coating is its lack of material efficiency. In general, only 2-5% of the material is dispensed onto the substrate, the remaining 98-95% being flung off into the coating bowl and disposed. On the other hand, very little material (if not at all) is lost by doctor blading. Roll to roll (**R2R**) processing has recently been developed to address the fast growing field of thin film PVs. These modules are printed on a roll of flexible substrate and can thus be produced at very high speeds (~ 2.5 m^2 min^{-1}) and for minimal prices.[12] In all cases, the active layer which results after evaporation of the solvent consists of intimately intermixed donor and acceptor molecules. As already mentioned, this morphology facilitates charge transfer and separation, which due to the dissociation length of the exciton is limited to approximately 10 nm.

Operating Principle and Output Parameters

Organic photovoltaics, regardless of the adopted architecture of the active layer (bilayer or BHJ[13]), are generally built using the same configuration. A transparent substrate (generally glass) is coated with a thin layer of conducting indium tin oxide (**ITO**) which serves as the **anode** (high work function electrode). In order to smoothen the irregular ITO surface, a layer of poly(3,4-ethylenedioxythiophene):poly-(styrenesulfonate) (**PEDOT:PSS**) is spun on top. The latter also serves as an electron blocking layer and is at the same time an efficient antistatic agent which prevents electrostatic discharges during film production. All these initial steps are carried out in air atmosphere. Since the presence of oxygen and/or humidity has a negative impact upon the solar cell performance (oxidation of the organic material or creation of traps which prevent efficient charge transfer), all the following steps must be carried out in a glove box (under protective atmosphere). A solution containing both the donor and the acceptor component (mixed in various ratios) is used for casting the composite BHJ **active layer** on top of PEDOT:PSS (while for a bilayer device the active layers are deposited stepwise). The thickness of the active layer thus obtained (after solvent evaporation) can easily be controlled by varying the concentration of the solution as well as the spin coating speed. The last steps in the preparation of the solar cell are performed by vacuum deposition. First, a very thin **buffer layer** (~ 1 nm) of Ca (calcium) or LiF (lithium fluoride) is deposited between the active layer and the cathode which serves as an electron injecting layer. The **cathode**, made out of a low work function metal, *e.g.* Al (aluminum), Au (gold) or Ag (silver), is ultimately evaporated. For laboratory tests, the process ends here. Nevertheless, for real-life modules, good device encapsulation is mandatory to assure long lifetimes. The protective barrier prevents oxygen and air penetration into the device.

The general mechanism responsible for energy generation (Figure 5) involves four steps. Upon photon absorption, an electron situated in the highest occupied molecular orbital (HOMO) of the donor material (often a conjugated polymer) is promoted to the lowest unoccupied molecular orbital (LUMO), generating an **exciton** (step 1). The latter, which is represented by a bound electron-hole pair, **diffuses** toward the donor-acceptor (D-A) interface (step 2) where it dissociates into free charges (step 3). The driving force for electron (charge) **transfer**, represented by the energy offset between

the LUMO levels of the donor and the acceptor (often a fullerene derivative), should be at least 0.3 eV (downhill). **Charge transport**, electrons being transported by the acceptor and the holes by the donor, followed by charge extraction (holes are collected at the anode and electrons at the cathode) at the electrodes (step 4) occurs in the final step.

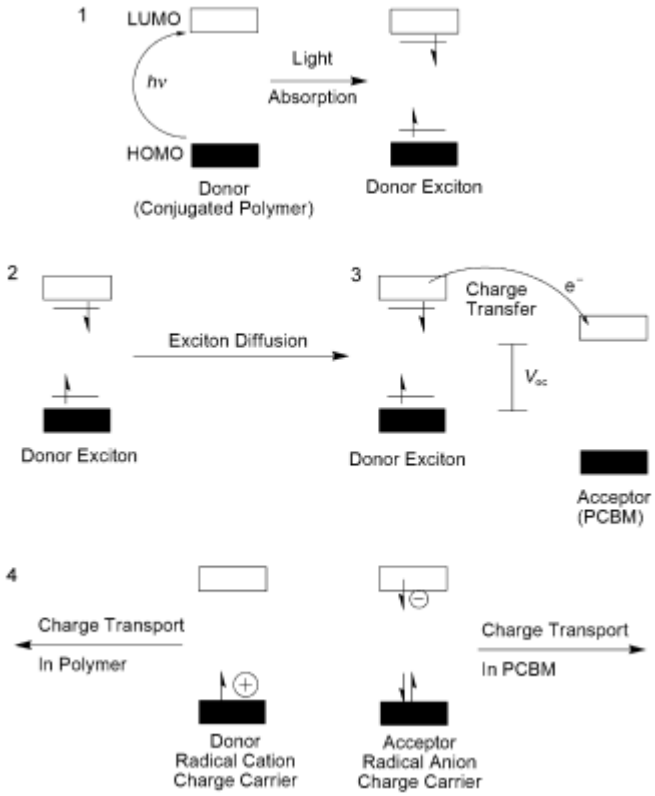

Figure 5. General mechanism for energy conversion in organic photovoltaics.[14]

The photovoltaic performance of a solar cell is evaluated under standard simulated conditions AM1.5G (Air Mass 1.5 Global spectrum on the ground when the sun is at 48.2° zenith angle (Figure 6a) with light intensity 100 mW cm^{-2})[15] by a series of output parameters, *i.e.* the current density at short circuit ($\boldsymbol{J_{sc}}$), the open circuit voltage ($\boldsymbol{V_{oc}}$), the fill factor (**FF**) and the power conversion efficiency (**PCE**) (Figure 6b).[9] J_{sc}, being (among others) determined by the number of excitons created during solar illumination, is related to the width of the absorption window of the photoactive material. The

broader the absorption wavelength range of the material, the more photons can be harvested and the higher the current can become. About 70% of the sunlight energy (photon flux) is distributed in the 400 to 900 nm wavelength region.[16]

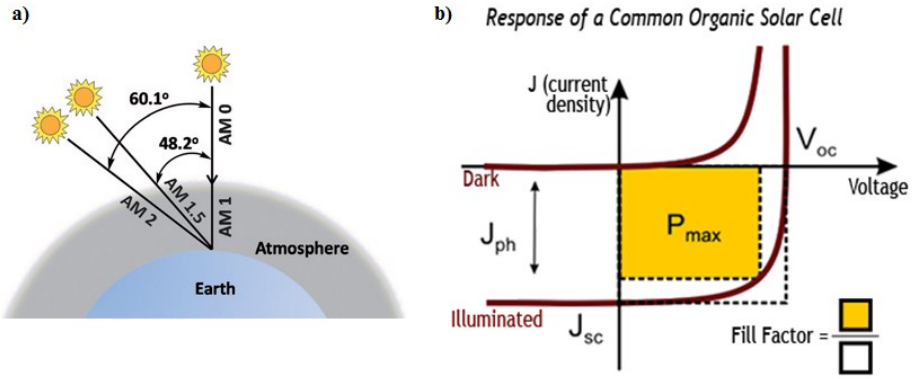

Figure 6. (a) Standards used for reporting solar cell efficiencies[5] and (b) response and output parameters of a solar cell, in dark and when illuminated (source: Thompson research group).[17]

As has been pointed out recently, superior purity and molecular weights (of the donor polymer materials) lead to a better organization (morphology) of the composite active layer and, corroborated with high charge mobility, this boosts up the current.[18] The V_{oc}, on the other hand, is the maximum voltage measured when no current is flowing through the cell. It correlates closely with the energy difference (the so called offset) between the HOMO of the donor and the LUMO of the acceptor material. Since fullerenes are almost exclusively used as the acceptor materials, and with very small variations in the first reduction potential between **$PC_{61}BM$** ([6,6]-phenyl-C_{61} butyric acid methyl ester) and other (functionalized) derivatives (+/- 100 mV) (Figure 7), it has become quite clear that the energy levels of the donor polymers should be altered to attain an ideal offset value of 1.2 eV, which would eventually lead to increased device performances.[19] Lowering of the HOMO level of the donor should hence be envisaged since this is regarded as a limiting parameter for the overall efficiency.

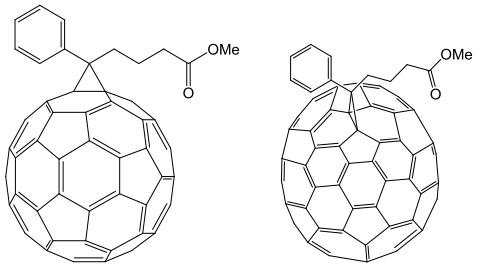

$PC_{61}BM$ **$PC_{71}BM$**

Figure 7. Most commonly used fullerene derivatives.

The maximum output power (**P_{max}**) of a solar cell, represented by the area of the yellow rectangle in Figure 6, is given by the product of J_m and V_m, *i.e.* the current and the voltage at the maximum power point, and represents the actual (real) power produced by a SC. The fill factor (**FF**) is a useful quantity for comparing P_{max} relative to the theoretical power (**P_{theor}**) given by the product of the (photo)current and (photo)voltage produced by the cell. For OPVs, FFs are generally ranging from 0.3 to 0.7. Low values arise from parasitic losses due to resistance within the cell itself. These losses mainly occur in the ITO or in large thickness active layers in which inefficient current generation leads to increased (series) resistance.[20] The FF can be calculated according to the following formula: $\mathrm{FF} = \frac{P_{max}}{P_{theor}} = \frac{J_{max} \times V_{max}}{J_{sc} \times V_{oc}}$

Finally, the power conversion efficiency (**PCE** or η) is expressed as the numerical quotient of P_{max} (the output power) and the total input photon irradiance. The efficiency of a solar cell can be calculated according to the following formula:

$$\eta(\%) = \frac{P_{out}}{P_{in}} = FF \cdot \frac{J_{sc} \times V_{oc}}{P_{in}} = \frac{J_{max} \times V_{max}}{P_{in}}$$

Care should be taken when reporting solar cell performances, making sure that the used standard (generally AM1.5G condition and light intensity 100 mW cm^{-2}) is clearly indicated and corrections of the spectral mismatch are done.

References

(1) http://www.indexmundi.com/g/g.aspx?v=81&c=xx&l=en

(2) Service, R. F. *Science* **2005**, *309*, 548.

(3) (a) Glasnović, Z.; Rogošić, M.; Margeta, J. *Sol. Energy* **2011**, *85*, 794; (b) Shaahid, S. M. *Renewable Sustainable Energy Rev.* **2011**, *15*, 3877; (c) Michel, H. *Angew. Chem. Int. Ed.* **2012**, *51*, 2516; (d) Ruggero, B. *Geothermics* **2012**, *41*, 1.

(4) Günes, S.; Neugebauer, H.; Sariciftci, N. S. *Chem. Rev.* **2007**, *107*, 1324.

(5) Mishra, A.; Bäuerle, P. *Angew. Chem. Int. Ed.* **2012**, *51*, 2020.

(6) www.konarka.com

(7) www.nrel.gov

(8) Pechettino, A. *Acad. Lincei Rend.* **1906**, *15*, 355.

(9) Tang, C. W. *Appl. Phys. Lett.* **1986**, *48*, 183.

(10) Sariciftci, N. S.; Braun, D.; Zhang, C.; Srdanov, V. I.; Heeger, A. J.; Stucky, G.; Wudl, F. *Appl. Phys. Lett.* **1993**, *62*, 585.

(11) Patrick, G. N.; Fernando, A. C. *Nanotechnology* **2010**, *21*, 492001.

(12) Espinosa, N.; Hosel, M.; Angmo, D.; Krebs, F. C. *Energy Environ. Sci.* **2012**, *5*, 5117.

(13) In this thesis/chapter we will only address BHJ solar cells for which the active layer is exclusively processed from solution.

(14) Thompson, B. C.; Fréchet, J. M. J. *Angew. Chem. Int. Ed.* **2008**, *47*, 58.

(15) Bird, R. E.; Hulstrom, R. L.; Lewis, L. J. *Sol. Energy* **1983**, *30*, 563.

(16) Moliton, A.; Nunzi, J.-M. *Polym. Int.* **2006**, *55*, 583.

(17) http://met.usc.edu/projects/solarcells.php

(18) (a) Van Mierloo, S.; Hadipour, A.; Spijkman, M.-J.; Van den Brande, N.; Ruttens, B.; Kesters, J.; D'Haen, J.; Van Assche, G.; de Leeuw, D. M.; Aernouts, T.; Manca, J.; Lutsen, L.; Vanderzande, D. J.; Maes, W. *Chem. Mater.* **2012**, *24*, 587; (b) Osaka, I.; Saito, M.; Mori, H.; Koganezawa, T.; Takimiya, K. *Adv. Mater.* **2012**, *24*, 425.

(19) Dennler, G.; Scharber, M. C.; Ameri, T.; Denk, P.; Forberich, K.; Waldauf, C.; Brabec, C. J. *Adv. Mater.* **2008**, *20*, 579.

(20) Schlenker, C. W.; Thompson, M. E. *Chem. Commun.* **2011**, *47*, 3702.

Review of Recent Literature on Polymer Solar Cells

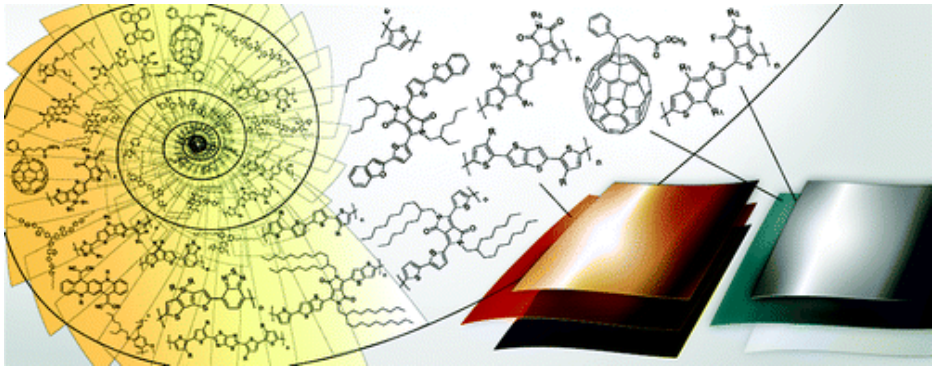

Three Generations of Conjugated Polymers

Since the discovery of ultrafast electron transfer between a conjugated polymer, *i.e.* poly[2-methoxy-5-(3',7'-dimethyloctyloxy)-1,4-phenylene vinylene] (**MDMO-PPV**) (Figure 8) and buckminsterfullerene (**C_{60}**) upon illumination,[1] the interest in developing new conjugated (polymer) materials for OPV applications has increased almost exponentially. A thorough understanding of the processes (both physical and chemical) taking place in the devices has allowed rational development of new solar cell architectures and materials that have eventually led to enhanced OPV performances.

Poly(*p*-phenylene vinylene)s (**PPV**s) constitute the **first generation** of semiconducting polymers employed in OPVs. This class of large band gap (in the range of 2.0 eV) materials, including the more soluble poly[2-methoxy-5-(2'-ethylhexyloxy)-1,4-phenylene vinylene] derivative (**MEH-PPV**) (Figure 8), allowed basic SC understanding and addressed the first device limitations. It soon became clear that the processing solvent had a tremendous influence on the morphology of the active layer (domain size) and, in consequence, on the device efficiency. For instance, the replacement of toluene by chlorobenzene afforded a better organization of the **MEH-PPV**:$PC_{61}BM$ blend (reduction of the surface roughness), which doubled the current and led to a significant increase in efficiency, from 0.9 to 2.5%.[2]

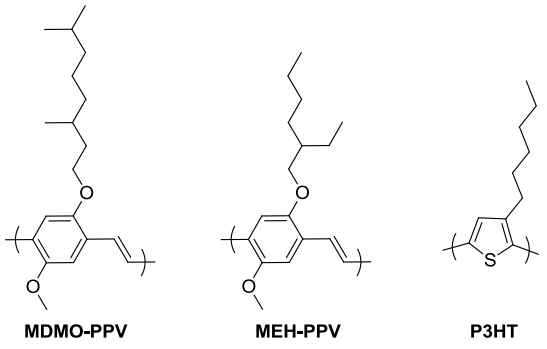

Figure 8. First and second generation polymers for PV devices.

A **second generation** of polymers, with lower band gaps and better organization properties (by showing a certain degree of crystallinity) has been developed afterwards. Mainly represented by poly(3-hexylthiophene) (**P3HT**) (Figure 8), this class of materials tends to organize in microcrystalline structures and therefore shows high charge mobilities and improved charge transport properties. In order to maximize these

features, chemists have developed new synthetic routes toward polythiophenes with increased degrees of regioregularity.[3] The first BHJ solar cells using a mixture of **P3HT**:$PC_{61}BM$ in the active layer showed efficiencies as low as 0.4%. Thermal annealing of the cells improved the morphology of the active layer, increased the current and subsequently enhanced the performance by 70%.[4] Shortly after the slow evaporation of the solvent, a spontaneous (vertical) phase separation of the $PC_{61}BM$ from the **P3HT** component occurs in the films (with thicknesses superior to 150 nm). In consequence, the bulk layer has a graded composition, with **P3HT** and $PC_{61}BM$ rich phases in the proximity of the ITO and of the metal electrode, respectively. During thermal annealing, the energy transferred in the system promotes molecular diffusion of $PC_{61}BM$ in the **P3HT** rich bottom phase, leading to a more balanced donor:acceptor composition within the bulk active layer.[5] Additionally, thermal annealing induces reorganization of **P3HT** into crystallites having a π–π stacking orientation perpendicular to the substrate (the so-called "*face-on*" orientation) (Figure 9), which facilitates charge transport and increases the current.[6] **P3HT** has been the benchmark material used in the last decade and has played a crucial role in the comprehension of the very complex processes occurring is OPVs, allowing the development of methods that enhance solar cell performances and stability (thermal annealing, cross

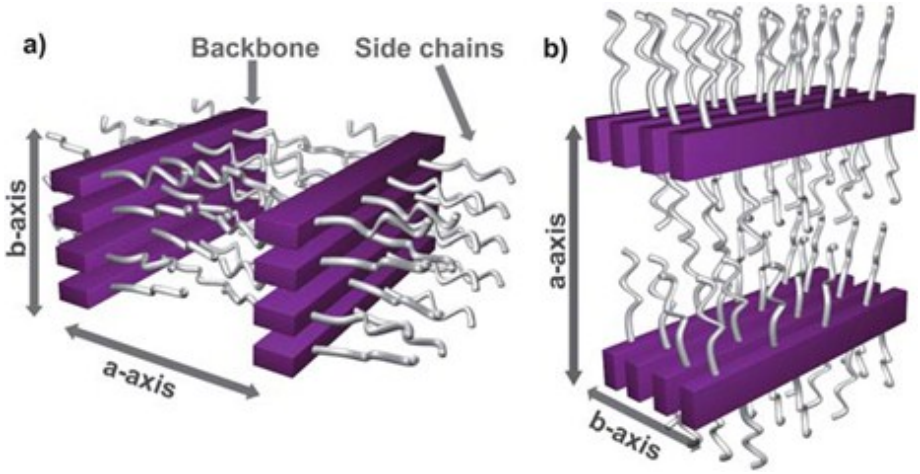

Figure 9. Graphical representation of a **P3HT** crystallite oriented a) face-on and b) edge-on. The purple blocks represent the thiophene backbone and the white cylinders the hexyl side chains.[6b]

linking, etc.). New materials were, however, required since the efficiencies of first and second generation polymers, for which the maximum predicted values were attained, were limited to no more than 5%.

The design and synthesis of a **third generation** of conjugated polymers, with band gaps below 1.6 eV (the so called "***low band gap***" polymers), led to efficiencies that nowadays overpass 10%.[7] Two approaches affording materials absorbing into the near infrared (NIR) region of the solar spectrum have been employed (Figure 10). In the **first strategy**, not very widely explored, an increase of the conjugation length along the polymer backbone was achieved by the incorporation of fused aromatic molecules for which the resonance structure is stabilized by a **quinoid form**. Since the aromatic structure is higher in energy, the polymer will be stabilized by the quinoid form, resulting in a reduction of the band gap. Polymers like poly(isothianaphthene) (**PITN**)[8] and poly(thieno[3,4-*b*]thiophene) (**PTT**)[9] have band gaps close to (or even below) 1.0 eV. The major drawback of this approach is that one is not able to achieve full control over the energy levels of the polymers, which in most cases do not possess a low-lying HOMO, ideally located around -5.4 eV.[10]

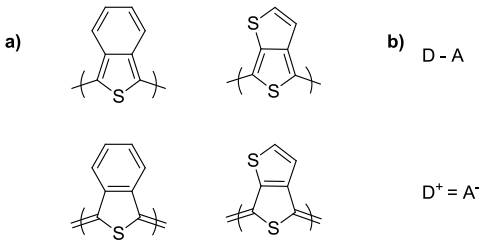

Figure 10. Approaches used in the development of low band gap polymers: a) quinoid stabilization of **PITN** and **PTT** and b) donor-acceptor alternation.

The **second strategy**, introduced in the beginning of the nineties by Havinga *et al.*,[11] is far more exploited than the former and is based on the alternation of electron rich and electron poor units along the polymer backbone. This push-pull approach increases the electron delocalization along the polymer chain. The formation of a low energy quinoid structure due to intramolecular charge transfer (**ICT**) from the donor to the acceptor unit effectively reduces the band gap of the material. As a result, a red shift of the absorption window toward the NIR region allows a better overlap with the photon flux and can lead to an increased J_{sc}.[12] As suggested by the term, the ICT process implies

the existence of charged species along the polymer backbone, the partial positive charge being located on the donor and the negative charge on the acceptor. In consequence, the bond length is reduced due to the dominant sp^2 character of the D-A bond, the conjugation length is increased and the HOMO/LUMO offset is lowered. The greatest advantage of this approach is that one is able, by varying the strength of the donors and/or acceptors (Figure 11), to fine tune the energy levels of the final polymers, the HOMO level being dictated merely by the donor and the LUMO by the acceptor. In general, this class of materials has a rather low degree of crystallinity (if any at all), which makes thermal annealing not effective or, in some cases, even detrimental for the device performance. Nevertheless, the use of processing additives (high boiling point solvents, *e.g.* 1,8-diiodooctane (**DIO**), 1,8-octanedithiol (**ODT**), etc.) may induce a better organization of the materials blend and therefore may improve the device efficiency.[13] A selection of some of the best performing materials that have been developed in the last decade is presented below. Emphasis is put on strategies that lead to superior light harvesting systems and/or optimized processing methods, affording record OPV efficiencies.

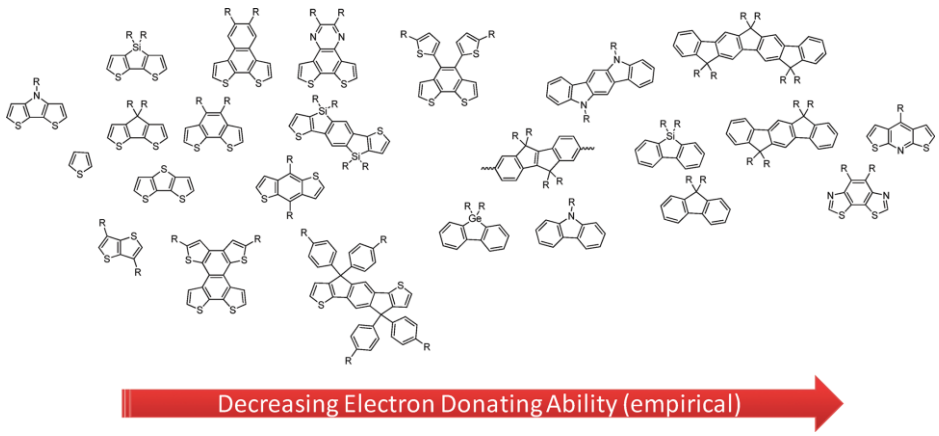

Figure 11. Building blocks with different donor strength incorporated in donor-acceptor polymers.[14]

State-of-the-Art Low Band Gap Polymers

By adopting the D-A strategy, the coupling of electron rich thiophene and electron accepting quinoxaline units was achieved by zerovalent nickel and palladium mediated polycondensations, *i.e.* Yamamoto and Stille cross-coupling reactions, respectively.[15] The resulting poly(thienoquinoxaline)s showed moderate optical properties (absorption maxima located at ~600 nm, band gaps of ~1.7 eV) and rather low solubility in common organic solvents. The polymers displayed low conductivities and reversible *n*- and *p*-doping characteristics. By introducing solubilizing side chains on the quinoxaline unit, the group of Andersson has developed a promising processable material, poly[2,3-bis(3-octyloxyphenyl)quinoxaline-5,8-diyl-*alt*-thiophene-2,5-diyl] (**TQ1**) (Figure 12). In combination with $PC_{61}BM$, **TQ1** showed a moderate performance in devices processed from chloroform solution (J_{sc} = 5.9 mA cm^{-2}, V_{oc} = 0.9 V, FF = 56%, η = 3%) which arose from the poor morphology of the active layer, which didn't perfectly promote charge separation and transport. By changing the solvent to *ortho*-dichlorobenzene (*o*-DCB) and by using the $PC_{71}BM$ derivative, which has an increased absorption in the visible region, the current (assured by the high molecular weight of the polymer, M_n = 4.1 x 10^4 g mol^{-1}) was doubled and the fill factor was increased to 70%, which led to an overall PCE of 6.0%, the best reported efficiency for this class of polymers.[16]

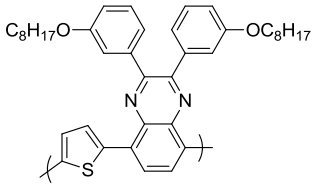

TQ1

Figure 12. Structure of polymer **TQ1**, a low band gap poly(thienoquinoxaline) derivative.

The synthesis of conjugated polymers in which fluorene (a rather weak donor, see Figure 11) is combined with a variety of donor-acceptor-donor (**D-A-D**) triads has resulted in a series of materials known as **APFO**s (Alternating Poly FluOrenes). A further distinction is made for those derivatives showing a green color in the neutral state, which are known as **APFO-Green**.[17] The solubility, optical properties, band gap and energy levels of these materials can be tuned by changing the strength of the

acceptor in the triad (the donor is invariably thiophene), which decreases when going from [1,2,5]thiadiazolo[3,4-*g*]quinoxaline to 2,1,3-benzothiadiazole (**BT**) and quinoxaline. In the **APFO** series, photovoltaic performances exceeding 3.5% were achieved for two polymers (Figure 13). Despite its large band gap (~2.4 eV), poly[(9,9-dioctylfluorenyl-2,7-diyl)-*co*-5,5-(4',7'-di-2-thienyl-2',1',3'-benzothiadiazole] (**APFO-3**), incorporating a BT acceptor moiety in the triad, appeared as an excellent donor material in combination with $PC_{61}BM$. The solar cells, with 3.5% efficiency, displayed a J_{sc} of 5.7 mA cm^{-2}, a FF of 60% and a V_{oc} of 1.02 V, the latter being related to the low lying HOMO (- 5.8 eV) of the polymer.[18] In poly[2,7-(9,9-dioctylfluoren)-*alt*-5,5-(5′,8′-di-2-thienyl-(2′,3′-bis-(3′′-octyloxyphenyl)quinoxaline))] (**APFO-15**), the BT was replaced by a quinoxaline unit, which is a weaker acceptor.[19] The solubilizing alkoxy substituents were introduced in the meta positions of the phenyl rings to prevent electron donation from the donor side chains to the quinoxaline unit, which would decrease its acceptor strength. The photovoltaic performance of the polymer was strongly influenced by the $PC_{61}BM$ loading. High concentrations of the acceptor reduced the optimum thickness of the active layer, which subsequently led to poor photon absorption. An efficiency of 3.7% was obtained with an optimum 1:3 (weight ratio (w/w)) **APFO-15**:$PC_{61}BM$. Once again, the high molecular weight material (M_n = 4.1 x 10^4 g mol^{-1}) granted optimal solar cell parameters (V_{oc} = 1.0 V, J_{sc} = 6.0 mA cm^{-2}, FF = 63%).

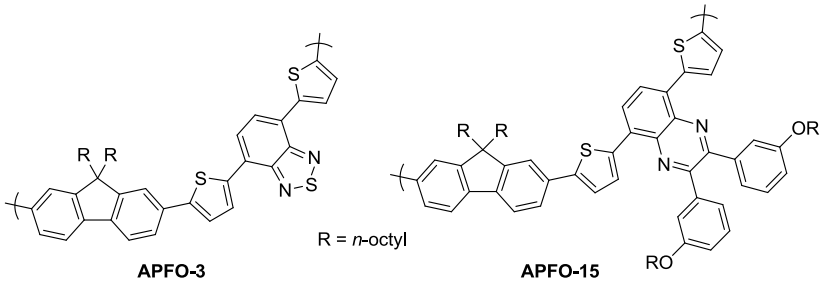

Figure 13. Best donor polymers in the **APFO** series.

The substitution of the phenyl rings in fluorene by thiophene units results in a promising electron-rich and planar derivative, *i.e.* 4*H*-cyclopenta[2,1-*b*:3,4-*b'*]dithiophene (**CPDT**). The CPDT derivative was combined with BT and afforded the first low band gap material (1.38 eV) to incorporate a CPDT donor unit in the polymer

chain.[20] The novel poly[2,6-(4,4-bis(2-ethylhexyl)-4*H*-cyclopenta[2,1-*b*:3,4-*b'*]dithiophene)-*alt*-4,7-(2,1,3-benzothiadiazole)] (**PCPDTBT**) (Figure 14), absorbing into the IR spectral region, showed high hole mobility values (2 x 10^{-2} cm^2 $V^{-1}s^{-1}$) and promising solar cell efficiencies of 2.60 and 3.16%, in combination with $PC_{61}BM$ and $PC_{71}BM$, respectively. The best devices were characterized by rather moderate output parameters: a J_{sc} of 11.0 mA cm^{-2}, a V_{oc} of 0.7 V, and a FF of 47%. Since thermal annealing or controlled solvent evaporation after film casting proved to be ineffective for this polymer, control of the morphology in the bulk could be achieved by incorporating small amounts of processing additives (ODT) in the composite solution. When used for processing of BHJ blends, additives have to fulfill two conditions: i) selective solvation of the fullerene, generally $PC_{71}BM$, and ii) have a higher boiling point than the processing solvent. When cast from a CB solution containing a few percentages of ODT, the pristine **PCPDTBT**:$PC_{71}BM$ film showed a 40 nm red shift in the high wavelength region of the spectrum, being an indication of stronger chain interactions occurring in films processed from the solvent mixture. As a result, the efficiency of the solar cells obtained with the processed films boosted to 5.5%.[13a] Based on TEM images, Cho *et al.* could conclude that the use of ODT leads to the formation of elongated (fiber like) structures that are responsible for the enhancement of the performance.[21] One should keep in mind that if any residual ODT is present in the blend, due to the proton accepting abilities of the sulfur atoms, it can act as a "hole trap". Better organization of the film in lamella-like structures, and in consequence improved mobility features (0.17 cm^2 $V^{-1}s^{-1}$) as desired in field effect transistors, have been obtained by replacing the 2-ethylhexyl branched side chains by long linear ones.[22]

An analogue polymer to **PCPDTBT** in which the carbon (C) bridge of the CDPT unit is replaced by silicon (Si) was reported by Gaudiana *et al*.[23] The longer Si-C bond modifies the geometry of the repeating unit, leading to a slightly increased deviation from planarity in poly[(4,4'-bis(2-ethylhexyl)dithieno[3,2-*b*:2',3'-*d*]silole)-2,6-diyl-*alt*-(4,7-bis(2-thienyl)-2,1,3-benzothiadiazole)-5,5'-diyl] (**Si-PCPDTBT**) (Figure 14) when compared to the motif present in the parent C-bridged polymer. The material, for which M_n values superior to 2.0 x 10^4 g mol^{-1} were obtained, displayed a higher degree of crystallinity, increased mobility and superior charge transport with respect to **PCPDTBT**. In blends with $PC_{71}BM$, the solar cells showed a FF of 62%, the moderate V_{oc} of 0.6 V being balanced by the excellent J_{sc} of 15 mA cm^{-2}, leading to 5.24%

certified efficiency. The good morphology of the blend and the high crystallinity of the polymer reduced the bimolecular recombination in the bulk.

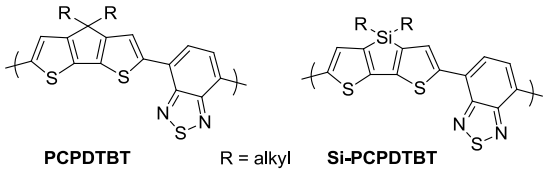

Figure 14. Structure of the C- and Si-bridged **PCPDTBT**-type low band gap polymers.

The promising (**Si**)**PCPDTBT** low band gap materials have been of great appeal and opened the door toward new related polymers in which the BT acceptor was replaced by other electron deficient units (of different strength), of which bis(2-thienyl)-2,1,3-benzothiadiazole (**TBTT**),[24] 2,1,3-benzoxadiazole (**BO**),[25] and 2,5-dithienylthiazolo[5,4-*d*]thiazole (**DTTzTz**)[26] showed the best solar cell performances. All new polymers (Figure 15) had band gaps in the range 1.5-1.8 eV. Poly[4,4-bis(2-ethylhexyl)-4*H*-cyclopenta[2,1-*b*:3,4-*b*′]dithiophene-2,6-diyl-*alt*-4,7-bis(2-thienyl)-2,1,3-benzothiadiazole-5′,5″-diyl] (**PCPDTTBTT**), reported by Moulé *et al.*, showed 2.1% efficiency in blends with $PC_{61}BM$.[24] The best films were obtained by using a solvent mixture consisting of 5% anisole in chlorobenzene (CB). The increased solubility of the polymer in less polar (co)solvents, such as anisole, improved the morphology of the active layer by decreasing the average domain size. Bijleveld *et al.* reported good efficiency for the copolymer incorporating the BO acceptor unit, *i.e.* **PCPDT-BO**. In combination with $PC_{61}BM$, the solar cells afforded efficiencies of 2.5%. Even though the cells had a high V_{oc} (0.8 V), the current (J_{sc} = 6.4 mA cm^{-2}) and FF (39%) were limited.[25] The combination of asymmetrically dialkylated CPDT and hexyl-substituted dithienylthiazolo[5,4-*d*]thiazole (**DTTzTz**) moieties afforded the narrow band gap copolymer poly([4-(2'-ethylhexyl)-4-octyl-4*H*-cyclopenta[2,1-*b*:3,4-*b'*]dithiophene-2,6-diyl]-*alt*-[2,5-di(3'-hexylthiophen-2'-yl)thiazolo[5,4-*d*]thiazole-5,5'-diyl]) (**PCPDT-DTTzTz**). When blended with $PC_{71}BM$, initial solar cell efficiencies were below 3%. Purification and fractionation of the polymer by preparative size exclusion chromatography (SEC) enhanced the organization of the semicrystalline polymer in the blend, which increased the current (from J_{sc} 9.0 to 11.3

mA cm^{-2}) and the FF (from 47 to 54%) and eventually led to an efficiency exceeding 4%. Nevertheless, the performance was inherently limited by the V_{oc} of 0.8 V.[26]

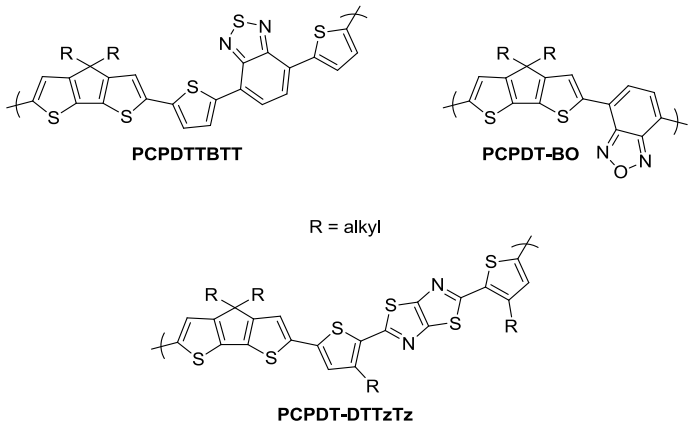

Figure 15. Chemical structure of **PCPDT-X** low band gap polymers.

The liquid crystalline poly[2,5-bis(3-hexadecylthiophen-2-yl)thieno[3,2-*b*]thiophene] (**pBTTT**) polymer (Figure 16) synthesized by McCulloch *et al.* appeared to be an excellent donor material for solar cell applications.[27] **pBTTT**, incorporating the rigid prequinoid thieno[3,2-*b*]thiophene unit intercalated between two substituted thiophenes, showed excellent electrical characteristics (mobility of 0.2-0.6 cm^2 $V^{-1}s^{-1}$, comparable with that of amorphous silicon). In combination with $PC_{71}BM$, the composite layer displayed superior organization features at an optimum 1:4 (w/w) polymer:fullerene loading, allowing intercalation of the $PC_{71}BM$ between the not very dense solubilizing side chains present along the polymer backbone and leading to good nanoscale phase separation.[28] Despite the good interdigitation in the blend, the resulting solar cells showed a moderate efficiency of 2.3% due to reduced light absorption in the thin films (~100 nm) and a mismatch between electron and hole mobility in the direction normal to the substrate.[29]

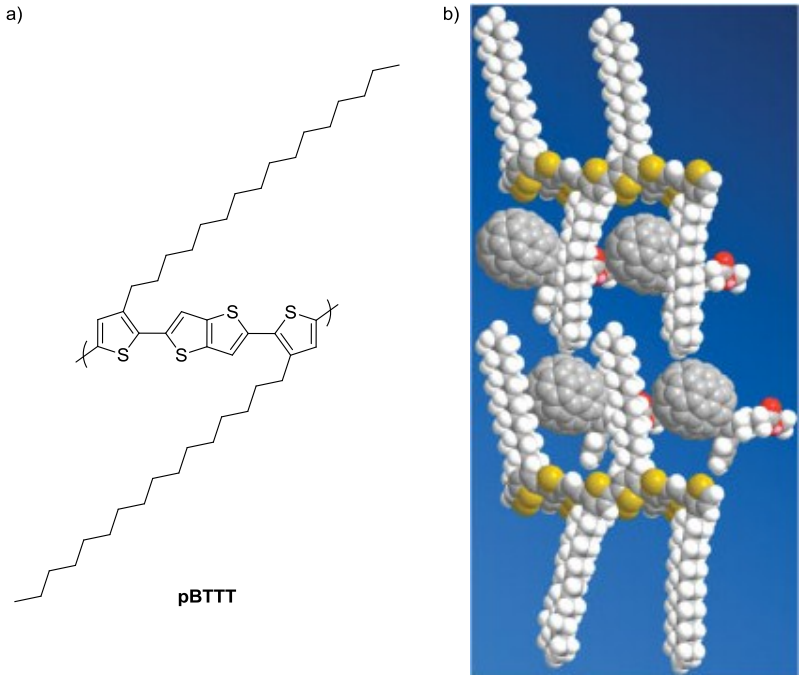

Figure 16. a) chemical structure of **pBTTT** and b) intercalation of $PC_{71}BM$ in the crystal lattice.[30]

The combination of thieno[3,4-*b*]thiophene (**TT**), with a different fusion pattern than the block used in **pBTTT**, and benzo[1,2-*b*:4,5-*b*']dithiophene (**BDT**) led to the development of the currently best performing class of polymers, known as poly[4,8-bis(substituted)-benzo[1,2-*b*:4,5-*b'*]dithiophene-2,6-diyl-*alt*-4-substituted-thieno[3,4-*b*]thiophene-2,6-diyl] polymers (**PBDTTT**) (Figure 17).[31] Both building blocks, alternating along the polymer chain, have a preferential quinoid structure stabilized by the fused aromatic rings. These narrow band gap materials (~1.6 eV) showed up as a very promising class of donor materials. Solar cell efficiencies, in combination with $PC_{71}BM$, were increased from 4.8 to 6.3% by replacing the ester group on the TT moiety in **PBDTT-E** with a ketone functionality in **PBDTT-C** (Figure 17).[32] It has been proven in numerous examples that the side chains have a crucial influence on the photovoltaic performance of materials. The introduction of branched substituents on the BDT unit increased the π-π interchain distance, which led to a drop in the efficiency. When introduced on the TT unit, however, this led to enhanced solar cell efficiencies since they do not interfere with the π-π stacking of the polymer chains.[33] Nevertheless, optimal interplay between π-π stacking (which enhances exciton diffusion) and

intercalation of the fullerene (which enhances electron-hole separation) has to be pursued in order to attain best performances. By varying the substituent (linear or branched) and the nature (alkyl or alkoxy) of the BDT side chains and the alkyl group of the ester-functionalized TT unit, a new series of **PTBx** (x = 1-7) polymers was developed (Figure 17). The energy levels of these polymers could be fine-tuned by modifying the acceptor strength of the TT unit by the introduction of electron withdrawing fluorine atoms. In this series, the highest efficiency (in combination with $PC_{71}BM$) was obtained for **PTB7**. When processed from solvent mixtures containing 3% DIO in CB, the FF increased from 55 to 69% and the J_{sc} increased from 13.6 to 14.5 mA cm^{-2}, leading to an overall PCE of 7.4%. The V_{oc} of 0.74 V remained unchanged by the processing additive. A more moderate efficiency was obtained for **PTB1**:$PC_{61}BM$ in the absence of additives (V_{oc} of 0.6 V, J_{sc} of 13.3 mA cm^{-2}, FF of 66%, and efficiency of 5.24%). Annealing the device had a negative impact on its performance. The highest influence was noticed for the J_{sc}, which was reduced by 50% to 6.9 mA cm^{-2}, decreasing the efficiency to 1.9%. Upon thermal annealing, the interfacial area between the donor and the acceptor was reduced, the absence of the microcrystalline network responsible for charge transport leading to a reduced J_{sc} and efficiency.[34] **PTB7** currently holds the record organic solar cell efficiency in single as well as in tandem devices.[7]

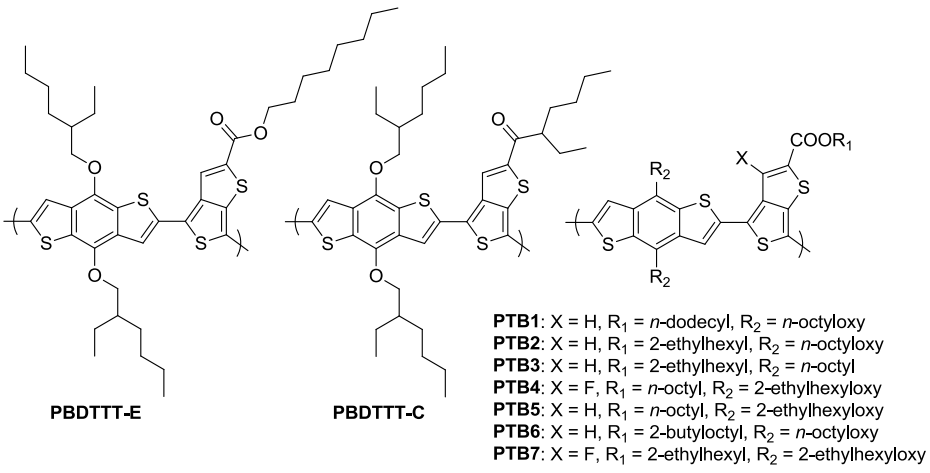

Figure 17. Chemical structures of the best performing polymers **PBDTTT** and **PTB**.

Brabec's Critical Triangle for Photovoltaics – Adaptation to Organic Solar Cells

Organic photovoltaics have a real potential to become a competitive market technology in the years to come. Meeting all requirements in Brabec's "**critical triangle for photovoltaics**"[35] (Figure 18) will need integrated efforts toward the development of highly efficient light harvesting and charge transporting materials with good thermal and photo-chemical stability that can be processed from solution. Failing in one of these issues means overall failure. Since semiconducting polymers are relatively cheap to produce, the major production **costs** arise from the use of expensive electrodes (such as ITO), encapsulation and energy consumption during the entire processing flow. New **inverted solar cell** architectures, in which ITO has been successfully replaced by a layer of TiO_x/Al, have shown comparable efficiencies to normal cell architectures and provide a real solution toward ITO-free devices.[36]

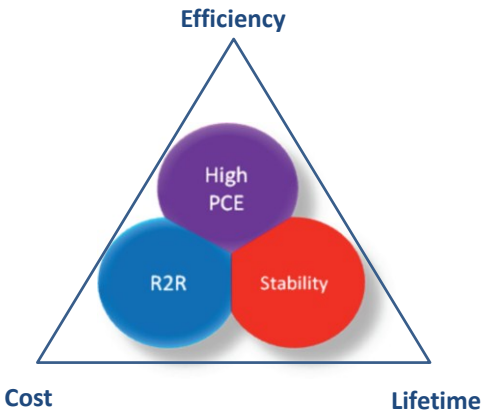

Figure 18. Adaptation of the critical triangle for organic photovoltaics.

The photoactive materials used in the active layer blends dictate the **efficiency** of a solar cell. With fullerene derivatives being able to accept up to six electrons,[37] the development of new electron deficient small molecules[38] or polymers[39] that would substitute them has so far not been very successful. In consequence, most efforts were directed toward the development of new donor polymers of which low band gap materials have shown the best efficiencies, the record for OPVs being already beyond 10%.[7]

The **stability** issue of a solar cell begins already with the processing of the active layer. The BHJ composite is a metastable structure which starts evolving as soon as the solvent evaporates from the film. Achieving a good morphology and maintaining it for years is a very challenging task. Strong interchain interactions in conjugated polymers render them insoluble and infusible. To obtain processable materials, the introduction of solubilizing side chains is mandatory. They are responsible for the semicrystalline feature of the polymer and influence the π-π stacking distance between the polymer chains, which has a direct impact on the electrical properties of the donor materials. Long linear substituents act as insulators and can reduce charge transfer to the acceptor material as well as charge hopping between polymer chains. Side chains render semiconducting polymers soluble in common organic solvents, making them excellent candidates for **R2R** processing but, at the same time, they increase the vulnerability of the materials toward photo-oxidation. So, one problem begins when another one ends. Degradation of the active layer has a direct and immediate impact on device performance, leading to a decrease in the PCE. Very efficient encapsulation should be ensured since this barrier between the solar cell and the environment determines the physical stability of a solar cell.[40] In inert atmosphere, the stability of light harvesting materials toward pure photo-chemical reactions is in the order of years.[41] Infiltration of oxygen and water in the cell leads to the formation of metal oxides at the electrodes.[42] In a first instance, oxygen present in the active layer prevents efficient charge transfer from the donor to the acceptor, acting as a trap for electrons.[43] The main mechanism leading to the degradation of the polymer has initially been attributed to direct interactions between singlet oxygen and the conjugated backbone of the polymer. It was later on proven that the active species, generated by the UV-initiated transformation of oxygen, was actually ozone.[44] The latter determines irreversible transformations of the semiconductor, starting with oxidation of the side chains which are regarded as the Achilles heel of the polymer and of the solar cell as a whole.[45]

The introduction of **thermo-cleavable side chains** enables solution processing of the polymer and allows the formation of a "**frozen**" **nano-morphology** in the active layer upon thermal elimination of the solubilizing component.[46] The latter can for instance be a tertiary alkyl ester group which affords, upon heating to 200 °C, the free carboxylic acid substituted polymer backbone, which is fully decarboxylated when temperatures as high as 300 °C are reached.[47] The residual, side-chain free, conjugated material is now

a rigid, insoluble, and highly stable (thermally as well as photo-chemically) component of the bulk layer. Additionally, upon cleavage of the side chains, the polymer loses its physical mobility due to an increase in the glass transition temperature (T_g).

A second approach to stabilize the blend morphology is based on the use of photoreactive species. Photocrosslinkable (co)polymers with at least 10% functionalities in the side chains (bromine,[48] azide,[49] or cinnamoyl[50]) showed increased stability compared to the non-functionalized materials. An alternative approach is to design and synthesize polymers starting from monomers (donors as well as acceptors) with superior photostability. For some of the best performing polymers, *e.g.* **PCPDTBT** and **PTBx**, stability is not at its highest, since CPDT and TT have proven to be among the most unstable donor and acceptor units, respectively.[51] The use of more stable derivatives such as thiophene or BDT and BT or thienopyrazine, these being just a few examples of donors and acceptors, respectively, should lead to highly **stable** and **efficient** conjugated materials suitable for **cheap** and fast module production, opening the door for organic photovoltaics toward a competitive market technology.

References

(1) Sariciftci, N. S.; Smilowitz, L.; Heeger, A. J.; Wudl, F. *Science* **1992**, *258*, 1474.

(2) Shaheen, S. E.; Brabec, C. J.; Sariciftci, N. S.; Padinger, F.; Fromherz, T.; Hummelen, J. C. *Appl. Phys. Lett.* **2001**, *78*, 841.

(3) (a) McCullough, R. D.; Lowe, R. D. *J. Chem. Soc., Chem. Commun.* **1992**, 70; (b) Chen, T. A.; O'Brien, R. A.; Rieke, R. D. *Macromolecules* **1993**, *26*, 3462; (c) Chen, T.-A.; Wu, X.; Rieke, R. D. *J. Am. Chem. Soc.* **1995**, *117*, 233; (d) Mauer, R.; Kastler, M.; Laquai, F. *Adv. Funct. Mater.* **2010**, *20*, 2085.

(4) Padinger, F.; Rittberger, R. S.; Sariciftci, N. S. *Adv. Funct. Mater.* **2003**, *13*, 85.

(5) Zeng, L.; Tang, C. W.; Chen, S. H. *Appl. Phys. Lett.* **2010**, *97*, 053305.

(6) (a) Chen, D.; Nakahara, A.; Wei, D.; Nordlund, D.; Russell, T. P. *Nano Lett.* **2010**, *11*, 561; (b) Treat, N. D.; Shuttle, C. G.; Toney, M. F.; Hawker, C. J.; Chabinyc, M. L. *J. Mater. Chem.* **2011**, *21*.

(7) Dou, L.; You, J.; Yang, J.; Chen, C.-C.; He, Y.; Murase, S.; Moriarty, T.; Emery, K.; Li, G.; Yang, Y. *Nat. Photon.* **2012**, *6*, 180.

(8) (a) Rose, T. L.; Liberto, M. C. *Synth. Met.* **1989**, *31*, 395; (b) Lapkowski, M.; Kiebooms, R.; Gelan, J.; Vanderzande, D.; Pron, A.; P. Nguyen, T.; Louarn, G.; Lefrant, S. *J. Mater. Chem.* **1997**, *7*, 873; (c) Paulussen, H.; Ottenbourgs, B.; Vanderzande, D.; Adriaensens, P.; Gelan, J. *Polymer* **1997**, *38*, 5221.

(9) (a) Corradini, A.; Mastragostino, M.; Panero, A. S.; Prosperi, P.; Scrosati, B.: *Synth. Met.* **1987**, *18*, 625; (b) Mastragostino, M.; Marinangeli, A. M.; Corradini, A.; Arbizzani, C. *Electrochim. Acta* **1987**, *32*, 1589.

(10) Zhou, H.; Yang, L.; Stoneking, S.; You, W. *ACS Appl. Mater. Interfaces* **2010**, *2*, 1377.

(11) (a) Havinga, E. E.; ten Hoeve, W.; Wynberg, H. *Polym. Bull.* **1992**, *29*, 119; (b) Havinga, E. E.; ten Hoeve, W.; Wynberg, H. *Synth. Met.* **1993**, *55*, 299; (c) van Mullekom, H. A. M.; Vekemans, J. A. J. M.; Havinga, E. E.; Meijer, E. W. *Mater. Sci. Eng., R* **2001**, *32*, 1.

(12) Kleinhenz, N.; Yang, L.; Zhou, H.; Price, S. C.; You, W. *Macromolecules* **2011**, *44*, 872.

(13) (a) Peet, J.; Kim, J. Y.; Coates, N. E.; Ma, W. L.; Moses, D.; Heeger, A. J.; Bazan, G. C. *Nat. Mater.* **2007**, *6*, 497; (b) Hwang, I.-W.; Cho, S.; Kim, J. Y.;

Lee, K.; Coates, N. E.; Moses, D.; Heeger, A. J. *J. Appl. Phys.* **2008**, *104*, 033706; (c) Lee, J. K.; Ma, W. L.; Brabec, C. J.; Yuen, J.; Moon, J. S.; Kim, J. Y.; Lee, K.; Bazan, G. C.; Heeger, A. J. *J. Am. Chem. Soc.* **2008**, *130*, 3619; (d) Pivrikas, A.; Neugebauer, H.; Sariciftci, N. S. *Sol. Energy* **2011**, *85*, 1226; (e) Chambon, S.; Mens, R.; Vandewal, K.; Clodic, E.; Scharber, M.; Lutsen, L.; Gelan, J.; Manca, J.; Vanderzande, D.; Adriaensens, P. *Sol. Energy Mater. Sol. Cells* **2012**, *96*, 210.

(14) Zhou, H.; Yang, L.; You, W. *Macromolecules* **2012**, *45*, 607.

(15) (a) Kanbara, T.; Miyazaki, Y.; Yamamoto, T. *J. Polym. Sci., Part A: Polym. Chem.* **1995**, *33*, 999; (b) Yamamoto, T.; Zhou, Z.-h.; Kanbara, T.; Shimura, M.; Kizu, K.; Maruyama, T.; Nakamura, Y.; Fukuda, T.; Lee, B.-L.; Ooba, N.; Tomaru, S.; Kurihara, T.; Kaino, T.; Kubota, K.; Sasaki, S. *J. Am. Chem. Soc.* **1996**, *118*, 10389.

(16) Wang, E.; Hou, L.; Wang, Z.; Hellström, S.; Zhang, F.; Inganäs, O.; Andersson, M. R. *Adv. Mater.* **2010**, *22*, 5240.

(17) Inganäs, O.; Zhang, F.; Tvingstedt, K.; Andersson, L. M.; Hellström, S.; Andersson, M. R. *Adv. Mater.* **2010**, *22*, E100.

(18) Björström Svanström, C. M.; Rysz, J.; Bernasik, A.; Budkowski, A.; Zhang, F.; Inganäs, O.; Andersson, M. R.; Magnusson, K. O.; Benson-Smith, J. J.; Nelson, J.; Moons, E. *Adv. Mater.* **2009**, *21*, 4398.

(19) Gadisa, A.; Mammo, W.; Andersson, L. M.; Admassie, S.; Zhang, F.; Andersson, M. R.; Inganäs, O. *Adv. Funct. Mater.* **2007**, *17*, 3836.

(20) Mühlbacher, D.; Scharber, M.; Morana, M.; Zhu, Z.; Waller, D.; Gaudiana, R.; Brabec, C. *Adv. Mater.* **2006**, *18*, 2884.

(21) Cho, S.; Lee, J. K.; Moon, J. S.; Yuen, J.; Lee, K.; Heeger, A. J. *Org. Electron.* **2008**, *9*, 1107.

(22) Zhang, M.; Tsao, H. N.; Pisula, W.; Yang, C.; Mishra, A. K.; Müllen, K. *J. Am. Chem. Soc.* **2007**, *129*, 3472.

(23) Gaudiana, R. K., Shi, X.; Waller, D.; Zhu, Z. U.S. Patent Application No. 2,008,087,324 (2008).

(24) Moulé, A. J.; Tsami, A.; Bünnagel, T. W.; Forster, M.; Kronenberg, N. M.; Scharber, M.; Koppe, M.; Morana, M.; Brabec, C. J.; Meerholz, K.; Scherf, U. *Chem. Mater.* **2008**, *20*, 4045.

(25) Bijleveld, J. C.; Shahid, M.; Gilot, J.; Wienk, M. M.; Janssen, R. A. J. *Adv. Funct. Mater.* **2009**, *19*, 3262.

(26) Van Mierloo, S.; Hadipour, A.; Spijkman, M.-J.; Van den Brande, N.; Ruttens, B.; Kesters, J.; D'Haen, J.; Van Assche, G.; de Leeuw, D. M.; Aernouts, T.; Manca, J.; Lutsen, L.; Vanderzande, D. J.; Maes, W. *Chem. Mater.* **2012**, *24*, 587.

(27) McCulloch, I.; Heeney, M.; Bailey, C.; Genevicius, K.; MacDonald, I.; Shkunov, M.; Sparrowe, D.; Tierney, S.; Wagner, R.; Zhang, W.; Chabinyc, M. L.; Kline, R. J.; McGehee, M. D.; Toney, M. F. *Nat. Mater.* **2006**, *5*, 328.

(28) Parmer, J. E.; Mayer, A. C.; Hardin, B. E.; Scully, S. R.; McGehee, M. D.; Heeney, M.; McCulloch, I. *Appl. Phys. Lett.* **2008**, *92*, 113309.

(29) Cates, N. C.; Gysel, R.; Beiley, Z.; Miller, C. E.; Toney, M. F.; Heeney, M.; McCulloch, I.; McGehee, M. D. *Nano Lett.* **2009**, *9*, 4153.

(30) Mayer, A. C.; Toney, M. F.; Scully, S. R.; Rivnay, J.; Brabec, C. J.; Scharber, M.; Koppe, M.; Heeney, M.; McCulloch, I.; McGehee, M. D. *Adv. Funct. Mater.* **2009**, *19*, 1173.

(31) Liang, Y.; Wu, Y.; Feng, D.; Tsai, S.-T.; Son, H.-J.; Li, G.; Yu, L. *J. Am. Chem. Soc.* **2008**, *131*, 56.

(32) Chen, H.-Y.; Hou, J.; Zhang, S.; Liang, Y.; Yang, G.; Yang, Y.; Yu, L.; Wu, Y.; Li, G. *Nat. Photon.* **2009**, *3*, 649.

(33) Szarko, J. M.; Guo, J.; Liang, Y.; Lee, B.; Rolczynski, B. S.; Strzalka, J.; Xu, T.; Loser, S.; Marks, T. J.; Yu, L.; Chen, L. X. *Adv. Mater.* **2010**, *22*, 5468.

(34) Guo, J.; Liang, Y.; Szarko, J.; Lee, B.; Son, H. J.; Rolczynski, B. S.; Yu, L.; Chen, L. X. *J. Phys. Chem. B* **2009**, *114*, 742.

(35) Brabec, C. J. *Sol. Energy Mater. Sol. Cells* **2004**, *83*, 273.

(36) Tang, Z.; Andersson, L. M.; George, Z.; Vandewal, K.; Tvingstedt, K.; Heriksson, P.; Kroon, R.; Andersson, M. R.; Inganäs, O. *Adv. Mater.* **2012**, *24*, 554.

(37) Xie, Q.; Perez-Cordero, E.; Echegoyen, L. *J. Am. Chem. Soc.* **1992**, *114*, 3978.

(38) (a) Woo, C. H.; Holcombe, T. W.; Unruh, D. A.; Sellinger, A.; Fréchet, J. M. J. *Chem. Mater.* **2010**, *22*, 1673; (b) Brunetti, F. G.; Gong, X.; Tong, M.; Heeger, A. J.; Wudl, F. *Angew. Chem. Int. Ed.* **2010**, *49*, 532.

(39) (a) Swaraj, S.; Wang, C.; Yan, H.; Watts, B.; Lüning, J.; McNeill, C. R.; Ade, H. *Nano Lett.* **2010**, *10*, 2863; (b) He, X.; Gao, F.; Tu, G.; Hasko, D.; Hüttner, S.; Steiner, U.; Greenham, N. C.; Friend, R. H.; Huck, W. T. S. *Nano Lett.* **2010**, *10*, 1302; (c) Falzon, M.-F.; Wienk, M. M.; Janssen, R. A. J. *J. Phys. Chem. C* **2011**, *115*, 3178.

(40) Søndergaard, R. R.; Makris, T.; Lianos, P.; Manor, A.; Katz, E. A.; Gong, W.; Tuladhar, S. M.; Nelson, J.; Tuomi, R.; Sommeling, P.; Veenstra, S. C.; Rivaton, A.; Dupuis, A.; Teran-Escobar, G.; Lira-Cantu, M.; Sapkota, S. B.; Zimmermann, B.; Würfel, U.; Matzarakis, A.; Krebs, F. C. *Sol. Energy Mater. Sol. Cells* **2012**, *99*, 292.

(41) Krebs, F. C.; Norrman, K. *Prog. Photovolt: Res. Appl.* **2007**, *15*, 697.

(42) Hermenau, M.; Riede, M.; Leo, K.; Gevorgyan, S. A.; Krebs, F. C.; Norrman, K. *Sol. Energy Mater. Sol. Cells* **2011**, *95*, 1268.

(43) Seemann, A.; Sauermann, T.; Lungenschmied, C.; Armbruster, O.; Bauer, S.; Egelhaaf, H. J.; Hauch, J. *Sol. Energy* **2011**, *85*, 1238.

(44) (a) Manceau, M.; Rivaton, A.; Gardette, J.-L.; Guillerez, S.; Lemaître, N. *Polym. Degrad. Stab.* **2009**, *94*, 898; (b) Chambon, S.; Rivaton, A.; Gardette, J.-L.; Firon, M. *Polym. Degrad. Stab.* **2011**, *96*, 1149.

(45) Jørgensen, M.; Norrman, K.; Gevorgyan, S. A.; Tromholt, T.; Andreasen, B.; Krebs, F. C. *Adv. Mater.* **2012**, *24*, 580.

(46) Brusso, J. L.; Lilliedal, M. R.; Holdcroft, S. *Polym. Chem.* **2011**, *2*, 175.

(47) (a) Liu, J.; Kadnikova, E. N.; Liu, Y.; McGehee, M. D.; Fréchet, J. M. J. *J. Am. Chem. Soc.* **2004**, *126*, 9486; (b) Helgesen, M.; Bjerring, M.; Nielsen, N. C.; Krebs, F. C. *Chem. Mater.* **2010**, *22*, 5617.

(48) (a) Kim, B. J.; Miyamoto, Y.; Ma, B.; Fréchet, J. M. J. *Adv. Funct. Mater.* **2009**, *19*, 2273; (b) Griffini, G.; Douglas, J. D.; Piliego, C.; Holcombe, T. W.; Turri, S.; Fréchet, J. M. J.; Mynar, J. L. *Adv. Mater.* **2011**, *23*, 1660.

(49) Kim, H. J.; Han, A. R.; Cho, C.-H.; Kang, H.; Cho, H.-H.; Lee, M. Y.; Fréchet, J. M. J.; Oh, J. H.; Kim, B. J. *Chem. Mater.* **2011**, *24*, 215.

(50) Campo, B.; Oosterbaan, W. D.; Gilot, J.; Cleij, T. J.; Lutsen, L.; Janssen, R. A. J.; Vanderzande, D. SPIE: San Diego, CA, USA, 2009; Vol. 7416; pp 74161G.

(51) Manceau, M.; Bundgaard, E.; Carle, J. E.; Hagemann, O.; Helgesen, M.; Sondergaard, R.; Jorgensen, M.; Krebs, F. C. *J. Mater. Chem.* **2011**, *21*, 4132.

Aim

The development of new light harvesting materials for organic photovoltaics (OPVs) has undergone an almost exponential growth during the last decade. Organic solar cells have the potential to become a competitive market technology, on conditions that the manufacturing costs are reduced and the power conversion efficiencies and lifetimes are at their maximum. Up to date, the efficiency record for OPVs (multiple cell configurations) is held by low band gap copolymers. These materials absorb into the near-IR region of the solar spectrum, where the highest photon flux is generated.

The research work described in this thesis was performed with the general goal to improve the efficiency of organic solar cells by developing light harvesting materials with enhanced optical properties. Our attention was focused on both donor, *i.e.* 4*H*-cyclopenta[2,1-*b*:3,4-*b'*]dithiophenes (**CPDTs**), as well as acceptor, *i.e.* quinoxaline (**Qx**), units. At first, the synthetic protocol for the CPDT building block had to be optimized. Variation of the alkyl side chains should allow to optimize the photovoltaic performance and the thermal stability of materials incorporating these donors, additionally gaining fundamental insights on the (nano)morphology formation and evolution of the polymer:fullerene active layer blend. New synthetic protocols had to be developed and optimized for the Qx building blocks as well. The main goal was the extension of the chromophore by the introduction of conjugated side chains (aliphatic or (hetero)aromatic), connected by ethenyl or butadienyl spacers to the Qx core.

The synthesized electron rich (CPDT) and electron poor (Qx) building blocks should further be integrated in donor-acceptor low band gap copolymers, made of either a combination of CPDT and Qx or with other appropriate acceptor and donor molecules, respectively. The emerging semiconducting polymers should then be employed and analyzed as light harvesting materials in the active layers of OPV devices and, depending on the outcome (and the insights gained), further steps should be taken.

Outline

Chapter 1 is dealing with the **optimization of the synthetic protocol** providing access to symmetrically substituted **cyclopenta[2,1-*b*:3,4-*b'*]dithiophene** (**CPDT**) building blocks. The presence of two branched or linear alkyl side chains allowed to synthesize solution processable **PCPDTBT low band gap polymers** by Suzuki polycondensation reactions with 2,1,3-benzothiadiazole-4,7-bis(boronic acid pinacol ester). The photovoltaic performance of the polymers was evaluated in bulk heterojunction (BHJ), bilayer and tandem organic solar cells. The influence of the number average molecular weight, the purity and the processability of the PCPDTBT polymers on the output parameters and, in consequence, the power conversion efficiencies (PCEs) of the devices was investigated.

In **Chapter 2**, **bromination** of a series of **CPDT** derivatives, **in the presence of NBS**, led to the formation of a new class of compounds, *i.e.* **2*H*-cyclopenta[2,1-*b*:3,4-*b'*]dithiophene-2,6(4*H*)-diones**. A key factor influencing their apparition was the number of equivalents of NBS employed during the reaction. Additionally, solvent effects and reaction times were investigated, affording a better understanding of the mechanism by which these derivatives are formed. Theoretical calculations supported the proposed reaction mechanism and confirmed the apparition of the diones as the thermodynamically favored products.

Chapter 3 describes the formation of 5*H*-spiro(benzo[1,2-*b*:6,5-*b'*]dithiophene-4,4'-cyclopenta[2,1-*b*:3,4-*b'*]dithiophen)-5-one via a **pinacol rearrangement reaction of CDPT-4-one**, induced by trivalent phosphorus reagents. The structure was proposed based on NMR, GC-MS and IR data and was finally confirmed by X-ray crystallography. Complete NMR characterization allowed full assignment of the carbon and hydrogen resonances. Theoretical calculations of the chemical shifts and the optimized geometry were in good agreement with the experimental data.

Chapter 4 reports on the synthesis of three **PCPDTBT low band gap copolymers** bearing either two 2-ethylhexyl, octyl or dodecyl side chains. The impact of the alkyl substituents on the thermal stability of these derivatives was monitored by UV-Vis/IR spectroscopy and a hyphenated TG-TD-GC/MS analysis. The influence of the synthetic route giving access to the dialkylated **CDPT** scaffold, *i.e.* direct alkylation or acid

mediated ring closure of a tertiary alcohol, was investigated by TG-TD-CG/MS. Synthesis of the monoalkyl-CPDT derivative, considered as a possible defect formed during the alkylation step, was also achieved. Its chemical behavior provided insight on the degradation processes occurring at the monomer stage.

Chapter 5 describes the synthesis of a series of **quinoxaline monomers with broadened absorption patterns** in the visible region of the spectrum. This was achieved by the introduction of ethenyl and/or butadienyl spacers between the solubilizing alkyl or (hetero)aryl side chains and the quinoxaline core. New synthetic routes giving access to donor-acceptor-donor (**D-A-D**) triads, bearing (bromo)thiophene end groups, were also explored. All monomers are promising coupling partners ready to be used in polycondensation reactions with a variety of donor materials toward low band gap copolymers for organic photovoltaics.

In **Chapter 6** the synthesis of a series of **poly(thienoquinoxaline)** derivatives was performed by Stille polycondensation reactions between **5,8-dibromoquinoxaline** and **2,5-bis(trialkylstannyl)thiophene** monomers. Considerable attention was devoted to monomer purity, as this had a direct impact on the degree of polymerization attained. The **photovoltaic performance** of these (electron) donor materials was evaluated in polymer:fullerene BHJ solar cells. Optimization of the molecular weight (distribution) of the polymers, the processing solvent and the polymer:fullerene ratio considerably improved the PCE of the devices.

Chapter 7 highlights the synthesis of a series of donor-acceptor, *i.e.* **PBDTQx**, **PBDT-DTQx** and **PCPDT-Qx**, **low band gap copolymers** by Stille polycondensation reactions between benzo[1,2-*b*:3,4-*b*]dithiophene (**BDT**) or **CPDT** donors and a variety of **quinoxaline** acceptors. In this series, as shown by UV-Vis spectroscopy, **PCPDT-Qx** displayed the most pronounced low band gap character (E_g^{OP} = 1.51 eV). Preliminary **photovoltaic evaluation** of these (electron) donor materials in BHJ solar cells, in combination with a fullerene acceptor, afforded promising results.

Chapter 1

PCPDTBT Polymers for Organic Photovoltaics – Debugging the One-Pot Synthesis Reaction of 4*H*-Cyclopenta[2,1-*b*:3,4-*b*']dithiophene

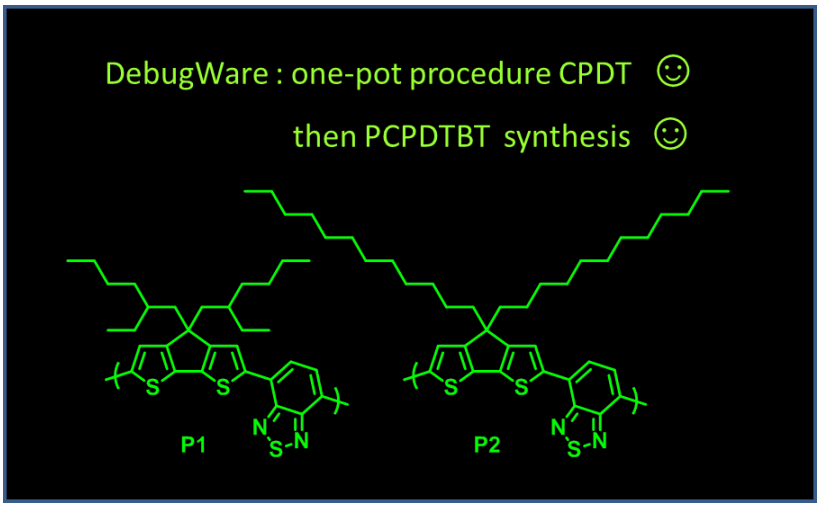

1.1. Introduction

Organic solar cells (OSCs) have emerged as a fast growing and cheap alternative for the conversion of light into energy, capable of occupying a particular part of the photovoltaic (PV) market, addressing specific needs such as flexibility, semi-transparency or low-light indoor applications. Best performing devices have recently surpassed the 10% power conversion efficiency (PCE) threshold,[1] which opens the door toward commercialization of large active area modules. To guarantee a permanent share in the PV market, OSCs with high and long-lasting efficiencies must be manufactured in a time- and cost-effective manner. Therefore, the development of new light harvesting materials with a reasonable stability is of major importance. Third generation conjugated polymers, also known as "*low band gap*" polymers (having band gaps below 1.6 eV), have so far been the most successful class of polymer materials for OSC applications.[2] These polymers are mainly synthesized by alternation of (heterocyclic) donor and acceptor units along the polymer backbone.

Being among the first of their kind, poly[2,6-(4,4-bis(2-ethylhexyl)-4*H*-cyclopenta[2,1-*b*:3,4-*b'*]dithiophene)-*alt*-4,7-(2,1,3-benzothiadiazole)] (**PCPDTBT**) has proven to be a promising material. The alternation of electron rich 4*H*-cyclopenta[2,1-*b*:3,4-*b'*]dithiophene (CPDT) and electron poor 2,1,3-benzothiadiazole (BT) units along the polymer backbone results in a narrow band gap material which absorbs in the near-IR region of the solar spectrum. In combination with $PC_{61}BM$ or $PC_{71}BM$, PCEs above 2.8% were achieved in bulk heterojunction (BHJ) solar cell configurations.[3] Better organization in the active layer, resulting mainly in an improved short circuit current density (J_{sc}), was induced by addition of processing additives. A doubling of the efficiency (5.5%) was achieved when a few percentages of 1,8-octanedithiol (ODT) were incorporated in the solution containing the donor and the acceptor components.[4] By preferential solvation of the fullerene derivative, the processing additive prevents its fast crystallization during film formation. This subsequently leads to a better organization of the bulk (the polymer organizes into fiber-like structures), which is responsible for the enhanced device performance.[5]

It is well known that alkyl substituents have a huge impact on the polymer (and blend) properties. Good solubility is crucial during the polymerization reaction, allowing to obtain high molecular weights. During processing of the solar cells from solution,

complete dissolution of the polymer in the blend is required to ensure formation of homogeneous thin films. In general, polymers bearing branched side chains show superior solubility compared with those bearing linear ones. Additionally, the substituents have a huge impact upon the orientation, organization and packing of the polymer chains. In the case of **PCPDTBT** derivatives, long linear substituents enhance polymer-polymer (π–π stacking) interactions, while branched ones hamper them.[6]

In this paper we present the synthesis of two **PCPDTBT**-type polymers, **P1** bearing two branched 2-ethylhexyl side chains and **P2** carrying two long linear dodecyl side chains. Both polymers were used as donor materials, in combination with a fullerene acceptor, in BHJ solar cells. The influence of solubility, molecular weight and purity of the polymer, as well as the influence of the processing additive upon the device performance is discussed. Considerable attention has been devoted to the optimization of the synthetic protocol toward the CPDT building block.

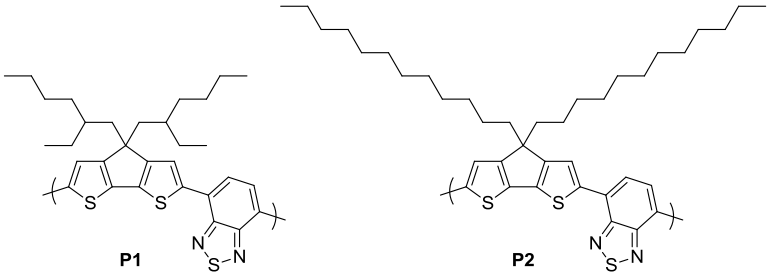

Figure 1.1. Structures of PCPDTBT-type polymers **P1** and **P2**.

1.2. Results and Discussion

1.2.1. Monomer Synthesis

The synthesis of 4*H*-cyclopenta[2,1-*b*:3,4-*b'*]dithiophene-4-one (CPDT-4-one) (**6**) was performed following the synthetic route described by Brzeziński *et al.* (Scheme 1.1).[7] This strategy is by far the most employed method giving access to the 4*H*-cyclopenta[2,1-*b*:3,4-*b'*]dithiophene (**7**) scaffold. The formation of the diiodoalcohol **4** consists of a one-pot reaction in which, in a first instance, halogen-metal exchange between 3-bromothiophene (**1**) and *n*-butyllithium (*n*-BuLi), followed by nucleophilic attack on thiophene-3-carbaldehyde (**2**), leads to the formation of a secondary alcoholate **3**. Ortholithiation of the thiophene rings followed by iodination yields a

diiodoalcohol **4**. Mild oxidation of the latter, using pyridinium chlorochromate (PCC), affords the diiodoketone **5**. Upon ring closure (Ullmann reaction) the cyclic ketone **6** is isolated as a purple crystalline solid.

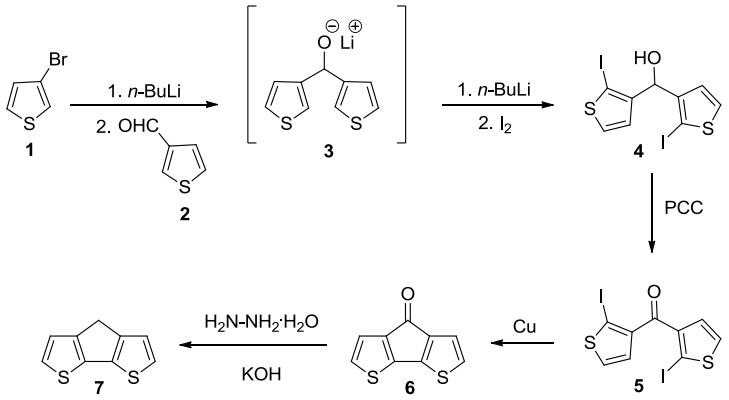

Scheme 1.1. Synthesis of the CPDT scaffold.

The main versatility of this synthetic approach is provided by the key intermediate **6**. The presence of the ketone functionality allows the use of this derivative in a series of transformations giving access to several material classes (Scheme 1.2). For instance, Huang-Minlon reduction has afforded the CPDT derivative **7**.[8] Pinacol rearrangement, mediated by trivalent organophosphorus reagents, afforded 5*H*-spiro[benzo[1,2-*b*:6,5-*b'*]dithiophene-4,4'-cyclopenta[2,1-*b*:3,4-*b'*]dithiophen]-5-one (**8**).[9] Wittig reactions with a large variety of (alkyl and/or aryl) phosphorus ylides afforded planar alkenyl derivatives **9**.[10] The introduction of a quinone moiety connected via azine linkages (**10**)[11] or a dicyanomethylene group (**11**) via Knoevenagel condensation with malononitrile[12] led to various functionalized donor-acceptor CPDT derivatives. Control over the energy levels of such materials is easily attained by varying the acceptor unit. The LUMO (lowest unoccupied molecular orbital) level is strongly dependent on the acceptor substituent (quinone or dicyanomethylene), whereas the HOMO (highest occupied molecular orbital) level is mainly determined by the CPDT unit. The corresponding (co)polymers, obtained by electropolymerization, have shown a highly amphoteric character.[11-12] The formation of 2,6-dibromo-4*H*-cyclopenta[2,1-*b*:3,4-*b*']dithiophen-4-one (**12**) upon bromination with *N*-bromosuccinimide (NBS) allowed its incorporation in various conjugated polymers.[13] $\Delta^{4,4'}$-Dicyclopenta[2,1-*b*:3,4-

b']dithiophene (**13**) can be synthesized in the presence of Lawesson's reagent or by $TiCl_4$ mediated McMurry coupling.[14] The former is preferred, though, due to higher selectivity and superior yields. Derivative **13** is ideal for building two-dimensional conjugated systems. Spiro compounds such as **14** can easily be synthesized by reacting ketone **6** with 2-lithiobiphenyl. The former can for instance be electropolymerized on the electrode surface and used in diodes.[15]

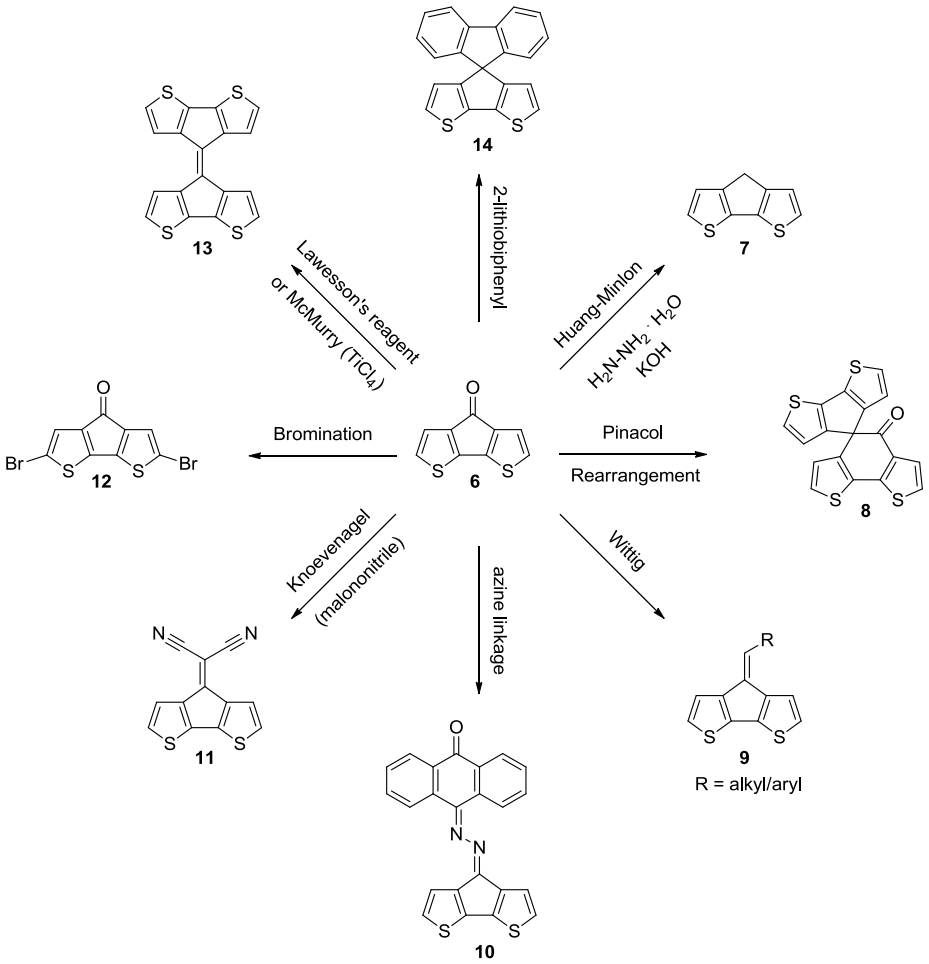

Scheme 1.2. Various transformations of CPDT-4-one **6**.

A few drawbacks associated with the classical synthetic approach toward CPDT-4-one precursor **6** are situated in the initial one-pot reaction, the formation of relatively

unstable derivatives and the use of highly toxic and carcinogenic hexavalent chromium (Cr^{VI}) oxidants, such as PCC (Scheme 1.1). A series of practical aspects and, where possible, ways of addressing the frailty of this synthetic route are discussed.

The first step in the one-pot synthesis is metal-halogen exchange between 3-bromothiophene (**1**) and *n*-BuLi. It was noticed that addition of the halogenated species to the base and immediate work-up after final iodine addition resulted in cleaner reactions and superior yields. Monitoring of the reaction by ^{1}H NMR and GC-MS (gas chromatography - mass spectrometry) showed that all three steps of the one-pot synthesis were neat and highly selective (Figure 1.2). Alcohol **2a**, isolated in 14% yield by Brzeziński *et al*.,[7] is formed by nucleophilic attack of unreacted *n*-BuLi on aldehyde **2**. Alcohol **3b**, the major reaction product after the first step, appeared to be a very unstable compound. As indicated by GC-MS, the latter was quickly oxidized (in air) to the corresponding ketone **3a**, the relative ratio of **3a** to **3b** being 2 to 1. Selective lithiation in positions 2 and 2' of the thiophene rings followed by iodination afforded (di)iodoalcohols **4** and **4a**, respectively. The crude reaction mixture consisted of **4**, the main reaction product, which was accompanied by small amounts of **4a**, **4b** and **4c** (the yields decreasing from **4b** to **4a** to **4c**). The formation of **4b** can be explained by the iodination of thiophene (from protonation of the initial lithiated species) or loss of the side chain, whereas **4c** is most probably formed by halogenation of **4b** during prolonged exposure to iodine.

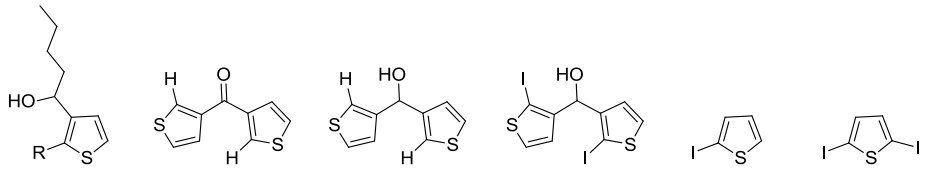

Figure 1.2. Intermediates formed during the one-pot reaction as identified by GC-MS.

Immediately after iodine addition, the reaction mixture is treated with a 20% aqueous solution (v/v) of sodium sulfite (Na_2SO_3). The excess of halogen oxidizes the sulfite to sulfate (Na_2SO_4), which leads to the formation of two moles of hydroiodic acid (HI) per mole of I_2 (Scheme 1.3, eq. 1). Subsequently, aqueous work-up, without adjusting the

pH of the solution with additional HI (the authors suggest pH values of ~5),[7] resulted in cleaner reaction mixtures. The excess iodine (I_2) can react with HI forming hydroiodic acid-iodine concentrate (HI_3) (eq. 2), a highly acidic (pH = 1.12 for 1% vol. aqueous solution)[16] dark brown viscous liquid which makes work-up very difficult and can eventually degrade the desired diiodoalcohol **4**. Moreover, air oxidation of HI to I_2 and water (eq. 3) requires additional neutralization of the generated halogen.

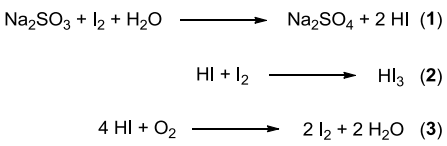

Scheme 1.3. Reactions occurring during work-up of the iodination reaction.

In order to avoid the slightest degradation of compound **4**, we have immediately pursued with the oxidation step followed by ring closure. Ketone **6** was isolated in 50% overall yield starting from 3-bromothiophene (compared to 66% for the literature procedure). Transformation of the carbonyl group following the Huang-Minlon modification of the Wolff-Kishner reduction afforded 4*H*-cyclopenta[2,1-*b*:3,4-*b'*]dithiophene (**7**) in 80% yield, as a white crystalline solid (Scheme 1.1).[8]

The introduction of solubilizing groups is mandatory to obtain solution processable materials. For CPDT derivatives, the introduction of alkyl groups at the bridging position is done in a straightforward manner. As mentioned before, the side chains have a strong influence on the solubility and organization of the polymer. As such, we decided to functionalize the CPDT derivatives with branched 2-ethylhexyl and linear dodecyl side chains, respectively. The synthesis of both derivatives (**15a** and **15b**) was achieved by alkylation of compound **7**, under basic conditions, in the presence of the respective alkyl bromide (Scheme 1.4). The final monomers were obtained *via* bromination of the alkyl-CPDTs **15a-b**, using a slight excess of NBS.[8] It has to be emphasized here that a (large) excess of NBS leads to the formation of a secondary reaction product, namely 2*H*-cyclopenta[2,1-*b*:3,4-*b'*]dithiophene-2,6(4*H*)-dione (**17a** and **17b**). The formation of the latter will be addressed in a forthcoming paper.

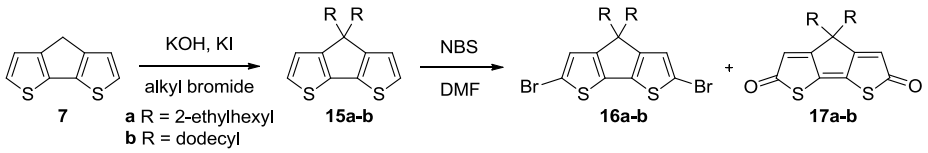

Scheme 1.4. Synthesis of CPDT monomers **16a-b**.

1.2.2. Synthesis and Characterization of PCPDTBT Polymers P1 and P2

CPDT-based polymers were synthesized, using a modified literature procedure,[6] by Suzuki polycondensation between the electron rich dibrominated CPDT units (**16a** and **16b**) and the commercially available electron poor 2,1,3-benzothiadiazole-4,7-bis(boronic acid pinacol ester) (**18**) (Scheme 1.5). The polymerization was carried out in a sealed tube using a biphasic solvent system consisting of toluene and an aqueous potassium carbonate (K_2CO_3) solution. A high-temperature phase transfer catalyst (Aliquat™ HTA-1) was used as well. The reaction, catalyzed by tetrakis(triphenyl-phosphine)palladium ($Pd(PPh_3)_4$), was continued for 3 days at 80 °C. End-capping was performed in two stages by addition of phenylboronic acid and bromobenzene, respectively. Purification of the polymers was done by repetitive Soxhlet extraction with methanol, acetone and hexane. Depending on the solubility, the final polymers were extracted with chloroform (**P1**) or chlorobenzene (**P2**) and were isolated as dark green powders upon precipitation in methanol.

The most soluble derivative (**P1**) was additionally purified by preparative GPC (gel permeation chromatography) or by using a thiol-functionalized metal scavenger kit, commercialized by Agilent Technologies under the name of PL-Thiol MP SPE (StratoSpheres). The additional purification steps were carried out with the goal of removing the slightest traces of residual palladium, originating from the catalyst, which was not washed out by Soxhlet extraction. The purified polymers are denoted as $\mathbf{P1_{GPC}}$ and $\mathbf{P1_{SPE}}$, respectively. The influence of the material purity on the solar cell performance was investigated (*vide infra*).

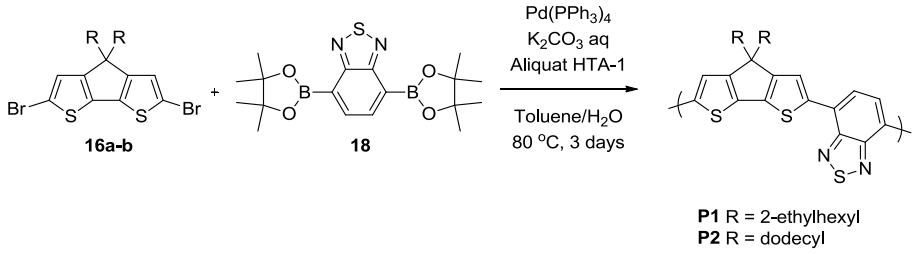

Scheme 1.5. **PCPDTBT** polymer synthesis *via* Suzuki polycondensation.

Both polymers were synthesized in yields ranging from 84 to 95% and their molecular weights were determined by GPC analysis (typically in tetrahydrofuran (THF) at 40 °C) (Table 1.1). For **P2**, carrying long linear alkyl chains, additional analysis was performed at higher temperatures in chlorobenzene (CB) (at 80 °C) and 1,2,4-trichlorobenzene (TCB) (at 135 °C), due to its pronounced tendency to aggregate and its relatively poor solubility in THF. For both **P1** and **P2**, optimization of the polymerization conditions allowed an almost doubling of the number average molecular weight (M_n).

In solution as well as in thin film, **P1** and **P2** showed very similar absorption spectra with two distinct absorption bands (Figure 1.3). The high energy band, located between 400 and 500 nm, is due to π-π* electronic transitions. The low energy band, located between 500 and 800 nm for **P1**, and extended toward 1000 nm for **P2**, has its origins in the intramolecular charge transfer (ICT) from the CPDT donor to the BT acceptor structural units. Going from solution to the solid state led to the apparition and/or enhancement of a shoulder toward the high wavelength end, which arises from π-π interactions between the polymer chains. This feature is generally stronger in derivatives bearing linear substituents, such as **P2**, for which a better packing of the polymer chains is achieved due to smaller interchain distances. Additionally, the degree of crystallinity and the tendency to aggregate improve with higher molecular weights. The low energy shoulder of the main absorption band, very pronounced for **P2**, is an indication of strong aggregation. At higher temperatures (at 180 °C in solution) this shoulder often disappears as break-up of the aggregates occurs.[17]

Table 1.1. Analytical GPC data of **PCPDTBT** polymers **P1** and **P2** obtained from different batches and after purification.

Polymer	M_n (g mol^{-1})	M_w (g mol^{-1})	PDI
P1'[a]	1.1 x 10^4	2.3 x 10^4	2.1
P1	1.8 x 10^4	3.6 x 10^4	2.0
P1$_{GPC\_1}$[b]	5.2 x 10^4	6.4 x 10^4	1.2
P1$_{GPC\_2}$[b]	3.6 x 10^4	5.4 x 10^4	1.5
P2'[a,c]	7.2 x 10^3	1.7 x 10^4	2.4
P2[c]	1.6 x 10^4	7.2 x 10^4	4.5
P2[d]	2.8 x 10^4	42.9 x 10^4	15.3[e]

[a] **P1'** and **P2'** are the same polymers from different polymerization batches; [b] **P1** was purified and fractionated by preparative GPC; [c] determined from CB; [d] determined from TCB [e] high PDI values are due to polymer aggregation.

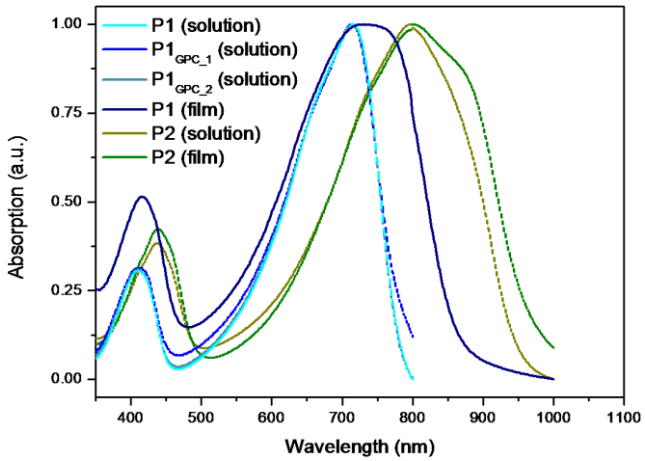

Figure 1.3. Absorption spectra of polymers **P1** and **P2** recorded from solutions and from thin films.

The energy levels of the polymers (Table 1.2), as determined by cyclic voltammetry, are in agreement with the values reported in literature for the parent **PCPDTBT**, having an identical structure to **P1**.[3] The relatively large difference between the optical

and electrochemical band gap of **P2** is probably due to polymer aggregation, which complicates precise determination of the absorption onset.

Table 1.2. Cyclic voltammetry data of the synthesized **PCPDTBT** polymers **P1**and **P2**.

Polymer	E^{ox}_{onset} (V)	E^{red}_{onset} (V)	HOMO (eV)	LUMO (eV)	E_g^{EC} (eV)	E_g^{OP} (eV)[a]
P1	0.15	-1.60	-5.08	-3.32	1.76	1.58
P1[b,c]	0.54	-1.18	-5.30	-3.57	1.73	1.38
P2	0.04	-1.56	-4.97	-3.36	1.61	1.27
P2[b,c]	0.37	-1.25	-5.12	-3.50	1.62	1.25

[a] In film; [b] literature values (ref. 3, 17); [c] determined *vs* normal hydrogen electrode (NHE).

1.2.3. Bilayer, Bulk Heterojunction and Tandem Organic Solar Cells

Two architectures were used for the construction of single module polymer solar cells (PSCs), *i.e.* the BHJ and the planar (bilayer) configuration. The BHJ solar cells were fabricated with a layered structure ITO/PEDOT:PSS/**PCPDTBT**:$PC_{71}BM$/Ca/Ag and the bilayer cells were made with a structure ITO/PEDOT:PSS/ **PCPDTBT**/$PC_{61}BM$/Ca/Ag. The output parameters were measured under air mass 1.5 global illumination conditions (AM 1.5G 100 mW cm^{-2}). A summary of all cell runs is given in Table 1.3 and the *J-V* curves are displayed in Figure 1.4.

For the BHJ solar cells processed using a blend of **P1**:$PC_{71}BM$, in the absence of ODT, a clear increase in efficiency, from 0.63 to 2.74%, was observed for polymers with higher molecular weights. Nevertheless, the gain in efficiency was only noticed when going from **P1'** to **P1** (purified and fractionated), a plateau for the PCE being reached for M_n values of 1.8 x 10^4 g mol^{-1}, and it did not change further when molecular weights were doubled or tripled. In all cases, except for **P1'**, the values for the V_{oc} levelled off at ~0.6 V and for the FF at ~0.4. Only the J_{sc} was directly impacted by the M_n values and increased for polymers with higher molecular weights. The latter show superior mobilities and have a better organization. This can lead to improved morphology in the active layer and hence higher PCEs.

Table 1.3. PSC performances of the synthesized **PCPDTBT** polymers **P1**and **P2**.

Donor Polymer	Processing Solvent(s)	M_n (g mol^{-1})	V_{oc} (V)	J_{sc} (mA cm^{-2})	FF	PCE (%)
P1'[a]	CB[b,c]	1.1 x 10^4	0.45	4.83	0.29	0.63
P1'[a]	CB + ODT[d]	1.1 x 10^4	0.57	7.13	0.34	1.37
P1[a]	CB[b,c]	1.8 x 10^4	0.64	9.49	0.45	2.71
P1[a]	CB + ODT[d]	1.8 x 10^4	0.62	9.50	0.44	2.58
P1[a]	ODCB[e]	1.8 x 10^4	0.66	7.20	0.40	1.90
P1$_{SPE}$[a,f]	CB + ODT[d]	/	0.62	8.22	0.41	2.10
P1$_{GPC_1}$[a,g]	CB[b,c]	5.2 x 10^4	0.62	10.2	0.42	2.68
P1$_{GPC_2}$[a,g]	CB[b,c]	3.6 x 10^4	0.64	9.75	0.44	2.74
P1$_{GPC_1+2}$[a,g]	CB + ODT[d]	/	0.63	8.22	0.50	2.59
P2[a]	ODCB[e,h]	2.8 x 10^4	0.37	4.75	0.41	0.72
P2'[a]	ODCB[e,h]	7.2 x 10^3	0.46	2.91	0.41	0.54
P2[i]	CB[b,c]	2.8 x 10^4	0.35	6.13	0.56	1.19

[a] BHJ solar cell configuration; [b] CB = chlorobenzene; [c] in CB, the polymer:$PC_{71}BM$ ratio was always 1:3 (w/w); [d] ODT = 1,8-octanedithiol; [e] ODCB = *ortho*-dichlorobenzene; [f] **P1$_{SPE}$** was purified with the PL-Thiol MP SPE metal scavenger kit; [g] **P1$_{GPC}$** was purified by preparative GPC; [h] in ODCB, the polymer:$PC_{61}BM$ ratio was always 1:2 (w/w); [i] planar (bilayer) solar cell configuration.

The addition of ODT was only beneficial for PSCs fabricated with the lowest molecular weight polymer **P1'**, for which the efficiency was doubled. When polymers with higher M_n values were used, the addition of ODT did not improve the SC performance any further. The V_{oc} and the FF slightly diminished or were left unchanged, while the J_{sc} was the most impacted output parameter. Drops in the current are most probably due to residual ODT which acts as a "hole trap", while small increases arise from a better organization in the bulk.[6] The highest efficiency (2.74%) was obtained with **P1$_{GPC_2}$**, which had a M_n of 3.6 x 10^4 g mol^{-1}. The evolution of the output parameters of PSCs fabricated with **P1**-type polymers in function of M_n is depicted in Figure 1.5.

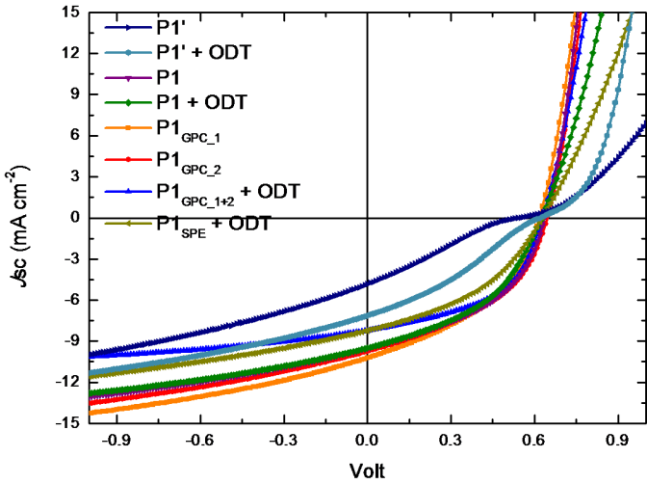

Figure 1.4. *J-V* curves for a series of BHJ solar cells fabricated with **P1**:$PC_{71}BM$ in the active layer.

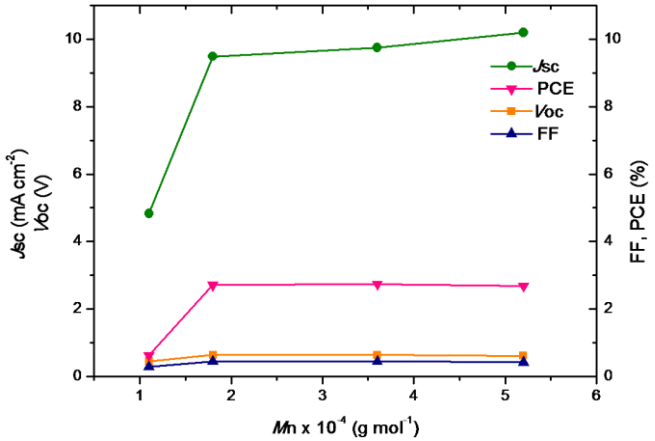

Figure 1.5. Influence of the M_n on the solar cell output parameters.

For the polymer which was additionally purified by preparative GPC, denoted as $\mathbf{P1_{GPC}}$, the solar cell performance was virtually unchanged as compared to **P1**, which was simply isolated after repetitive Soxhlet extractions. The polymer fraction purified using the metal scavenger kit, denoted as $\mathbf{P1_{SPE}}$, showed slightly lower efficiency (and J_{sc} values), probably due to some loss of the high molecular weight fraction on the filter. In consequence, for this class of materials, which has a very low tendency to organize (crystallize), the additional purification steps do not really ameliorate the material's performance in PSCs.

The combination of a large band gap material such as **P3HT** (poly(3-hexylthiophene)) and the low band gap **PCPDTBT** polymer allows, due to the complementary absorption ranges of these materials, a very good coverage of the solar spectrum, leading to enhanced photon absorption. The integration of these two materials in tandem solar cells previously led to 6.5% efficiency when the bottom and the front cell were connected in parallel configuration.[18] Using the same architecture, the bottom cell and the top cell were prepared using a mixture of **P1**:$PC_{71}BM$ (1:2 w/w ratio) and **P3HT**: $PC_{61}BM$ (1:1 w/w ratio), respectively. The output parameters and the *J-V* curves of the single as well as the tandem cells with series and parallel connections are displayed in Table 1.4 and Figure 1.6, respectively.

Table 1.4. Summary of the output parameters for single and tandem organic solar cells made with **P1** (bottom) and **P3HT** (top) in combination with $PC_{61}BM$.

Cell (connection)	V_{oc} (V)	J_{sc} (mA cm^{-2})	FF	PCE (%)
Top (single)	0.59	7.49	0.66	2.90
Bottom (single)	0.66	6.75	0.38	1.70
Tandem (series)	1.25	3.88	0.42	2.10
Tandem (parallel)	0.62	10.51	0.49	3.20

When the bottom and the top cells were connected in series, the efficiency of the tandem device was 2.10 %, the V_{oc} of 1.25 V being (within approximation) the sum of the values obtained for the single cells. On the other hand, for the parallel connection, the current of the tandem device (J_{sc} of 10.51 mA cm^{-2}) was close the sum of the values obtained for each of the individual cells, which enhanced the efficiency of the device to 3.2%. The modest efficiency of the tandem devices as compared to the literature reference can mainly be attributed to the considerably lower efficiencies of the single cells. The origin of the lower J_{sc} and FF for the **PCPDTBT** (**P1**) single cell remains unclear, as an in-house control experiment afforded a single cell with 3.0% efficiency for the same material batch.

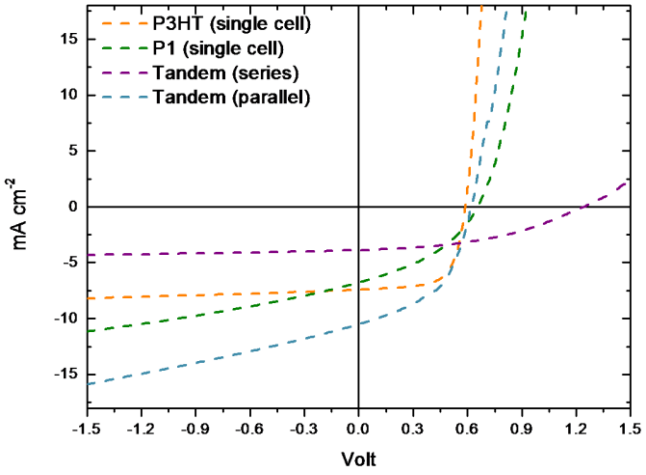

Figure 1.6. *J-V* curves for single and tandem cells made of **P1** and **P3HT** in combination with $PC_{71/61}BM$.

For polymer **P2**, the best solar cell results for the BHJ configuration were obtained from ODCB, using a 1:2 (w/w) polymer:$PC_{61}BM$ ratio. The modest efficiency (0.72%, Table 1.3) could be due to several factors. First of all, the relatively low solubility of the material in the processing solvent prevented its complete dissolution. Filtration prior to film casting probably depleted the composite solution of the highest molecular weight fraction. Secondly, the high tendency of this polymer to aggregate can lead to the formation of inhomogeneous and rough films, with increased phase separation between the donor and the acceptor.

The limited solubility of **P2** in common organic solvents such as chloroform or THF allowed full solution processing of a planar bilayer solar cell. The polymer film was spin coated from a CB solution on top of the ITO. After drying, a layer of $PC_{61}BM$ was deposited from a chloroform solution and the cathode was evaporated by vacuum deposition. Improved J_{sc} and FF led to an almost doubling of the PCE (to 1.2%, Table 1.3).

The presence of charge transfer complex (CTC) ground states was evidenced by Fourier-transform photocurrent spectroscopy (FTPS) (Figure 1.7). This sensitive technique allows the detection of the very weak signals of the CT state, which become visible if the external quantum efficiency (EQE) of the solar cell is plotted on a logarithmic scale. The formation of the CTC leads to the apparition of a new subgap absorption band having its origin in the electronic charge transfer from the donor

polymer to the fullerene acceptor. In BHJ solar cells processed from **P2** in combination with $PC_{61}BM$, the energy of the CT state was located at 1.10 eV. This was slightly reduced to 1.00 eV in BHJ solar cells processed with ODT as an additive, as well as in the bilayer device configuration. The energies of the CT states determined for **P2** are somewhat reduced compared to the ones reported in literature for the parent **PCPDTBT** polymer.[19] The lower values can be explained by the smaller band gap of polymer **P2**.

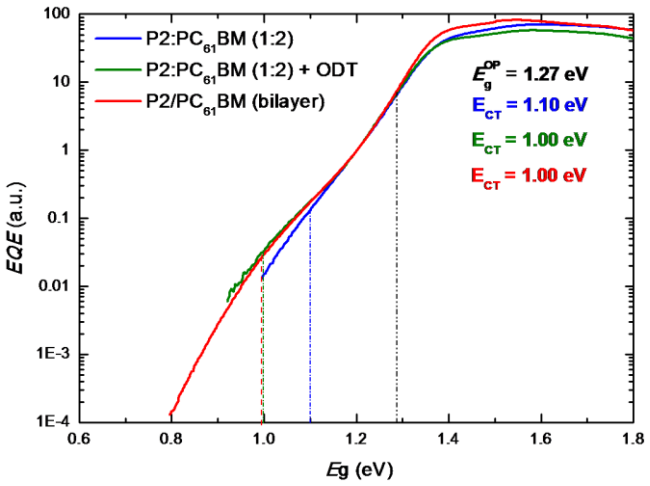

Figure 1.7. Logarithmic plot of the EQE spectra of solar cells fabricated from **P2** and $PC_{61}BM$, revealing the formation of CTCs.

1.3. Conclusions

The synthesis of two low band gap polymers from the **PCPDTBT** family, *i.e.* **P1** and **P2**, bearing different solubilizing alkyl chains, was accomplished. Careful synthetic optimization led to small modifications of the one-pot synthesis reaction giving access to the CPDT scaffold, which afforded cleaner reactions with higher reproducibility. The photovoltaic performance of polymers **P1** and **P2** was evaluated in various solar cell configurations, *i.e.* bulk heterojunction, planar bilayer and tandem solar cells. For **P1,** having an identical structure to the **PCPDTBT** reference polymer, a good correlation between the values of the output parameters of the BHJ solar cells, *i.e.* J_{sc} and PCE, and the M_n values of the polymers issued from various batches was found. The presence of ODT as a processing additive appeared to be beneficial only for devices fabricated

from the polymers with the lowest M_n values, leading to a doubling of the efficiency. In all other cases, ODT did not improve the efficiency or even slightly decreased it. The purity of the polymer isolated by simple precipitation after repetitive Soxhlet extraction was comparable with other samples for which additional purification steps using preparative GPC or a thiol-functionalized metal scavenger kit were performed. Regardless of the purification method, the polymers showed similar PCEs in BHJ solar cells. The modest efficiencies probably be attributed to the rather low molecular weights obtained in the Suzuki polycondensations. The use of the FTPS technique revealed the formation of a sub band gap emission arising from the CTC between polymer **P2** and $PC_{61}BM$.

1.4. Experimental Section

Materials and Methods

NMR chemical shifts (δ, in ppm) were determined relative to the residual $CHCl_3$ absorption (7.26 ppm) or the ^{13}C resonance shift of $CDCl_3$ (77.16 ppm). Gas chromatography-mass spectrometry (GC-MS) analyses were carried out applying Chrompack Cpsil5CB or Cpsil8CB capillary columns. Molecular weights and molecular weight distributions were determined relative to polystyrene standards (Polymer Labs) by gel permeation chromatography (GPC). Chromatograms were recorded on a Spectra Series P100 (Spectra Physics) equipped with two mixed-B columns (10 µm, 0.75 cm x 30 cm, Polymer Labs) and a refractive index detector (Shodex) at 40 °C. THF was most often used as the eluent at a flow rate of 1.0 mL min^{-1}. If chlorobenzene was used as the eluent, the temperature was raised to 80 °C. For the GPC samples in 1,2,4-trichlorobenzene (at 135 °C), the chromatograms were recorded on a PSS-WinGPC (PSS) (pump: alliance GPC 2000) equipped with a PLgel MIXED-B column (particle size: 10 mm, dimension: 0.80 cm x 30 cm) and a refractive index detector at a flow rate of 1.0 mL min^{-1}. Preparative GPC was performed on JAIGEL *2H* and *2.5H* columns attached to a LC system equipped with a UV detector (path 0.5 mm) and a switch for recycling and collecting the eluent ($CHCl_3$: flow rate 3.5 mL min^{-1} and injection volume 1.0 mL). Polymer purification using the thiol-functionalized metal scavenger kit, commercialized by Agilent Technologies under the name of PL-Thiol MP SPE (StratoSpheres), was performed on a polymer solution with

a concentration of 5 mg mL^{-1} in THF. The purified polymer was collected from the cartridge by gravity flow. Solution UV-Vis absorption measurements were performed with a scan rate of 600 nm min^{-1} in a continuous run from 1000 or 800 to 200 nm. Thin film electrochemical measurements were performed with an Eco Chemie Autolab PGSTAT 30 Potentiostat/Galvanostat using a conventional three-electrode cell under N_2 atmosphere (electrolyte: 0.1 mol L^{-1} $TBAPF_6$ in anhydrous CH_3CN). For the measurements, a $Ag/AgNO_3$ reference electrode (0.01 mol L^{-1} $AgNO_3$ and 0.1 mol L^{-1} $TBAPF_6$ in anhydrous CH_3CN), a platinum counter electrode and an indium tin oxide (ITO) coated glass substrate as working electrode were used. The polymers were deposited by drop-casting directly onto the ITO substrates. Cyclic voltammograms were recorded at 50 mV s^{-1}. From the onset potentials of the oxidation and reduction the position of the energy levels could be estimated. All potentials were referenced using a known standard, ferrocene/ferrocenium, which in CH_3CN solution is estimated to have an oxidation potential of -4.98 eV *vs*. vacuum. Polymer BHJ solar cells were fabricated by spin coating a **PCPDTBT**:$PC_{61}BM$ or **PCPDTBT**:$PC_{71}BM$ (Solenne) blend in a 1:2 or 1:3 w/w ratio, respectively, with or without 1,8-octanedithiol (24 mg mL^{-1}) (Sigma Aldrich) as an additive, sandwiched between a transparent anode and an evaporated metal cathode. The bilayer solar cell was fabricated by spin coating a layer of **P2** (from a chlorobenzene solution with a concentration of 10 mg mL^{-1}) followed by a layer of $PC_{61}BM$ (from a chloroform solution with a concentration of 10 mg mL^{-1}). The tandem solar cells were fabricated by spin coating a **P1**:$PC_{71}BM$ blend in a 1:2 w/w ratio for the bottom cell and a P3HT:$PC_{61}BM$ blend in a 1:1 w/w ratio for the top cell. A transparent TiO_x layer was then spin coated from ethanol, followed by evaporation of a layer of MoO_3. For all three solar cell architectures, the transparent anode was an ITO covered glass substrate which was coated with a 30 nm poly(3,4-ethylenedioxythiophene)/poly(styrene sulfonic acid) PEDOT/PSS (CLEVIOS P VP.AI 4083) layer applied by spin coating. The ITO glass substrate was cleaned by ultrasonification (sequentially) in soap solution, deionized water, acetone and isopropanol. The cathode, a bilayer of 50 nm Ca and 100 nm Ag, was thermally evaporated. For the BHJ devices, **PCPDTBT** and $PC_{61}BM$ (1:2 w/w ratio) or $PC_{71}BM$ (1:3 w/w ratio) were dissolved together in *ortho*-dichlorobenzene or chlorobenzene to give an overall 30 or 40 mg mL^{-1} solution, respectively, which was stirred overnight at 80 °C inside a glovebox. For the bilayer configuration, **P2** and $PC_{61}BM$ were dissolved

separately in chlorobenzene and chloroform, respectively. The solutions with a concentration of 10 mg mL^{-1} were stirred overnight at 80 and 50 °C, respectively, inside a glovebox. Solar cell efficiencies were characterized under simulated 100 mW cm^{-2} AM 1.5 G irradiation from a Xe arc lamp with an AM 1.5 global filter.

Synthesis

Unless stated otherwise, all reagents and chemicals were obtained from commercial sources and used without further purification. 2,1,3-Benzothiadiazole-4,7-bis(boronic acid pinacol ester) (95%) (**18**) was purchased from Sigma Aldrich and used without further purification.

Bis(2-iodo-3-thienyl)methanol (4) was synthesized according to a modified literature procedure.[7] A solution of 3-bromothiophene (6.52 g, 40 mmol) in dry diethyl ether (30 mL) was added dropwise to a solution of *n*-BuLi (16.0 mL, 2.5 M in hexane) in dry diethyl ether (20 mL) cooled at -78 °C. The mixture was allowed to react at -78 °C for 2 h and then a solution of thiophene-3-carbaldehyde (4.48 g, 40 mmol) in dry diethyl ether (30 mL) was added dropwise. The mixture was allowed to react for 30 minutes at -78 °C and was then brought to r.t. and stirred for another 30 minutes. The mixture was again cooled to -10 °C and *n*-BuLi (35.2 mL, 2.5 M in hexane) was added dropwise. The mixture was allowed to react for 1 h at -10 °C, and then for 1 h at r.t. The mixture was then cooled to 0 °C and a solution of I_2 (31.98 g, 126 mmol) in dry diethyl ether (250 mL) was added dropwise. After the addition, the mixture was brought to r.t. and an aqueous Na_2SO_3 solution (20% vol., 100 mL) was added. The organic layer was washed with an aqueous Na_2SO_3 solution (20% vol., 250 mL), a saturated Na_2CO_3 solution and brine, and dried over anhydrous $MgSO_4$. The solvent was removed under reduced pressure and the crude product was used in the next step without further purification. Material identity was confirmed by GC-MS and ^{1}H NMR.

Bis(2-iodo-3-thienyl)ketone (5) was synthesized according to a literature procedure.[7] The product was used in the next step without further purification. Material identity and purity were confirmed by GC-MS and ^{1}H NMR.

4*H*-Cyclopenta[2,1-*b*:3,4-*b'*]dithiophene-4-one (**6**) was synthesized according to a literature procedure.[7] The residue was purified by column chromatography (silica, eluent CH_2Cl_2) to afford the title compound as a purple solid (3.85 g, 50% yield starting

from 3-bromothiophene). Material identity and purity were confirmed by GC-MS and ^{1}H NMR.

4*H*-Cyclopenta[2,1-*b*:3,4-*b'*]dithiophene (7) was synthesized according to a literature procedure.[8] Material identity was confirmed by GC-MS and ^{1}H NMR.

4,4-Bis(2-ethylhexyl)-4*H*-cyclopenta[2,1-*b*:3,4-*b'*]dithiophene (15a) and **2,6-dibromo-4,4-bis(2-ethylhexyl)-4*H*-cyclopenta[2,1-*b*:3,4-*b'*]dithiophene (16a)** were synthesized according to a literature procedure.[20] Material identity and purity were confirmed by GC-MS and ^{1}H NMR.

Poly[2,6-(4,4-bis(2-ethylhexyl)-4*H*-cyclopenta[2,1-*b*:3,4-*b'*]-dithiophene)-*alt*-4,7-(2,1,3-benzothiadiazole)] (PCPDTBT) (P1) was synthesized using a **general polymerization procedure** from **16a** and **18** according to a modified literature procedure.[6] The phase transfer catalyst (PTC) Aliquat 336 was replaced by a high temperature resistant PTC, *i.e.* Aliquat^{TM} HTA-1. **P1** was isolated as a dark green powder (yield: 84%). GPC (THF, PS standards) M_n = 1.8 x 10^4 g mol^{-1}, M_w = 3.6 x 10^4 g mol^{-1}, PDI = 2.0.

4,4-Didodecyl-4*H*-cyclopenta[2,1-*b*:3,4-*b'*]dithiophene (15b) and **2,6-dibromo-4,4-didodecyl-4*H*-cyclopenta[2,1-*b*:3,4-*b'*]dithiophene (16b)** were synthesized according to a literature procedure.[17] Material identity and purity were confirmed by GC-MS and ^{1}H NMR.

Poly[2,6-(4,4-didodecyl)-4*H*-cyclopenta[2,1-*b*:3,4-*b'*]-dithiophene)-*alt*-4,7-(2,1,3-benzothiadiazole)] (PCPDTBT) (P2) was synthesized according to the general polymerization procedure from **16b** and **18**. **P2** was isolated as a dark green powder (yield: 95%). GPC (CB, PS standards) M_n = 1.6 x 10^4 g mol^{-1}, M_w = 7.2 x 10^4 g mol^{-1}, PDI = 4.5.

1.5. References

(1) Dou, L.; You, J.; Yang, J.; Chen, C.-C.; He, Y.; Murase, S.; Moriarty, T.; Emery, K.; Li, G.; Yang, Y. *Nat. Photon.* **2012**, *6*, 180.

(2) (a) Van Mierloo, S.; Adriaensens, P. J.; Maes, W.; Lutsen, L.; Cleij, T. J.; Botek, E.; Champagne, B.; Vanderzande, D. J. *J. Org. Chem.* **2010**, *75*, 7202; (b) Carsten, B.; He, F.; Son, H. J.; Xu, T.; Yu, L. *Chem. Rev.* **2011**, *111*, 1493; (c) Son, H. J.; He, F.; Carsten, B.; Yu, L. *J. Mater. Chem.* **2011**, *21*, 18934; (d) Zhou, H.; Yang, L.; You, W. *Macromolecules* **2012**, *45*, 607; (e) Kettle, J.; Waters, H.; Horie, M.; Chang, S. W. *J. Phys. D: Appl. Phys.* **2012**, *45*, 125102; (f) Horie, M.; Kettle, J.; Yu, C.-Y.; Majewski, L. A.; Chang, S.-W.; Kirkpatrick, J.; Tuladhar, S. M.; Nelson, J.; Saunders, B. R.; Turner, M. L. *J. Mater. Chem.* **2012**, *22*, 381; (g) Rosch, R.; Tanenbaum, D. M.; Jorgensen, M.; Seeland, M.; Barenklau, M.; Hermenau, M.; Voroshazi, E.; Lloyd, M. T.; Galagan, Y.; Zimmermann, B.; Wurfel, U.; Hosel, M.; Dam, H. F.; Gevorgyan, S. A.; Kudret, S.; Maes, W.; Lutsen, L.; Vanderzande, D.; Andriessen, R.; Teran-Escobar, G.; Lira-Cantu, M.; Rivaton, A.; Uzunoglu, G. Y.; Germack, D.; Andreasen, B.; Madsen, M. V.; Norrman, K.; Hoppe, H.; Krebs, F. C. *Energy Environ. Sci.* **2012**, *5*, 6521.

(3) Mühlbacher, D.; Scharber, M.; Morana, M.; Zhu, Z.; Waller, D.; Gaudiana, R.; Brabec, C. *Adv. Mater.* **2006**, *18*, 2884.

(4) Peet, J.; Kim, J. Y.; Coates, N. E.; Ma, W. L.; Moses, D.; Heeger, A. J.; Bazan, G. C. *Nat. Mater.* **2007**, *6*, 497.

(5) Cho, S.; Lee, J. K.; Moon, J. S.; Yuen, J.; Lee, K.; Heeger, A. J. *Org. Electron.* **2008**, *9*, 1107.

(6) Zhang, M.; Tsao, H. N.; Pisula, W.; Yang, C.; Mishra, A. K.; Müllen, K. *J. Am. Chem. Soc.* **2007**, *129*, 3472.

(7) Brzeziński, J. Z.; Reynolds, J. R. *Synthesis* **2002**, 1053.

(8) Coppo, P.; Cupertino, D. C.; Yeates, S. G.; Turner, M. L. *Macromolecules* **2003**, *36*, 2705.

(9) Marin, L.; Zhang, Y.; Robeyns, K.; Champagne, B.; Lutsen, L.; Vanderzande, D.; Adriaensens, P.; Maes, W. *Trivalent Phosphorus Reagent Induced Pinacol Rearrangement of 4H-Cyclopenta[2,1-b:3,4-b']dithiophen-4-one, manuscript in preparation*

(10) Coppo, P.; Adams, H.; Cupertino, D. C.; Yeates, S. G.; Turner, M. L. *Chem. Commun.* **2003**, 2548.

(11) Kozaki, M.; Igarashi, H.; Okada, K. *Chem. Lett.* **2004**, *33*, 156.

(12) Ferraris, J. P.; Lambert, T. L. *J. Chem. Soc., Chem. Commun.* **1991**, 1268.

(13) Pal, B.; Yen, W.-C.; Yang, J.-S.; Chao, C.-Y.; Hung, Y.-C.; Lin, S.-T.; Chuang, C.-H.; Chen, C.-W.; Su, W.-F. *Macromolecules* **2008**, *41*, 6664.

(14) Loganathan, K.; Cammisa, E. G.; Myron, B. D.; Pickup, P. G. *Chem. Mater.* **2003**, *15*, 1918.

(15) Ong, T.-T.; Ng, S.-C.; Chan, H. S. O.; Vardhanan, R. V.; Kumura, K.; Mazaki, Y.; Kobayashi, K. *J. Mater. Chem.* **2003**, *13*, 2185.

(16) http://iofina.com/iofina-chemical/products

(17) Coffin, R. C.; Peet, J.; Rogers, J.; Bazan, G. C. *Nat. Chem.* **2009**, *1*, 657.

(18) Kim, J. Y.; Lee, K.; Coates, N. E.; Moses, D.; Nguyen, T.-Q.; Dante, M.; Heeger, A. J. *Science* **2007**, *317*, 222.

(19) Vandewal, K.; Gadisa, A.; Oosterbaan, W. D.; Bertho, S.; Banishoeib, F.; Van Severen, I.; Lutsen, L.; Cleij, T. J.; Vanderzande, D.; Manca, J. V. *Adv. Funct. Mater.* **2008**, *18*, 2064.

(20) Karsten, B. P.; Bijleveld, J. C.; Viani, L.; Cornil, J.; Gierschner, J.; Janssen, R. A. J. *J. Mater. Chem.* **2009**, *19*, 5343.

Chapter 2

Reaction of 4*H*-Cyclopenta[2,1-*b*:3,4-*b*']dithiophenes with NBS - A Route Toward 2*H*-Cyclopenta[2,1-*b*:3,4-*b*']dithiophene-2,6(4*H*)-diones

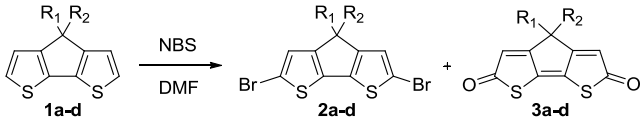

a $R_1 = R_2$ = 2-ethylhexyl, **b** $R_1 = R_2$ = dodecyl, **c** R_1 = 2-ethylhexyl, R_2 = octyl
d R_1 = 2-ethylhexyl, R_2 = methyl nonanoate

2.1. Introduction

Organic photovoltaics (OPVs) have emerged as an environmentally friendly technology that converts solar light into energy. An appealing feature of OPVs is the relatively low production cost for large area modules by roll to roll (R2R) printing techniques.[1] Due to the high extinction coefficients of organic semiconductors, the thicknesses of the active layers can be in the order of hundreds of nanometers only, which ultimately leads to lightweight and flexible modules able to efficiently convert solar irradiance to electricity.[2] With the solar irradiation photon flux peaking around 700 nm, various narrow band gap materials have recently been designed and used in bulk heterojunction (BHJ) organic solar cells.[3,4] Poly[(4,4-bis(2-ethylhexyl)-4*H*-cyclopenta[2,1-*b*:3,4-*b'*]dithiophene-2,6-diyl)-*alt*-(2,1,3-benzothiadiazole-4,7-diyl)] (**PCPDTBT**) (Figure 2.1), was among the first low band gap copolymers (1.3 eV) that afforded power conversion efficiencies above 2.8% in combination with a fullerene acceptor.[5] In the presence of suitable processing additives, the efficiency was almost doubled, surpassing the 5% threshold.[6] This resulted in **PCPDTBT** being currently one of the most widely studied low band gap polymers for OPVs. This copolymer, in which electron rich 4*H*-cyclopenta[2,1-*b*:3,4-*b'*]dithiophene (CPDT) and electron poor 2,1,3-benzothiadiazole units (BT) alternate along the backbone, is generally synthesized by Suzuki or Stille polycondensations.[7] These reactions occur *via* a step-wise growth of the polymer chain and require a precise 1:1 ratio of functionalities, halide and boronic ester or trialkyl tin for Suzuki and Stille polycondensations, respectively. Not fulfilling this precise feed ratio of monomers in the polymerization mixture leads to the formation of low molecular weight species which show poor optical properties and can in consequence not be used in the fabrication of highly efficient solar cell devices.

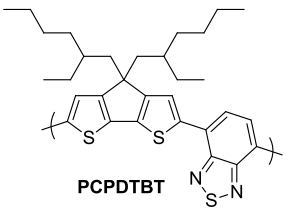

Figure 2.1. Chemical structure of a **PCPDTBT** narrow band gap copolymer.[5-6]

When Suzuki polycondensation (SPC) is the method of choice for the synthesis of **PCPDTBT**,[7c] the toxic tin side products generated in the Stille polycondensation are avoided. The SPC is usually carried out between the dibrominated CPDT and the bis(boronic acid pinacol ester) derivative of 2,1,3-benzothiadiazole. The latter can be synthesized in two steps starting from BT by direct bromination, using a mixture of bromine in hydrobromic acid,[8] followed by palladium catalyzed halogen-metal exchange in the presence of bis(pinacolato)diboron.[7b] On the other hand, dibrominated CPDT derivatives are obtained upon bromination using *N*-bromosuccinimide (NBS).[7d,9] In order to meet the precise 1:1 stoichiometry required in the SPC, high purity of the difunctional monomers is required. Coupling units bearing only one of these functionalities, *i.e.* boronic ester or bromine, act as "end-cappers" or "dead end chains" and lead to the formation of lower molecular weight polymer/oligomer materials. Such monofunctional compounds must therefore be carefully removed by tedious purification or, ideally, not be formed during the transformations.

In this paper we present a detailed study of the bromination reaction of CPDT derivatives, by means of NBS, giving access to either 2,6-dibromo-4,4-bis(alkyl)-4*H*-cyclopenta[2,1-*b*:3,4-*b'*]dithiophenes or 2*H*-cyclopenta[2,1-*b*:3,4-*b'*]dithiophene-2,6(4*H*)-diones. A possible mechanism leading to the formation of the latter, which arise as a new class of compounds within the CPDT family, is proposed. The influence of the solvent, reaction time and the number of equivalents of NBS on the selectivity of the reaction is discussed.

2.2. Results and Discussion

2.2.1. Synthetic Exploration

The synthesis of CPDT derivatives has been studied intensively and improved steadily over the years. The groups of Gronowitz[10] and Wynberg[11] have conducted elaborated studies and have dedicated long years of research to this class of compounds. Among the six isomers that can be obtained depending on the annulation of the thiophene rings, 4*H*-cyclopenta[2,1-*b*:3,4-*b'*]dithiophene has gained much attention in the past years and is, to the best of our knowledge, the sole isomer that has been used for the synthesis of low band gap polymers for solar cell applications. The presence of solubilizing alkyl side chains on the bridging carbon atom is mandatory to obtain solution processable

materials. Most synthetic routes toward the CPDT scaffold involve multistep synthetic routes,[12] many of which use harsh reaction conditions and/or controversial reagents, such as the Wolff-Kishner reduction and the oxidation of secondary alcohols using pyridinium chlorochromate (PCC), respectively. More recently, CPDT derivatives bearing various functionalities in the side chains have been synthesized using a three-step approach.[13] This route enables the synthesis of both symmetrically and asymmetrically alkyl-substituted (linear or branched) CPDT derivatives, and the introduction of ester-functionalized side chains by variation of the keto(ester) precursor. Regardless of the synthetic approach used for the synthesis of the CPDT scaffold, bromination in positions 2 and 6 of the aromatic unit is required to afford the CPDT monomer possessing bromine groups ready to be subjected to SPC.[4c,14]

In order to dibrominate 4,4-bis(2-ethylhexyl)-substituted CPDT derivative **1a** (Scheme 2.1), and exclude the presence of the monobrominated derivative in the reaction mixture, we have conducted the bromination reaction for 8 to 24 h in the dark and under inert atmosphere, by using an excess of NBS (2.5 up to 3.2 equivalents) in a 2 mM solution of the CPDT derivative in *N*,*N*-dimethylformamide (DMF). Under these conditions, no monobrominated product was detected and the yields of the isolated dibrominated CPDT **2a** (Scheme 2.1) were varying between 40 and 80%.

Reactions which afforded compound **2a** in isolated yields as low as 40% have drawn our attention. The ^{1}H NMR spectrum of the crude reaction mixtures (Figure 2.2) showed, besides the expected "triplet-like" resonance pattern of the dibrominated CPDT **2a**, located around 6.93 ppm, and the aliphatic protons of the alkyl chains present on the CPDT bridging carbon atom (in this case two 2-ethylhexyl groups), the presence of an additional "triplet" around 6.01 ppm. In this particular case, both "triplets" were located in the low field region with the same integrated value, pointing to a 1:1 ratio of two products. The presence of a secondary product formed during the bromination reaction was also confirmed by GC-MS. It should be emphasized here that the resonance of the unique aromatic proton belonging to the dibrominated CPDT derivative **2a** (situated at 6.93 ppm) shows up as an apparent triplet (there is no *J*-coupling) due to the presence of different stereoisomers. In the case where there is one linear and one branched 2-ethylhexyl side chain (**2c** and **2d**), an apparent doublet was observed, whereas in the case of two linear substituents (**2b**) only a sharp singlet was noticed.

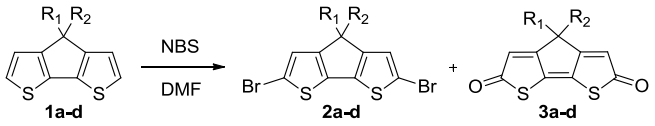

a $R_1 = R_2$ = 2-ethylhexyl, **b** $R_1 = R_2$ = dodecyl, **c** R_1 = 2-ethylhexyl, R_2 = octyl, **d** R_1 = 2-ethylhexyl, R_2 = methyl nonanoate

Scheme 2.1. Bromination of CPDTs **1a-d** with NBS, affording dibromo-CPDTs **2a-d** and CPDT-2,6-diones **3a-d**.

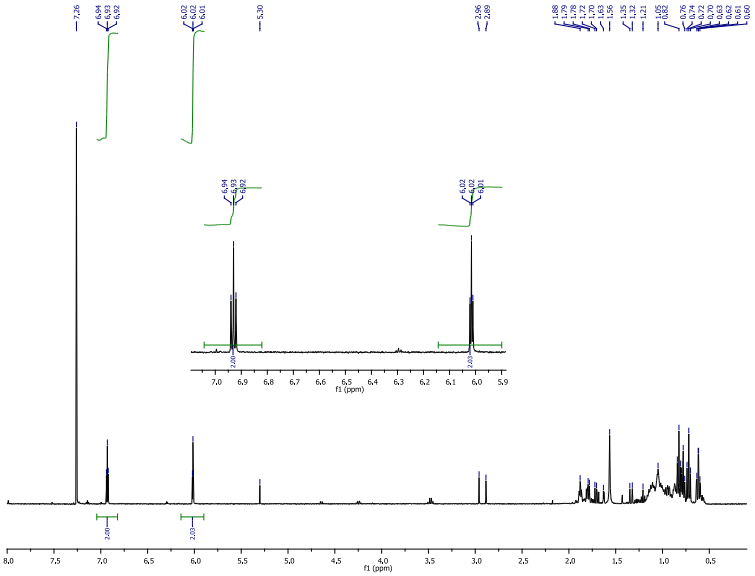

Figure 2.2. ^{1}H NMR spectrum of a (low yield) crude reaction mixture after treatment of CPDT **1a** with NBS.

Both reaction products were then separated and purified by means of column chromatography (silica) to recover the dibrominated CPDT **2a** (clear oil, 40% yield) and the secondary product **3a** (yellow oil, 40% yield), respectively. Complete ^{1}H and ^{13}C NMR analysis, corroborated with GC-MS analysis and IR spectroscopy, allowed to identify the isolated secondary product as 4,4-bis(2-ethylhexyl)-2*H*-cyclopenta[2,1-*b*:3,4-*b'*]dithiophene-2,6(4*H*)-dione (**3a**), a new compound within the 4*H*-cyclopenta[2,1-*b*:3,4-*b'*]dithiophene family (Scheme 2.1). ^{1}H NMR revealed that the triplet-like signal located around 6.01 ppm results from the proton in the α position of the carbonyl group, the latter being confirmed by the presence of a characteristic C=O resonance around 194 ppm in the ^{13}C NMR spectrum. IR spectroscopy confirmed the

presence of the carbonyl groups, by an absorption peak located at 1700 cm^{-1}. GC-MS analysis provided a molar mass of the isolated product (*m/z* 432), in accordance with the proposed structure. The formation of the CPDT-2,6-dione was not limited to the bis(2-ethylhexyl) derivative, but was also encountered for a few analogous CPDT compounds **1b-d** (Scheme 2.1). The experiments that were conducted using 3.5 equivalents of NBS in DMF allowed us to isolate both the initially targeted dibrominated CPDTs **2a-d** together with the diones **3a-d**. All novel materials were fully characterized by ^{1}H and ^{13}C NMR, GC-MS and IR.

2.2.2. Reaction Mechanism

Several processes can account for the formation of compound **3a**: (1) Diels-Alder addition between singlet oxygen ($^{1}O_2$) (presumably generated *in situ*) and the non-brominated CPDT derivative,[15] (2) hydrolytic opening of the thiophene ring followed by dehydration *via* bromine and (3) overbromination of the dibrominated compound leading to the formation of the thiolactone **2a''** (Scheme 2.3), followed by fast oxidation of the latter in air, toward the dione **3a**. In order to elucidate the mechanism which led to the formation of diketo-CPDT **3a**, these possible mechanisms have been analyzed.

(1) It is well known that thiophene derivatives, and especially photoactive materials such as poly(3-alkylthiophenes), have a rather low photochemical stability which, in the presence of oxygen and/or air, leads to their degradation. The photodegradation products are believed to be formed via an adduct between the thiophene ring (part of the π conjugated system in the case of polymers) and oxygen, generating carbonyl and sulfonic derivatives or that, alternatively, the pathway may involve the side chain.[16] Such degradations being considerably reduced or even absent when the thiophene derivatives are irradiated under inert atmosphere highlight the key role of oxygen in the formation of the photodegradation products.

Since the bromination reaction of CPDT has been conducted in the dark and under inert atmosphere, this mechanism is not likely to take place. Moreover, the dibrominated derivative **2a** is stable in air and NMR analysis demonstrated that it does not degrade (on a reasonable time scale).

To exclude the involvement of $^{1}O_2$, all further experiments were carried out under oxygen free atmosphere, by using degassed solvents and chemicals. Additionally, only

2.1 equivalents of NBS were used in a 1 mM solution in DMF. Even when taking all these precautions, GC-MS and NMR analysis showed the formation of **3a** already after 2 h. At this stage of the reaction, also monobrominated CPDT was still present in low concentrations. After 3 h, the monobrominated CPDT was not detected anymore and the reaction was stopped. This showed that the exclusion of oxygen from the reaction medium does not completely avoid the formation of the dione. The mechanism leading to the formation of compound **3a** hence probably does not involve $^1O_2$.

(2) In an attempt to brominate 2-bromo-3,5-di-*tert*-butylthiophene with bromine in an acetic acid-nitric acid mixture in the presence of silver nitrate, Gronowitz *et al*.[17] isolated the corresponding hydroxyfuranone in 70% yield. The formation of the latter was supposed to occur by hydrolytic opening of the thiophene ring followed by dehydration *via* bromine. Also this mechanism does not seem to be responsible for the formation of compound **3a**, as the replacement of the sulfur atom in the CPDT ring was not observed.

(3) Upon bromination of naphtho[1,2-*c*]thiophene (**4**) using a mixture of NBS in acetic acid, Lin *et al.*[18] have recovered the expected dibrominated compound **5** together with two other secondary products, *i.e.* thiolactone **6** and thioanhydride **7** (Scheme 2.2). Even though the bromination reaction was conducted for only 20 minutes, with just 2.0 equivalents of NBS (an equimolar amount), the formation of the dibrominated compound was not exclusive, as three products were formed in a 1:0.6:1 (**5**:**6**:**7**) ratio. The proposed mechanism involves further electrophilic attack of the dibrominated derivative leading to the tribrominated species **9**, which affords the thiolactone **6** upon aqueous work-up. Exposure of the latter to air leads to the formation of the thioanhydride **7**. The crucial role of a bromonium intermediate in the NBS promoted rearrangement of 1,1-diarylmethylenecyclopentanes has recently been pointed out and supports the proposed reaction pathway.[19]

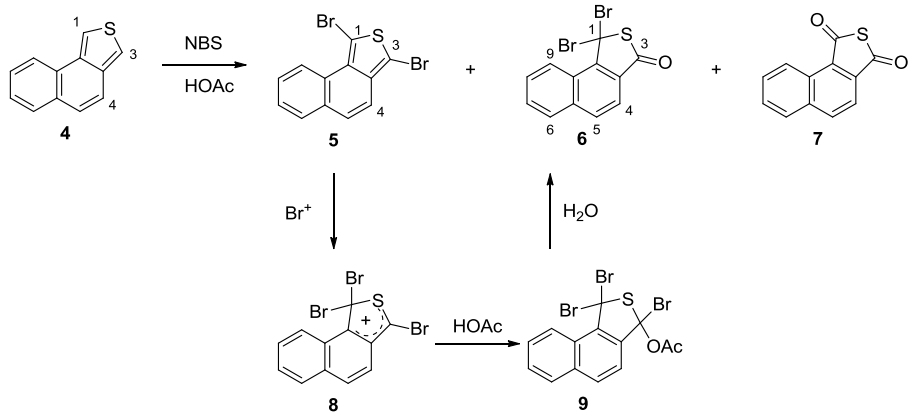

Scheme 2.2. Bromination of naphtho[1,2-c]thiophene (**4**).[18]

Additionally, palladium mediated reactions between a series of variously substituted CPDT derivatives and sodium dicyanomethanide, followed by oxidation with aqueous bromine, have led to the formation of quinoid 2,6-dihydro-4*H*-cyclopenta[2,1-*b*:3,4-*b'*]dithiophene derivatives.[20]

By analogy, the same sequence of reactions, *i.e.* electrophilic attack followed by hydrolysis and fast oxidation, can account for the formation of dione **3a** (Scheme 2.3). Here, overbromination at C2 of the CPDT ring affords the positively charged intermediate **2a'**, which is stabilized by several resonance forms. The resonance form bearing the positive charge at the 6-position leads, upon aqueous work-up, to thiolactone **2a''**. Surprisingly, this product has never been detected by GC-MS or NMR analysis, suggesting that this compound is very efficiently oxidized to compound **3a**. The loss of aromaticity in compound **3a** is reflected in the chemical shift of the two protons of the fused heterocycle at $\delta = 6.01$ ppm, well below the normal chemical shift range of aromatic (CPDT) protons. The driving force can be found in the formation of a stable quinoid derivative.[21] The dione formation was enhanced by the use of an excess of NBS, which suggests that, under these conditions, the dione is thermodynamically favored, whereas the dibrominated CPDT derivative appears under more kinetic conditions.

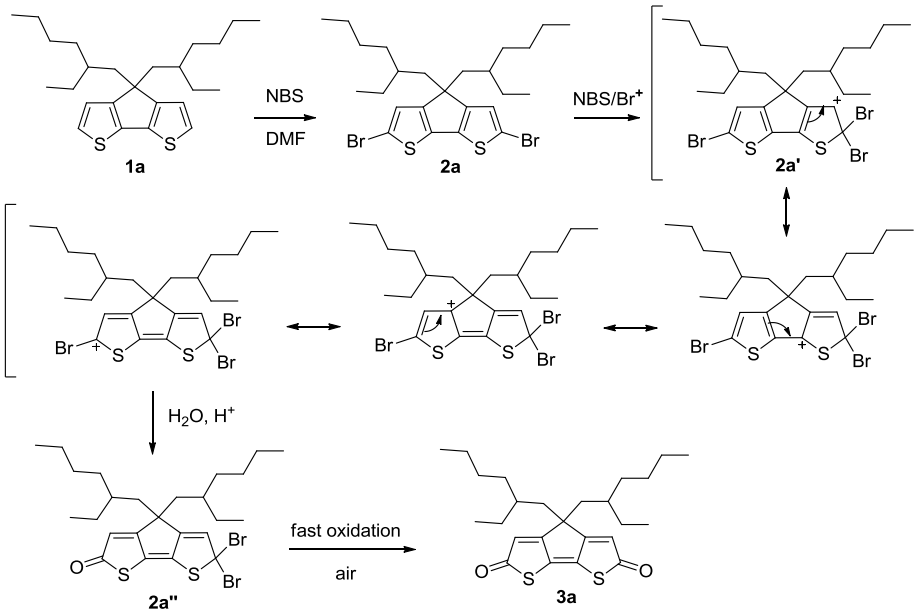

Scheme 2.3. Proposed mechanism for the formation of CPDT-2,6-dione **3a**.

2.2.3. Theoretical Calculations

To support this interpretation, theoretical calculations were carried out for reactions involving the model compounds **1e**, **2e**, **2e''**, and **3e**, for which the 2-ethylhexyl side chains were truncated to ethyl groups, together with NBS, succinimide (NS), HBr, and water. The results, summarized in Figure 2.3, showed that the formation of dibromo-CPDT **2e** from 4,4-diethyl-CPDT **1e** stabilizes the system by about 46.0 kcal/mol according to B3LYP/6-311+G(d,p) calculations, and by 51.8 kcal/mol when employing the MP2/6-311+G(d,p) method, indicating that the formation of the dibrominated compound is a thermodynamically favored process. Moreover, the formation of CPDT-dione **3e** further stabilizes the system by 62.6 [31.6] kcal/mol according to calculations carried out at the B3LYP/6-311+G(d,p) [MP2/6-311+G(d,p)] levels, respectively. This substantiates the experimental hypothesis that the dione is thermodynamically favored. During the formation of dibromo-CPDT **2e**, part of the product reacts further with NBS to form **3e**, provided NBS is in excess. This is also consistent with the experimental findings. The calculations also showed that the formation of the dione derivative **3e** through the intermediate **2e''** is a thermodynamically favored process. The formation of **2e''** leads to additional ΔG stabilization by 33.7 [17.6] kcal/mol with respect to **2e'**

and then, the transformation of the former to **3e** also involves an additional stabilization by 28.9 [14.0] kcal/mol according to B3LYP/6-311+G(d,p) [MP2/6-311+G(d,p)] calculations.

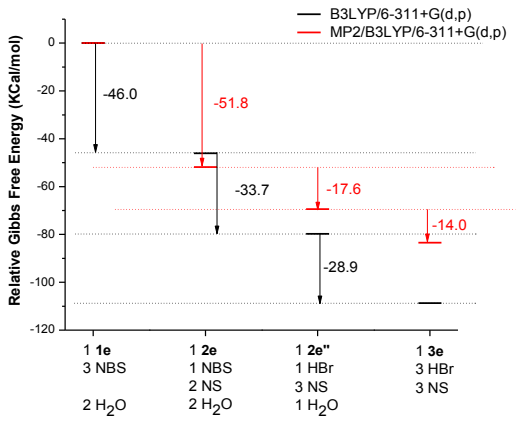

Figure 2.3. Variation of the Gibbs free energy along the reaction coordinate.

Theoretically calculated NMR chemical shifts were in good agreement with the experimental ones, which provided additional evidence for the molecular structure. The calculated ^{1}H NMR chemical shifts (corrected using the α/β linear regressions)[22] for the α and β hydrogen atoms on the thiophene rings of **1e** amounted to 7.19 and 7.05 ppm, respectively, matching rather well the experimental values of 7.10 and 6.91 ppm for **1a**. In **2e**, the corresponding chemical shift for the β hydrogen decreased slightly to 6.90 ppm, close to the experimental value of 6.93 ppm for **2a**. The calculated ^{1}H NMR chemical shift of the β hydrogen atoms in **3e** appeared at 5.97 ppm, in line with the experimental shift at 6.01 ppm for **3a**, proving that the crude reaction mixture also contains **3a**. In addition, calculations on **2e''** show that the β hydrogen atoms on the dibrominated and on the carbonyl sides have chemical shifts of 6.45 and 5.97 ppm, respectively. The resonance at 6.45 ppm can hence be applied as a fingerprint to detect the possible existence of **2e''**.

Among all parameters influencing the reaction, *e.g.* concentration of the starting product in DMF, reaction time and the presence/absence of oxygen, the number of equivalents of NBS seemed to have the greatest impact on the percentage of dibrominated products, and in consequence of the diones, obtained during the

bromination reaction of the CPDT derivatives **1a-d**. We therefore decided to perform the bromination reaction of **1c** (R_1 = 2-ethylhexyl, R_2 = octyl) (in DMF) using an excess of NBS ranging from 2.1 to 5.0 equivalents, the reaction time being limited to 3 h.

This series of experiments (Table 2.1) pointed out that by using only a slight excess of NBS (2.1 or 2.5 equiv), the dione formation was (almost) suppressed. The use of 3.0, 3.5 and 4.0 equiv of NBS afforded the dione in 15, 50 and 73%, respectively. The use of 5.0 equiv of NBS afforded the dione as the unique reaction product. The mole fractions of **2c** and **3c** in the crude reaction mixture, as deduced from the integration of the protons located at 6.93 and 6.01 ppm in the ^{1}H NMR spectrum, respectively, showed a sigmoid variation with the number of equivalents of NBS used, which could be an indication of an autocatalytic reaction (Figure 2.4).[23]

Table 2.1. Influence of the number of equivalents of NBS on the reaction product distribution **2c**:**3c**.

equiv NBS	2c (%)[a]	3c (%)[a]
2.1	98	2
2.5	100[b]	0
3.0	85	15
3.5	50	50
4.0	27	73
5.0	0	100

[a] Deduced from the integration of the protons situated at 6.93 and 6.01 ppm, belonging to compounds **2c** and **3c**, respectively; concentration of **1c**: 0.02 mM in DMF, equivalents of NBS varying from 2.1 to 5.0, reaction time: 3 h at r.t. [b] Within the ^{1}H NMR detection limit.

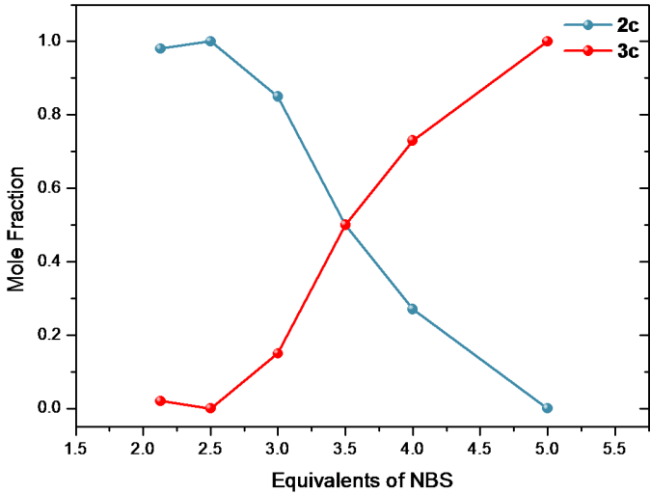

Figure 2.4. Influence of the number of equivalents of NBS on the reaction product ratio **2c**:**3c**.

2.2.4. Study of Solvent Effects - *In Situ* ^{1}H NMR Experiments

To get more insight into the reaction mechanism and to be able to follow the evolution of the reaction mixture in time, we have performed a series of *in situ* ^{1}H NMR experiments. For this purpose, we have conducted the bromination reaction directly in an NMR tube. A solution of **1c** in the corresponding deuterated solvent or solvent mixture (chloroform, DMF, acetic acid, chloroform:acetic acid = 1:1 (v/v)) was placed in the tube to which NBS (4.0 equiv) was added as a solid. The mixture was well stirred by means of a vortex (the tube was protected from light by wrapping it in aluminum foil). After having homogenized the solution, a clear change in color was noticed (the mixture turned from pale yellow to green). The tube was placed in the NMR and a first spectrum was recorded (generally 3 to 10 minutes after the addition of NBS). At the end of the reaction, water was added and the aqueous layer was extracted with diethyl ether. Depending on the solvent, different results were obtained.

$CDCl_3$

The first spectrum (recorded 5 minutes after the sample was prepared) showed that the starting product was fully converted to the dibromo-CPDT **2c**. No traces of the monobrominated derivative or other secondary products could be detected at this stage of the reaction. The reaction was allowed to run for 3 days, with spectra recorded every hour. The system looked stable and did not evolve in the next 5 h. No major changes were noticed until the end of the experiment, except for two minor "doublet-like"

signals located at 6.30 and 7.10 ppm. At the end of the reaction the mixture was gradually hydrolyzed by the addition of 10 + 20 μL of water. Again, no major changes were noticed. On the other hand, after work-up, the ^{1}H NMR spectrum of the fully hydrolyzed mixture showed the presence of the dibrominated CPDT **2c** and dione **3c**, the corresponding "doublets" being located at 6.93 and 6.01 ppm, respectively, together with two other minor "doublet-like" signals located at 6.30 and 7.10 ppm, as the major peaks.

DMF-d_7

The first spectrum (recorded 5 minutes after the sample was prepared) revealed the presence of the dibrominated CPDT together with traces of the monobrominated derivative. The reaction was then allowed to run for 3 days, ^{1}H NMR spectra being recorded every hour. The last recorded spectrum showed almost no changes compared to the one recorded after 1 h, which showed a main peak corresponding to the dibrominated product and two additional small peaks, like in the case of chloroform. The spectrum of the hydrolyzed sample showed the peak located at 6.01 ppm, corresponding to the dione, as the major signal, in an almost 9:1 ratio with respect to the dibrominated CPDT. Surprisingly enough, GC-MS analysis of an aliquot collected after 45 minutes and the one of the hydrolyzed sample had the same composition. These facts strongly suggest that the formation of the dione is significantly enhanced upon hydrolysis and/or exposure to air. Under these conditions (4.0 equiv of NBS, DMF as a solvent) it became very clear that the reaction time has little influence, if any, on the formation of the dione.

CH_3COOD and CH_3COOD:$CDCl_3$ (1:1 v/v)

For the reactions performed in acetic acid or a mixture acetic acid:chloroform, *in situ* ^{1}H NMR experiments pointed again toward an increase in the percentage of the dione upon aqueous work-up and, in consequence, a decrease in the percentage of the dibrominated product.

In summary, *in-situ* ^{1}H NMR experiments allowed us to identify the strong dependence of the reaction products upon the solvent. No clear intermediates could be identified and/or isolated. These findings point to a crucial change in composition upon aqueous work-up and support the suggested mechanism by which the dione is formed, *i.e.*

overbromination followed by hydrolysis and fast oxidation (as shown by GC-MS analysis).

Knowing that in DMF the use of 4.0 equivalents of NBS afforded the dione as the major reaction product (~73 % yield), we have investigated the influence of other solvents and/or solvent mixtures, generally used for brominations using NBS, on the reaction outcome. The polarity and the character (protic or aprotic) of the solvent were varied. As displayed in Table 2.2, the use of non-polar solvents such as carbon tetrachloride or chloroform led exclusively to the formation of the dibrominated compound **2c**. The use of polar protic solvents or a 1:1 mixture with a non-polar solvent, such as acetic acid:chloroform, afforded the dibrominated compound **2c** as the main reaction product, together with small amounts of dione **3c**. The percentage of **3c** was higher in pure acetic acid. These findings suggest that the formation of **3c** was enhanced by the polarity of the mixture. 1,2-Dimethoxyethane (DME) and DMF are both polar aprotic solvents, perfectly miscible with water. Moreover, the system NBS-DME is known as a powerful oxidizing medium for secondary alcohols.[20c,24] Surprisingly enough, bromination of **1c** appeared to proceed differently in these two very similar solvents. In DME, the formation of **3c** did not occur, whereas in DMF the latter stands for the major reaction product. In acetone, **2c** was the sole reaction product, the presence of **3c** not being detected.

Table 2.2. Influence of the solvent on the bromination of **1c**, using 4.0 equiv of NBS.

Solvent (mixture)	Nature	Dipole Moment (D)[a]	Dielectric constant (ε)[a]	2c (%)	3c (%)	Miscibility with water
CCl_4	non-polar	0	2.24	100	0	N
$CHCl_3$	non-polar	1.01	4.81	100	0	N
DME	polar aprotic	1.71	7.20	100	0	Y
AcOH	polar protic	1.74	6.15	83	17	Y
Acetone	polar aprotic	2.88	21.0	100	0	Y
DMF	polar aprotic	3.82	36.70	27	73	Y
$CHCl_3$:AcOH 1:1	/	/	/	96	4	/

[a] CRC Handbook of Chemistry and Physics: A Ready-Reference of Chemical and Physical Data, 85th ed. Edited by David R. Lide (National Institute of Standards and Technology). CRC Press LLC: Boca Raton, FL. 2004.

2.3. Conclusions

In this study we have carefully investigated the bromination reaction for a series of CPDT derivatives, with NBS as the bromine source. In DMF, full control over the reaction products could be achieved depending on the equivalents of NBS used during the reaction. The use of 2.1 equivalents of NBS afforded the dibrominated CPDT derivatives as the unique reaction products. On the other hand, the use of 5.0 equivalents of NBS led to the exclusive formation of 2*H*-cyclopenta[2,1-*b*:3,4-*b'*]dithiophene-2,6(4*H*)-diones, which arise as a new class of compounds issued from the 4*H*-cyclopenta[2,1-*b*:3,4-*b'*]dithiophene family. The formation of the diones is supposed to occur *via* a bromination-hydrolysis sequence, followed by fast air oxidation of a thiolactone intermediate. The obtained insights are of high relevance for all people involved in the synthesis and application of CPDT-based materials in organic electronics. The chemical reactivity of this new class of compounds toward various transformations, *e.g.* reductions, Knoevenagel reactions, condensations, dimerizations, etc., specific to carbonyl functionalities, is currently under investigation within our group.

2.4. Experimental Section

Materials and Methods

NMR chemical shifts (δ, in ppm) were determined relative to the residual $CHCl_3$ absorption (7.26 ppm) or the ^{13}C resonance shift of $CDCl_3$ (77.16 ppm). Gas chromatography-mass spectrometry (GC-MS) analyses were carried out applying Chrompack Cpsil5CB or Cpsil8CB capillary columns. The structures of the model compounds were optimized using density functional theory (DFT) with the B3LYP hybrid exchange-correlation functional and the 6-311+G(d,p) basis set. Based on the optimized structures at the B3LYP/6-311+G(d,p) level, the chemical shifts of all systems were calculated with the B3LYP functional and the 6-311+G(2d,p) basis set together with the GIAO method to ensure origin-independence. The Møller-Plesset second-order perturbation theory (MP2) method was also employed to calculate the reaction ΔG values on the basis of geometrical structures optimized at the B3LYP/6-311+G(d,p) level. For both the structure optimizations and property calculations, the Polarizable Continuum Model (PCM) using the integral equation formalism (IEFPCM) was employed to account for solvent (DMF) effects. All calculations were performed using Gaussian09.[25]

Synthesis

General procedure 1 (allowing to obtain both the dibrominated and the dione products): 4,4-Bis(2-ethylhexyl)-4*H*-cyclopenta[2,1-*b*:3,4-*b'*]dithiophene (**1a**) (0.797 g, 1.98 mmol) was dissolved in DMF (100 mL) and the mixture was cooled to 0 ^oC by means of an ice-bath (the reaction was run in the dark and under N_2 balloon pressure). Subsequently, a solution of NBS (3.0 equiv, 0.178 g, 5.97 mmol) in DMF (100 mL) was added drop-wise during 30 minutes and the mixture was allowed to react at r.t. overnight. The mixture was again cooled to 0 ^oC water (100 mL) was added and the aqueous layer was extracted with diethyl ether. The combined organic layers were washed with water and brine, dried over anhydrous $MgSO_4$ and filtered. Evaporation of the solvent under reduced pressure afforded a dark yellow viscous oil. The crude mixture was purified by means of column chromatography (silica) using a gradient of hexane-ethyl acetate from 0% (isolation of the dibrominated compound **2a**) to 10% (isolation of the dione **3a**).

2,6-Dibromo-4,4-bis(2-ethylhexyl)-4*H*-cyclopenta[2,1-*b*:3,4-*b*']dithiophene (2a):[7d] light-yellow oil (0.400 g, 36%). ^{1}H NMR (300 MHz, $CDCl_3$) δ 6.94/6.93/6.92 (3 x s, intensity ratio 1/2/1, 2H), 1.85-1.75 (m, 4H), 1.32-1.21 (m, 2H), 0.90-0.85 (m, 16H), 0.80-0.76 (m, 6H), 0.64-0.60 (m, 6H).

4,4-Bis(2-ethylhexyl)-2*H*-cyclopenta[2,1-*b*:3,4-*b*']dithiophene-2,6(4*H*)-dione (3a): yellow oil (0.342 g, 40%). GC-MS (EI) *m/z* 432 [M^+]; HRMS (EI) calcd for $C_{25}H_{36}O_2S_2$ 432.2157 found *m/z* 432.2166; ^{1}H NMR (300 MHz, $CDCl_3$) δ 6.02/6.01/6.00 (3 x s, intensity ratio 1/2/1, 2H), 1.92-1.82 (m, 4H), 1.15-0.99 (m, 18H), 0.81 (t, J = 6.0 Hz, 6H), 0.71 (t, J = 6.0 Hz, 6H); ^{13}C NMR (75 MHz, $CDCl_3$) δ 193.7 (C=O), 176.1, 145.7, 115.5 (CH), 52.1, 44.5 (CH_2), 35.6 (CH), 33.9 (CH_2), 28.2 (CH_2), 27.1 (CH_2), 22.8 (CH_2), 14.1 (CH_3), 10.3 (CH_3); IR (NaCl, cm^{-1}) ν_{max} 3077 (w, unsaturated C-H), 2958/2927/2871/2857 (s, saturated C-H), 1700 (s, CO); UV-Vis ($CHCl_3$, nm) λ_{max} (log ε) 278 (4.422), 381 (4.456).

2,6-Dibromo-4,4-didodecyl-4*H*-cyclopenta[2,1-*b*:3,4-*b*']dithiophene (2b):[14] According to general procedure 1. 4,4-Didodecyl-4*H*-cyclopenta[2,1-*b*:3,4-*b*']dithiophene (**1b**) (0.370 g, 0.718 mmol), NBS (0.383 g, 2.16 mmol), DMF (50 mL), eluent hexane; light yellow oil (0.510 g, 72%); GC-MS (EI) *m/z* 671/673/675 [M^+]; ^{1}H NMR (300 MHz, $CDCl_3$) δ 6.92 (s, 2H), 1.77-1.72 (m, 4H), 1.29-1.14 (m, 40H), 0.87 (t, J = 6.0 Hz, 6H).

4,4-Didodecyl-2*H*-cyclopenta[2,1-*b*:3,4-*b*']dithiophene-2,6(4*H*)-dione (3b): light-yellow oil (0.078 g, 20%). MS (CI) *m/z* 544 [M^+]; HRMS (EI) calcd for $C_{33}H_{52}O_2S_2$ 544.3409 found *m/z* 544.3370; ^{1}H NMR (300 MHz, $CDCl_3$) δ 6.01 (s, 2H), 1.86-1.82 (m, 4H), 1.29-1.20 (m, 40H), 0.87 (t, J = 6.0 Hz, 6H); ^{13}C NMR (75 MHz, $CDCl_3$) δ 194.3 (C=O), 176.1, 145.3, 115.1, 52.6, 39.4 (CH_2), 32.0 (CH_2), 29.8 (CH_2), 29.77 (CH_2), 29.75 (CH_2), 29.70 (CH_2), 29.6 (CH_2), 29.4 (CH_2), 29.4 (CH_2), 22.8 (CH_2), 14.2 (CH_3); IR (NaCl, cm^{-1}) ν_{max}, 3076 (w, unsaturated C-H), 2958/2923/2852 (s, saturated C-H), 1703 (s, CO); UV-Vis ($CHCl_3$, nm) λ_{max} (log ε) 380 (4.497).

General procedure 2: 4-(2-Ethylhexyl)-4-octyl-4*H*-cyclopenta[2,1-*b*:3,4-*b'*]dithiophene (**1c**) (0.276 g, 0.68 mmol) was dissolved in DMF (10 mL) and the mixture was cooled to 0 °C by means of an ice-bath (the reaction was run in the dark and under N_2 balloon pressure). Subsequently, a solution of NBS (4.0 equiv, 0.484 g, 2.72 mmol) in DMF (10 mL) was added drop-wise and the mixture was allowed to

react at r.t. overnight. The mixture was again cooled to 0 °C, water (100 mL) was added and the aqueous layer was extracted with diethyl ether. The combined organic layers were washed with water and brine, dried over anhydrous $MgSO_4$ and filtered. Evaporation of the solvent under reduced pressure afforded a dark yellow viscous oil. The crude mixture was purified by means of column chromatography (silica) using a gradient of hexane-ethyl acetate from 0% (isolation of the dibrominated compound **2c**) to 10% (isolation of the dione **3c**).

2,6-Dibromo-4-(2-ethylhexyl)-4-octyl-4H-cyclopenta[2,1-*b*:3,4-*b'*]dithiophene (2c): slightly yellow oil (0.060 g, 16%); GC-MS (EI) *m/z* 558/560/562 [M^+]; ^{1}H NMR (300 MHz, $CDCl_3$) δ 6.94/6.93 (2 x s, intensity ratio 1/1, 2H), 1.83 (t, J = 4.8 Hz, 2H), 1.78-1.72 (m, 2H), 1.27-0.89 (m, 21H), 0.86 (t, J = 7.1 Hz, 3H), 0.79 (t, J = 6.9 Hz, 3H), 0.64 (t, J = 7.4 Hz, 3H); ^{13}C NMR (75 MHz, $CDCl_3$) δ 155.9/155.8, 136.6/136.5, 125.0/124.9, 111.05/111.0, 55.1, 41.6, 39.4, 35.5, 34.1, 31.9, 30.0, 29.43, 29.40, 28.6, 27.4, 24.4, 22.9, 22.8, 14.3, 14.2, 10.8; IR (NaCl, cm^{-1}) ν_{max} 3082 (w, unsaturated C-H), 2957/2926/2855 (w, saturated C-H); UV-Vis ($CHCl_3$, nm) λ_{max} (log ε) 250 (3.984), 339 (4.282).

4-(2-Ethylhexyl)-4-octyl-2*H*-cyclopenta[2,1-*b*:3,4-*b'*]dithiophene-2,6(4*H*)-dione (3c): deep yellow oil (0.205 g, 70 %); GC-MS (EI) *m/z* 432 [M^+]; HRMS (EI) calcd for $C_{25}H_{36}O_2S_2$ 432.2157 found *m/z* 432.2164; ^{1}H NMR (300 MHz, $CDCl_3$) δ 6.01/6.00 (2 x s, intensity ratio 1/1, 2H), 1.88-1.86 (m, 2H), 1.84-1.80 (m, 2H), 1.26-0.98 (m, 21H), 0.83 (t, J = 6.9 Hz, 3H), 0.80 (t, J = 6.9 Hz, 3H), 0.70 (t, J = 7.2 Hz, 3H); ^{13}C NMR (75 MHz, $CDCl_3$) δ 193.99/193.95 (C=O), 176.2/176.1, 145.4, 115.3/115.2, 52.3, 43.1, 40.9, 35.9, 33.8, 31.8, 29.7, 29.2, 28.3, 27.0, 24.4, 22.9, 22.6, 14.15, 14.10, 10.4; IR (NaCl, cm^{-1}) ν_{max} 3066 (w, unsaturated C-H), 2957/2926/2855 (s, saturated C-H), 1701 (s, CO); UV-Vis ($CHCl_3$, nm) λ_{max} (log ε) 381 (4.253).

Methyl-9-(2,6-dibromo-4-(2-ethylhexyl)-4*H*-cyclopenta[2,1-*b*:3,4-*b'*]dithiophene-4-yl)nonanoate (2d). According to general procedure 1. Methyl 9-(4-(2-ethylhexyl)-4*H*-cyclopenta[2,1-*b*:3,4-*b'*]dithiophene-4-yl)nonanoate (**1d**) (0.315 g, 0.685 mmol), NBS (2.1 equiv, 0.260 g, 1.46 mmol), DMF (17.5 mL), eluent hexane:ethyl acetate 9:1; yellow oil (0.266 g, 63%); GC-MS (EI) *m/z* 616/618/620 [M^+]; ^{1}H NMR (300 MHz, $CDCl_3$) δ 6.92/6.91 (2 x s, intensity ratio 1/1, 2H), 3.64 (s, 3H), 2.26 (t, J = 7.5 Hz, 2H), 1.81 (t, J = 4.8 Hz, 2H), 1.76-1.70 (m, 2H), 1.61-1.51 (m, 2H), 1.30-0.88 (m,

19H), 0.77 (t, *J* = 6.9 Hz, 3H), 0.62 (t, *J* = 7.4 Hz, 3H); ^{13}C NMR (75 MHz, $CDCl_3$) δ 174.5 (CO-O), 155.9/155.8, 136.6/136.5, 125.0/124.9, 111.1/111.0, 55.1, 51.6, 41.7, 39.4, 35.4, 34.2, 34.1, 29.9, 29.31, 29.26, 29.18, 28.6, 27.4, 25.0, 24.3, 22.9, 14.2, 10.8; IR (NaCl, cm^{-1}) ν_{max} 3084 (w, unsaturated C-H), 2928/2855 (s, saturated C-H), 1739 (s, CO-O); UV-Vis ($CHCl_3$, nm) λ_{max} (log ε) 250 (3.884), 339 (4.297).

Methyl-9-(4-(2-ethylhexyl)-4*H*-cyclopenta[2,1-*b*:3,4-*b'*]dithiophene-4yl)nonanoate-2,6(4*H*)-dione (3d). According to general procedure 2. Methyl 9-(4-(2-ethylhexyl)-4*H*-cyclopenta[2,1-*b*:3,4-*b'*]dithiophene-4-yl)nonanoate (**1d**) (0.100 g, 0.216 mmol), NBS (4.0 equiv, 0.154 g, 0.866 mmol), DMF (10 mL), eluent hexane/ethyl acetate 80:20; yellow oil (0.067 g, 63%); GC-MS (EI) *m/z* 490 [M^+]; HRMS (EI) calcd for $C_{27}H_{38}O_4S_2$ 490.2212 found *m/z* 490.2208; ^{1}H NMR (300 MHz, $CDCl_3$) δ 6.010/6.005 (2 x s, intensity ratio 1/1, 2H), 3.66 (s, 3H), 2.28 (t, *J* = 7.5 Hz, 2H), 1.89-1.81 (m, 4H), 1.63-1.54 (m, 2H), 1.28-1.05 (m, 19H), 0.82 (t, *J* = 6.8 Hz, 3H), 0.72 (t, *J* = 7.2 Hz, 3H); ^{13}C NMR (75 MHz, $CDCl_3$) δ 194.1 (CO), 176.2/176.1 (CO-O), 174.3, 145.5, 115.3, 52.4, 51.6, 43.2, 41.0, 35.9, 34.1, 33.9, 29.7, 29.2, 29.13, 29.08, 28.3, 27.1, 24.9, 24.4, 22.9, 14.1, 10.4.; IR (NaCl, cm^{-1}) ν_{max} 3073 (w, unsaturated C-H), 2928/2855 (s, saturated C-H), 1739 (s, CO-O), 1700 (s, CO); UV-Vis ($CHCl_3$, nm) λ_{max} (log ε) 381 (4.424).

2.5. References

(1) Espinosa, N.; Hosel, M.; Angmo, D.; Krebs, F. C. *Energy Environ. Sci.* **2012**, *5*, 5117.

(2) Günes, S.; Neugebauer, H.; Sariciftci, N. S. *Chem. Rev.* **2007**, *107*, 1324.

(3) (a) Bundgaard, E.; Krebs, F. C. *Sol. Energy Mater. Sol. Cells* **2007**, *91*, 954; (b) Po, R.; Maggini, M.; Camaioni, N. *J. Phys. Chem. C* **2009**, *114*, 695; (c) Brabec, C. J.; Gowrisanker, S.; Halls, J. J. M.; Laird, D.; Jia, S.; Williams, S. P. *Adv. Mater.* **2010**, *22*, 3839; (d) Boudreault, P.-L. T.; Najari, A.; Leclerc, M. *Chem. Mater.* **2010**, *23*, 456.

(4) (a) Liang, Y.; Yu, L. *Acc. Chem. Res.* **2010**, *43*, 1227; (b) Hellstrom, S.; Lindgren, L. J.; Zhou, Y.; Zhang, F.; Inganas, O.; Andersson, M. R. *Polym. Chem.* **2010**, *1*, 1272; (c) Bronstein, H.; Chen, Z.; Ashraf, R. S.; Zhang, W.; Du, J.; Durrant, J. R.; Shakya Tuladhar, P.; Song, K.; Watkins, S. E.; Geerts, Y.; Wienk, M. M.; Janssen, R. A. J.; Anthopoulos, T.; Sirringhaus, H.; Heeney, M.; McCulloch, I. *J. Am. Chem. Soc.* **2011**, *133*, 3272.

(5) Mühlbacher, D.; Scharber, M.; Morana, M.; Zhu, Z.; Waller, D.; Gaudiana, R.; Brabec, C. *Adv. Mater.* **2006**, *18*, 2884.

(6) Peet, J.; Kim, J. Y.; Coates, N. E.; Ma, W. L.; Moses, D.; Heeger, A. J.; Bazan, G. C. *Nat. Mater.* **2007**, *6*, 497.

(7) (a) Schlüter, A. D. *J. Polym. Sci., Part A: Polym. Chem.* **2001**, *39*, 1533; (b) Zhang, M.; Tsao, H. N.; Pisula, W.; Yang, C.; Mishra, A. K.; Müllen, K. *J. Am. Chem. Soc.* **2007**, *129*, 3472; (c) Murage, J.; Eddy, J. W.; Zimbalist, J. R.; McIntyre, T. B.; Wagner, Z. R.; Goodson, F. E. *Macromolecules* **2008**, *41*, 7330; (d) Bijleveld, J. C.; Shahid, M.; Gilot, J.; Wienk, M. M.; Janssen, R. A. J. *Adv. Funct. Mater.* **2009**, *19*, 3262; (e) Kettle, J.; Horie, M.; Majewski, L. A.; Saunders, B. R.; Tuladhar, S.; Nelson, J.; Turner, M. L. *Sol. Energy Mater. Sol. Cells* **2011**, *95*, 2186; (f) Kowalski, S.; Allard, S.; Scherf, U. *ACS Macro Lett.* **2012**, 465.

(8) Pilgram, K.; Zupan, M.; Skiles, R. *J. Heterocycl. Chem.* **1970**, *7*, 629.

(9) Coppo, P.; Cupertino, D. C.; Yeates, S. G.; Turner, M. L. *Macromolecules* **2003**, *36*, 2705.

(10) (a) Gronowitz, S. E., B.; : *Arkiv för kemi* **1963**, *21*, 335; (b) Gronowitz, S. S., J.E.; Erikksson, B.; *Arkiv för kemi* **1967**, *28*, 99.

(11) (a) Wynberg, H.; Kraak, A. *J. Org. Chem.* **1964**, *29*, 2455; (b) Kraak, A.; Wiersema, A. K.; Jordens, P.; Wynberg, H. *Tetrahedron* **1968**, *24*, 3381.

(12) (a) Lucas, P.; Mehdi, N. E.; Ho, H. A.; Bélanger, D.; Breau, L. *Synthesis* **2000**, *2000*, 1253; (b) Brzeziński, J. Z.; Reynolds, J. R. *Synthesis* **2002**, *2002*, 1053.

(13) Van Mierloo, S.; Adriaensens, P. J.; Maes, W.; Lutsen, L.; Cleij, T. J.; Botek, E.; Champagne, B. t.; Vanderzande, D. J. *J. Org. Chem.* **2010**, *75*, 7202.

(14) Coffin, R. C.; Peet, J.; Rogers, J.; Bazan, G. C. *Nat. Chem.* **2009**, *1*, 657.

(15) Wasserman, H. H.; Ives, J. L. *Tetrahedron* **1981**, *37*, 1825.

(16) Caronna, T.; Forte, M.; Catellani, M.; Meille, S. V. *Chem. Mater.* **1997**, *9*, 991.

(17) Gronowitz, S. B., G.L.; *Acta Chem. Scand.* **1965**, *19*, 1180.

(18) Lin, L. T.; Hart, H. *J. Org. Chem.* **1982**, *47*, 3570.

(19) Chang, M.-Y.; Lin, C.-H. *J. Chin. Chem. Soc.* **2011**, *58*, 853.

(20) (a) Chonan, T.; Takahashi, K. *Bull. Chem. Soc. Jpn.* **2004**, *77*, 1487; (b) Cai, N.; Moon, S.-J.; Cevey-Ha, L.; Moehl, T.; Humphry-Baker, R.; Wang, P.; Zakeeruddin, S. M.; Grätzel, M. *Nano Lett.* **2011**, *11*, 1452; (c) Xu, D.; Wang, S.; Shen, Z.; Xia, C.; Sun, W. *Org. Biomol. Chem.* **2012**, *10*, 2730.

(21) (a) Agostinelli, T.; Caironi, M.; Natali, D.; Sampietro, M.; Dassa, G.; Canesi, E. V.; Bertarelli, C.; Zerbi, G.; Cabanillas-Gonzalez, J.; De Silvestri, S.; Lanzani, G. *J. Appl. Phys.* **2008**, *104*, 114508; (b) Di Motta, S.; Negri, F.; Fazzi, D.; Castiglioni, C.; Canesi, E. V. *J. Phys. Chem. Lett.* **2010**, *1*, 3334.

(22) Diliën, H.; Marin, L.; Botek, E.; Champagne, B.; Lemaur, V.; Beljonne, D.; Lazzaroni, R.; Cleij, T. J.; Maes, W.; Lutsen, L.; Vanderzande, D.; Adriaensens, P. J. *J. Phys. Chem. B* **2011**, *115*, 12040.

(23) Frenklach, M.; Clary, D. *Ind. Eng. Chem. Fundam.* **1983**, *22*, 433.

(24) Corey, E. J.; Ishiguro, M. *Tetrahedron Lett.* **1979**, *20*, 2745.

(25) Frisch, M. J. T., G. W.; Schlegel, H. B.; Scuseria, G. E.; Robb, M. A.; Cheeseman, J. R.; Scalmani, G.; Barone, V.; Mennucci, B.; Petersson, G. A.; Nakatsuji, H.; Caricato, M.; Li, X.; Hratchian, H. P.; Izmaylov, A. F.; Bloino, J.; Zheng, G.; Sonnenberg, J. L.; Hada, M.; Ehara, M.; Toyota, K.; Fukuda, R.; Hasegawa, J.; Ishida, M.; Nakajima, T.; Honda, Y.; Kitao, O.; Nakai, H.; Vreven,

T.; Montgomery, Jr., J. A.; Peralta, J. E.; Ogliaro, F.; Bearpark, M.; Heyd, J. J.; Brothers, E.; Kudin, K. N.; Staroverov, V. N.; Kobayashi, R.; Normand, J.; Raghavachari, K.; Rendell, A.; Burant, J. C.; Iyengar, S. S.; Tomasi, J.; Cossi, M.; Rega, N.; Millam, N. J.; Klene, M.; Knox, J. E.; Cross, J. B.; Bakken, V.; Adamo, C.; Jaramillo, J.; Gomperts, R.; Stratmann, R. E.; Yazyev, O.; Austin, A. J.; Cammi, R.; Pomelli, C.; Ochterski, J. W.; Martin, R. L.; Morokuma, K.; Zakrzewski, V. G.; Voth, G. A.; Salvador, P.; Dannenberg, J. J.; Dapprich, S.; Daniels, A. D.; Farkas, Ö.; Foresman, J. B.; Ortiz, J. V.; Cioslowski, J.; Fox, D. J.; Wallingford CT, Gaussian 09, Revision A.1, 2009.

Chapter 3

Trivalent Phosphorus Reagent Induced Pinacol Rearrangement of 4*H*-Cyclopenta[2,1-*b*:3,4-*b*′]-dithiophen-4-one

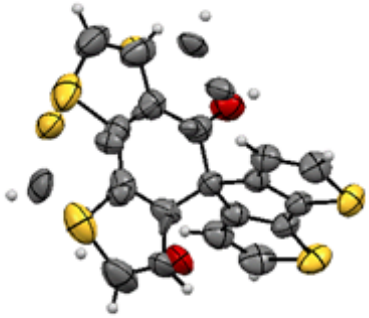

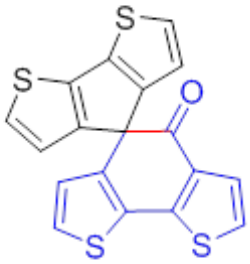

3.1. Introduction

Low band gap (co)polymers have recently received considerable attention in the field of organic light harvesting materials.[1] The alternation of electron rich and electron poor units along the backbone increases the conjugation length, lowers the band gap of the materials (generally below 1.6 eV), and therefore allows a better matching between the available and the absorbed photon flux. 4*H*-Cyclopenta[2,1-*b*:3,4-*b'*]dithiophen-4-one (**8**) (*vide infra*) is a key intermediate used in the synthesis of various cyclopentadithiophene-based (CPDT) light harvesting materials, ranging from small molecules (typically used in dye sensitized solar cells)[2] to conjugated low band gap polymers (used in bulk heterojunction organic solar cells).[3] The presence of the keto function on the bridging carbon atom allows to perform a broad variety of transformations, such as reductions,[4] Knoevenagel condensations,[5] and homo-couplings.[6] The reductive coupling of aromatic monoketones, *e.g.* cyclopentadithiophenones (CPDT-ones) and 9-fluorenone, has been widely studied.[7] The corresponding 1,2-diols can undergo chemical and/or photochemical pinacol-type rearrangements in the presence of Brønsted acids and/or UV-irradiation, respectively.[8] The formation of a variety of mixed heterocyclic fulvalenes using different CDPT-ones and/or fluorenone has been reported by Wynberg *et al*.[9]

In this paper we report on the reactions of 4*H*-cyclopenta[2,1-*b*:3,4-*b'*]dithiophen-4-one with various trivalent phosphorus derivatives, with an emphasis on the final reaction products depending on the applied reagents.

3.2. Results and Discussion

3.2.1. Synthetic Exploration

The acid induced pinacol rearrangement of 7,7'-dihydroxy-7,7'-bi(7*H*-cyclopenta[1,2-*c*:3,4-*c'*]dithiophene) (**2**),[10] obtained after reductive coupling of 7*H*-cyclopenta[1,2-*c*:3,4-*c'*]dithiophen-7-one (**1**), has been reported to occur via a carbinol intermediate **3** which, upon deprotonation, leads to the formation of the corresponding pinacolone **4**, *i.e.* spiro-7'*H*-cyclopenta[1,2-*c*:3,4-*c'*]dithiophene-7',8-7*H*,8*H*-cyclohexa[3,4-*a*:3,4-*c*]dithiophene-7-one (Scheme 3.1).[7a] On the other hand, UV-irradiation of 9,9'-bifluorene-9,9'-diol (**5**) in neutral solutions led to the formation of 9-fluorenone (**6**) and the corresponding pinacolone **7** in ratios varying from 8.6:1 to 2:1, respectively,

depending on the nature of the solvent (Scheme 3.2).[11] The pinacolone is generated by C-O bond heterolysis of the diol, which subsequently undergoes rearrangement and deprotonation. The same rearrangement product could also be synthesized in one step, starting from 9-fluorenone and triethyl phosphite.[12]

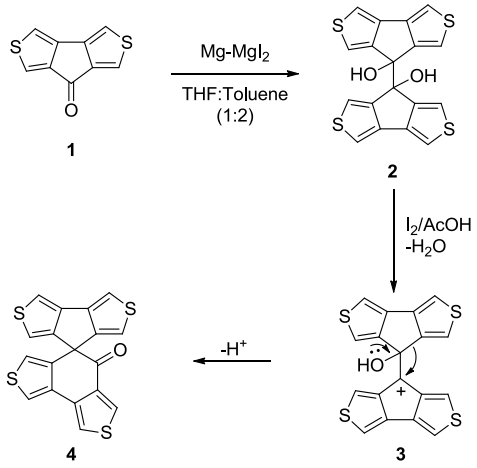

Scheme 3.1. Acid induced pinacol rearrangement of 7*H*-cyclopenta[1,2-*c*:3,4-*c'*]dithiophen-7-one (**1**).

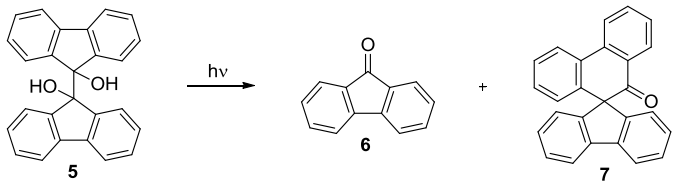

Scheme 3.2. Photochemical pinacol rearrangement of 9,9'-bifluorene-9,9'-diol (**5**).

As we have been exploring novel synthetic pathways toward asymmetrically substituted cyclopentadithiophenes,[13] and their integration in low band gap copolymers for organic photovoltaics,[14] we have exploited the reactivity of 4*H*-cyclopenta[2,1-*b*:3,4-*b'*]dithiophen-4-one (**8**) in similar rearrangement protocols. Reaction of CPDT-one **8** with two equivalents of triethyl phosphite in refluxing *o*-xylene afforded a novel product, tentatively assigned as pinacolone **11** (Scheme 3.3 and *vide infra*), in 61% yield, together with triethyl phosphate and very low amounts of starting material. The formation of such a pinacol rearrangement product under similar conditions has, to the best of our knowledge, not yet been reported in the CPDT series, but has been observed

for fluorenone. The latter affords the corresponding pinacolone upon reaction with either triethyl phosphite[12,15] or tri(isopropyl) phosphite[16] in high to moderate yields. Such reactions are known to proceed via a three-step mechanism, which can hence be translated to the CPDT-pinacolone synthesis (Scheme 3.3): i) Attack of the phosphorus atom on the oxygen atom of the cyclic ketone, which results in the formation of a 1:1 dipolar adduct, an intramolecular phosphonium salt in which the negative charge is stabilized by delocalization, here in cyclopentadienide **9**. ii) The reaction of adduct **9** with another equivalent of CPDT-one **8**, leading to the formation of the 2:1 adduct **10** in which a pentacovalent oxyphosphorane is generated. iii) Thermal decomposition of **10** into spiro compound **11** (the pinacol rearrangement product) and triethyl phosphate, a reaction for which the expulsion of the pentacovalent phosphate ester is the driving force.[17]

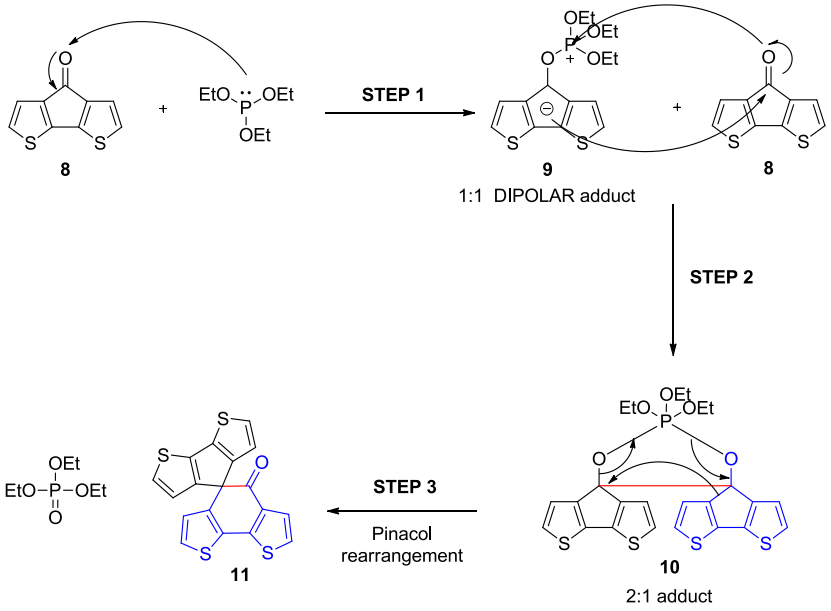

Scheme 3.3. Proposed reaction mechanism for the synthesis of pinacolone **11**.

The proposed spiro structure of the isolated product **11** was confirmed by IR, GC-MS and NMR analysis. The carbonyl function was readily identified in the IR spectrum, which showed a characteristic C=O stretching band at 1664 cm^{-1}. GC-MS analysis provided the molecular mass of the product (*m/z* = 368) and further indicated CO loss.

^{1}H NMR analysis showed the presence of eight aromatic protons, the lowest field one located at 7.43 ppm being assigned to the proton situated at the β-position of the carbonyl function (*vide infra* Section 3.2.2).

Under similar conditions, application of triphenylphosphine or tricyclohexylphosphine in refluxing *o*-xylene afforded, even after three days, only the unreacted CPDT-one **8**. This result is in agreement with the findings of Borowitz *et al.*,[12] who also mentioned a lack of reactivity between 9-fluorenone and the above mentioned phosphines. On the other hand, the more nucleophilic tri(*n*-butyl)phosphine exclusively afforded, upon reaction with fluorenone, the bicyclopentadienylene derivative. In this case, the 2:1 adduct did not undergo pinacol rearrangement, but reacted further with another molecule of phosphine leading to the formation of a so called "open" dipolar phosphorane, which then rearranged to the corresponding bicyclidene. Surprisingly, the reaction of CPDT-one **8** with a large excess of tri(*n*-butyl)phosphine led, after three days of reflux, also to the formation of pinacolone **11** (Scheme 3.4). This suggests that phosphorane **12**, incorporating the tri(*n*-butyl)phosphine moiety, exists majorly/exclusively in its cyclic form and does not open and subsequently convert to bis-CPDT adduct **15** (Scheme 3.4). The latter has previously been obtained starting from **8** using a small excess of Lawesson's reagent.[18]

3.2.2. NMR Characterization

A series of NMR experiments such as APT (Attached Proton Test), short-range/long-range HETCOR, and selective proton irradiation was performed, allowing complete chemical shift assignment of the ^{13}C and ^{1}H resonances of pinacolone **11**. Such detailed chemical shift information can - besides providing strong structural proof - also be useful for implementation in NMR chemical shift prediction software. Figure 3.1 provides an arbitrary numbering scheme for the carbon and hydrogen atoms of 5*H*-spiro(benzo[1,2-*b*:6,5-*b'*]dithiophene-4,4'-cyclopenta[2,1-*b*:3,4-*b'*]dithiophen)-5-one (**11**), together with its optimized structure viewed along the CPDT plane and along the benzodithiophene plane, respectively.

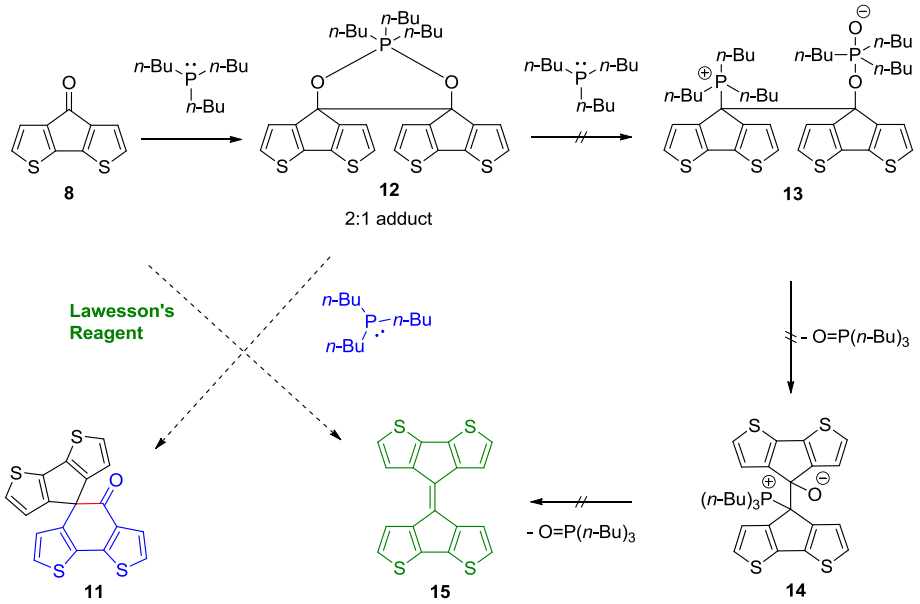

Scheme 3.4. Reaction of CPDT-one **8** with tri(*n*-butyl)phosphine.

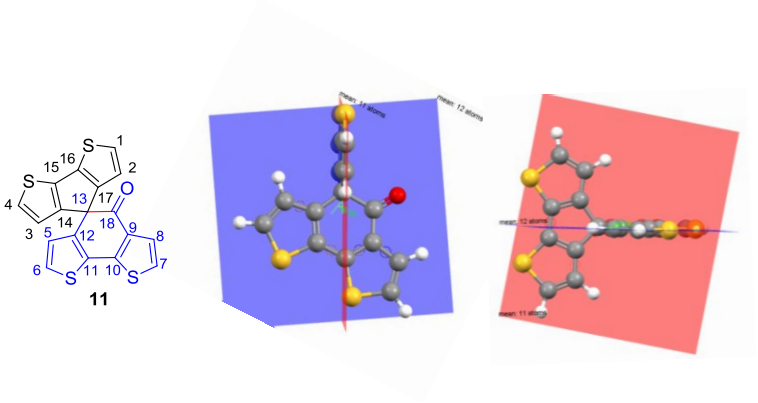

Figure 3.1. Arbitrary numbering of the carbon and hydrogen atoms (left) and optimized structure of pinacolone **11** along the 4,4'-cyclopenta[2,1-*b*:3,4-*b'*]dithiophene plane (center) and along the 5*H*-spiro(benzo[1,2-*b*:6,5-*b'*]dithiophene)-5-one plane (right).

As an additional tool for the NMR structural elucidation, chemical shift calculations were performed and the theoretical values were compared to the experimental ones. The APT spectrum confirmed the presence of the carbonyl group of pinacolone **11** (δ = 190.1 ppm), together with the quaternary aliphatic carbon atom at the spiro position (δ = 63.9 ppm). This pulse sequence also revealed the presence of eight protonated and eight non-protonated aromatic carbon atoms of the thiophene rings. HETCOR

experiments (HETeronuclear CORrelation) allowed us to determine the direct and long-range ^{1}H -^{13}C connectivities. As can be seen in the long-range HETCOR spectrum (Figure 3.2), the proton situated in β-position with respect to the carbonyl function couples to the carbonyl ^{13}C signal, the value of the coupling constant being $^{3}J_{C\text{-}H}$ = 2.0 Hz. An overview of the experimental and theoretical proton and carbon chemical shift assignments of derivative **11** is presented in Table 3.1 and 3.2, respectively. The optimized geometry of pinacolone **11** (Figure 3.1) shows that the CPDT core is almost perpendicular to the benzodithiophenone core, the dihedral angle between the planes being 89°. Having this in mind and looking at the ^{13}C spectrum, it can be expected that the chemical environment of the quaternary carbon atoms of the pairs C15/C16 and C14/C17 of the CPDT core is identical. The same holds for the protonated carbon atoms of the pairs C1/C4 and C2/C3 of the CPDT core. The carbon atoms of these pairs will therefore have the same chemical shifts and will integrate for a double intensity. From the APT experiment it appears that the signals at 190.1, 152.5, 147.9, 141.3, 140.3, 133.6, 129.0 and 63.9 ppm arise from the 10 quaternary carbons, of which the 190.1 and 63.9 ppm signals belong to the carbonyl group and the "spiro" carbon atom, respectively, and the signals at 152.5 and 140.3 ppm have a double intensity. The signals at 127.4, 127.2, 127.0, 126.4, 123.2 and 121.9 ppm arise from the 6 protonated carbons, those at 127.0 and 121.9 ppm having a double intensity.

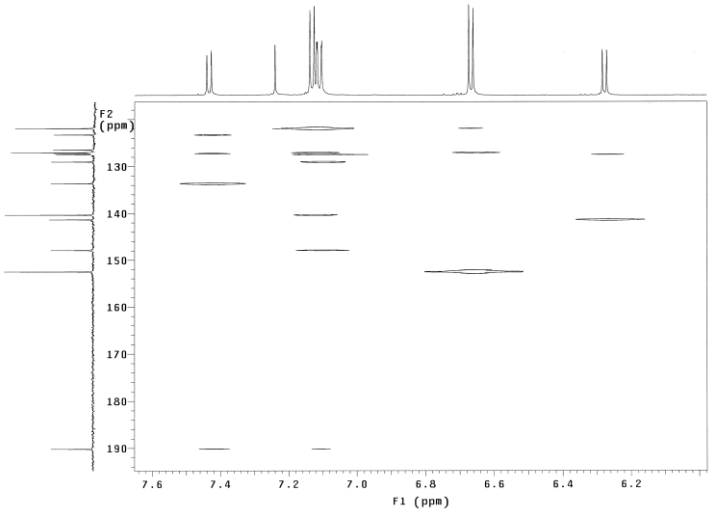

Figure 3.2. Long-range HETCOR spectrum of pinacolone **11**.

The ^{1}H spectrum shows four doublets at 7.43 (1H), 7.11 (1H), 7.10 (1H) and 6.27 (1H) ppm, all with a vicinal ^{3}J-coupling constant of 5.2 Hz, next to two doublets at 7.13 (2H) and 6.66 (2H) ppm, both with a vicinal ^{3}J -coupling constant of 5.0 Hz. It is clear that the four 1H-doublets arise from the benzodithiophenone core protons H5-H8, while the two 2H-doublets belong to the CPDT core protons H1-H4. While the H2/H3 protons are located directly in the shielding zone of the benzodithiophenone structure, the H1/H4 protons appear further away from it and moreover are situated in α-position of the electron-withdrawing sulfur atom (deshielding). Based on these arguments, the H1/H4 protons can be assigned to the doublet at 7.13 ppm and the H2/H3 protons to the doublet at 6.66 ppm. By analogy, the H6 and H7 protons in α-position of the sulfur atoms can be assigned to the 1H-doublets at 7.10 and 7.11 ppm (*vide infra*). The H5 proton is located directly in the shielding zone of the CPDT ring and its resonance therefore appears more upfield at 6.27 ppm. The H8 proton on the other hand is situated further away from the CPDT ring and in the direct deshielding zone of the carbonyl group, explaining its downfield resonance at 7.43 ppm.

A short-range HETCOR experiment (optimized toward the $^{1}J_{C\text{-}H}$ or direct C-H coupling) then allowed to assign the carbon atoms C1/C4, C2/C3, C5 and C8 to the resonance signals at 127.0, 121.9, 127.4 and 127.2 ppm, respectively. The two remaining protonated carbons, C6 and C7, could be assigned to the signals at 126.4 and 123.2 ppm based on a long-range HETCOR experiment. Figure 3.2 shows clear correlations between the carbon signal at 123.2 ppm and H8 (7.43 ppm) and between the carbon signal at 126.4 ppm and H5 (6.27 ppm). Since C6(C7) cannot couple to H8(H5), these correlations allowed the assignment of C6 and C7. Close inspection of the short-range HETCOR spectrum then allowed the assignment of H6 and H7 to the proton resonances at 7.10 and 7.11 ppm, respectively.

This leaves the eight quaternary carbons to be assigned to the carbon signals at 152.5 (2C), 147.9, 141.3, 140.3 (2C), 133.6 and 129.0 ppm via the long-range HETCOR spectrum. Figure 3.2 shows a strong $^{3}J_{C\text{-}H}$ coupling (2.0 Hz) between the carbonyl carbon (190.1 ppm) and H8 (7.43 ppm), next to a weaker $^{4}J_{C\text{-}H}$ coupling with H7 (7.11 ppm), confirming the assignment of H8 and H7 (and C8 and C7 via short-range HETCOR). Starting from H8 and supported by theoretical calculations, C9 could easily be assigned to the carbon signal at 133.6 ppm based on a strong $^{2}J_{C\text{-}H}$ correlation. Analogously, the 141.3 ppm signal showing a strong $^{2}J_{C\text{-}H}$ correlation with H5 at 6.27

ppm can be identified as C12. The carbon resonance at 147.9 ppm correlates to the 7.11 ppm doublet of H7 and very weakly to the 7.43 ppm doublet of H8 (only seen after blowing up the vertical scale), and can therefore be assigned as C10. On the other hand, the 129.0 ppm carbon signal correlates to H6 at 7.10 ppm and very weakly (only seen after blowing up the vertical scale) to H5 at 6.27 ppm, and therefore can be assigned to C11. Due to the anisotropy of the CPDT ring, its four quaternary carbon atom resonances appear as two distinctive double intensity signals located at 152.5 and 140.3 ppm, respectively. The peak located at 152.5 ppm strongly correlates ($^{2}J_{C\text{-}H}$ - two bonds away from each other) with the 6.66 ppm 2H-doublet (H2 and H3) and can be assigned to C14 and C17. The peak located at 140.3 ppm correlates ($^{3}J_{C\text{-}H}$ - three bonds away from each other) with the 7.13 ppm 2H-doublet (H1 and H4) and can be assigned to C15 and C16.

Table 3.1. Overview of the experimental and theoretical carbon signal assignments.

Carbon atom	Experimental	Calculated	Corrected	
	Chemical Shift	Chemical Shift	Linear regression[a]	α/β Linear regression[b]
	δ (ppm)	δ (ppm)	δ (ppm)	δ (ppm)
C1	127.0	135.9	128.1	125.5
C2	121.9	125.5	118.0	123.2
C3	121.9	125.8	118.4	123.5
C4	127.0	135.6	127.7	125.2
C5	127.4	132.1	124.4	128.3
C6	126.4	136.6	128.7	126.0
C7	123.2	131.7	124.0	122.0
C8	127.2	130.8	123.1	127.3
C9	133.6	139.1	131.1	133.6
C10	147.9	162.0	153.2	146.6
C11	129.0	140.6	132.6	129.3
C12	141.3	149.9	141.5	141.8
C13	63.9	69.1	63.8	
C14	152.5	161.7	152.9	150.8
C15	140.3	152.6,	144.1	139.0
C16	140.3	152.0	143.6	138.5
C17	152.5	161.2	152.3	150.4
C18	190.1	195.8	185.7	

[a] Calculated value corrected with linear regression of y = 0.9618x - 2.6581; [b] Calculated value corrected with α/β linear regression.

Table 3.2. Overview of the experimental and theoretical proton signal assignments.

Hydrogen atom	Experimental		Calculated	Corrected	
	Chemical Shift	Coupling constant	Chemical Shift	Linear regression[a]	α/β Linear regression[b]
	δ (ppm)	(*J* = Hz)	δ (ppm)	δ (ppm)	δ (ppm)
H1	7.13 (d)	5.0	7.44	7.10	7.15
H2	6.66 (d)	5.0	6.76	6.59	6.51
H3	6.66 (d)	5.0	6.77	6.59	6.51
H4	7.13(d)	5.0	7.43	7.10	7.15
H5	6.27 (d)	5.2	6.31	6.19	6.08
H6	7.10 (d)	5.2	7.34	7.02	7.06
H7	7.11 (d)	5.2	7.31	6.99	7.02
H8	7.43 (d)	5.2	7.56	7.29	7.26

[a] Calculated value corrected with linear regression of y = 0.9451x + 0.1186; [b] Calculated value corrected with α/β linear regression.

3.2.3. Single-Crystal X-Ray Diffraction

Final unambiguous structural proof was provided by single-crystal X-ray diffraction, showing the two fused heterocycles in an almost perpendicular conformation (Figure 3.3).

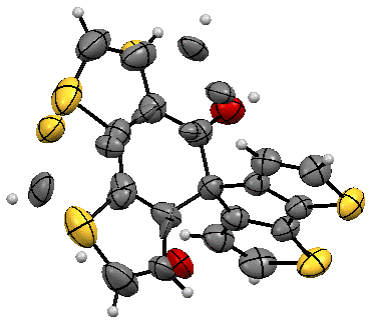

Figure 3.3. X-ray crystal structure of 5*H*-spiro(benzo[1,2-*b*:6,5-*b'*]dithiophene-4,4'-cyclopenta[2,1-*b*:3,4-*b'*]dithiophen)-5-one (**11**).

3.3. Conclusions

In this paper we have reported on the reaction of 4*H*-cyclopenta[2,1-*b*:3,4-*b'*]dithiophen-4-one (**8**) with trivalent organophosphorus reagents. The results have shown that such a protocol leads to the formations of pinacolone **11** when triethyl phosphite is applied, whereas no reactivity is observed with triphenylphosphine. To the best of our knowledge, this is the first time that a one-step synthesis of this kind of CPDT pinacol rearrangement products is reported. Unlike in the fluorenone case, the use of the more nucleophilic tri(*n*-butyl)phosphine does not lead to the formation of a bicyclidene, but affords the same pinacol rearrangement product. Thorough NMR characterization allowed full ^{1}H and ^{13}C chemical shift assignment of the CPDT-pinacolone product, providing further support for the structure assignment. Theoretical chemical shift calculations were in good agreement with the experimentally observed values. A single-crystal X-ray structure of the pinacolone was obtained as well, with a solid-state conformation matching closely to the calculated optimum structure.

3.4. Experimental Section

Materials and Methods

NMR chemical shifts (δ, in ppm) were determined relative to the residual $CHCl_3$ absorption (7.24 ppm) or the ^{13}C resonance shift of $CDCl_3$ (77.70 ppm). Gas chromatography-mass spectrometry (GC-MS) analyses were carried out applying Chrompack Cpsil5CB or Cpsil8CB capillary columns. Solution UV-Vis absorption measurements were performed with a scan rate of 600 nm min^{-1} in a continuous run from 800 to 200 nm. Infrared spectra were collected with a resolution of 4 cm^{-1} (16 scans) using films drop-cast on a NaCl disk from a $CHCl_3$ solution. Unless stated otherwise, all reagents and chemicals were obtained from commercial sources and used without further purification.

Synthesis

Pinacolone **11** (5*H*-spiro(benzo[1,2-*b*:6,5-*b'*]dithiophene-4,4'-cyclopenta[2,1-*b*:3,4-*b'*]dithiophen)-5-one) was synthesized following two standard procedures.

a. Procedure using triethyl phosphite: 4*H*-Cyclopenta[2,1-*b*:3,4-*b'*]dithiophen-4-one (**8**) (48 mg, 0.249 mmol) was dissolved in *o*-xylene (5 mL), to which triethyl phosphite

(0.085 mL, 0.498 mmol) was added, and the mixture was allowed to react at 150 °C for 3 days. Removal of the solvent under reduced pressure afforded a pale-yellow solid. Purification of the crude product by means of column chromatography (silica, eluent 20% CH_2Cl_2 in hexane) afforded pinacolone **11** as a yellowish solid (28 mg, 0.076 mmol, 61%). mp 184.6-185.0 °C

b. Procedure using tri(*n*-butyl)phosphine: 4*H*-Cyclopenta[2,1-*b*:3,4-*b'*]dithiophen-4-one (**8**) (100 mg, 0.520 mmol) was dissolved in a large excess of tri(*n*-butyl)phosphine (2.5 mL) and the mixture was allowed to react at 160 °C for 3 days. The excess of tri(*n*-butyl)phosphine was removed by Kugelrohr distillation (120 °C, 1.2 10^{-1} mbar) affording a pale-yellow solid. Purification of the crude product by means of column chromatography (silica, eluent 20% CH_2Cl_2 in hexane) afforded pinacolone **11** as a yellowish solid (40 mg, 0.108 mmol, 42%). GC-MS (EI) *m/z* 368 [M^+], 339 [M^+-CO]; HRMS (EI) calcd for $C_{18}H_8OS_4$ 367.9458, found *m/z* 367.9457; ^{1}H NMR (400 MHz, $CDCl_3$) δ 7.43 (d, *J* = 5.2 Hz, 1H), 7.14-7.10 (dd, *J* = 5.0/5.2 Hz, 4H), 6.66 (d, *J* = 5.0 Hz, 2H), 6.27 (d, *J* = 5.2 Hz, 1H); ^{13}C NMR (75 MHz, $CDCl_3$) δ 190.1 (C=O), 152.5, 147.9, 141.3, 140.3, 133.6, 129.0, 127.4 (CH), 127.2 (CH), 127.0 (2xCH), 126.4 (CH), 123.2 (CH), 121.9 (2xCH), 63.9; IR (NaCl, cm^{-1}) ν_{max} 3103/3007 (w, unsaturated C-H), 1664 (s, C=O); UV-vis ($CHCl_3$, nm) λ_{max} (log ε) 257 (3.908), 323 (3.653), 368 (3.334).

NMR Characterization

All ^{1}H and ^{13}C liquid-state NMR experiments were performed at room temperature on a Varian Inova 300 or 400 spectrometer in a 5 mm four-nucleus PFG probe. The chemical shift scales were calibrated to $CDCl_3$: ^{1}H = 7.24 ppm and ^{13}C = 77.70 ppm. The proton spectra were acquired with a 90° pulse of 4.3 μs, a spectral width of 4500 Hz, an acquisition time of 3.5 s, a preparation delay of 8 s and 20 accumulations, processed with a line broadening of 0.2 Hz. The carbon spectra were acquired with a 90° pulse of 12 μs, a spectral width of 16500 Hz, an acquisition time of 0.8 s, a preparation delay of 60 s and 2500 accumulations, processed with a line broadening of 3 Hz. The long-range HETCOR experiment was optimized for *J* = 4 Hz.

Details on the Computational Procedures

The ground state geometries were optimized at the density functional theory (DFT) level of approximation by employing the B3LYP exchange-correlation (XC) functional and the 6-31G* basis set. The chemical shifts (δ) of all systems were calculated as the difference of isotropic shielding constants (σ) with respect to TMS. All σ values were obtained with the B3LYP XC functional and the 6-311+G(2d,p) basis set together with the GIAO method to ensure origin-independence, following the approach that was employed and tested recently for PVC oligomers, fluoroionophores, and poly(thienylene vinylene) (PTV) model compounds.[19] As shown in these previous studies, linear fits between experimental and theoretical δ values of representative model compounds can facilitate the interpretation of the NMR spectra of more complex and larger compounds and can therefore provide a way of correcting the calculated properties from systematic errors. Preliminary investigations on PTV model compounds have been reported before,[19] and the theoretically estimated δ values were obtained from the calculated values using the following relationships (in ppm):

sp^2 in α	^{13}C: δ(estimated) = 0.8099 δ[IEF-PCM/B3LYP/6-311+G(2d,p)] + 15.39	(1a)
	^{1}H: δ(estimated) = 0.8653 δ[IEF-PCM/B3LYP/6-311+G(2d,p)] + 0.67	(1b)
sp^2 in β	^{13}C: δ(estimated) = 0.7618 δ[IEF-PCM/B3LYP/6-311+G(2d,p)] + 27.61	(2a)
	^{1}H: δ(estimated) = 0.8845 δ[IEF-PCM/B3LYP/6-311+G(2d,p)] + 0.61	(2b)
other sp^2	^{13}C: δ(estimated) = 0.6510 δ[IEF-PCM/B3LYP/6-311+G(2d,p)] + 40.36	(3a)
	^{1}H: δ(estimated) = 0.8911 δ[IEF-PCM/B3LYP/6-311+G(2d,p)] + 0.52	(3b)
other atoms	^{13}C: δ(estimated) = 0.9618 δ[IEF-PCM/B3LYP/6-311+G(2d,p)] - 2.66	(4a)
	^{1}H: δ(estimated) = 0.9451 δ[IEF-PCM/B3LYP/6-311+G(2d,p)] + 0.12	(4b)

All the theoretical chemical shifts reported in this paper have been corrected by one of the linear regression equations. Solvent (here $CHCl_3$) effects were taken into account

within the integral equation formalism of the polarizable continuum model (IEF-PCM)[20] for the calculations of the isotropic shielding constants of all compounds (including TMS).

3.5. References

(1) (a) Bundgaard, E.; Krebs, F. C. *Sol. Energy Mater. Sol. Cells* **2007**, *91*, 954; (b) Cheng, Y.-J.; Yang, S.-H.; Hsu, C.-S. *Chem. Rev.* **2009**, *109*, 5868; (c) Po, R.; Maggini, M.; Camaioni, N. *J. Phys. Chem. C* **2009**, *114*, 695; (d) Boudreault, P.-L. T.; Najari, A.; Leclerc, M. *Chem. Mater.* **2010**, *23*, 456; (e) Brabec, C. J.; Gowrisanker, S.; Halls, J. J. M.; Laird, D.; Jia, S.; Williams, S. P. *Adv. Mater.* **2010**, *22*, 3839; (f) Cao, J.; Zhang, W.; Xiao, Z.; Liao, L.; Zhu, W.; Zuo, Q.; Ding, L. *Macromolecules* **2012**, *45*, 1710.

(2) (a) Li, R.; Liu, J.; Cai, N.; Zhang, M.; Wang, P. *J. Phys. Chem. B* **2010**, *114*, 4461; (b) Bendall, J. S.; Etgar, L.; Tan, S. C.; Cai, N.; Wang, P.; Zakeeruddin, S. M.; Gratzel, M.; Welland, M. E. *Energy Environ. Sci.* **2011**, *4*, 2903.

(3) (a) Peet, J.; Kim, J. Y.; Coates, N. E.; Ma, W. L.; Moses, D.; Heeger, A. J.; Bazan, G. C. *Nat. Mater.* **2007**, *6*, 497; (b) Zhang, M.; Tsao, H. N.; Pisula, W.; Yang, C.; Mishra, A. K.; Müllen, K. *J. Am. Chem. Soc.* **2007**, *129*, 3472; (c) Bijleveld, J. C.; Shahid, M.; Gilot, J.; Wienk, M. M.; Janssen, R. A. J. *Adv. Funct. Mater.* **2009**, *19*, 3262; (d) Horie, M.; Majewski, L. A.; Fearn, M. J.; Yu, C.-Y.; Luo, Y.; Song, A.; Saunders, B. R.; Turner, M. L. *J. Mater. Chem.* **2010**, *20*, 4347; (e) Manceau, M.; Bundgaard, E.; Carle, J. E.; Hagemann, O.; Helgesen, M.; Sondergaard, R.; Jorgensen, M.; Krebs, F. C. *J. Mater. Chem.* **2011**, *21*, 4132.

(4) Coppo, P.; Cupertino, D. C.; Yeates, S. G.; Turner, M. L. *Macromolecules* **2003**, *36*, 2705.

(5) Reddy, J. S.; Kale, T.; Balaji, G.; Chandrasekaran, A.; Thayumanavan, S. *J. Phys. Chem. Lett.* **2011**, *2*, 648.

(6) Luo, J.; Huang, K.-W.; Qu, H.; Zhang, X.; Zhu, L.; Chan, H. S. O.; Chi, C. *Org. Lett.* **2010**, *12*, 5660.

(7) (a) Heeres, G. J.; Wynberg, H. *Synth. Commun.* **1972**, *2*, 335; (b) Tanaka, K.; Kishigami, S.; Toda, F. *J. Org. Chem.* **1990**, *55*, 2981.

(8) (a) Berson, J. A. *Angew. Chem. Int. Ed.* **2002**, *41*, 4655; (b) Mladenova, G.; Singh, G.; Acton, A.; Chen, L.; Rinco, O.; Johnston, L. J.; Lee-Ruff, E. *J. Org. Chem.* **2004**, *69*, 2017.

(9) (a) Heeres, G. J.; Wynberg, H. *Tetrahedron* **1972**, *28*, 5237; (b) Adam, M.; Enkelmann, V.; Räder, H.-J.; Röhrich, J.; Müllen, K. *Angew. Chem. Int. Ed.* **1992**,

31, 309; (c) Yamamoto, H. M.; Hagiwara, M.; Kato, R. *Synth. Met.* **2003**, *133–134*, 449.

(10) The naming of compound **2** employed here is taken from reference 7a. The authors assigned the carbonyl as position 7.

(11) Hoang, M.; Gadosy, T.; Ghazi, H.; Hou, D.-F.; Hopkinson, A. C.; Johnston, L. J.; Lee-Ruff, E. *J. Org. Chem.* **1998**, *63*, 7168.

(12) Borowitz, I. J.; Anschel, M. *Tetrahedron Lett.* **1967**, *8*, 1517.

(13) Van Mierloo, S.; Adriaensens, P. J.; Maes, W.; Lutsen, L.; Cleij, T. J.; Botek, E.; Champagne, B. t.; Vanderzande, D. J. *J. Org. Chem.* **2010**, *75*, 7202.

(14) Van Mierloo, S.; Hadipour, A.; Spijkman, M.-J.; Van den Brande, N.; Ruttens, B.; Kesters, J.; D'Haen, J.; Van Assche, G.; de Leeuw, D. M.; Aernouts, T.; Manca, J.; Lutsen, L.; Vanderzande, D. J.; Maes, W. *Chem. Mater.* **2012**, *24*, 587.

(15) Poshkus, A. C.; Herweh, J. E. *J. Org. Chem.* **1964**, *29*, 2567.

(16) Ramirez, F.; Smith, C. P. *Chem. Commun.* **1967**, 662.

(17) Ramirez, F.; Ramanathan, N. *J. Org. Chem.* **1961**, *26*, 3041.

(18) Loganathan, K.; Cammisa, E. G.; Myron, B. D.; Pickup, P. G. *Chem. Mater.* **2003**, *15*, 1918.

(19) (a) d'Antuono, P.; Botek, E.; Champagne, B.; Spassova, M.; Denkova, P. *J. Chem. Phys.* **2006**, *125*, 144309; (b) d'Antuono, P.; Botek, E.; Champagne, B.; Wieme, J.; Reyniers, M.-F.; Marin, G.B.; Adriaensens, P.; Gelan, J.M. *J. Phys. Chem. B* **2008**, *112*, 14804; (c) Botek, E.; d'Antuono, P.; Jacques, A.; Carion, R.; Champagne, B.; Maton, L.; Taziaux, D.; Habib-Jiwan, J.-L. *Phys. Chem. Chem. Phys.* **2010**, *12*, 14172; (d) Diliën, H.; Marin, L.; Botek, E.; Champagne, B.; Lemaur, V.; Beljonne, D.; Lazzaroni, R.; Cleij, T. J.; Maes, W.; Lutsen, L.; Vanderzande, D.; Adriaensens, P. J. *J. Phys. Chem. B* **2011**, *115*, 12040.

(20) (a) Tomasi, J.; Persico, M. *Chem. Rev.* **1994**, *94*, 2027; (b) Tomasi, J.; Mennucci, B.; Cammi, R. *Chem. Rev.* **2005**, *105*, 2999.

Chapter 4

Thermally Induced Degradation of PCPDTBT Low Band Gap Polymers

4.1. Introduction

Organic photovoltaics (OPVs) have the potential of becoming a strong renewable energy market technology if the requirements of the "critical triangle for photovoltaics", *i.e.* (low) cost, (high) efficiency, and (prolonged) lifetime, are simultaneously fulfilled.[1] The low production costs (due to solution processability) and low amounts of organic semiconductors needed (due to their high extinction coefficients) in the fabrication of OPVs by roll to roll (R2R) printing make these materials cheap and viable alternatives for their inorganic counterparts.[2] With certified efficiencies having surpassed the 10% threshold for single module as well as for tandem configurations, and considering their almost exponential evolution over the last decade, the efficiency requirement of OPVs can also honorably be fulfilled.[3] The last and most difficult requirement is the stability of the devices. Photovoltaic (PV) modules, being continuously exposed to external stress factors such as light, heat and humidity, require efficient encapsulation, a barrier that prevents oxygen and humidity to penetrate in the device, and light harvesting materials that are stable under severe photo-thermal conditions.[4,5]

One of the most powerful and most widely applied material combinations within the OPV field is the bulk heterojunction (BHJ) active layer blend composed of a conjugated (low band gap) polymer donor material and a fullerene acceptor.[6] The introduction of solubilizing (alkyl) side chains is mandatory to obtain conjugated polymers that can be processed from solution. In terms of stability, these functionalities are, however, regarded as the Achilles heel of a polymer. It has been proven that under accelerated (artificial) aging conditions the semiconducting polymers start degrading. In a first step, the side chains are oxidatively cleaved off, starting a chain reaction that eventually leads to the degradation of the conjugated backbone. Additionally, defects that are built up during the polymer synthesis and which are, in consequence, present along the conjugated polymer backbone, can considerably speed up the degradation process. This leads to the alteration of the optical and conducting properties of the photoactive materials, and the reduction of the solar cell efficiencies.[7]

The stability of a solar cell being strongly dependent on the integrity of the photoactive material, which depends on a series of external and internal factors, *i.e.* humidity, the presence of oxygen and reactive species generated within the system (*e.g.* free

radicals), it is important to determine the evolution of the system under certain stress conditions, *e.g.* increased temperature, photo- and thermo-oxidation, humidity, or a combination of them. Such elaborate studies have been conducted on poly[2-methoxy-5-(3',7'-dimethyloctyloxy)-1,4-phenylene vinylene] (MDMO-PPV), poly(3-hexylthiophene) (P3HT) and poly(9,9-dialkyl-9*H*-fluorene) (PF) derivatives.[7b,7d,8] Under induced stress, these polymers were shown to degrade in two stages. In an initial step, degradation or loss of the side chains was observed, followed, in a second step, by degradation of the main polymer backbone. The solubilizing side chains (alkoxy or alkyl) and the exocyclic vinylene bonds (in MDMO-PPV) were proven to be the weakest points of the photoactive materials. The degradation process being very complex, the nature of the side chains, the position of the substituents and the aromatic repeating units playing a key role, a general degradation pathway applicable for all conjugated polymers could not be determined yet and does not seem very plausible.

In PFs for instance, the monoalkylfluorene defect is believed to be responsible for the apparition of a low energy green emission band (the "G-band") due to the formation, upon oxidation, of a keto functionality on the bridging carbon atom of the fluorene unit, *i.e.* 9-fluorenone.[9] The G-band was drastically suppressed in fully alkylated PFs for which the monomer was obtained *via* a cyclization step rather than by alkylation of the 9-position, typically carried out under basic conditions.[10] Nevertheless, the formation of the keto defect was not fully prevented, its apparition being also noticed in ladder type polymers, suggesting a more complex degradation process for this class of materials.[11] The concentrations of the monoalkylfluorene and of the (oxidatively) generated fluorenone did not correlate with the intensity of the G-band, the latter being substantially enhanced in PF films which underwent additional thermal treatment. Ultimately, metal impurities in the polymer (nickel or palladium) can contribute to the oxidation process as well.[8]

In this paper we present a detailed study on the behavior of a series of **PCPDTBT** polymers with different alkyl side chain patterns (Figure 4.1) under induced thermal stress. **P1** and **P1'** bear two branched 2-ethylhexyl side chains, while **P2'** and **P3** are decorated with two linear octyl and dodecyl side chains, respectively. The possible influence of the synthetic route giving access to the alkyl-substituted 4*H*-cyclopenta[2,1-*b*:3,4-*b'*]dithiophene (CPDT) building blocks, as well as the nature of

the side chains, on the thermal stability of the materials are discussed. All polymers were synthesized by palladium catalyzed Suzuki polycondensation reactions. The evolution of the optical properties of thin films prepared from the above mentioned polymers was investigated by UV-Vis spectroscopy. Possible changes in the chemical structures were monitored by IR spectroscopy. The degradation pattern(s) of the polymer side chains and main backbone were investigated by TG-TD-GC/MS.

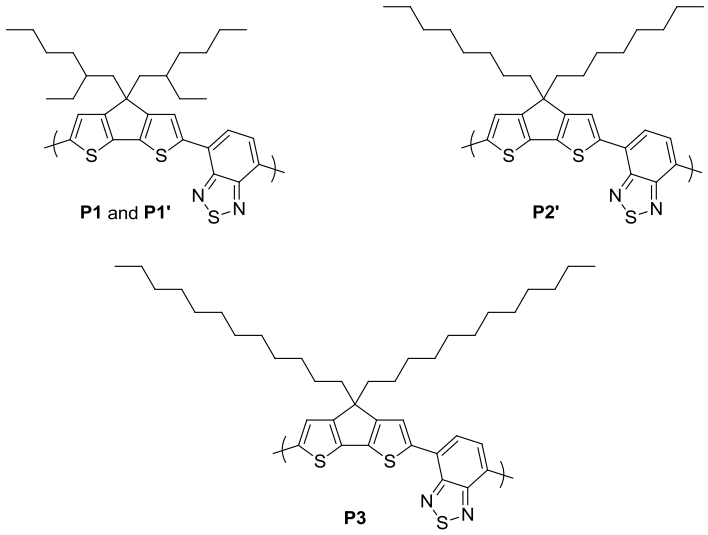

Figure 4.1. Structures of **PCPDTBT**-type polymers **P1**-**P3**.

4.2. Results and Discussion

4.2.1. Synthesis and Characterization of PCPDTBT Polymers P1-P3

The synthesis of the dialkylated CPDT derivatives (**1a-c**) was achieved using two different strategies. Derivatives **1a** and **1c** (Scheme 4.1) were synthesized by the "traditional" route, involving direct alkylation of 4*H*-cyclopenta[2,1-*b*:3,4-*b'*]dithiophene under basic conditions in the presence of 2-ethylhexyl and dodecyl bromide, respectively, followed by bromination with *N*-bromosuccinimide (NBS).[12] Derivatives **1a'** and **1b'** were obtained upon bromination (with NBS) of the CPDT scaffold prepared *via* a three-step synthetic protocol recently developed in our group.[13,14] In the first step, 3-bromo-2,2'-bithiophene was synthesized by Kumada coupling of 2-thienylmagnesium bromide with 2,3-dibromothiophene. Lithiation in position 3, followed by treatment with the corresponding dialkyl ketones afforded

dialkylated tertiary alcohol derivatives. The CPDT scaffold was ultimately obtained by means of Friedel-Crafts dehydration cyclization in sulfuric acid medium. Polymers **P1**-**P3** were then obtained by Suzuki polycondensation of the CPDT derivatives **1a-c** and the commercially available 2,1,3-benzothiadiazole-4,7-bis(boronic acid pinacol ester) (**2**) using a modified literature procedure (Scheme 4.1).[15] End-capping was performed in two stages by addition of phenylboronic acid and bromobenzene, respectively. Regardless of the method by which the CPDT scaffold was prepared, all polymers were considered "defect free" materials (*vide infra*). Polymers **P1** and **P3**, for which the alkyl chains were introduced to the CPDT ring, may possibly contain a very low percentage of monoalkylated CPDTs, which were left undetected (by ^{1}H NMR) during the monomer synthesis and were built-in in the final polymers. Polymers **P1'** and **P2'**, for which the CPDT scaffold was obtained by a final ring closure reaction, are free of any monoalkyl defects. Molecular weights of the polymers were determined by gel permeation chromatography (GPC) analysis in tetrahydrofuran (THF) at 40 ^{o}C for **P1** and **P1'**, and in chlorobenzene (CB) at 80 ^{o}C for **P2'** and **P3** (Table 4.1).

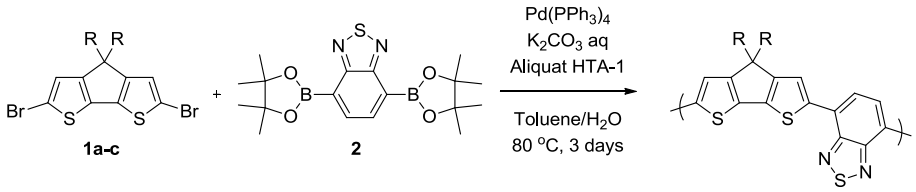

1a and **1a'** R = 2-ethylhexyl
1b' R = octyl
1c R = dodecyl

P1 and **P1'** R = 2-ethylhexyl
P2' R = octyl
P3 R = dodecyl

Scheme 4.1. **PCPDTBT** polymers syntheses *via* Suzuki polycondensation.

Table 4.1. Analytical GPC data of **PCPDTBT** polymers **P1**, **P1'**, **P2'** and **P3**.

Polymer	M_n (g mol^{-1})	M_w (g mol^{-1})	PDI
P1[a]	1.8 x 10^4	3.6 x 10^4	2.0
P1'[a]	1.1 x 10^4	2.3 x 10^4	2.1
P2'[b]	8.3 x 10^3	1.4 x 10^4	1.6
P3[b]	1.6 x 10^4	7.2 x 10^4	4.5

[a] Determined from THF; [b] Determined from CB.

4.2.2. Synthesis of 4-(2-Ethylhexyl)-4*H*-cyclopenta[2,1-*b*:3,4-*b'*]dithiophene

Based on the structural resemblance between fluorene and CPDT, having two aryl rings connected by an sp^3-hybridized carbon bridge, and the similar conditions used to synthesize the dialkylated building blocks (*via* direct alkylation and/or ring closure), one might presume a possible common degradation pathway for these materials, *i.e*. the apparition of the keto defect. To verify this assumption, we have synthesized a monoalkylated CPDT, with the goal to deliberately incorporate this "defect" in the final donor-acceptor **PCPDTBT** polymers (for comparison).

Alkylation of CPDT **3** using 1.1 equivalent of *n*-BuLi and 2-ethylhexylbromide afforded monoalkyl-CPDT derivative **4a** as the major reaction product, together with small amounts of **4b** (Scheme 4.2).[16] Due to the reasonable difference in polarity, derivatives **4a** and **4b** could be separated by means of column chromatography (on silica). It became clear that, in the case of CPDT derivatives, where the mono- and the dialkylated derivatives are perfectly separable, the presence of the monoalkyl defect in the dialkyl-CPDT fraction was rather unlikely. Subsequent bromination of **4a** in the presence of NBS was required before proceeding to the Suzuki polycondensation reaction. The formation of the desired dibrominated product **5a** was confirmed by ^{1}H NMR of the crude reaction mixture. Purification of the latter by means of column chromatography (on silica), using hexane as an eluent led, however, to the exclusive isolation of the corresponding (oxidized) 2,6-dibromo-4-(2-ethylhexylidene)-4*H*-cyclopenta[2,1-*b*:3,4-*b'*]dithiophene (**5b**). The formation of alkylidene derivative **5b** is believed to occur during the purification step and/or during the handling and analysis of the fractions recovered after chromatography.

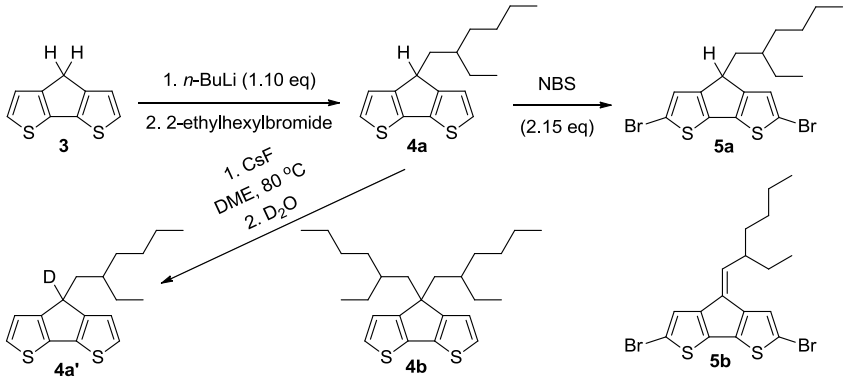

Scheme 4.2. Synthesis of monoalkylated CPDT derivatives **5a** and **5b**.

The relatively unstable nature of products **4a** and **5a**, under basic and/or acidic conditions, could arise from the presence of the labile proton situated on the bridging carbon atom of the CPDT unit. Even under the mildest basic conditions that one could use in the Suzuki polycondensation reaction, *i.e.* CsF (cesium fluoride) in 1,2-dimethoxyethane (DME),[17] the abstraction of the proton in position 4 of the CPDT occurred. Addition of deuterium oxide (D_2O) at the end of the reaction resulted in an exchange of D and H atoms. In ^1H NMR this led to the disappearance of the corresponding signal, located at 3.70 ppm. In consequence, the instability of **4a** and **5a** hampered the synthesis of the corresponding **PCPDTBT**-like polymers, incorporating different percentages (*e.g.* 10% up to 100%) of the monoalkyl defects in the backbone. Nevertheless, these findings pointed out a possible degradation pathway of the monoalkyl-CPDT, leading to the formation of an alkene rather than a keto functionality, the latter being the main identified defect (degradation product) occurring in monoalkylfluorenes.

4.2.3. UV-Vis Spectroscopy Study of PCPDTBT Polymers under Thermal Stress

For semicrystalline polymers such as P3HT, short exposure (in the order of minutes) of polymer films at temperatures between 100 and 150 ^{o}C has proven to be beneficial for the organization of the polymer chains. Annealed films show a higher degree of crystallinity and hence improved conducting (electrical) properties compared to the "as cast" ones.[18] Higher temperatures and/or prolonged exposure times eventually result in the degradation of the material, this process being considerably accelerated in the presence of oxygen and/or humidity. Cleavage of the alkyl side chains accompanied by scission of the polymer backbone results in a loss of conjugation. These structural changes cause an alteration of the chromophore structure which leads to a modification of the absorption spectrum of the photoactive species.[19]

The evolution of the optical properties of thin films prepared by drop casting from a chlorobenzene solution of polymers **P1**-**P3**, exposed to temperatures ranging from 150 up to 230 ^{o}C, in air or under inert atmosphere, was followed by UV-Vis spectroscopy. For polymers **P2'** and **P3**, carrying linear alkyl side chains, an annealing effect was observed at temperatures of 150 ^{o}C (Figure 4.2). The enhancement of the shoulder on the low energy band, located between 800 and 1000 nm, can be attributed to a better organization and interaction between the polymer chains. Under inert atmosphere the chromophore appeared to be stable for up to 1 day under a continuous thermal stress of 150 ^{o}C. In contrast, **P1'**, carrying 2-ethylhexyl branched side chains, showed a lower degree of ordering, marked by the absence of a shoulder on the low energy side of the spectrum. Additionally, annealing at 150 ^{o}C for 1 day led to a small decrease in the low energy absorption band of **P1'**.

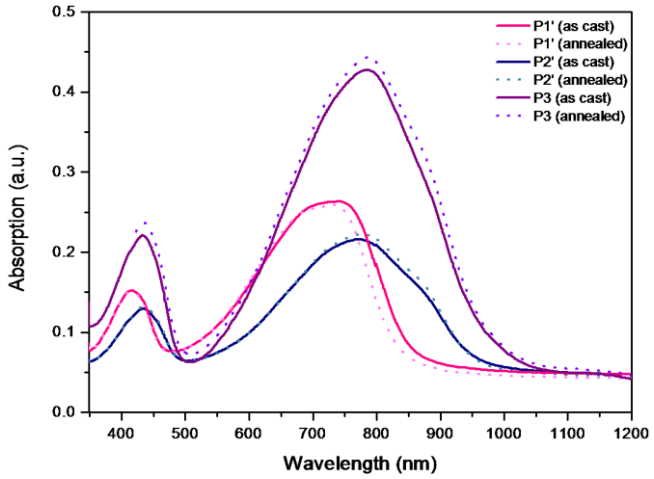

Figure 4.2. UV-Vis spectra (not normalized) of polymer thin films as cast (solid line) and annealed (dotted line) for 1 day at 150 °C.

Annealing at higher temperatures (1 day at 200 °C) had a negative effect on the thin films (Figure 4.3). Most impact was seen for **P1**, which displayed a clear decrease in the intensity of the low energy absorption band, most probably due to an alteration of the chromophore. **P2'** and **P3** showed no or very little degradation, respectively, which suggest superior thermal stability of the polymers bearing linear side chains.

When subjected to repetitive heating-cooling cycles (Figure S4.1), which are very common processes occurring in the lifecycle of solar cells, all polymers seemed to be affected to a much lesser extent than during the isothermal experiments. During the step-heating experiments, temperatures up to 250 °C were reached. These extreme temperatures are far too high compared with the ones reached in a working solar cell under normal conditions. Nevertheless, this series of experiments gives a good indication of the stability of the polymers when exposed to elevated temperatures. As already observed from the isothermal heating experiments, **P1'** was the least stable in the series (Figure 4.4), followed by **P3**, which showed minor changes (Figure 4.6) and **P2'**, for which the heating-cooling cycles actually enhanced the optical properties of the polymer (Figure 4.5).

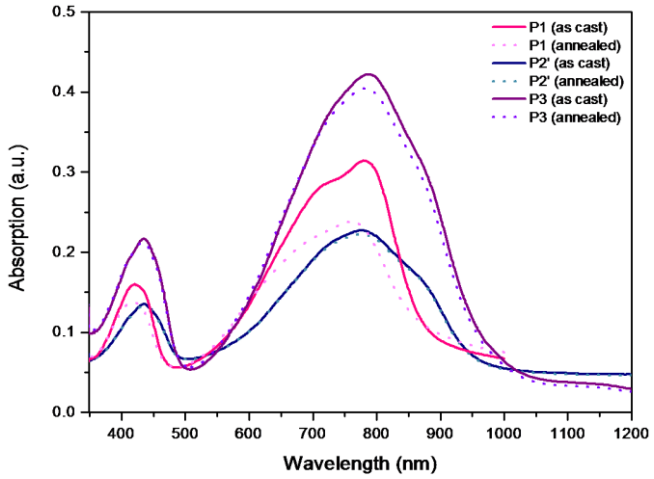

Figure 4.3. UV-Vis spectra (not normalized) of polymer thin films as cast (solid line) and annealed (dotted line) for 1 day at 200 ºC.

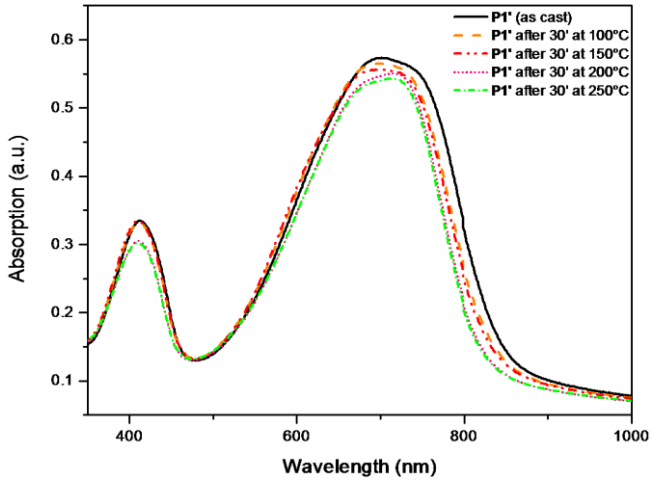

Figure 4.4. UV-Vis spectra (not normalized) of polymer **P1'** for the as cast film and after sequential heating-cooling cycles.

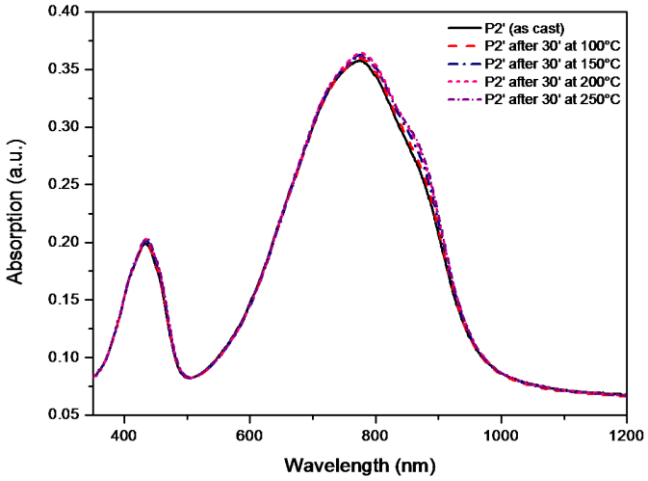

Figure 4.5. UV-Vis spectra (not normalized) of polymer **P2'** for the as cast film and after sequential heating-cooling cycles.

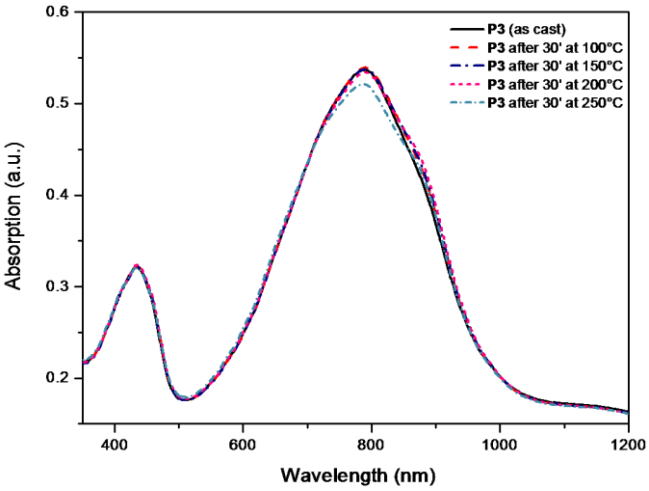

Figure 4.6. UV-Vis spectra (not normalized) of polymer **P3** for the as cast film and after sequential heating-cooling cycles.

4.2.4. IR Spectroscopy Study of PCPDTBT Polymers under Thermal Stress

IR spectroscopy is a powerful technique which enables real-time follow-up of the evolution of the chemical composition and structure of a specific material or compound. In IR, the detection of functional groups, in particular carbon-heteroatom (*e.g.* N or O) bonds, allows a precise identification of these functionalities which give unique and specific fingerprints. The technique can as well be used in the determination

of trace impurities present in a given sample.[20] The general detection limit is about 1% but can go as low as 0.1% in certain cases.[21]

During the step-heating experiment, polymer thin films fabricated from **PCPDTBT** polymers **P1**-**P3**, drop cast from chlorobenzene solutions, were subjected to repetitive heating-cooling cycles (*vide supra*). The evolution of the chemical composition (structural modifications) within these films was monitored by *in situ* IR spectroscopy. Unlike MDMO-PPV, where the phenyl rings are linked by vinylene connectors, **PCPDTBT** polymers are made of alternating electron donor CPDT and electron acceptor BT units, interconnected by C-C single bonds. The only functionalities present along the polymer backbone are the solubilizing alkyl chains. Due to a reduced number of functional groups present in **PCPDTBT**-type materials, polymers **P1**-**P3** will probably give rise to a reduced variety and number of degradation products. Knowing that PFs are characterized by the apparition of a keto defect upon thermal stress and under oxygen/air atmosphere, and having in mind the structural resemblance between fluorene and CPDT derivatives, such defect was expected to occur under the same conditions. Therefore, this series of experiments was conducted by continuously flushing the measurement cell with compressed air.

The results showed very similar behavior for **P1'** (Figure 4.7) and **P2'** (Figure 4.8). In both cases, a reduction of the intensities of the C-H stretching bands located between 2960 and 2850 cm^{-1} was observed (see Table S4.1), in the same temperature interval of 200-225 ^{o}C. These bands were drastically reduced at 225 ^{o}C, their complete disappearance occurring already at 250 ^{o}C.

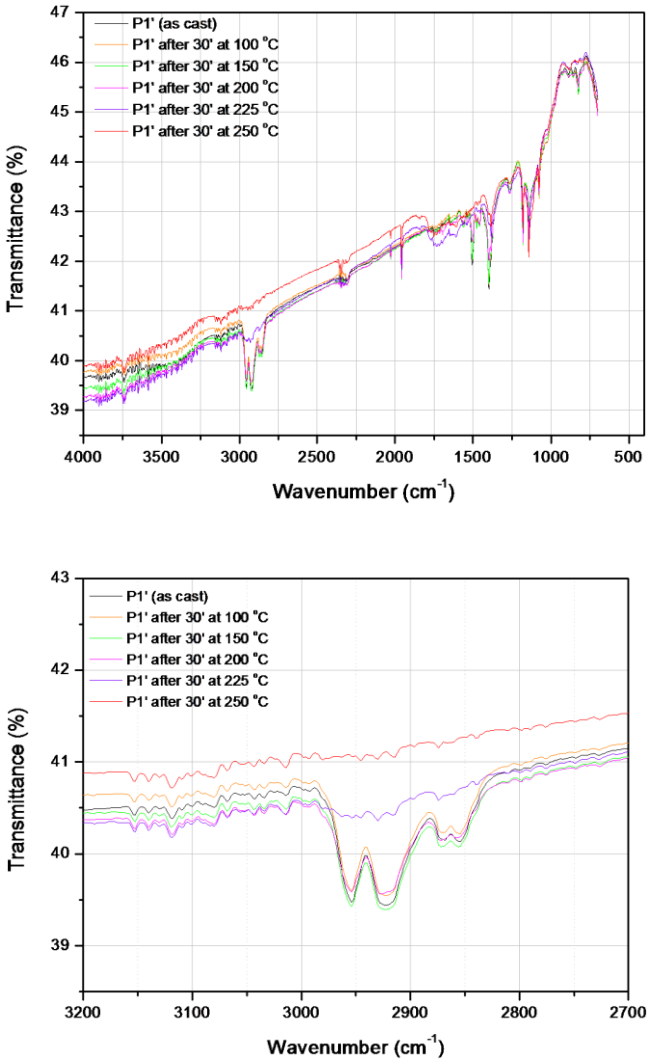

Figure 4.7. IR spectra of polymer **P1'** (top) for the as cast film and after sequential heating-cooling cycles and a zoom of the alkyl C-H stretching region (bottom).

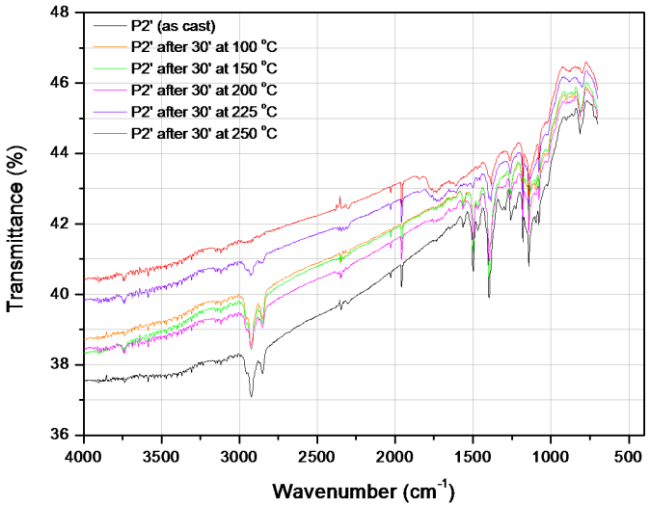

Figure 4.8. IR spectra of polymer **P2'** for the as cast film and after sequential heating-cooling cycles.

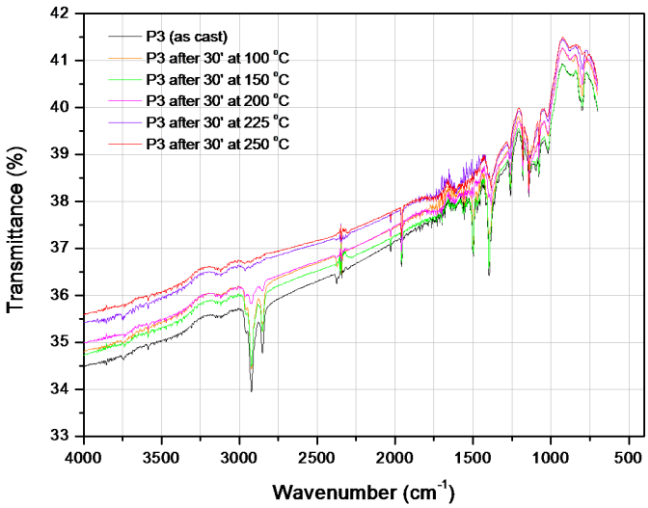

Figure 4.9. IR spectra of polymer **P3** for the as cast film and after sequential heating-cooling cycles.

For **P3** (Figure 4.9), a strong reduction of the C-H stretching band intensity was already noticed after heating the film at 200 °C, drastic reduction occurring above 225 °C. The slightly different behavior of **P2'** and **P3**, both carrying linear chains, is difficult to explain. A very important issue concerning conjugated polymers is the purity of these materials. The presence of traces of residual metal catalysts has proven to accelerate the degradation of photoactive species.[8] Additionally, the protocol used for the synthesis of

the CPDT building blocks, as well as small impurities still present in the final polymers, might also have a contribution to the stability of these materials.

Traces of silicone grease, *i.e.* polydimethylsiloxane (PDMS), alter the film forming properties of the polymers. This optically clear and heat resistant compound will lead to extremely "slippery" hydrophobic polymer solutions, which afford inhomogeneous films. The contamination can occur during the reaction and even during Soxhlet extraction of the polymers, where silicon grease is used for lubricating the glass stopcocks and joints. For **P3**, PDMS contamination was noticed by IR, as unambiguously identified by the fingerprint located at 1261 cm^{-1} ($\upsilon_{C\text{-}Si}$, see Figure S4.2). Subsequent washing of the polymer with dichloromethane, a solvent which preferentially dissolves PDMS, allowed almost complete removal of this impurity. The purified polymer showed improved film forming properties which resulted in more homogeneous films. Additionally, the characteristic band of PDMS was considerably reduced.

At temperatures above 150 ^{o}C, all polymers showed a reduction of the (aliphatic) C-H stretching bands located between 2960-2850 cm^{-1} and the band located at 1500 cm^{-1} (CPDT unit), which was accompanied by the apparition of a broad band situated between 1800 and 1600 cm^{-1}. The origin of this band most probably resides in the formation of degradation products possessing carbonyl functionalities, *e.g.* aromatic and/or aliphatic ketones, carboxylic acids, etc. The latter are hard to identify since the presence of a broad band belonging to the O-H vibrations (above 3000 cm^{-1}) is not distinguishable. A possible way for identifying these carbonyl functionalities could be to apply a chemical derivatization method.[22]

4.2.5. TG-TD-GC/MS Study of PCPDTBT Polymers

Thermogravimetric analysis (TGA) is a very useful technique which allows the quantification of the volatile organic compounds (VOCs) that evolve from a given sample at elevated temperatures. Heating the samples up to ~1000 ^{o}C in a N_2 atmosphere, at a rate of 20 $^{o}C\ min^{-1}$, resulted in pyrolysis of the studied polymer species. The degradation process normally occurs in two steps, *i.e.* degradation of the side chains followed by degradation of the backbone. TGA screening experiments were conducted for the determination of the temperature interval(s) where weight loss was

observed. After this screening, combined TG-TD-GC/MS (thermogravimetry-thermal desorption-gas chromatography/mass spectrometry) experiments were carried out, in which the VOCs evolving from the polymers during the TGA were trapped on Tenax columns, in two steps, according to the predetermined temperature intervals. This hyphenated technique allows, in a second step, the thermal desorption of the VOCs and separation of the analytes in function of their interaction with the stationary phase (based on the intrinsic properties of the analytes such as molecular weight, volatility, polarity, etc.). Identification of the thermal decomposition products helps to elucidate the degradation mechanism taking place in these polymers.

The preliminary TGA results showed that **P1** and **P1'** lose 20% weight at ~450 ^{o}C, while **P2'** and **P3** showed an initial 27 and 22% weight loss, respectively, at ~475 ^{o}C (Figure 4.10, Table 4.2). The total weight loss, recorded at ~960 ^{o}C, was 83, 55 and 73% for **P1**/**P1'**, **P2'** and **P3**, respectively. This result is in agreement with the observed stability of the polymers during the UV-Vis experiments, which increases from **P1**/**P1'** to **P3** and **P2'**.

Table 4.2. Overview of the theoretical (estimated) weight loss and the values issued from TGA.

Polymer	Theoretical		TGA			
	Side Chains	Backbone	Weight Loss (%)/ Temperature (^{o}C)			
	%	%	1st step	2nd step	3rd step	Total
P1 and **P1'**	42.3	57.7	20/447	75/910	/	83/963
P2'	42.3	57.7	27/473	52/672	/	55/962
P3	52.4	47.6	22/472	47/577	58/640	73/963

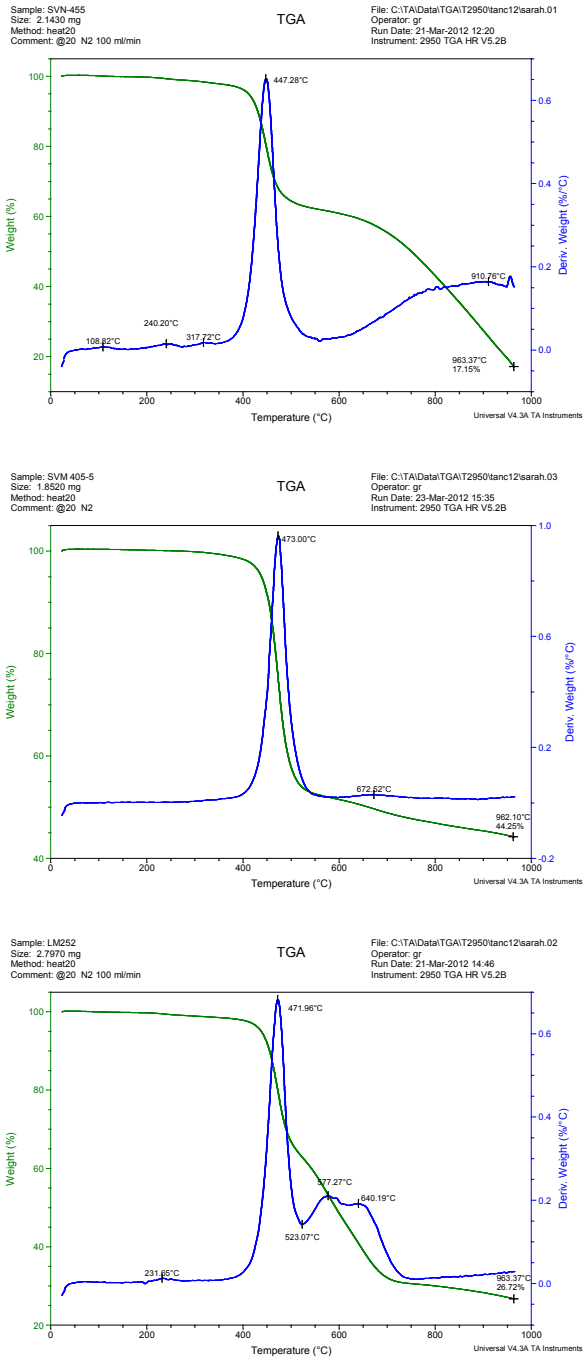

Figure 4.10. TGA data for polymers **P1**/**P1'** (top), **P2'** (middle) and **P3** (bottom).

According to TGA, two temperature ranges were selected for the TG-TD-GC/MS study, *i.e.* 20-550 °C and 550-1000 °C. During the first step, the expected major degradation process is the loss and/or fragmentation of the side chains present on the CPDT carbon bridge. Surprisingly, side chain degradation was not only restricted to cleavage of the 2-ethyhexyl, octyl and dodecyl substituents in **P1**/**P1'**, **P2'**, and **P3**, respectively, but was also accompanied by degradation of the cyclopentadiene ring (Figure 4.11, Table 4.3). In such cases, α- and β-cleavage of the alkyl chains, bonds *b* and *a*, respectively, was accompanied by cleavage of both *c* bonds (Figure 4.11). The presence of alkanes and alkenes for which the number of carbon atoms was superior to the length of the alkyl substituents present on the CPDT bridge can arise from cleavage of the *c* bonds and/or during a termination step, in which two free (alkyl) radicals combine in a natural way. Side chain degradation was not complete in the first temperature range and continued at temperatures superior to 550 °C. Above this temperature, degradation of the polymer backbone also took place. Thiophene, 2,1,3-benzothiadiazole, benzene and cyclopentadiene appeared as most abundant volatiles. The presence of thiophene and 2,1,3-benzothiadiazole provides a proof of polymer chain scission. Benzene units could occur following further degradation of the 2,1,3-benzothiadiazole unit and/or loss of the benzene groups introduced during the end-capping step. Finally, the detection of cyclopentadiene could be explained by further degradation of the CPDT unit.

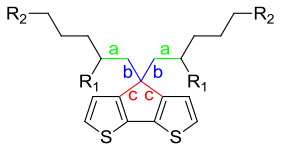

P1/P1' $R_1 = C_2H_5$, $R_2 = CH_3$
P2' $R_1 = H$, $R_2 = C_3H_7$
P3 $R_1 = H$, $R_2 = C_7H_{15}$

Figure 4.11. Side chain cleavage accompanied by degradation of the CPDT unit.

TG-TD-GC/MS revealed identical degradation pathways for both **P1** and **P1'**, being an indication that the synthetic route used for the generation of the CDPT unit has no (or very little) influence on the thermal stability of **PCPDTBT** low band gap copolymers.

Table 4.3. Most abundant degradation compounds revealed by TG-TD-GC/MS analysis.

P1 and P1'	
1st step (20-550 °C)	**2nd step (550-1000 °C)**
Heptane	Butane + butene
3-Methylheptane + alkene	Benzene[a]
Tridecane	Thiophene
Pentadecane	2,1,3-Benzothiadiazole
1-Hexene	Undecene
Butane + butene	Heptane
	Triphenylphosphine oxide[a]
P2'	
Hexane + hexene	Benzene
Heptane + heptene	Thiophene
Octane + octene	Heptane + heptene
Undecene	Octane + octane
2,1,3-Benzothiadiazole	2,1,3-Benzothiadiazole
P3	
Undecane + alkene(s)	Undecane + alkene(s)
Dodecane + dodecene	Dodecane + dodecene
Pentadecane	Octane
Decane + decene	Nonene
Pentane + pentene	Cyclopentadiene
Benzene[a]	Triphenylphosphine oxide
	Siloxane[b]

[a] Detected in **P1'**; [b] Small amounts were detected in all samples, with the highest degree of contamination noticed for **P3**.

4.3. Conclusions

The synthesis of a series of low band gap **PCPDTBT** polymers (**P1**/**P1'**, **P2'** and **P3**, bearing two branched 2-ethylhexyl and two linear octyl and dodecyl side chains on the CPDT ring, respectively) was accomplished and their thermally induced degradation was monitored by UV-Vis and IR spectroscopy, and TG-TD-GC/MS. Deliberate incorporation of monoalkyl defects along the polymer chain, presumed to be responsible for accelerated degradation of the material (leading to keto defects) in terms of optical and electrical characteristics, was shown impossible due to the very unstable nature of the dibrominated monoalkyl-CPDT derivative. In ambient conditions, the latter was oxidized during the purification step (on silica) leading to the formation of an alkene.

The optical properties of thin films of the **PCPDTBT** polymers were investigated under isothermal and step-heating conditions. As revealed by UV-Vis spectroscopy, the optical properties of **P2'** and **P3** remained virtually unchanged when heated to 200 ^{o}C for 1 day, while **P1**/**P1'** showed a noticeable decrease in absorption when exposed to 150 ^{o}C. Repetitive heating-cooling cycles had an annealing effect for **P2'**, while **P3** and (more pronounced) **P1'** showed degradation of the chromophore.

The IR study revealed that the intensities of the C-H vibrations of the side chains decreased at temperatures above 150 ^{o}C and in the presence of air and/or oxygen, this being accompanied by the apparition of a broad band between 1800 and 1600 cm^{-1}, suggesting the formation of carbonyl derivatives. This technique also revealed PDMS contamination of the polymers, which explained the poor film-forming properties.

TGA in a N_2 atmosphere revealed a two-step thermal degradation process of the polymers. The first step, between 20 and ~550 ^{o}C, was mainly characterized by degradation of the alkyl side chains. This process continued on a second stage, from 550 ^{o}C up to ~960 ^{o}C, and was accompanied by additional degradation of the polymer backbone. A combined TG-TD-GC/MS analysis allowed identification of the alkane and alkene derivatives released upon α- and β-cleavage of the side chains, as well as aromatic units from degradation of the polymer backbone. Traces of PDMS were detected in all polymers, the highest degree of contamination being noticed for **P3**. Additionally, residual triphenylphosphine oxide, presumably from the palladium catalyst ($Pd(PPh_3)_4$) used in the polymerization reaction, was detected for **P1'** and **P3**.

TG-TD-GC/MS also revealed that the synthetic route by which the CDPT scaffold was obtained had no or very little influence on the stability of the final polymers.

In general, this study showed that **P2'**, bearing linear octyl side chains, had superior thermal stability compared to **P3** and **P1**/**P1'**, bearing linear dodecyl and branched 2-ethylhexyl side chains, respectively. It became clear that the pendant alkyl groups, introduced merely for granting solubility to the final polymers, are not just dormant entities, but dictate both the performance of the device (by altering the active layer blend nanomorphology) and the (thermal) stability of the photoactive material (blend).

On the other hand, this study also revealed that the thermal degradation pathway of **PCPDTBT** derivatives probably does not involve keto intermediates, as has been demonstrated for PFs, as such signatures were not clearly identified. These findings are in agreement with and support the changes noticed during the synthesis and bromination of the monoalkylated CPDT derivative.

4.4. Experimental Section

Materials and Methods

NMR chemical shifts (δ, in ppm) were determined relative to the residual $CHCl_3$ absorption (7.26 ppm) or the ^{13}C resonance shift of $CDCl_3$ (77.16 ppm). Gas chromatography-mass spectrometry (GC-MS) analyses were carried out applying Chrompack Cpsil5CB or Cpsil8CB capillary columns. Molecular weights and molecular weight distributions were determined relative to polystyrene standards (Polymer Labs) by gel permeation chromatography (GPC). Chromatograms were recorded on a Spectra Series P100 (Spectra Physics) equipped with two mixed-B columns (10 µm, 0.75 cm x 30 cm, Polymer Labs) and a refractive index detector (Shodex) at 40 °C. THF was most often used as the eluent at a flow rate of 1.0 mL min^{-1}. If chlorobenzene was used as the eluent, the temperature was raised to 80 °C. In situ UV-Vis measurements were performed on a Cary 500 UV-Vis-NIR spectrophotometer, specially adapted by Varian to contain a Harrick high-temperature cell, with a scan rate of 600 nm min^{-1} in a continuous run from 1000 to 200 nm. The polymers were drop-cast from a chlorobenzene solution (10 mg mL^{-1}) on a quartz glass substrate, which was heated in the Harrick high temperature cell specially adapted by Harrick to be positioned in the beam of the UV-Vis-NIR-spectrophotometer. The temperature of the film was controlled by a dual channel temperature controller from Watlow (serial number 999). Spectra were taken every 10 min. The heating rate was 2 °C min^{-1} up to 250 °C. All measurements were performed under a continuous flow of nitrogen. Step-heating experiments with in situ collection of infrared spectra were performed in a Harrick high-temperature cell (purchased from Safir), which was positioned in the beam of a Perkin-Elmer Spectrum One FT-IR spectrometer. Infrared spectra were collected with a resolution of 4 cm^{-1} (16 scans) using films drop-cast from a chlorobenzene solution (10 mg mL^{-1}) on a NaCl disk. The temperature of the film was controlled by a dual channel temperature controller from Watlow (serial number 999). All experiments were performed at a heating rate of 2 °C min^{-1} under a continuous flow of compressed air. TGA measurements were performed on a TA instrument 951 thermogravimetric analyzer with a continuous nitrogen flow of 80 mL min^{-1} and a heating rate of 20 °C min^{-1}. Polymer samples (5 mg) were inserted in the solid state. Collection of released volatiles occurred on self-packed Tenax tubes (Tenax TA 60/80

Grace) in 2 fractions: 20-550 °C and 550-1000 °C. Samples were thermally desorbed with a Unity-1 thermal desorber (Markes) equipped with an Ultra-TD autosampler (Markes), operating under the following experimental conditions: tube desorption 20 min at 270 °C, cold trap temperature -10 °C, heating of general purpose cold trap 15 min at 320 °C, helium desorption flow 20 mL min^{-1}, inlet and outlet split flow 75 mL min^{-1}. Analytes were transferred to a Trace Ultra GC Thermo gas chromatograph equipped with a ZB5-MS, 30 m x 0.25 mm x 0.25 $\mu(d_f)$ fused silica column. The initial temperature (30 °C) was maintained for 5 min, ramp rate of 8 °C min^{-1} to 100 °C, hold time 0 min, ramp rate of 12 °C min^{-1} to 310 °C, with a subsequent hold time 5 min. Mass spectrometric analyses were carried out on a DSQ-I mass spectrometer (Thermo) in EI^+ mode (electron energy 70 eV), scan conditions: 33 to 480 *m/z* in 0.4 s.

Synthesis

Unless stated otherwise, all reagents and chemicals were obtained from commercial sources and used without further purification. 2,1,3-Benzothiadiazole-4,7-bis(boronic acid pinacol ester) (95%) (**2**) was purchased from Sigma Aldrich and used without further purification.

2,6-Dibromo-4,4-bis(2-ethylhexyl)-4*H*-cyclopenta[2,1-*b*:3,4-*b'*]dithiophene (1a/1a') were synthesized according to literature procedures.[13,23] Material identity was confirmed by GC-MS and ^{1}H NMR.

Poly[2,6-(4,4-bis(2-ethylhexyl)-4*H*-cyclopenta[2,1-*b*:3,4-*b'*]-dithiophene)-*alt*-4,7-(2,1,3-benzothiadiazole)] (PCPDTBT) (P1/P1') was synthesized using a **general polymerization procedure** from **1a/1a'** and **2** according to a modified literature procedure.[15] The phase transfer catalyst (PTC) Aliquat 336 was replaced by a high temperature resistant PTC, *i.e.* Aliquat^{TM} HTA-1. **P1** was isolated as a dark green powder (yield: 84%).[24] GPC (THF, PS standards) M_n = 1.8 x 10^4 g mol^{-1}, M_w = 3.6 x 10^4 g mol^{-1}, PDI = 2.0. **P1'** was isolated as a dark green powder (yield: 72%). GPC (THF, PS standards) M_n = 1.1 x 10^4 g mol^{-1}, M_w = 2.3 x 10^4 g mol^{-1}, PDI = 2.1.

2,6-Dibromo-4,4-dioctyl-4*H*-cyclopenta[2,1-*b*:3,4-*b'*]dithiophene (1b') was synthesized according to a literature procedure.[13] Material identity was confirmed by GC-MS and ^{1}H NMR.

Poly[2,6-(4,4-dioctyl-4*H*-cyclopenta[2,1-*b*:3,4-*b'*]dithiophene)-*alt*-4,7-(2,1,3-benzothiadiazole)] (PCPDTBT) (P2') was synthesized according to the general polymerization procedure from **1b'** and **2**. **P2** was isolated as a dark green powder (yield: 72%).[25] GPC (CB, PS standards) M_n = 8.3 x 10^3 g mol^{-1}, M_w = 1.4 x 10^4 g mol^{-1}, PDI = 1.6.

2,6-dibromo-4,4-didodecyl-4*H*-cyclopenta[2,1-*b*:3,4-*b'*]dithiophene (1c) was synthesized according to a literature procedure.[26] Material identity was confirmed by GC-MS and ^{1}H NMR.

Poly[2,6-(4,4-didodecyl)-4*H*-cyclopenta[2,1-*b*:3,4-*b'*]-dithiophene)-*alt*-4,7-(2,1,3-benzothiadiazole)] (PCPDTBT) (P3) was synthesized according to the general polymerization procedure from **1c** and **2**. **P3** was isolated as a dark green powder (yield: 95%).[26] GPC (CB, PS standards) M_n = 1.6 x 10^4 g mol^{-1}, M_w = 7.2 x 10^4 g mol^{-1}, PDI = 4.5.

4*H*-Cyclopenta[2,1-*b*:3,4-*b'*]dithiophene (3) was synthesized according to a literature procedure.[12a] Material identity was confirmed by GC-MS and ^{1}H NMR.

4-(2-Ethylhexyl)-4*H*-cyclopenta[2,1-*b*:3,4-*b'*]dithiophene (4a): *n*-BuLi (2.5 M in hexane, 0.39 mL) was added dropwise to a solution of **3** (0.160 g, 0.90 mmol) in THF (8 mL), cooled to 0 ^{o}C by means of an ice bath. The mixture was allowed to warm-up to r.t. and was left at this temperature for 1.5 h. A solution of 2-ethylhexyl bromide (0.191 g, 0.99 mmol) in THF (5 mL) was then added and the mixture was allowed to react at r.t. overnight. The reaction was quenched by addition of water. The organic layer was separated and the aqueous layer was extracted with diethyl ether. The combined organic extracts were dried over $MgSO_4$, filtered and concentrated by evaporation *in vacuo*. The residue was purified by column chromatography (silica, eluent hexane) to afford a colorless oil (0.146 g, 56%). GC-MS (EI) *m/z* 290 [M^+]; ^{1}H NMR (300 MHz, $CDCl_3$) δ 7.15 (d, J = 4.8 Hz, 2H), 7.05 (d, J = 4.8 Hz, 1H), 7.04 (d, J = 5.1 Hz, 1H), 3.70 (t, J = 8.1 Hz, 1H), 1.66-1.58 (m, 2H), 1.49-1.39 (m, 1H), 1.32-1.24 (m, 8H), 0.92-0.86 (m, 6H); ^{13}C NMR (75 MHz, $CDCl_3$) δ 154.90, 154.84, 137.5, 124.4, 122.8, 42.4, 37.4, 36.1, 32.8, 28.7, 25.9, 23.2, 14.3, 10.6.

2,6-Dibromo-4-(2-ethylhexyl)-4*H*-cyclopenta[2,1-*b*:3,4-*b'*]dithiophene (5a) and **2,6-dibromo-4-(2-ethylhexylidene)-4*H*-cyclopenta[2,1-*b*:3,4-*b'*]dithiophene (5b)**: 4-(2-Ethylhexyl)-4*H*-cyclopenta[2,1-*b*:3,4-*b'*]dithiophene (**4a**) (0.400 g, 1.38 mmol) was dissolved in DMF (25 mL) and the mixture was cooled to 0 ^{o}C by means of an ice-bath

(the reaction was run in the dark and under nitrogen atmosphere). Subsequently, a solution of NBS (0.491 g, 2.76 mmol) in DMF (25 mL) was added drop-wise and the mixture was allowed to react at r.t. for 1 h. Water (10 mL) was added and the aqueous layer was extracted with CH_2Cl_2. The combined organic layers were dried over $MgSO_4$, filtered and concentrated by evaporation *in vacuo*. The crude product was purified by column chromatography (silica, eluent hexane).

The crude reaction mixture as analyzed by GC-MS and ^{1}H NMR (see Figure S4.3), consisted of a mixture of **5a** and **5b**, which were present in a ~1:0.1 ratio. GC-MS (EI) *m/z* 446/448/450 and 444/446/448 [M^+]. Upon column chromatographic purification, a yellow oil was recovered (0.492 g, 80%), which was identified as pure **5b**. ^{1}H NMR (300 MHz, $CDCl_3$) δ 7.17 (s, 1H), 7.15 (s, 1H), 6.13 (d, J = 10.8 Hz, 1H), 2.80-2.71 (m, 1H), 1.68-1.57 (m, 2H), 1.47-1.37 (m, 2H), 1.29-1.25 (m, 4H), 0.91-0.83 (m, 6H); ^{13}C NMR (75 MHz, $CDCl_3$) δ 144.0, 140.44, 140.36, 139.1, 135.4, 130.5, 125.6, 122.8, 111.0, 110.4, 42.5, 35.3, 29.9, 28.7, 23.0, 14.1, 12.1.

4.5. References

(1) Brabec, C. J. *Sol. Energy Mater. Sol. Cells* **2004**, *83*, 273.

(2) Espinosa, N.; Hosel, M.; Angmo, D.; Krebs, F. C. *Energy Environ. Sci.* **2012**, *5*, 5117.

(3) Source: NREL

(4) In this paper we will only address conjugated polymers.

(5) (a) Manceau, M.; Bundgaard, E.; Carle, J. E.; Hagemann, O.; Helgesen, M.; Sondergaard, R.; Jorgensen, M.; Krebs, F. C. *J. Mater. Chem.* **2011**, *21*, 4132; (b) Jørgensen, M.; Norrman, K.; Gevorgyan, S. A.; Tromholt, T.; Andreasen, B.; Krebs, F. C. *Adv. Mater.* **2012**, *24*, 580.

(6) Heeger, A. J. *Chem. Soc. Rev.* **2010**, *39*, 2354.

(7) (a) Chambon, S.; Rivaton, A.; Gardette, J.-L.; Firon, M.; Lutsen, L. *J. Polym. Sci., Part A: Polym. Chem.* **2007**, *45*, 317; (b) Manceau, M.; Rivaton, A.; Gardette, J.-L.; Guillerez, S.; Lemaître, N. *Polym. Degrad. Stab.* **2009**, *94*, 898; (c) Manceau, M.; Chambon, S.; Rivaton, A.; Gardette, J.-L.; Guillerez, S.; Lemaître, N. *Sol. Energy Mater. Sol. Cells* **2010**, *94*, 1572; (d) Chambon, S.; Rivaton, A.; Gardette, J.-L.; Firon, M. *Polym. Degrad. Stab.* **2011**, *96*, 1149.

(8) Grisorio, R.; Suranna, G. P.; Mastrorilli, P.; Nobile, C. F. *Adv. Funct. Mater.* **2007**, *17*, 538.

(9) (a) List, E. J. W.; Guentner, R.; Scanducci de Freitas, P.; Scherf, U. *Adv. Mater.* **2002**, *14*, 374; (b) Craig, M. R.; de Kok, M. M.; Hofstraat, J. W.; Schenning, A. P. H. J.; Meijer, E. W. *J. Mater. Chem.* **2003**, *13*, 2861.

(10) Cho, S. Y.; Grimsdale, A. C.; Jones, D. J.; Watkins, S. E.; Holmes, A. B. *J. Am. Chem. Soc.* **2007**, *129*, 11910.

(11) Liu; Qiu, S.; Wang, B.; Zhang, W.; Lu, P.; Xie, Z.; Hanif, M.; Ma, Y.; Shen, J. *J. Phys. Chem. B* **2005**, *109*, 23366.

(12) (a) Coppo, P.; Cupertino, D. C.; Yeates, S. G.; Turner, M. L. *Macromolecules* **2003**, *36*, 2705; (b) Coppo, P.; Turner, M. L. *J. Mater. Chem.* **2005**, *15*, 1123.

(13) Van Mierloo, S.; Adriaensens, P. J.; Maes, W.; Lutsen, L.; Cleij, T. J.; Botek, E.; Champagne, B.; Vanderzande, D. J. *J. Org. Chem.* **2010**, *75*, 7202.

(14) The prime (') denotes that the monomer is prepared via the more recent three-step protocol.

(15) Zhang, M.; Tsao, H. N.; Pisula, W.; Yang, C.; Mishra, A. K.; Müllen, K. *J. Am. Chem. Soc.* **2007**, *129*, 3472.

(16) Zotti, G.; Schiavon, G.; Berlin, A.; Fontana, G.; Pagani, G. *Macromolecules* **1994**, *27*, 1938.

(17) (a) Cammidge, A. N.; Crepy, K. V. L. *Chem. Commun.* **2000**, 1723; (b) Van Mierloo, S.; Hadipour, A.; Spijkman, M.-J.; Van den Brande, N.; Ruttens, B.; Kesters, J.; D'Haen, J.; Van Assche, G.; de Leeuw, D. M.; Aernouts, T.; Manca, J.; Lutsen, L.; Vanderzande, D. J.; Maes, W. *Chem. Mater.* **2012**, *24*, 587.

(18) Treat, N. D.; Shuttle, C. G.; Toney, M. F.; Hawker, C. J.; Chabinyc, M. L. *J. Mater. Chem.* **2011**, *21*, 15224.

(19) (a) Rivaton, A.; Chambon, S.; Manceau, M.; Gardette, J.-L.; Lemaître, N.; Guillerez, S. *Polym. Degrad. Stab.* **2010**, *95*, 278; (b) Manceau, M.; Gaume, J.; Rivaton, A.; Gardette, J.-L.; Monier, G.; Bideux, L. *Thin Solid Films* **2010**, *518*, 7113.

(20) Fux, P. *Analyst* **1989**, *114*, 445.

(21) Bard, C. C.; Porro, T. J.; Rees, H. L. *Anal. Chem.* **1955**, *27*, 12.

(22) Wilhelm, C.; Gardette, J.-L. *J. Appl. Polym. Sci.* **1994**, *51*, 1411.

(23) Karsten, B. P.; Bijleveld, J. C.; Viani, L.; Cornil, J.; Gierschner, J.; Janssen, R. A. J. *J. Mater. Chem.* **2009**, *19*, 5343.

(24) Bijleveld, J. C.; Shahid, M.; Gilot, J.; Wienk, M. M.; Janssen, R. A. J. *Adv. Funct. Mater.* **2009**, *19*, 3262.

(25) Zoombelt, A. P.; Mathijssen, S. G. J.; Turbiez, M. G. R.; Wienk, M. M.; Janssen, R. A. J. *J. Mater. Chem.* **2010**, *20*, 2240.

(26) Coffin, R. C.; Peet, J.; Rogers, J.; Bazan, G. C. *Nat. Chem.* **2009**, *1*, 657.

4.6. Supporting Information

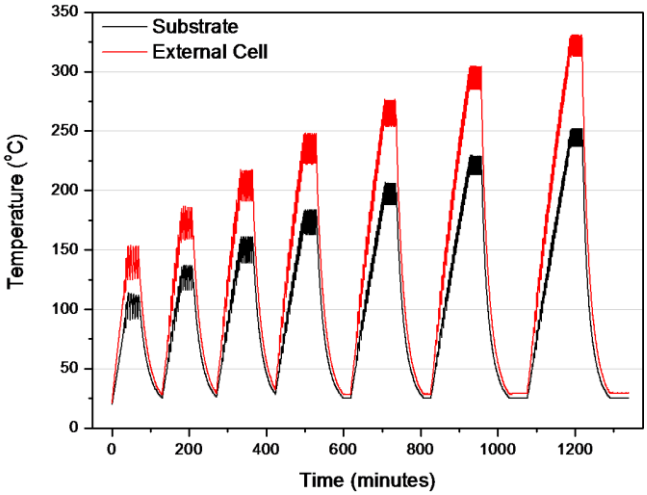

Figure S4.1. Profile of the temperature *vs* time used in the step-heating experiment.

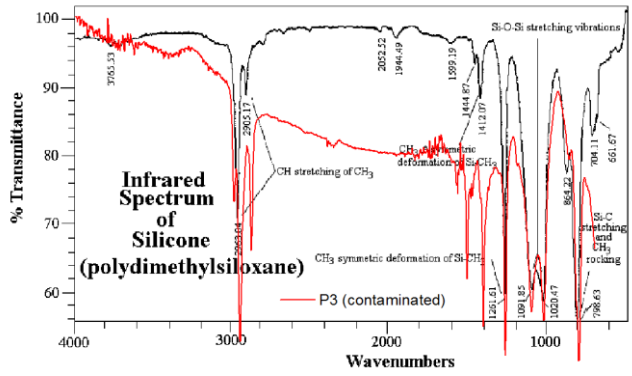

Figure S4.2. IR spectra of a contaminated sample of polymer **P3** as cast film.

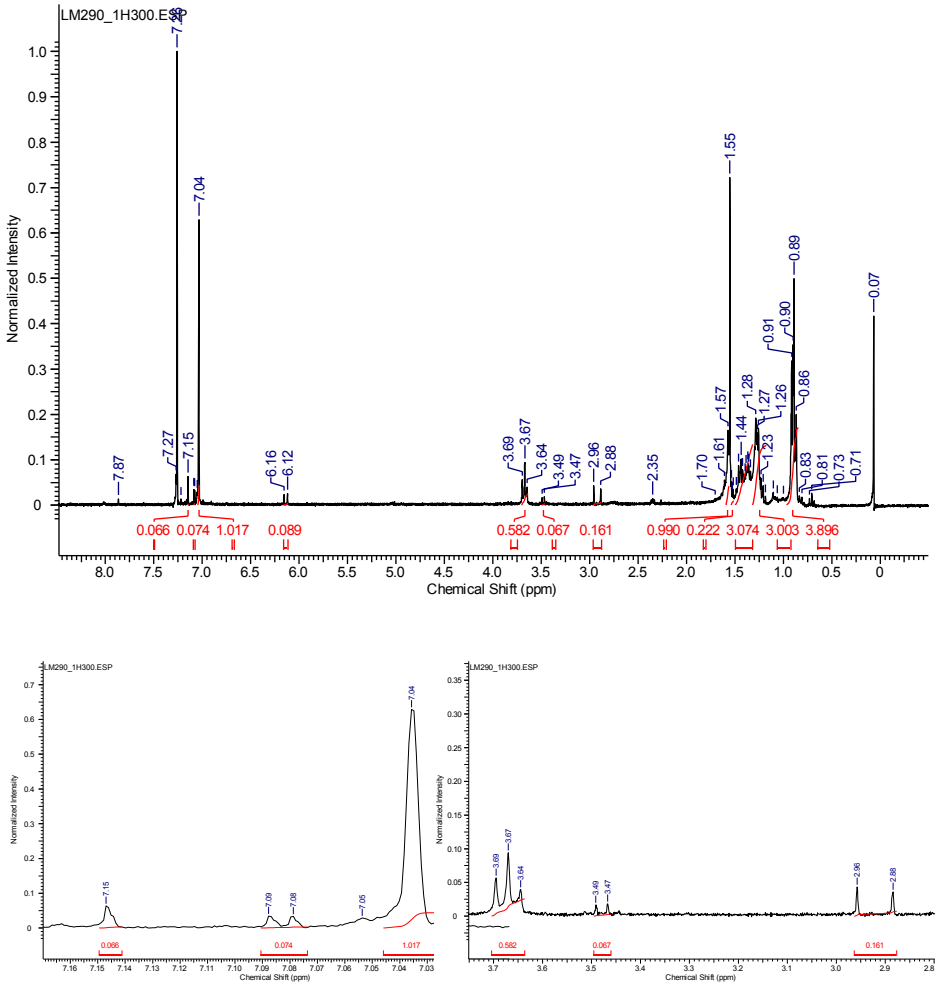

Figure S4.3. ^{1}H NMR spectrum of the crude reaction mixture after bromination of **4a**, indicating the formation of **5a** as the major reaction product and **5b** being present in very small amounts.

Table S4.1. Assignment of the main IR features of **P1**/**P1'**, **P2'** and **P3**.

P1/P1' (υ cm^{-1})	**P2'** (υ cm^{-1})	**P3** (υ cm^{-1})	**Assignment**
2954	2956	2958	CH_3 asymmetric stretching
2922	2926	2922	CH_2 asymmetric stretching
2890	/	/	CH_3 symmetric stretching
2856	2850	2852	CH_2 symmetric stretching
1958	1958	1958	C=C asymmetric stretching
1506	1500	1498	C=C stretching out of phase
1398	1400	1398	C=C stretching in phase
1180		1180	=C-H bending in plane
1142		1142	ring deformation in plane
1076		1076	CH_3, CH_2 rocking
822	814	814	=C-H in plane bending
	804	798	=C-H out of plane bending

Chapter 5

Quinoxaline Derivatives with Broadened Absorption Patterns Toward 2D-Conjugated Low Band Gap Copolymers for Organic Photovoltaics

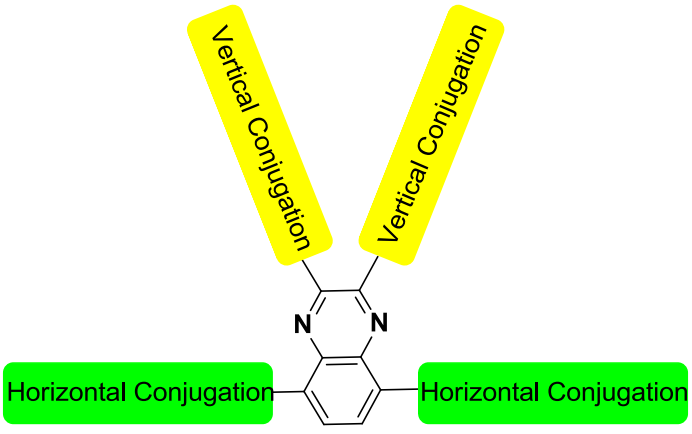

5.1. Introduction

The number of studies on the design and synthesis of light harvesting organic materials used in optoelectronic devices, *i.e.* organic light emitting diodes (OLEDs), field effect transistors (OFETs) and photovoltaics (OPVs), has increased almost exponentially in the last decade. Depending on the device architecture and function, the photoactive materials need to fulfill certain criteria in order to deliver optimal output parameters. In OLEDs for instance, materials that emit light in the visible range of the solar spectrum with high electroluminescence quantum efficiencies are required.[1] For OFETs, organic semiconductors with high charge carrier mobilities are desirable. Additionally, a high degree of crystallinity and tendency to self-assemble facilitate unidirectional charge transport.[2] In OPVs, materials with a broad (absorption) coverage of the solar spectrum, ideally extended toward the low energy side of the spectrum where the photon flux is most abundant, are required.[3] The use of either individual or a combination of conjugated heteroaromatic building blocks in the synthesis of optically active materials has proven to be very successful. In general, the use of a strong chromophore is required, and integration in donor-acceptor architectures is one of the most versatile approaches used for tuning the band gap, *i.e.* the energy levels of the material.

While polymer OPV materials are almost exclusively processed from solution, small molecules are traditionally processed by vacuum deposition techniques. Solution processing is strongly preferred due to reduced energy consumption and lower manufacturing costs. Therefore, there is also increased interest in solution processing of small molecules as active (light harvesting) donor and acceptor materials in organic photovoltaics.[4] To encompass the strong π-π interchain interactions of conjugated (polymer) materials, solubilizing side chains are generally introduced. Most often, these are linear or branched alkyl groups, connected to the (hetero)aromatic unit by C-C or C-O single bonds. The side chains not only render the material soluble in common organic solvents, simplifying synthetic protocols and material purification, but they also have a huge impact on the organization and interactions between individual molecules and/or polymer chains.[5] As a rule of thumb, linear substituents enhance the degree of order while branched chains introduce disorder. On the other hand, linear substituents generally induce a lower degree of solubility compared to the branched ones. Side chains can additionally be used as a tool for controlling the optical properties

of the π-conjugated monomers and polymers. The introduction of ethenyl spacers between the side chains and the heteroaromatic unit leads to an extension of the conjugated system. In most cases this results in a broadening of the absorption window of the photoactive species and it also has an impact on the conducting properties and the degree of order (interactions) within the material.[6]

The electron deficient quinoxaline (Qx) moiety has been introduced on numerous occasions as an interesting candidate for integration in organic electronics.[7,8] In the OPV field, a number of donor-acceptor copolymers incorporating quinoxaline units as the electron poor components have appeared, showing rather high solar cell efficiencies.[8]

In this paper we present a series of novel 2D-conjugated quinoxaline derivatives specifically designed for optoelectronic applications. For all these materials the side chains, *i.e.* alkyl, aryl or heteroaryl units, are separated from the electron deficient quinoxaline core by ethenyl and/or butadienyl spacers. As reference materials, derivatives for which the side chains are directly attached to the quinoxaline core by C-C single bonds were synthesized as well. The influence of the side chains on the optical, chemical and physical properties of the materials is discussed. Some of the quinoxaline materials were also applied in cross coupling reactions, which afforded a series of donor-acceptor-donor type small molecules with enhanced optical characteristics. The gain in absorption which is achieved at the monomer stage is preserved, and even enhanced, when the conjugation in the horizontal (quinoxaline) plane is extended. As a result, these compounds are promising materials for applications in optoelectronic devices, notably when incorporated in low band gap copolymers.

5.2. Results and Discussion

5.2.1. Synthesis and Optical Characterization of 5,8-Dibromoquinoxaline Monomers

Electron deficient quinoxaline heterocycles have proven to be very versatile building blocks that can easily be functionalized.[8-9] Addition of bromine atoms in positions 5 and 8 makes them very suitable coupling partners for Suzuki and/or Stille polycondensation reactions.[8a,10] Therefore, at a first stage, the bromine atoms were

introduced on the precursor level, *i.e.* 2,1,3-benzothiadiazole (**1**), using a mixture of Br_2 and HBr (Scheme 5.1).[11] Sulfur extrusion in the presence of $NaBH_4$ afforded the corresponding diamine **3**.[12] The quinoxaline cores were then obtained by condensation reactions between diketones **4** and 3,6-dibromo-*o*-phenylenediamine (**3**). At this point, the introduction of the different side chains, which are directly attached to the quinoxaline core by a C-C single bond, can be achieved by employing different diketones **4**. Thus, 2,3-diphenyl-5,8-dibromoquinoxaline (**M1**), 2,3-bis(thien-2-yl)-5,8-dibromoquinoxaline (**M2**), and 2,3-bis[5-(2-ethylhexyl)thien-2-yl]-5,8-dibromoquinoxaline (**M3**) were synthesized in good yields (66-95%) by *p*-toluenesulfonic acid (*p*-TsOH) mediated condensation of diphenylethanedione, 1,2-di(thiophen-2-yl)ethane-1,2-dione and 1,2-bis(5-(2-ethylhexyl)thien-2-yl)ethane-1,2-dione, respectively, with diamine **3** (Scheme 5.1).[13] These derivatives (**M1**-**M3**) further on served as reference compounds for the evaluation of the optical properties of the quinoxaline derivatives bearing ethenyl and butadienyl spacers between the (donor) side chains and the quinoxaline core. Further use of these monomers in polymer materials was not envisaged since they would most probably lead to insoluble derivatives that do not allow solution processing.

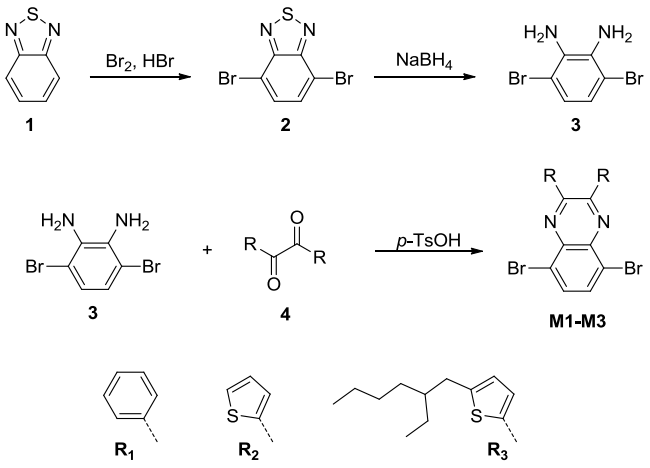

Scheme 5.1. Synthesis of quinoxaline monomers **M1**-**M3**.

For the synthesis of Qx derivatives with broadened absorption patterns, the quinoxaline derivative **M0**, bearing bromomethyl groups in positions 2 and 3, was synthesized as a common precursor (Scheme 5.2). Further transformations involved an Arbuzov

reaction (leading to the formation of a phosphonate), followed by Horner-Wadsworth-Emmons condensation in the presence of an (alkenyl)aldehyde **A4**-**A9**. 2D-Conjugated quinoxaline monomers **M4**-**M9** were synthesized in this way in good yields (56-80% starting from **M0**).

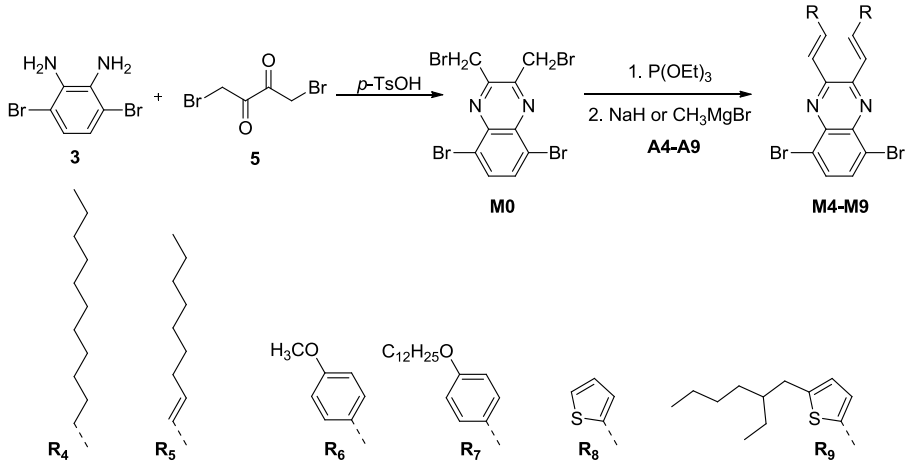

Scheme 5.2. Synthesis of 2D-conjugated quinoxaline monomers **M4**-**M9**.

The UV-Vis spectra of monomers **M1**-**M3** (Figure 5.1) showed a bathochromic shift upon going from phenyl to thienyl and 5-(2-ethylhexyl)thienyl substituents. While **M1** was characterized by a unique absorption band with a maximum at ~350 nm, for **M2**, and even more pronounced for **M3**, the absorption window was extended toward the visible region of the spectrum and displayed a second absorption band covering the 350-450 nm range. The replacement of the phenyl units by (substituted) thienyl groups creates an enhanced 2D-conjugation pathway within the molecules, with additional intramolecular charge transfer (from the donor side chains to the acceptor quinoxaline core). For **M3**, the alkyl substituent in position 5 of the thiophene ring seemed to slightly increase the donor strength of the appended side chains, resulting in enhanced intramolecular charge transfer within the system.

The introduction of ethenyl and butadienyl spacers between the quinoxaline core and the linear alkyl substituents afforded monomers **M4** and **M5**, respectively. The absorption spectra of these derivatives were characterized by a main band located in the UV region and a weak secondary band extended into the visible range (Figure 5.1). The incorporation of a conjugated butadienyl spacer in **M5** resulted in a red-shift of the

main and secondary absorption bands with ~50 nm compared to **M4**. The replacement of the alkyl end groups by alkoxyphenylene and thienyl (hetero)aromatic moieties in **M6**/**M7** and **M8**, respectively, resulted in an additional red-shift for both absorption bands, and the low energy band (between 400 and 500 nm) became progressively (slightly) more intense as a result of enhanced conjugation between the quinoxaline core and the (hetero)arylene-vinylene side chains. **M6** and **M8** were again merely synthesized for comparison and were not used in further transformations due to the likeliness of solubility issues. The contribution of the additional alkyl chains in **M7** on the absorption pattern was negligible. As a consequence, regardless of the length of the alkyl substituent of the ether functionality, and even in absence of a substituent, the absorption spectra of **M6**, **M7** and **M8** were almost overlapping. Monomer **M9**, bearing 5-(2-ethylhexyl)thien-2-yl side chains connected by ethenyl linkers to the quinoxaline core, displayed the best optical properties. In case of the thienyl substituents, the additional alkyl side chains resulted in an absorption spectrum with an enhanced coverage of the solar spectrum, characterized by three distinct maxima located at 350, 415 and 450 nm, with a shoulder extending beyond 500 nm.

At this point we can conclude that **M9** appeared as the best Qx monomer in terms of optical absorption. This derivative, decorated with pendant 2-ethylhexyl branched alkyl side chains, also showed excellent solubility in common organic solvents. Monomers **M6** and **M7** are situated right behind. The latter have shown, however, some solubility issues, which rendered purification and further transformations somewhat difficult. Based on their excellent processability and still appealing optical characteristics, **M4** and **M5** were also employed further on in various cross coupling reactions.

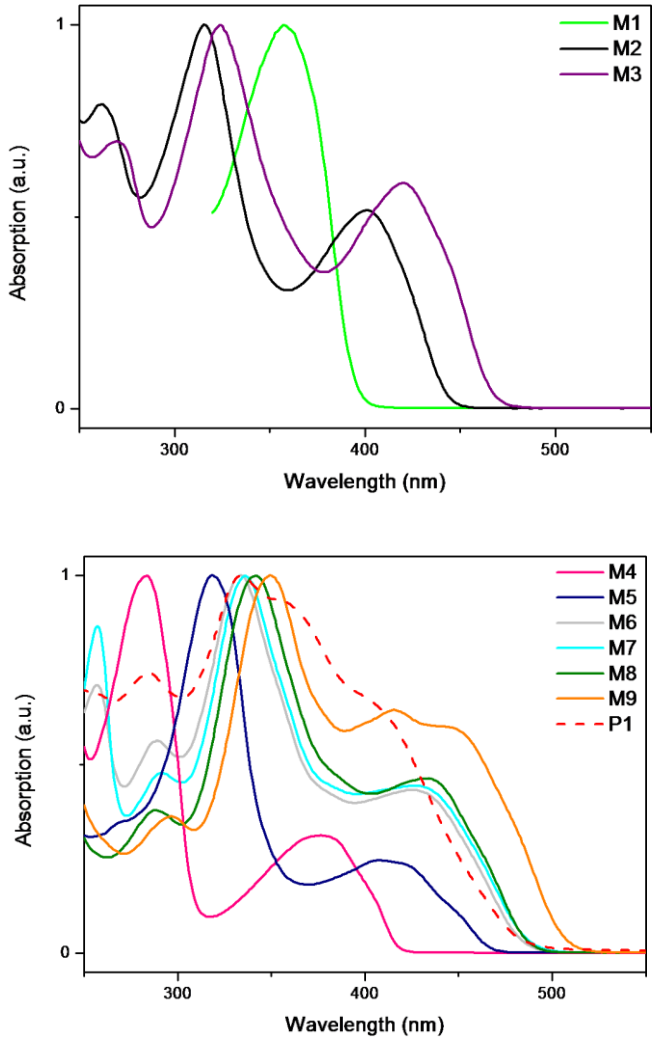

Figure 5.1. UV-Vis spectra (normalized, from chloroform solution) of Qx monomers **M1**-**M9** and polymer **P1**.

5.2.2. Synthesis and Optical Characteristics of Donor-Acceptor-Donor Triads

Preliminary tests showed that **P1** (M_n = 6.8 x 10^4 g mol^{-1}, PDI = 6.0) (Scheme 5.3), the homopolymer synthesized by Ni^0 mediated Yamamoto polycondensation of Qx monomer **M7**, showed almost identical absorption spectra with its monomer (Figure 5.1).[14] In **P1**, the contribution of the vertical conjugation induced by the side chains appeared, surprisingly enough, to be significantly diminished compared to the monomer. Additionally, no further increase in the conjugation length was observed in

the (horizontal) quinoxaline plane, most probably caused by pronounced twisting along the polymer backbone which drastically disrupts the conjugation.[14]

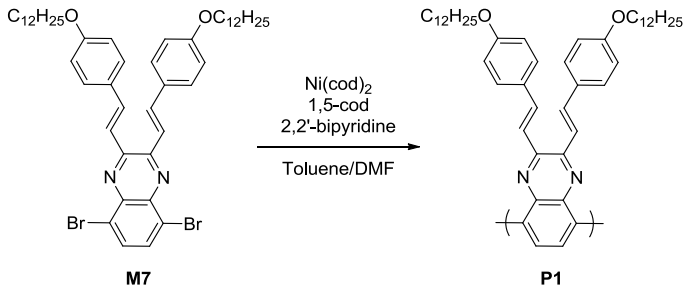

Scheme 5.3. Synthesis of Qx homopolymer **P1** by Yamamoto polycondensation.

Minimizing the steric hindrance between two neighboring quinoxaline units can be achieved by the introduction of spacers, *e.g.* vinylene spacers or small aromatic units such as thiophene.[15] The most convenient way to assemble such expanded units is by means of Suzuki or Stille cross coupling reactions.[16] For toxicity reasons the former is, whenever possible, preferred. Therefore, we decided to assemble thiophene-Qx-thiophene triads by Suzuki cross coupling reactions (Scheme 5.4). This should allow to minimize sterically induced twists in the horizontal backbone and to enhance the conjugation within the expanded quinoxaline molecules. 2-Thiopheneboronic acid (**6**) was readily synthesized starting from thiophene.[17] In order to promote the transmetallation, the activation of boronates is achieved by employing a base. Very often these are aqueous carbonate or phosphate solutions, leading to biphasic reaction mixtures. As such, the use of a phase transfer catalyst is required. Moreover, the basic reaction conditions are not always compatible with the functional groups present or may give solubility problems. In these cases, the use of "water-free" Suzuki conditions, in which *e.g.* CsF is employed as a base, is required.[18] Due to the relatively poor solubility of **M7** in a biphasic solvent system and its tendency to precipitate, the use of a homogenous reaction mixture was mandatory for the synthesis of **M10** (Scheme 5.4). The optimized conditions were then also employed for the synthesis of monomers **M11**-**M13**. Even when using a three-fold excess of the boronic acid (6 equiv), the triads were obtained in relatively low yields (41-78%). The low efficiency of the

coupling reaction could be due to low reactivity of the quinoxaline monomers toward such transformations or the non-optimized water-free Suzuki conditions.

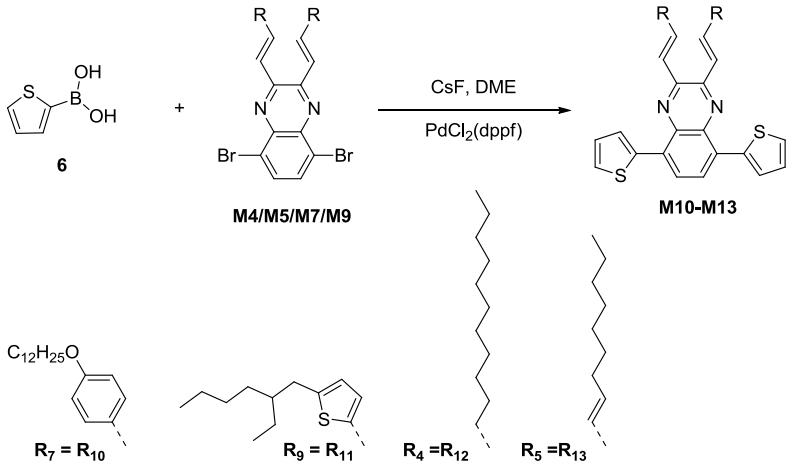

Scheme 5.4. Synthesis of donor-acceptor-donor triads **M10-M13** *via* Suzuki cross coupling reactions.

For derivatives **M10**-**M13**, the introduction of thiophene groups in positions 5 and 8 of the quinoxaline unit had little influence on their optical properties (Figure 5.2). Compared with the corresponding monomers, the onset of the absorption spectra of the donor-acceptor-donor triads was almost unchanged. This could be due to a competition between the vertical and the horizontal conjugation within the system, induced by the conjugated side chains and the thiophene units. Nevertheless, the main absorption bands, located between 300 and 400 nm, were broadened and slightly red-shifted. Once more, the derivative with the 5-(2-ethylhexyl)thien-2-yl side chains showed the most promising (broadest and most red-shifted) absorption profile.

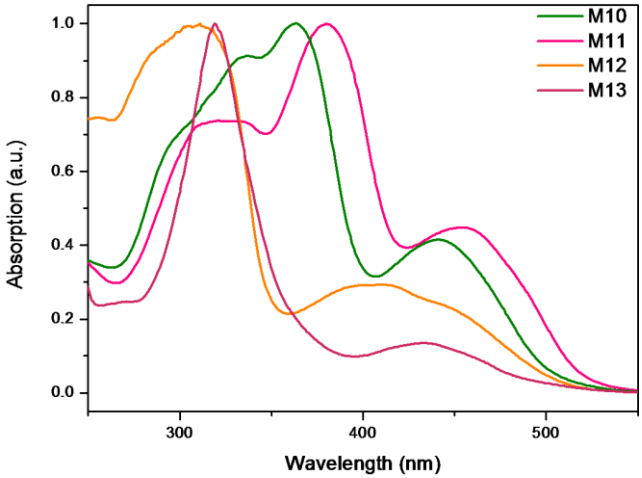

Figure 5.2. UV-Vis spectra (normalized, from chloroform solution) of donor-acceptor-donor triads **M10-M13**.

At this point it became clear that future polymerization of the novel quinoxaline monomers **M4-M9** by Suzuki polycondensation reactions (toward Qx polymers applicable in OPVs), for which efficient coupling of the monomers using a precise 1:1 feed ratio is required, was not viable. It was envisaged that introducing bromine atoms in position 5 of the thiophene rings of the triads **M10-M13** would lead to a more reactive unit toward Suzuki reactions. In order to exploit this possibility and to obtain the dibrominated triads, a new synthetic pathway was required as it was expected that the presence of the ethenyl and/or butadienyl spacers could create problems. The introduction of the side chains, and in consequence the spacers, should preferably be accomplished in the final step of the synthetic protocol, the bromine atoms being already present at this point. Retrosynthetic analysis indicated that two possible pathways (A and B) could be employed for the synthesis of the target triads **M14-M17** (Scheme 5.5). The introduction of the conjugated side chains could be achieved passing by bisphosphonate intermediate **12**. The latter could be synthesized by direct bromination of triad **11** or could be generated *in situ* by treatment of derivative **9** with triethyl phosphite. For pathway A, precursor **9** could be obtained by direct bromination of triad **8** in the presence of *N*-bromosuccinimide (NBS). The quinoxaline core **8** could be obtained by sulfur extrusion followed by condensation with 1,4-dibromo-2,3-butanedione (**5**). The Suzuki cross coupling reaction could thus be performed at the

precursor stage, between thiophene-2-boronic acid and 4,7-dibromo-2,1,3-benzothiadiazole (**2**) or, alternatively, 2-bromothiophene and 2,1,3-benzothiadiazole-4,7-bis(boronic acid pinacol ester) (**13**). In pathway B, bisphosphonate triad **11** could be synthesized by Suzuki coupling between Qx **10** and thiophene-2-boronic acid.

Following synthetic pathway A (Scheme 5.6.), the synthesis of Qx monomer **M17** could be accomplished. Initial screening of the Suzuki coupling reaction between thiophene-2-boronic acid and 4,7-dibromo-2,1,3-benzothiadiazole (**2**), using a series of conditions in which the base (K_2CO_3 and CsF), the solvent (toluene, toluene:H_2O and 1,2-dimethoxyethane) and the palladium catalyst ($PdCl_2$(dppf) and $Pd(PPh_3)_4$) were varied, showed rather poor efficiency of the coupling reaction. The major products isolated were the starting material **2** and the mono-coupled product, which were accompanied by very low amounts of the expected bicoupled product **7**. These three derivatives being very hard to separate by column chromatography, we have tempted to push the reaction toward the formation of compound **7** by treating the crude reaction mixture with an additional amount of thiophene-2 boronic acid. This resulted in full conversion of the mixture to the bicoupled product.

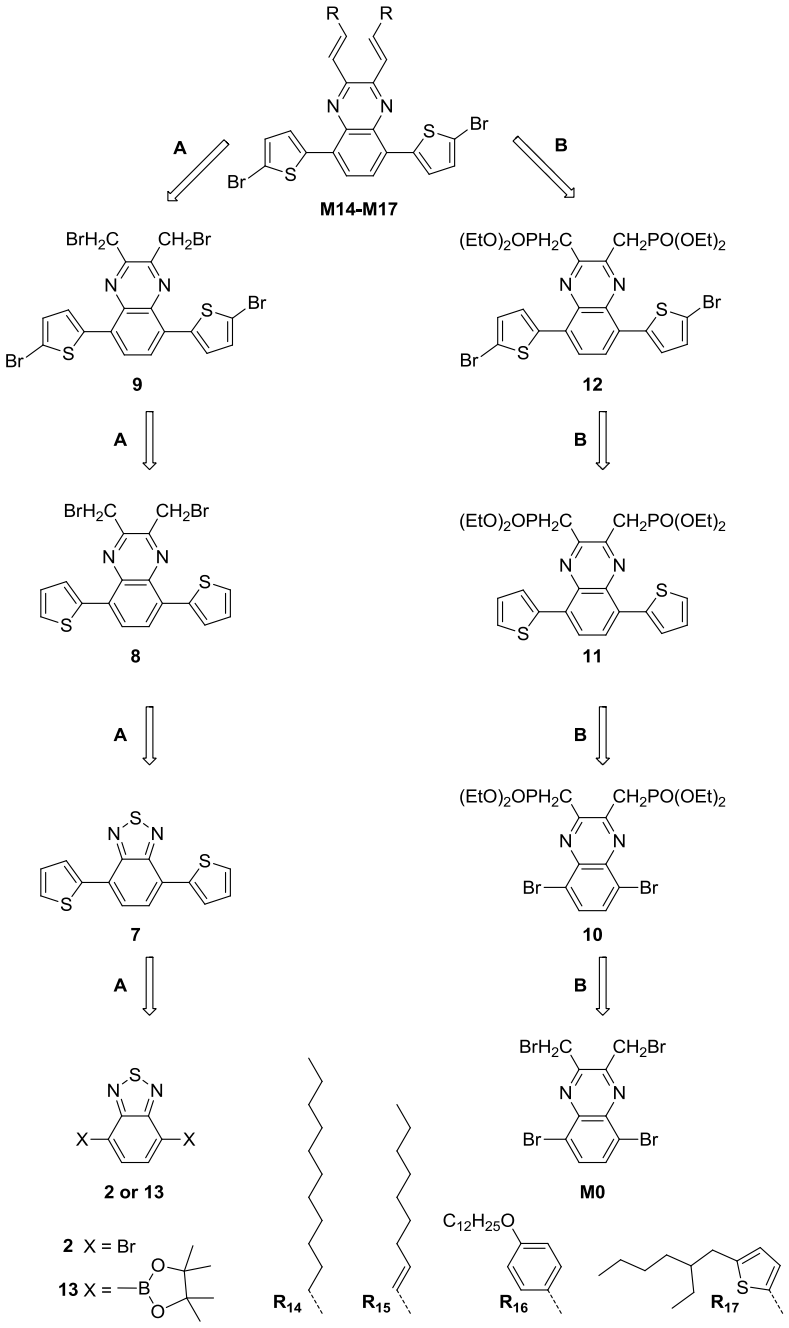

Scheme 5.5. Retrosynthetic analysis for the dibrominated triads **M14**-**M17**.

Introduction of bromine atoms in triad **7** was successful, but further treatment with $LiAlH_4$ (in view of generating the corresponding diamine) resulted in a cleavage of the bromine atoms and afforded, upon condensation with 1,4-dibromo-2,3-butanedione (**5**), the non-brominated derivative **8** instead of triad **9**. The thiophene bromination step leading to **9** was therefore postponed and performed on triad **8** (which was smoothly obtained from **7**).

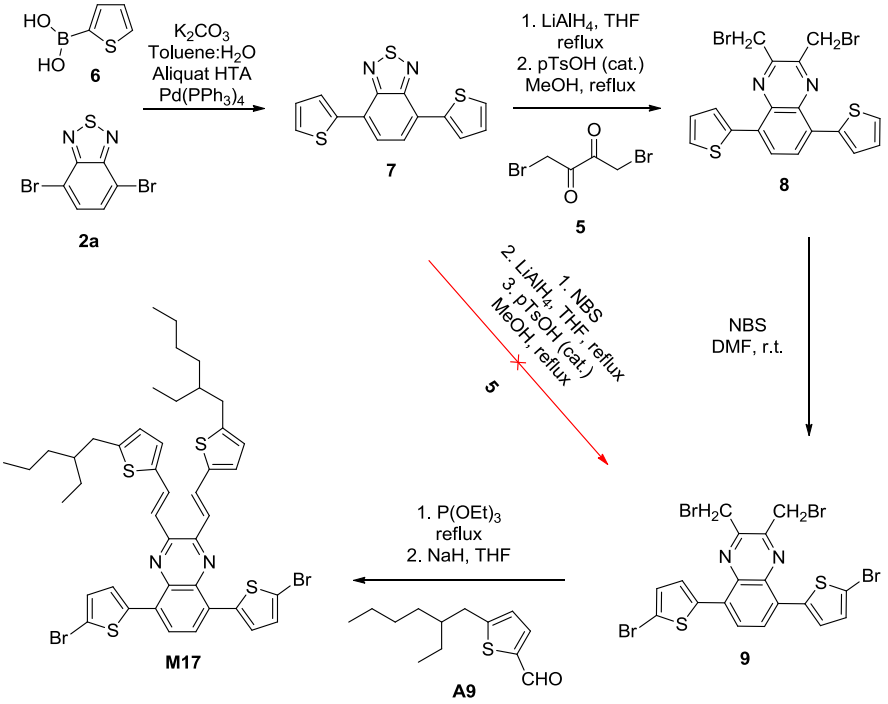

Scheme 5.6. Synthesis of Qx monomer **M17** bearing adjacent 2-bromothiophene units.

Treatment of triad **7** with $LiAlH_4$ resulted in the formation of the corresponding diamine. Due to the very unstable character of this derivative, it was used further on as isolated upon extraction and was immediately employed in the acid mediated condensation with 1,4-dibromo-2,3-butanedione (**5**), which led to the formation of derivative **8**, albeit in low overall yield (12%). Subsequent bromination in the presence of NBS afforded dibrominated derivative **9**. Generation of intermediate **12** upon treatment with triethyl phosphite, followed by basic treatment and reaction with an aldehyde, can provide access to derivatives **M14**-**M17** (Scheme 5.5). Being interested

in derivatives that possess the broadest possible absorption windows, and bearing in mind the solubility issues of the derivatives with alkoxyphenylene substituents, only the synthesis of dibrominated triad **M17** was pursued.

Following (retro)synthetic pathway B, derivative **10** resulted as the sole reaction product upon reaction of quinoxaline **M0** and triethyl phosphite. Subsequent Suzuki coupling using an excess of thiophene-2-boronic acid (6.0 equiv) afforded triad **11**. Derivative **12** was then obtained by direct bromination of **11** with NBS. Basic treatment of **12** with NaH, followed by reaction with aldehyde **A7**, led to the formation of monomer **M17** in low yield. The very polar nature of the phosphonate functionalities present in compounds **11** and **12** makes work-up, purification and isolation (by means of column chromatography) very difficult, time-consuming and renders this synthetic route inefficient.

Preliminary polymerization reactions between dibrominated triad **M17**, isolated as a purple solid, and 2,1,3-benzothiadiazole-4,7-bis(boronic acid pinacol ester) (**13**) resulted in insoluble green polymers. The reason could be that the two branched side chains present on the quinoxaline unit are not sufficient for rendering the resulting polymers soluble. As a result, the introduction of additional solubilizing side chains on the thiophene units was investigated.

The most straightforward and facile manner to accomplish this was the introduction of alkyl (hexyl) side chains in position 3 of the thiophene rings. For this purpose, the synthesis of 2-bromo-3-hexylthiophene (**14**) (Scheme 5.7) was performed following a literature procedure.[19] Subsequent Suzuki coupling with 2,1,3-benzothiadiazole-4,7-bis(boronic acid pinacol ester) (**13**) afforded triad **15**. This approach was by far more efficient than in the previous case (synthesis of **7**), the yields and selectivity of the reaction being clearly superior for the bicoupled product. The main drawback of this reaction is the relatively expensive derivative **13**, but the atom economy (2.5 *vs* 6 equiv) of the reaction strongly favors this route. The following steps in the synthetic protocol were identical as for the synthesis of **M17**. The final triad **M18** was isolated as a deep orange oil. The introduction of 3-hexylthiophene groups led to significant modifications in the physical properties of the final monomer, for which purification was much facilitated as a result of the increased solubility of this derivative. Incorporation of this monomer in low band gap copolymers will most probably grant good solubility to the resulting polymers.

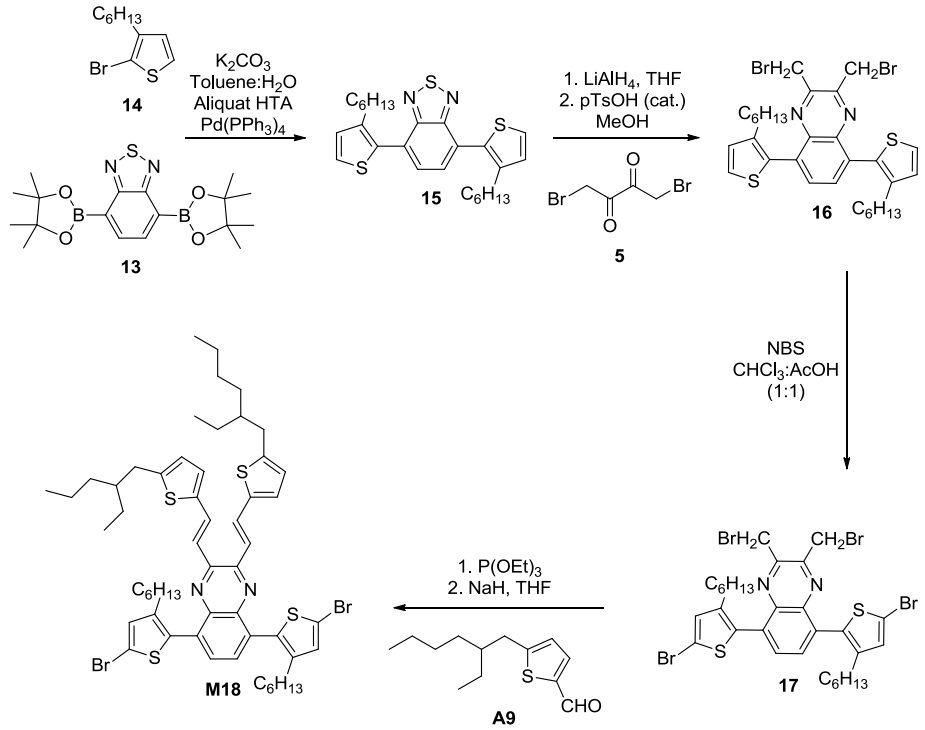

Scheme 5.7. Synthesis of triad **M18**, bearing solubilizing hexyl groups on the adjacent thiophene units.

The optical properties of this macromonomer (Figure 5.3) make it attractive to be incorporated in low band gap materials, of which the properties can be further tuned by varying the comonomer. The presence of hexyl groups on the adjacent thiophene rings of **M18**, introduced for granting solubility to the final polymers, led to a slight decrease of the conjugation compared to **M17**, for which the structure adopted a more planar configuration.

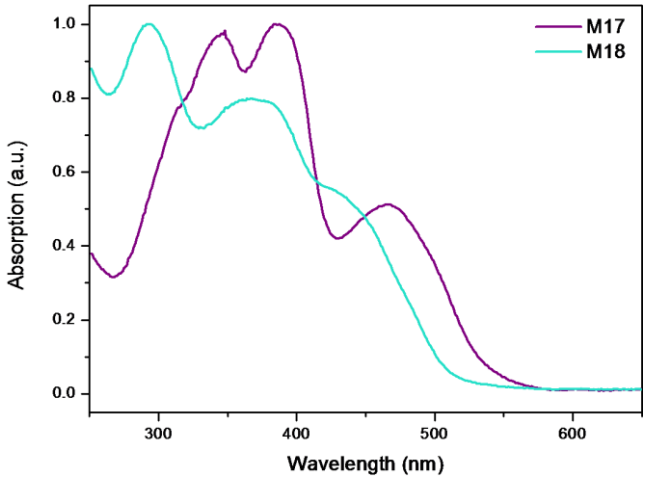

Figure 5.3. UV-Vis spectra (normalized, from chloroform solution) of donor-acceptor-donor triads **M17-M18**.

5.3. Conclusions

In this paper we have reported on the synthesis of a series of novel 2D-conjugated quinoxaline derivatives with absorption windows extended into the visible range of the solar spectrum. This was accomplished by the introduction of ethenyl or butadienyl spacers between the required solubilizing alkyl side chains and the quinoxaline core. This led to a broadening of the absorption window by approximately a factor of two, mainly due to the apparition of a second band in the low energy part of the spectrum, having its origin in the intramolecular charge transfer from the donor side chains to the electron poor quinoxaline core. In an attempt to extend the conjugation in the horizontal direction as well, various synthetic protocols toward thiophene-Qx-thiophene triads were explored. A rather low reactivity of the Qx derivatives toward Suzuki cross coupling reactions was noticed. Preliminary polycondensation reactions (*e.g.* Suzuki and/or Stille) using the corresponding dibrominated triads have shown promising results. The introduction of additional solubilizing groups on the thiophene units in the backbone was proven to be crucial to render the polymers soluble. The synthesis of low band gap polymers incorporating these Qx building blocks and the evaluation of these materials in BHJ organic solar cells will be reported in a separate forthcoming paper.

5.4. Experimental Section

NMR chemical shifts (δ, in ppm) were determined relative to the residual $CHCl_3$ absorption (7.26 ppm) or the ^{13}C resonance shift of $CDCl_3$ (77.16 ppm). Gas chromatography-mass spectrometry (GC-MS) analyses were carried out applying Chrompack Cpsil5CB or Cpsil8CB capillary columns. Exact mass measurements were performed in the EI mode at a resolution of 10000. Molecular weights and molecular weight distributions were determined relative to polystyrene standards (Polymer Labs) by gel permeation chromatography (GPC). Chromatograms were recorded on a Spectra Series P100 (Spectra Physics) equipped with two mixed-B columns (10 µm, 0.75 cm x 30 cm, Polymer Labs) and a refractive index detector (Shodex) at 40 °C. THF was used as the eluent at a flow rate of 1.0 mL min^{-1}. Solution UV-Vis absorption measurements were performed with a scan rate of 600 nm min^{-1} in a continuous run from 200 to 800 nm. Infrared spectra were collected with a resolution of 4 cm^{-1} (16 scans) using films drop-cast on a NaCl disk from a $CHCl_3$ solution. Unless stated otherwise, all reagents and chemicals were obtained from commercial sources and used without further purification. Diethyl ether and tetrahydrofuran (THF) were dried prior to use by distillation from Na/benzophenone. 2,1,3-Benzothiadiazole-4,7-bis(boronic acid pinacol ester) (95%) (**13**) was obtained from Sigma Aldrich and used without further purification. Diones **4** were obtained from commercial sources.

4,7-Dibromo-2,1,3-benzothiadiazole (**2**),[11] 3,6-dibromo-*o*-phenylenediamine (**3**),[20] 2,3-diphenyl-5,8-dibromoquinoxaline (**M1**),[21] and 4-(dodecyloxy)benzaldehyde (**A7**)[22] were synthesized according to literature procedures. Material identity and purity was confirmed by GC-MS and ^1H NMR.

5,8-Dibromo-2,3-bis(bromomethyl)quinoxaline (M0): **General procedure 1**: A mixture of 3,6-dibromo-*o*-phenylenediamine (**3**) (0.778 g, 2.92 mmol), 1,4-dibromobutane-2,3-dione (**5**) (0.713 g, 2.92 mmol), and a catalytic amount of *p*-toluenesulfonic acid (*p*-TsOH) (0.055 g, 10 mol%) in methanol (15 mL) was reacted at reflux temperature for 3 h. The resulting mixture was allowed to cool to r.t. and the yellow precipitate was filtered off and washed with methanol. Column chromatography (silica, eluent 30% $CHCl_3$ in hexane) afforded **M0** as amber crystals (1.251 g, 91%). Material identity and purity were confirmed by GC-MS and ^1H NMR.[15b]

5,8-Dibromo-2,3-bis(thiophen-2-yl)quinoxaline (M2): According to general procedure 1: **3** (0.800 g, 3.00 mmol), 1,2-di(thiophen-2-yl)ethane-1,2-dione (0.670 g, 3.00 mmol), *p*-TsOH (0.057 g, 10 mol%), methanol (40 mL), eluent 30% $CHCl_3$ in hexane, yellow-green solid (1.159 g, 85%). GC-MS (EI) *m/z* 450/452/454 [M^+]; ^{1}H NMR (300 MHz, $CDCl_3$) δ 7.84 (s, 2H), 7.56 (dd, *J* = 0.9/3.6 Hz, 2H), 7.48 (dd, *J* = 0.9/2.7 Hz, 2H), 7.05 (dd, *J* = 2.7/3.6 Hz, 2H); ^{13}C NMR (75 MHz, $CDCl_3$) δ 147.4, 141.0, 138.9, 133.3, 130.6, 130.3, 127.9, 123.2.

5,8-Dibromo-2,3-bis(5-(2-ethylhexyl)thiophen-2-yl)quinoxaline (M3): According to general procedure 1: **3** (0.236 g, 0.89 mmol), 1,2-bis[5-(2-ethylhexyl)thien-2-yl]ethane-1,2-dione (0.396 g, 0.89 mmol), *p*-TsOH (0.015 g, 10 mol%), methanol (20 mL), eluent 10% $CHCl_3$ in hexane, yellow-green solid (0.401 g, 66%). MS (CI) *m/z* 675/677/679 [MH^+]; ^{1}H NMR (300 MHz, $CDCl_3$) δ 7.78 (s, 2H), 7.40 (d, *J* = 2.7 Hz, 2H), 6.70 (d, *J* = 2.7 Hz, 2H), 2.80 (d, *J* = 5.1 Hz, 4H), 1.68-1.62 (m, 2H), 1.40-1.25 (m, 16H), 0.93-0.90 (m, 12H); ^{13}C NMR (75 MHz, $CDCl_3$) δ 150.9, 147.3, 138.5, 132.7, 130.4, 126.1, 122.9, 41.5, 34.6, 32.5, 28.9, 25.7, 23.1, 14.3, 10.9.

5,8-Dibromo-2,3-di((*E*)-tridec-1-en-1-yl)quinoxaline (M4): **General procedure 2**: **M0** (1.100 g, 2.32 mmol) was dissolved in triethyl phosphite (5 mL) and the mixture was reacted at 165 ^{o}C for 2 h. The excess of triethyl phosphite was then removed under reduced pressure. The residue (orange solid) was dissolved in THF (50 mL) and transferred by cannula to a suspension of NaH (0.188 g, 4.70 mmol) in THF (50 mL), cooled at 0 ^{o}C. The mixture was allowed to react for 1 h at 0 ^{o}C, and then a solution of dodecenal (**A4**) (0.942 g, 5.10 mmol) in THF (50 mL) was added dropwise and the mixture was reacted at r.t. overnight. The solid, recovered by filtration, was purified by column chromatography (silica, eluent 30% $CHCl_3$ in hexane) to afford a slightly yellow solid (1.007 g, 67%). GC-MS (EI) *m/z* 646/648/650 [M^+]; ^{1}H NMR (300 MHz, $CDCl_3$) δ 8.16 (d, *J* = 15.3 Hz, 2H), 7.78 (s, 2H), 7.66 (d, *J* = 8.6 Hz, 4H), 7.52 (d, *J* = 15.3 Hz, 2H), 6.96 (d, *J* = 8.6 Hz, 4H), 4.02 (t, *J* = 6.0 Hz, 4H), 1.82 (m, 4H) 1.51-1.19 (br m, 36H), 0.88 (t, *J* = 6.3 Hz, 6H); ^{13}C NMR (75 MHz, $CDCl_3$) δ 150.0, 144.5, 139.6, 132.2, 123.9, 123.5, 33.7, 32.1, 29.83, 29.80, 29.77, 29.67, 29.58, 29.50, 28.9, 22.8, 14.3; mp 57 °C

5,8-Dibromo-2,3-di((1*E*,3*E*)-undeca-1,3-dien-1-yl)quinoxaline (M5): According to general procedure 2: **M0** (1.100 g, 2.32 mmol), triethyl phosphite (5 mL), THF (50

mL), NaH (0.188 g, 4.70 mmol), THF (50 mL), *trans*-2-decenal (**A5**) (0.725 g, 4.70 mmol), THF (50 mL), eluent 30% $CHCl_3$ in hexane, yellow solid (0.801 g, 59%). GC-MS (EI) *m/z* 586/588/590 [M^+]; ^{1}H NMR (300 MHz, $CDCl_3$) δ 7.85-7.77 (m, 4H), 6.93 (d, *J* = 15.0 Hz, 2H), 6.45-6.37 (m, 2H), 6.27-6.18 (m, 2H), 2.28-2.21 (m, 4H), 1.58-1.20 (br m, 16H), 0.90 (t, *J* = 6.9 Hz, 6H); ^{13}C NMR (75 MHz, $CDCl_3$) δ 150.8, 143.6, 141.3, 140.1, 132.7, 130.8, 124.0, 123.0, 51.6, 33.9, 32.6, 29.9, 29.7, 23.4, 14.8; mp 89 °C

5,8-Dibromo-2,3-bis((*E*)-4-methoxystyryl)quinoxaline (M6): **General procedure 3**: **M0** (4.500 g, 9.50 mmol) was dissolved in triethyl phosphite (20 mL) and the mixture was reacted at 165 ^{o}C for 2 h. The excess of triethyl phosphite was then removed under reduced pressure and the residue (orange solid) was subsequently dissolved in THF (100 mL). The mixture was cooled to 0 ^{o}C and a solution of MeMgBr (3.0 M in diethyl ether, 6.40 mL) was added dropwise. The mixture was allowed to react for 30 minutes at r.t., then *p*-anisaldehyde (2.723 g, 20.0 mmol) was added and the mixture was reacted at r.t. overnight. The reaction was quenched by the addition of a saturated NH_4Cl solution and the mixture was extracted with $CHCl_3$. The organic extracts were dried over $MgSO_4$, filtered and concentrated by evaporation *in vacuo*. The residue was purified by column chromatography (silica, eluent $CHCl_3$) to afford a light-orange solid (4.210 g, 80%). MS (EI) *m/z* 552/554/556 [M^+]; ^{1}H NMR (300 MHz, $CDCl_3$) δ 8.19 (d, *J* = 15.3 Hz, 2H), 7.78 (s, 2H), 7.67 (d, *J* = 8.9 Hz, 4H), 7.54 (d, *J* = 15.3 Hz, 2H), 6.97 (d, *J* = 8.9 Hz, 4H), 3.88 (s, 6H); ^{13}C NMR (75 MHz, $CDCl_3$) δ 160.9, 150.3, 139.8, 139.7, 132.3, 129.6, 129.3, 123.5, 119.1, 114.5, 55.6; mp 229 °C

5,8-Dibromo-2,3-bis((*E*)-4-(dodecyloxy)styryl)quinoxaline (M7): According to general procedure 2: **M0** (4.998 g, 10.6 mmol), triethyl phosphite (20 mL), THF (100 mL), NaH (0.885 g, 22.2 mmol), THF (50 mL), 4-dodecyloxybenzaldehyde (**A7**) (6.428 g, 22.2 mmol), THF (50 mL), eluent 30% $CHCl_3$ in hexane, bright-yellow solid (6.417 g, 71%). GC-MS (EI) *m/z* 858/860/862 [M^+]; ^{1}H NMR (300 MHz, $CDCl_3$) δ 8.16 (d, *J* = 15.3 Hz, 2H), 7.78 (s, 2H), 7.66 (d, *J* = 8.6 Hz, 4H), 7.52 (d, *J* = 15.3 Hz, 2H), 6.96 (d, *J* = 8.6 Hz, 4H), 4.02 (t, *J* = 6.0 Hz, 4H), 1.82 (m, 4H) 1.51-1.19 (br m, 36H), 0.88 (t, *J* = 6.3 Hz, 6H); ^{13}C NMR (75 MHz, $CDCl_3$) δ 161.1, 150.9, 140.4, 140.2, 132.8, 130.1, 129.6, 124.0, 119.4, 115.5, 66.8, 32.6, 30.4, 30.34, 30.28, 30.10, 30.05, 29.9, 26.7, 23.4, 14.8.

5,8-Dibromo-2,3-bis((*E*)-2-(thien-2-yl)vinyl)quinoxaline (M8): According to general procedure 3: **M0** (1.000 g, 2.11 mmol), triethyl phosphite (5 mL), THF (10 mL), MeMgBr (3.0 M in diethyl ether, 1.50 mL), thiophene-2-carbaldehyde (**A8**) (0.515 g, 4.60 mmol), THF (100 mL), eluent 30% $CHCl_3$ in hexane, light-green solid (0.639 g, 60%). GC-MS (EI) *m/z* 502/504/506 [M^+]; ^{1}H NMR (300 MHz, $CDCl_3$) δ 8.33 (d, J = 15.3 Hz, 2H), 7.79 (s, 2H), 7.43-7.37 (m, 6H), 7.12-7.09 (m, 2H); ^{13}C NMR (75 MHz, $CDCl_3$) δ 148.5, 140.9, 138.7, 131.7, 131.5, 129.1, 127.3, 126.4, 122.5, 119.1.

2-(2-Ethylhexyl)thiophene: *n*-BuLi (2.5 M in hexane, 50 mL) was added dropwise to a THF (50 mL) solution of thiophene (10.500 g, 125 mmol) cooled to -40 ^{o}C. The mixture was allowed to react at this temperature for 1 h, and then at r.t. for an additional 1 h. 2-Ethylhexyl bromide (22.140 g, 125 mmol) was added dropwise and the reaction was continued overnight. The mixture was poured in cold water (100 mL) and extracted with hexane. The organic extracts were dried over $MgSO_4$, filtered and concentrated by evaporation *in vacuo*. The residue was purified by vacuum distillation (92 ^{o}C, 2.0 mbar) to afford a colorless oil (8.543 g, 58%). GC-MS (EI) *m/z* 196 [M^+]; ^{1}H NMR (300 MHz, $CDCl_3$) δ 7.12 (dd, J = 1.2/5.1 Hz, 1H), 6.92 (dd, J = 3.3/5.1 Hz, 1H), 6.73 (dd, J = 1.2/3.3 Hz, 1H), 2.77 (d, J = 6.6 Hz, 2H), 1.62-1.55 (m, 1H), 1.39-1.29 (m, 8H), 0.87 (t, J = 7.2 Hz, 6H); ^{13}C NMR (75 MHz, $CDCl_3$) δ 144.5, 126.7, 125.1, 123.0, 41.6, 34.0, 32.5, 29.0, 25.6, 23.2, 14.3, 11.0.

5-(2-Ethylhexyl)thiophene-2-carbaldehyde (A9): To a solution of 2-(2-ethylhexyl)thiophene (3.927 g, 20.0 mmol) in THF (100 mL), cooled at -78 ^{o}C, *n*-BuLi (2.5 M in hexane, 8.0 mL) was added dropwise and the mixture was allowed to react for 1 h at this temperature and 1 h at r.t. *N*-Formylpiperidine (2.263 g, 20 mmol) was added at -78 ^{o}C and the mixture was further reacted at r.t. overnight. The reaction was quenched by the addition of HCl (2.0 M, 50 mL), and the mixture was extracted with CH_2Cl_2. The organic extracts were dried over $MgSO_4$, filtered and concentrated by evaporation *in vacuo*. The residue was purified by column chromatography (silica, eluent 10% ethyl acetate in hexane) to afford a light-yellow oil (3.679 g, 82%). GC-MS (EI) *m/z* 224 [M^+]; ^{1}H NMR (300 MHz, $CDCl_3$) δ 9.81 (s, 1H), 7.60 (d, J = 3.9 Hz, 1H), 6.88 (d, J = 3.9 Hz, 1H), 2.80 (d, J = 6.7 Hz, 2H), 1.66-1.61 (m, 2H), 1.35-1.25 (m, 8H), 0.90 (m, 6H); ^{13}C NMR (75 MHz, $CDCl_3$) δ 182.3, 156.1, 141.7, 136.8, 126.7, 41.2, 34.6, 32.1, 28.6, 25.3, 22.7, 13.9, 10.6.

5,8-Dibromo-2,3-bis((*E*)-2-(5-(2-ethylhexyl)thien-2-yl)vinyl)quinoxaline (M9): According to general procedure 2: **M0** (2.188 g, 4.62 mmol), triethyl phosphite (10 mL), THF (50 mL), NaH (0.374 g, 9.36 mmol), THF (50 mL), 5-(2-ethylhexyl)thiophene-2-carbaldehyde (**A9**) (2.100 g, 9.36 mmol), THF (50 mL), eluent 30% $CHCl_3$ in hexane, orange oil (1.891 g, 56%). MS (EI) *m/z* 726/728/730 [M^+]; ^{1}H NMR (300 MHz, $CDCl_3$) δ 8.27 (d, J = 15.1 Hz, 2H), 7.76 (s, 2H), 7.27 (d, J = 15.1 Hz, 2H), 7.18 (d, J = 3.6 Hz, 2H), 6.76 (d, J = 3.6 Hz, 2H), 2.80 (d, J = 3.1 Hz, 4H), 1.69-1.61 (m, 2H) 1.44-1.25 (br m, 16H), 0.95-0.90 (m, 12H); ^{13}C NMR (75 MHz, $CDCl_3$) δ 149.8, 147.9, 139.9, 139.6, 133.2, 132.3, 130.6, 126.6, 123.4, 118.8, 41.6, 34.8, 32.5, 29.0, 25.7, 23.2, 14.3, 11.0.

Poly[2,3-bis((*E*)-4-(dodecyloxy)styryl)quinoxaline-5,8-diyl] (P1): $Ni(cod)_2$ (0.970 g, 3.48 mmol) and 2,2'-bipyridine (0.543 g, 3.48 mmol) were placed in a Schlenk tube inside a glove box. DMF (5 mL), toluene (5 mL) and 1,5-cyclooctadiene (0.376 g, 3.48 mmol), degased by bubbling through N_2 gas for 20 minutes, were added and the mixture was vigorously stirred for 20 minutes at 60 ^{o}C. A solution of **M7** (1.248 g, 1.45 mmol) in toluene (22 mL) was then added and the mixture was allowed to react for 2 days at 75 ^{o}C. The polymer was poured in a solution of methanol:HCl (600 mL, 1:1, v/v), collected by filtration and purified by repetitive Soxhlet extraction with methanol, acetone and hexane. The final polymer was extracted with chloroform and was isolated as yellow fibers upon precipitation in methanol (0.978 g, 96%); UV-Vis ($CHCl_3$, nm) λ_{max} 334/359/411; GPC (THF, PS standards) M_n = 6.8 x 10^4 g mol^{-1}, M_w = 4.1 x 10^5 g mol^{-1}, PDI = 6.0.

2,3-Bis[(*E*)-4-(dodecyloxy)styryl]-5,8-di(thien-2-yl)quinoxaline (M10): **General procedure 4**: **M7** (108 mg, 0.13 mmol), thiophene-2-boronic acid (100 mg, 0.78 mmol, 6 equiv) and CsF (118 mg, 0.78 mmol) were placed in a Schlenk tube and dissolved in DME (10 mL). The mixture was degassed by bubbling through N_2 gas for 20 minutes, and then $PdCl_2$(dppf) (3mol%) was added, the tube was sealed and the mixture was reacted at 90 ^{o}C overnight. After cooling to r.t., water was added and the mixture was extracted with $CHCl_3$. The organic extracts were dried over $MgSO_4$, filtered and concentrated by evaporation *in vacuo*. The residue was purified by column chromatography (silica, eluent 30% $CHCl_3$ in hexane), followed by recrystallization from methanol to afford a dark-red solid (58.6 mg, 52%). MS (EI) *m/z* 867 [M^+]; ^{1}H

NMR (300 MHz, $CDCl_3$) δ 8.25 (d, J = 15.5 Hz, 2H), 8.04 (s, 2H), 7.82 (dd, J = 1.1/3.7 Hz, 2H), 7.66 (d, J = 8.7 Hz, 4H), 7.56 (d, J = 15.5 Hz, 2H), 7.55 (dd, J = 1.1/5.1 Hz, 2H), 7.21 (dd, J = 3.7/5.1 Hz, 2H), 6.97 (d, J = 8.7 Hz, 4H), 4.02 (t, J = 6.6 Hz, 4H), 1.87-1.78 (m, 4H), 1.51-1.44 (m, 4H), 1.40-1.25 (br m, 32H), 0.89 (t, J = 6.9 Hz, 6H); ^{13}C NMR (75 MHz, $CDCl_3$) δ 160.3, 148.4, 139.4, 139.1, 137.9, 131.0, 129.5, 129.3, 128.9, 126.6, 126.5, 126.2, 120.0, 115.0, 68.3, 32.1, 29.82, 29.80, 29.77, 29.74, 29.57, 29.50, 29.4, 26.2, 22.9, 14.3.

2,3-Bis((*E*)-2-(5-(2-ethylhexyl)thien-2-yl)vinyl)-5,8-di(thien-2-yl)quinoxaline (M11): According to general procedure 4: **M9** (0.298 g, 0.41 mmol), thiophene-2-boronic acid (0.316 g, 2.47 mmol, 6 equiv), CsF (0.375 g, 2.47 mmol), DME (10 mL), $PdCl_2$(dppf) (3mol%), eluent 30% $CHCl_3$ in hexane, recrystallization from methanol, deep-orange solid (0.124 g, 41%). MS (EI) *m/z* 736 [M^+]; ^{1}H NMR (300 MHz, $CDCl_3$) δ 8.32 (d, J = 15.2 Hz, 2H), 8.00 (s, 2H), 7.78 (dd, J = 1.2/3.9 Hz, 2H), 7.54 (dd, J = 1.2/5.1 Hz, 2H), 7.32 (d, J = 15.2 Hz, 2H), 7.21-7.16 (m, 4H), 6.77 (d, J = 3.6 Hz, 2H), 2.81 (d, J = 6.9 Hz, 4H), 1.72-1.65 (m, 2H), 1.45-1.20 (br, 16H), 0.96-0.91 (m, 12H); ^{13}C NMR (75 MHz, $CDCl_3$) δ 147.8, 147.2, 140.4, 139.0, 137.8, 132.8, 131.0, 129.8, 128.9, 126.56, 126.50, 126.4, 126.1, 120.0, 41.6, 34.8, 31.4, 29.9, 29.0, 25.7, 14.32, 11.0.

5,8-Di(thien-2-yl)-2,3-di((*E*)-tridec-1-en-1-yl)quinoxaline (M12): According to general procedure 4: **M4** (0.388 g, 0.60 mmol), thiophene-2-boronic acid (0.460 g, 3.60 mmol), CsF (0.546 g, 3.60 mmol), DME (10 mL), $PdCl_2$(dppf) (3mol%), eluent 30% CH_2Cl_2 in hexane, deep-orange solid (0.280 g, 71%). MS (EI) *m/z* 654 [M^+]; ^{1}H NMR (300 MHz, $CDCl_3$) δ 8.03 (s, 2H), 7.80 (dd, J = 1.3/3.8 Hz, 2H), 7.51 (dd, J = 1.3/5.1 Hz, 2H), 7.47-7.37 (m, 2H), 7.18 (dd, J = 3.8/5.1 Hz, 2H), 6.95 (d, J = 15.3 Hz, 2H), 2.46-2.39 (m, 4H), 1.66-1.57 (m, 4H), 1.47-1.20 (br m, 28H), 0.88 (t, J = 6.9 Hz, 6H); ^{13}C NMR (75 MHz, $CDCl_3$) δ 147.9, 143.6, 139.1, 137.8, 131.0, 128.8, 126.6, 126.3, 126.1, 124.6, 33.7, 32.1, 29.88, 29.82, 29.7, 29.5, 29.2, 22.9, 14.3.

5,8-Di(thien-2-yl)-2,3-di[(1*E*,3*E*)-undeca-1,3-dien-1-yl]quinoxaline (M13): According to general procedure 4: **M5** (0.300 g, 0.51 mmol), thiophene-2-boronic acid (0.391 g, 3.06 mmol, 6 equiv), CsF (0.464 g, 3.06 mmol), DME (10 mL), $PdCl_2$(dppf) (3mol%), eluent 30% $CHCl_3$ in hexane, recrystallization from methanol, deep-orange solid (0.169 g, 56%). GC-MS (EI) *m/z* 594 [M^+]; ^{1}H NMR (300 MHz, $CDCl_3$) δ 7.98

(s, 2H), 7.85 (dd, *J* = 11.0/15.1 Hz, 2H), 7.77 (dd, *J* = 1.1/3.8 Hz, 2H), 7.53 (dd, *J* = 1.1/5.1 Hz, 2H), 7.18 (dd, *J* = 3.8/5.1 Hz, 2H), 6.95 (d, *J* = 15.1 Hz, 2H), 6.45-6.37 (m, 2H), 6.22-6.13 (m, 2H), 2.28-2.21 (m, 4H), 1.54-1.45 (m, 4H), 1.40-1.27 (br m, 16H), 0.92 (t, *J* = 7.0 Hz, 6H); ^{13}C NMR (75 MHz, $CDCl_3$) δ 148.2, 141.6, 140.2, 139.1, 137.7, 131.0, 130.6, 128.8, 126.5, 126.4, 126.1, 123.6, 33.3, 32.0, 29.42, 29.35, 29.2, 22.8, 14.3.

4,7-Di(thien-2-yl)-2,1,3-benzothiadiazole (7): **General procedure 5**: 4,7-dibromo-2,1,3-benzothiadiazole (0.441 g, 1.50 mmol) and thiophene-2-boronic acid (1.151 g, 9.00 mmol) were placed in a Schlenk tube which was brought under inert atmosphere. All solvents and basic solutions were previously degassed by bubbling through N_2 gas for 20 minutes. Toluene (28 mL), K_2CO_3 (2.0 M, 14 mL), H_2O (7 mL) and Aliquat HTA (4-5 drops) were added and the mixture was vigorously stirred for 10 minutes at r.t. $PdCl_2$(dppf) (3mol%) was then added and the mixture was allowed to react for 3 days at 80 ^{o}C. After cooling to r.t., the mixture was extracted with $CHCl_3$. The organic extracts were dried over $MgSO_4$, filtered and concentrated by evaporation *in vacuo*. The residue was purified by column chromatography (silica, eluent 30% $CHCl_3$ in hexane) to afford a bright orange solid (0.058 g, 13%). NOTE! The crude mixture consisted mostly of starting material **2a** and monocoupled product (0.056 g, 10%). Treatment of this mixture with additional thiophene-2-boronic acid (1.151 g, 9.00 mmol), under the same reaction conditions, led to the exclusive formation of **8**. Material identity and purity was confirmed by MS, ^{1}H NMR and ^{13}C NMR.[23]

4-Bromo-7-(thien-2-yl)-2,1,3-benzothiadiazole (monocoupled product): yellow-orange solid. GC-MS (EI) *m/z* 296/298 [M^+]; ^{1}H NMR (400 MHz, $CDCl_3$) δ 8.10 (dd, *J* = 1.1/3.6 Hz, 1H), 7.84 (d, *J* = 7.7 Hz, 1H), 7.73 (d, *J* = 7.7 Hz, 1H), 7.48 (dd, *J* = 1.1/5.1 Hz, 1H), 7.21 (dd, *J* = 3.6/5.1 Hz, 1H); ^{13}C NMR (100 MHz, $CDCl_3$) δ 153.8, 151.8, 138.5, 132.3, 128.21, 128.11, 127.4, 127.1, 125.9, 112.4.

2,3-Bis(bromomethyl)-5,8-di(thien-2-yl)quinoxaline (8): **General procedure 6**: A solution of $LiAlH_4$ (4.0 M in THF, 4.7 mL) was added dropwise to a solution of **7** (0.631 g, 2.10 mmol) in THF (50 mL). The mixture was reacted at reflux overnight. After cooling to r.t., ethanol (20 mL) and H_2O (50 mL) were added and the mixture was extracted with diethyl ether. The organic extracts were dried over $MgSO_4$, filtered and concentrated by evaporation *in vacuo*. The residue, obtained as a pale-yellow solid, was

directly used in the condensation reaction step without further purification [^{1}H NMR (400 MHz, $CDCl_3$) δ 7.37 (dd, J = 1.2/5.2 Hz, 2H), 7.19 (dd, J = 1.2/3.5 Hz, 2H), 7.14 (dd, J = 3.5/5.2 Hz, 2H), 6.88 (s, 2H), 3.88 (br s, 4H)]. 1,4-Dibromobutane-2,3-dione (**5**) (1.463 g, 6.00 mmol) and a catalytic amount of *p*-TsOH (0.035 g, 10 mol%) were added, the solids were dissolved in methanol (100 mL) and the mixture was reacted at reflux for 3 h. After cooling to r.t., the mixture was extracted with $CHCl_3$. The organic extracts were dried over $MgSO_4$, filtered and concentrated by evaporation *in vacuo*. The residue, purified by column chromatography (silica, eluent 30% $CHCl_3$ in hexane), afforded **8** as a dark-pink solid (0.121 g, 12%). GC-MS (EI) *m/z* 478/480/482 [M^+]; ^{1}H NMR (400 MHz, $CDCl_3$) δ 8.15 (s, 2H), 7.87 (dd, J = 1.1/3.8 Hz, 2H), 7.53 (dd, J = 1.1/5.1 Hz, 2H), 7.20 (dd, J = 3.8/5.1 Hz, 2H), 5.02 (s, 4H); ^{13}C NMR not recorded due to poor solubility of the product.

2,3-Bis(bromomethyl)-5,8-bis(5-bromothiophen-2-yl)quinoxaline (9): **General procedure 7**: NBS (0.065 g, 0.37 mmol) was added to a solution of **8** (0.072 g, 0.15 mmol) in DMF (70 mL). The mixture was allowed to react at r.t., protected from light, for 5 h. Water was added and the mixture was extracted with $CHCl_3$. The organic extracts were dried over $MgSO_4$, filtered and concentrated by evaporation *in vacuo*. The residue, purified by column chromatography (silica, eluent 30% $CHCl_3$ in hexane), afforded dibrominated compound **9** as a purple solid (0.071 g, 75%). GC-MS (EI) *m/z* 636/638/640 [M^+]; ^{1}H NMR (400 MHz, $CDCl_3$) δ 8.10 (s, 2H), 7.54 (d, J = 4.0 Hz, 2H), 7.12 (d, J = 4.0 Hz, 2H), 5.04 (s, 4H); ^{13}C NMR (100 MHz, $CDCl_3$) δ 150.0, 139.2, 137.5, 130.9, 129.5, 127.0, 126.3, 117.7, 29.9.

Tetraethyl[(5,8-di(thien-2-yl)quinoxaline-2,3-diyl)bis(methylene)]bis(phospho-nate) (11): **M0** (0.469 g, 0.99 mmol) was dissolved in triethyl phosphite (5 mL) and the mixture was reacted at 165 ^{o}C for 2 h. The excess of triethyl phosphite was removed under reduced pressure and the residue (orange solid) was subsequently dissolved in DME (20 mL) and placed in a Schlenk tube. Thiophene-2-boronic acid (0.767 g, 6.00 mmol) and CsF (0.911 g, 6.00 mmol) were added and the mixture was degassed by bubbling through N_2 gas for 20 minutes, then $PdCl_2$(dppf) (3mol%) was added, the tube was sealed and the mixture was reacted at 90 ^{o}C overnight. Upon cooling to r.t., water was added and the mixture was extracted with $CHCl_3$. The organic extracts were dried over $MgSO_4$, filtered and concentrated by evaporation *in vacuo*. The residue was

purified by column chromatography (silica, eluent CH_2Cl_2, then a gradient of ethyl acetate in CH_2Cl_2 from 50 to 100%, followed by pure acetone) to afford a brown-yellow oil (0.170 g, 29%). MS (ESI) *m/z* 595 $[M+H]^+$.

5,8-Bis(5-bromothiophen-2-yl)-2,3-bis((*E*)-2-(5-(2-ethylhexyl)thiophen-2-yl)vinyl)-quinoxaline (M17): According to general procedure 2: **9** (0.102 g, 0.16 mmol), triethyl phosphite (5 mL), THF (10 mL), NaH (0.014 g, 0.37 mmol), THF (25 mL), 5-(2-ethylhexyl)thiophene-2-carbaldehyde (**A9**) (0.191 g, 0.85 mmol), THF (10 mL), eluent gradient of 15 to 30% $CHCl_3$ in hexane, orange-red solid (0.051 g, 36%). MS (ESI^+) *m/z* 1808.8 $[2M+Na]^+$; ^1H NMR (400 MHz, $CDCl_3$) δ 8.31 (d, J = 15.2 Hz, 2H), 7.87 (s, 2H), 7.45 (d, J = 4.2 Hz, 2H), 7.20 (d, J = 15.2 Hz, 2H), 7.16 (d, J = 3.7 Hz, 2H), 7.09 (d, J = 4.2 Hz, 2H), 6.78 (d, J = 3.7 Hz, 2H), 2.82 (d, J = 7.0 Hz, 4H), 1.67 (m, 2H), 1.41-1.25 (br m, 30H), 0.97-0.85 (m, 12H); ^{13}C NMR (100 MHz, $CDCl_3$) δ 148.6, 148.0, 140.7, 140.2, 137.5, 134.0, 131.0, 130.5, 129.4, 127.1, 125.6, 125.3, 119.7, 117.5, 42.2, 35.4, 33.1, 29.6, 26.3, 23.8, 14.9, 11.6.

4,7-Bis(3-hexylthiophen-2-yl)-2,1,3-benzothiadiazole (15): According to general procedure 5: 2,1,3-Benzothiadiazole-4,7-bis(boronic acid pinacol ester) (**13**) (1.718 g, 4.43 mmol), 2-bromo-3-hexylthiophene (**14**) (2.741 g, 11.1 mmol, 2.5 equiv), toluene (70 mL), K_2CO_3 (2.0 M, 35 mL), H_2O (25 mL), Aliquat HTA (4-5 drops), $PdCl_2$(dppf) (3mol%), eluent 10% $CHCl_3$ in hexane, orange oil (1.492 g, 72%). MS (EI) *m/z* 468 $[M^+]$; ^1H NMR (300 MHz, $CDCl_3$) δ 7.65 (s, 2H), 7.44 (d, J = 5.2 Hz, 2H), 7.10 (d, J = 5.2 Hz, 2H), 2.66 (t, J = 7.8 Hz, 4H), 1.67-1.57 (m, 4H), 1.30-1.16 (br m, 12H), 0.82 (t, J = 7.2 Hz, 6H); ^{13}C NMR (75 MHz, $CDCl_3$) δ 154.4, 141.8, 132.3, 130.0, 129.4, 127.6, 126.0, 31.7, 30.8, 29.5, 29.2, 22.7, 14.2.

2,3-Bis(bromomethyl)-5,8-bis(3-hexylthien-2-yl)quinoxaline (16): According to general procedure 6: $LiAlH_4$ (4.0 M in THF, 0.44 mL), **15** (0.163 g, 0.35 mmol), THF (50 mL), pale-yellow solid, directly used in the condensation reaction step without further purification (GC-MS (EI) *m/z* 440 $[M^+]$). 3,6-Bis(3-hexylthiophen-2-yl)benzene-1,2-diamine, 1,4-dibromobutane-2,3-dione (**5**) (0.195 g, 0.8 mmol), *p*-TsOH (0.007 g, 10 mol%), methanol (75 mL), eluent 30% $CHCl_3$ in hexane, yellow oil (0.108 g, 48%). GC-MS (EI) *m/z* 646/648/650 $[M^+]$; ^1H NMR (300 MHz, $CDCl_3$) δ 7.82 (s, 2H), 7.43 (d, J = 5.1 Hz, 2H), 7.10 (d, J = 5.1 Hz, 2H), 4.89 (s, 4H), 2.54 (t, J = 7.8 Hz, 4H), 1.60 (m, 4H), 1.28-1.10 (br m, 12H), 0.79 (t, J = 6.9 Hz, 6H); ^{13}C NMR

(75 MHz) δ 150.4, 141.9, 140.2, 133.9, 132.5, 128.9, 125.8, 31.7, 30.8, 30.7, 29.7, 29.3, 22.7, 14.2.

5,8-Bis(5-bromo-3-hexylthien-2-yl)-2,3-bis(bromomethyl)quinoxaline (17): According to general procedure 7: NBS (0.064 g, 0.36 mmol), **16** (0.103 g, 0.16 mmol), $CHCl_3$:ethyl acetate (1:1) (13 mL), eluent 20% CH_2Cl_2 in hexane, yellow-brown oil (0.100 g, 78%). MS (EI) *m/z* 806/808 [M^+]; ^{1}H NMR (300 MHz, $CDCl_3$) δ 7.79 (s, 2H), 7.05 (s, 2H), 5.02 (s, 4H), 2.50 (t, J = 7.6 Hz, 4H), 1.60 (m, 4H), 1.27-1.17 (br m, 12H), 0.80 (t, J = 6.9 Hz, 6H); ^{13}C NMR (75 MHz, $CDCl_3$) δ 150.4, 142.6, 139.9, 133.8, 133.1, 132.3, 131.7, 113.1, 44.2, 31.7, 30.5, 29.6, 29.2, 22.7, 14.2.

5,8-Bis(5-bromo-3-hexylthien-2-yl)-2,3-bis((*E*)-2-(5-(2-ethylhexyl)thien-2-yl)vinyl)-quinoxaline (M18): According to general procedure 2: **17** (0.185 g, 0.23 mmol), triethyl phosphite (5 mL), THF (40 mL), NaH (0.019 g, 0.50 mmol), THF (40 mL), 5-(2-ethylhexyl)thiophene-2-carbaldehyde (**A9**) (0.148 g, 0.66 mmol), THF (25 mL), eluent 10% $CHCl_3$ in hexane, orange-red oil (0.110 g, 45%). MS (ESI+) *m/z* 1062.8 [M+H]$^+$; ^{1}H NMR (300 MHz, $CDCl_3$) δ 8.32 (d, J = 15.0 Hz, 2H), 7.83 (s, 2H), 7.46 (s, 2H), 7.45 (d, J = 15.0 Hz, 2H), 7.31 (d, J = 3.3 Hz, 2H), 6.94 (d, J = 3.3 Hz, 2H), 2.99 (d, J = 6.6 Hz, 4H), 2.83 (d, J = 7.5 Hz, 4H), 1.86-1.76 (m, 2H), 1.61-1.36 (br m, 28H), 1.15-0.98 (br m, 18H); ^{13}C NMR (75 MHz, $CDCl_3$) δ 147.9, 147.3, 141.9, 140.1, 139.4, 134.8, 132.5, 131.9, 131.4, 130.2, 129.9, 126.5, 119.5, 113.0, 41.6, 34.8, 32.5, 31.7, 30.8, 29.7, 29.2, 29.0, 25.7, 23.2, 22.7, 14.3, 14.2, 11.0.

5.5. References

(1) Joseph, S.; Ruth, S. *J. Phys. D: Appl. Phys.* **2008**, *41*, 133001.

(2) (a) Zhang, M.; Tsao, H. N.; Pisula, W.; Yang, C.; Mishra, A. K.; Müllen, K. *J. Am. Chem. Soc.* **2007**, *129*, 3472; (b) Lee, J. S.; Son, S. K.; Song, S.; Kim, H.; Lee, D. R.; Kim, K.; Ko, M. J.; Choi, D. H.; Kim, B.; Cho, J. H. *Chem. Mater.* 2012, *24*, 1316.

(3) Delgado, J. L.; Bouit, P.-A.; Filippone, S.; Herranz, M. A.; Martin, N. *Chem. Commun.* **2010**, *46*, 4853.

(4) (a) Sun, Y.; Welch, G. C.; Leong, W. L.; Takacs, C. J.; Bazan, G. C.; Heeger, A. J. *Nat. Mater.* **2012**, *11*, 44; (b) Mishra, A.; Bäuerle, P. *Angew. Chem. Int. Ed.* **2012**, *51*, 2020; (c) Schwenn, P. E.; Gui, K.; Nardes, A. M.; Krueger, K. B.; Lee, K. H.; Mutkins, K.; Rubinstein-Dunlop, H.; Shaw, P. E.; Kopidakis, N.; Burn, P. L.; Meredith, P. *Adv. Energy Mater.* **2011**, *1*, 73; (d) Li, G.; Zhu, R.; Yang, Y. *Nat. Photon.* **2012**, *6*, 153.

(5) (a) Biniek, L.; Fall, S.; Chochos, C. L.; Anokhin, D. V.; Ivanov, D. A.; Leclerc, N.; Lévêque, P.; Heiser, T. *Macromolecules* **2010**, *43*, 9779; (b) Egbe, D. A. M.; Adam, G.; Pivrikas, A.; Ramil, A. M.; Birckner, E.; Cimrova, V.; Hoppe, H.; Sariciftci, N. S. *J. Mater. Chem.* **2010**, *20*, 9726; (c) Szarko, J. M.; Guo, J.; Liang, Y.; Lee, B.; Rolczynski, B. S.; Strzalka, J.; Xu, T.; Loser, S.; Marks, T. J.; Yu, L.; Chen, L. X. *Adv. Mater.* **2010**, *22*, 5468; (d) Mavrinskiy, A.; Nielsen, C. B.; Reynolds, J. R.; Müllen, K.; Pisula, W. *Chem. Mater.* **2011**, *23*, 1939.

(6) Duan, R.; Ye, L.; Guo, X.; Huang, Y.; Wang, P.; Zhang, S.; Zhang, J.; Huo, L.; Hou, J. *Macromolecules* **2012**, *45*, 3032.

(7) (a) Champion, R. D.; Cheng, K.-F.; Pai, C.-L.; Chen, W.-C.; Jenekhe, S. A. *Macromol. Rapid Commun.* **2005**, *26*, 1835; (b) Chang, D. W.; Lee, H. J.; Kim, J. H.; Park, S. Y.; Park, S.-M.; Dai, L.; Baek, J.-B. *Org. Lett.* **2011**, *13*, 3880.

(8) (a) Kitazawa, D.; Watanabe, N.; Yamamoto, S.; Tsukamoto, J. *Appl. Phys. Lett.* **2009**, *95*, 053701; (b) Li, H.; Tam, T. L.; Lam, Y. M.; Mhaisalkar, S. G.; Grimsdale, A. C. *Org. Lett.* **2010**, *13*, 46; (c) Zhang, J.; Cai, W.; Huang, F.; Wang, E.; Zhong, C.; Liu, S.; Wang, M.; Duan, C.; Yang, T.; Cao, Y. *Macromolecules* **2011**, *44*, 894; (d) He, Z.; Zhang, C.; Xu, X.; Zhang, L.; Huang, L.; Chen, J.; Wu, H.; Cao, Y. *Adv. Mater.* **2011**, *23*, 3086; (e) Cheng, Y.-J.; Wu,

J.-S.; Shih, P.-I.; Chang, C.-Y.; Jwo, P.-C.; Kao, W.-S.; Hsu, C.-S. *Chem. Mater.* **2011**, *23*, 2361; (f) Zhang, X.; Shim, J. W.; Tiwari, S. P.; Zhang, Q.; Norton, J. E.; Wu, P.-T.; Barlow, S.; Jenekhe, S. A.; Kippelen, B.; Bredas, J.-L.; Marder, S. R. *J. Mater. Chem.* **2011**, *21*, 4971; (g) Lee, S. K.; Lee, W.-H.; Cho, J. M.; Park, S. J.; Park, J.-U.; Shin, W. S.; Lee, J.-C.; Kang, I.-N.; Moon, S.-J. *Macromolecules* **2011**, *44*, 5994; (h) Popere, B. C.; Della Pelle, A. M.; Thayumanavan, S. *Macromolecules* **2011**, *44*, 4767; (i) Huang, Y.; Zhang, M.; Ye, L.; Guo, X.; Han, C. C.; Li, Y.; Hou, J. *J. Mater. Chem.* **2012**, *22*, 5700; (j) Wang, E.; Hou, L.; Wang, Z.; Hellström, S.; Zhang, F.; Inganäs, O.; Andersson, M. R. *Adv. Mater.* **2010**, *22*, 5240.

(9) Meshram, H. M.; Santosh Kumar, G.; Ramesh, P.; Chennakesava Reddy, B. *Tetrahedron Lett.* **2010**, *51*, 2580.

(10) Tsami, A.; Yang, X.-H.; Farrell, T.; Neher, D.; Holder, E. *J. Polym. Sci., Part A: Polym. Chem.* **2008**, *46*, 7794.

(11) Pilgram, K.; Zupan, M.; Skiles, R. *J. Heterocycl. Chem.* **1970**, *7*, 629.

(12) Edelmann, M. J.; Raimundo, J.-M.; Utesch, N. F.; Diederich, F.; Boudon, C.; Gisselbrecht, J.-P.; Gross, M. *Helv. Chim. Acta* **2002**, *85*, 2195.

(13) Lee, B. H.; Jaung, J. Y.; Cho, J.-w.; Yoon, K. J. *Polym. Bull.* **2003**, *50*, 9.

(14) Yamamoto, T.; Sugiyama, K.; Kushida, T.; Inoue, T.; Kanbara, T. *J. Am. Chem. Soc.* **1996**, *118*, 3930.

(15) (a) Tsami, A.; Yang, X.-H.; Galbrecht, F.; Farrell, T.; Li, H.; Adamczyk, S.; Heiderhoff, R.; Balk, L. J.; Neher, D.; Holder, E. *J. Polym. Sci., Part A: Polym. Chem.* **2007**, *45*, 4773; (b) Huo, L.; Tan, Z. a.; Zhou, Y.; Zhou, E.; Han, M.; Li, Y. *Macromol. Chem. Phys.* **2007**, *208*, 1294; (c) Huo, L.; Tan, Z. a.; Wang, X.; Zhou, Y.; Han, M.; Li, Y. *J. Polym. Sci., Part A: Polym. Chem.* **2008**, *46*, 4038.

(16) (a) Milstein, D.; Stille, J. K. *J. Am. Chem. Soc.* **1978**, *100*, 3636; (b) Miyaura, N.; Suzuki, A. *Chem. Rev.* **1995**, *95*, 2457.

(17) Bidan, G.; De Nicola, A.; Enée, V.; Guillerez, S. *Chem. Mater.* **1998**, *10*, 1052.

(18) (a) Cammidge, A. N.; Crepy, K. V. L. *Chem. Commun.* **2000**, 1723; (b) Van Mierloo, S.; Hadipour, A.; Spijkman, M.-J.; Van den Brande, N.; Ruttens, B.; Kesters, J.; D'Haen, J.; Van Assche, G.; de Leeuw, D. M.; Aernouts, T.; Manca, J.; Lutsen, L.; Vanderzande, D. J.; Maes, W. *Chem. Mater.* **2012**, *24*, 587.

(19) Van Mierloo, S.; Chambon, S.; Boyukbayram, A. E.; Adriaensens, P.; Lutsen, L.; Cleij, T. J.; Vanderzande, D. *Magn. Reson. Chem.* **2010**, *48*, 362.

(20) Naef, R.; Balli, H. *Helv. Chim. Acta* **1978**, *61*, 2958.

(21) Yamamoto, T.; Zhou, Z.-h.; Kanbara, T.; Shimura, M.; Kizu, K.; Maruyama, T.; Nakamura, Y.; Fukuda, T.; Lee, B.-L.; Ooba, N.; Tomaru, S.; Kurihara, T.; Kaino, T.; Kubota, K.; Sasaki, S. *J. Am. Chem. Soc.* **1996**, *118*, 10389.

(22) Lensen, M. C.; Elemans, J. A. A. W.; van Dingenen, S. J. T.; Gerritsen, J. W.; Speller, S.; Rowan, A. E.; Nolte, R. J. M. *Chem. Eur. J.* **2007**, *13*, 7948.

(23) Beaujuge, P. M.; Ellinger, S.; Reynolds, J. R. *Adv. Mater.* **2008**, *20*, 2772.

Chapter 6

Synthesis and Photovoltaic Performance of Poly(thienoquinoxaline) Low Band Gap Copolymers with Conjugated Side Chains

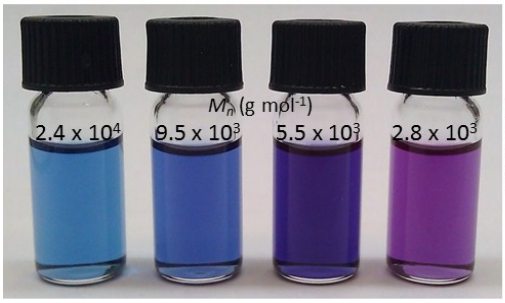

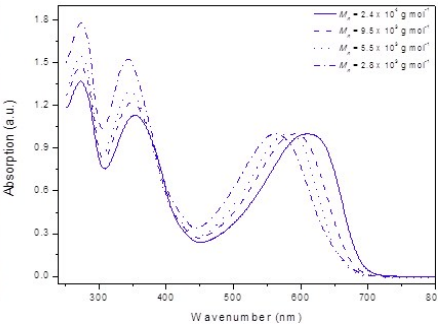

6.1. Introduction

Over the last decade, the architectures and the materials employed in the fabrication of organic (polymer) solar cells have recorded remarkable advances, which allows nowadays the production (and commercialization) of lightweight and relatively cheap organic photovoltaic (OPV) modules, which are manufactured by roll to roll printing on flexible substrates. Efforts to develop new conjugated polymers for OPVs have nowadays led to materials that afford power conversion efficiencies (PCEs) as high as 10%.[1] In general, the amount of light a photoactive material can absorb goes hand in hand with the amount of energy a solar cell can produce. Means of maximizing this feature, for instance, consist in the development of conjugated polymers which additionally absorb in the near-IR region of the solar spectrum, *i.e.* the low energy side. The trivial appellation of such materials is low band gap polymers.[2] The most common approach used in the synthesis of such materials is the alternation of electron rich and electron poor (heterocyclic) units along the polymer backbone.[3] By varying the electron donating and accepting strength of the building blocks, one can fine tune the energy levels of the conjugated polymers.[4] 2,1,3-Benzothiadiazole is among the strongest electron poor units used in the synthesis of highly efficient materials, of which poly[2,6-(4,4-bis(2-ethylhexyl)-4*H*-cyclopenta[2,1-*b*;3,4-*b*′]dithiophene)-*alt*-4,7-(2,1,3-benzothiadiazole)] (PCPDTBT) is the most well-known example.[5] The weaker benzotriazole acceptor, or its fluorinated variant, have been incorporated in semiconducting copolymers affording PCEs above 7%.[6] Quinoxaline (Qx) derivatives show an average electron acceptor strength. Side chains can easily be introduced in positions 2 and 3, which grant solubility and facile processability to the photoactive materials, a highly required feature for fast (roll to roll) printing of (organic) optoelectronic devices. Due to their electron deficient character, Qx units can be used for the synthesis of (electron) acceptor (n-type) polymers. In combination with poly(3-hexylthiophene) (P3HT), which served as the donor material, modest PCEs have been achieved in "all polymer" bulk heterojunction (BHJ) solar cells.[7] The low device performance was attributed to the poor electron mobility of the acceptor material. The largest number of donor-acceptor (D-A) polymers incorporating Qx units along the conjugated backbone are used as (electron) donor (p-type) materials.[8] Among the most popular ones, the alternating polyfluorene (APFO) series and poly(thienoquinoxaline)

derivatives (such as TQ1) have delivered PCEs close to 6%, in combination with a fullerene acceptor.[9]

In this paper we present the synthesis and photovoltaic performances of a series of poly(thienoquinoxaline) derivatives, **P1**-**P3**. The novelty of these materials consists in the Qx units, in which a two dimensional (2D) conjugation[10] is created by introducing ethenyl and/or butadienyl spacers between the solubilizing donating side chains and the electron accepting quinoxaline core. At the monomer stage, the contribution of the vertical conjugation leads to a noticeable extension of the absorption window toward the visible range of the spectrum.[11] All polymers were synthesized by Stille polycondensation reactions. The photovoltaic performance of the donor materials was evaluated in BHJ solar cells, with normal or inverted configuration, in combination with $PC_{61}BM$ and/or $PC_{71}BM$ as an acceptor.

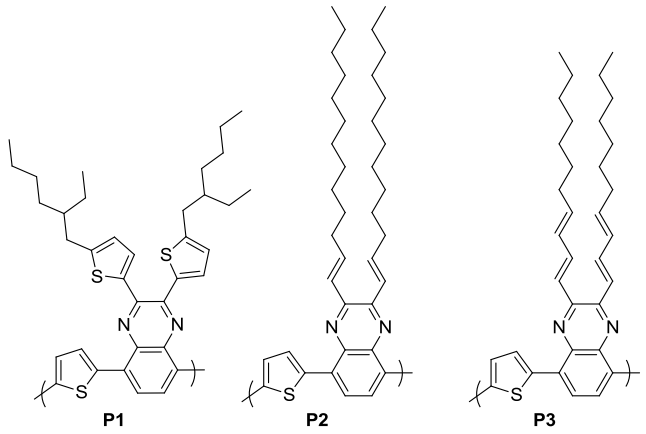

Figure 6.1. Structures of the synthesized poly(thienoquinoxaline) polymers **P1**-**P3**.

6.2. Results and Discussion

6.2.1. Synthesis and Characterization of Poly(thienoquinoxaline) Derivatives P1-P3

The synthesis of the quinoxaline monomer **M1**, having 5-(2-ethylhexyl)thienyl substituents directly connected to the quinoxaline core, was readily achieved in three steps starting from 2,1,3-benzothiadiazole (**1**) (Scheme 6.1). Bromination using a mixture of Br_2 and HBr followed by sulfur extrusion in the presence of $NaBH_4$ afforded the corresponding diamine **3**. Subsequently, **M1** was obtained by condensation of

diamine **3** with diketone **4**. Polymer **P1** was synthesized by Stille polycondensation, under conventional heating, in combination with 2,5-bis(tributylstannyl)thiophene (**5**), obtained from commercial sources. The polymerization was performed in a sealed tube using toluene as a solvent. The reaction, catalyzed by tetrakis(triphenylphosphine)-palladium ($Pd(PPh_3)_4$), was continued for 5 days at 100 ^oC. End-capping was performed in two stages, by addition of 2-tributylstannylthiophene (4 equiv) and 2-bromothiophene (2 equiv), respectively. Purification of the polymer was done by repetitive Soxhlet extraction with methanol, acetone, hexane and dichloromethane. The final polymer **P1** was extracted with chlorobenzene and was isolated as a dark green powder upon precipitation in methanol (M_n = 5.0 x 10^3 g mol^{-1}, M_w = 9.5 x 10^3 g mol^{-1}, PDI = 1.9, as determined by gel permeation chromatography (GPC) from a chlorobenzene solution at 80 ^oC) (Table 6.1).

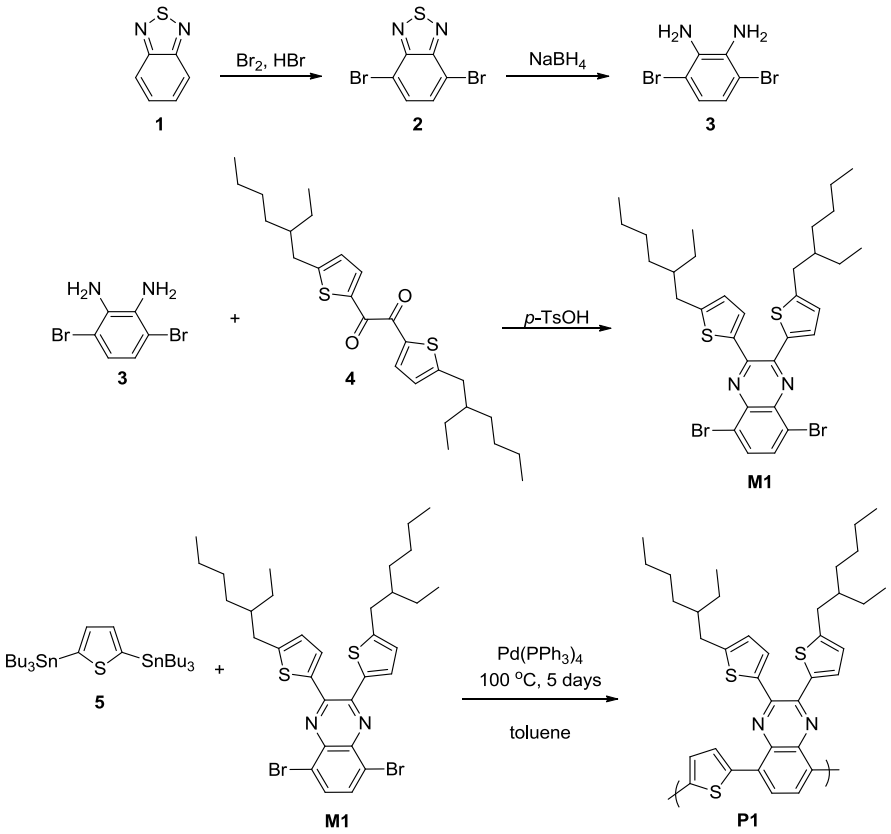

Scheme 6.1. Synthesis of quinoxaline monomer **M1** and poly(thienoquinoxaline) **P1**.

Table 6.1. Analytical GPC data (THF) of polymers **P1**-**P3** obtained from different batches and after purification.

Polymer	M_n (g mol^{-1})	M_w (g mol^{-1})	PDI
P1[a,b]	5.0 x 10^3	9.5 x 10^3	1.9
P2[b]	5.7 x 10^3	1.1 x 10^4	1.9
P2'[b]	1.3 x 10^4	3.4 x 10^4	2.6
P2'$_{GPC\_1}$[b,c]	1.6 x 10^4	3.5 x 10^4	2.2
P2'$_{GPC\_2}$[b,c]	2.6 x 10^4	4.0 x 10^4	1.5
P2'$_{GPC\_3}$[b,c]	5.5 x 10^3	6.1 x 10^3	1.1
P2'$_{GPC\_4}$[b,c]	2.8 x 10^3	3.2 x 10^3	1.1
P2''[b,d]	8.3 x 10^3	2.0 x 10^4	2.4
P3[b,c]	8.8 x 10^3	2.6 x 10^4	2.9
P3$_{GPC_1}$[b,e]	1.3 x 10^4	3.5 x 10^4	2.7
P3$_{GPC_2}$[b,e]	1.6 x 10^4	4.0 x 10^4	2.5
P3$_{GPC_3}$[b,e]	1.5 x 10^4	4.5 x 10^4	3.0
P3'[e,f]	6.5 x 10^3	1.5 x 10^4	2.3

[a] determined from CB; [b] conventional heating, [c] after Soxhlet extraction, the polymer was additionally purified and fractionated by preparative GPC; [d] an excess of 0.05 mol% of 2,5-bis(trimethylstannyl)thiophene (**8**) was used; [e] heated by microwave irradiation; [f] GPC result of the crude polymer.

The synthesis of monomers **M2** and **M3** was achieved passing by quinoxaline precursor **7** (Scheme 6.2). The latter was obtained by condensation of 3,6-dibromo-*o*-phenylenediamine (**3**) and 1,4-dibromobutane-2,3-dione (**6**). Transformation of the methylene bromide groups in phosphonates, followed by proton abstraction and treatment with dodecanal or *trans*-2-decenal afforded monomers **M2** and **M3**, respectively. The corresponding polymers, **P2** and **P3**, were initially synthesized by Stille polycondensation in combination with 2,5-bis(tributylstannyl)thiophene (**5**) under conventional heating conditions (*vide supra*).

The obtained molecular weights for **P1-P3** were rather low (Table 6.1), presumably due to the relatively high content of impurities present in the commercial bisstannyl product (97% pure). We have therefore further on replaced this derivative by 2,5-bis(trimethylstannyl)thiophene (**8**), synthesized by lithiation of 2,5-dibromothiophene, followed by stannylation in the presence of trimethyltin chloride. After repetitive recrystallizations from methanol, this monomer was obtained more than 99.5% pure. The latter was used in combination with **M2** and afforded the polymer denoted as **P2'**, for which indeed a higher molecular weight was obtained (Table 6.1). The final polymers **P2**/**P2'** and **P3** were isolated as dark blue powders upon precipitation in methanol. The polymers were isolated in yields ranging from 61 to 89% and their molecular weights were determined by GPC analysis (typically in THF at 40 ^{o}C).

It has previously been demonstrated that small adjustments of the stoichiometric feed of the coupling partners, deviating from the exact 1.00:1.00 ratio of the monomers which is a *conditio sine qua non* for obtaining high molecular weight polymers by step-growth polycondensation reactions, can lead to significantly higher degrees of polymerization.[12] If the catalyst used is a bivalent palladium (Pd(II)) complex, a small amount of the organostannyl derivative is presumed to be consumed in the generation of zerovalent palladium (Pd(0)).[3] In case of a Pd(0) catalyst (as in this case), the major effect causing a stoichiometric mismatch is probably the purity of the monomers. Determining the exact percentages of impurities, *e.g.* monofunctional species, residual tin derivatives, etc., can be used for compensation with a slight excess of the bisstannyl monomer, but this is not a trivial exercise.

The impact of the stoichiometry of the monomers upon the molecular weight was investigated for polymer **P2'** (Table 6.1, the resulting polymer is denoted as **P2''**). For this experiment, a polymerization reaction in which an excess of 0.05 mol% of 2,5-bis(trimethylstannyl)thiophene (**8**) was used, was carried out using conventional heating. The results showed that when the precise 1.00:1.00 stoichiometry was used (**P2'**), the number average molecular weight (M_n = 1.3 x 10^4 g mol^{-1}) was almost doubled compared to a 1.00:1.05 feed ratio of the dibrominated and organostannyl monomers (**P2''**) (M_n = 8.3 x 10^3 g mol^{-1}). This suggests that in the case where both coupling partners are highly pure (above 99.5%), and when a Pd(0) complex is used, a small stoichiometric imbalance has a negative impact on the molecular weight of the polymer.

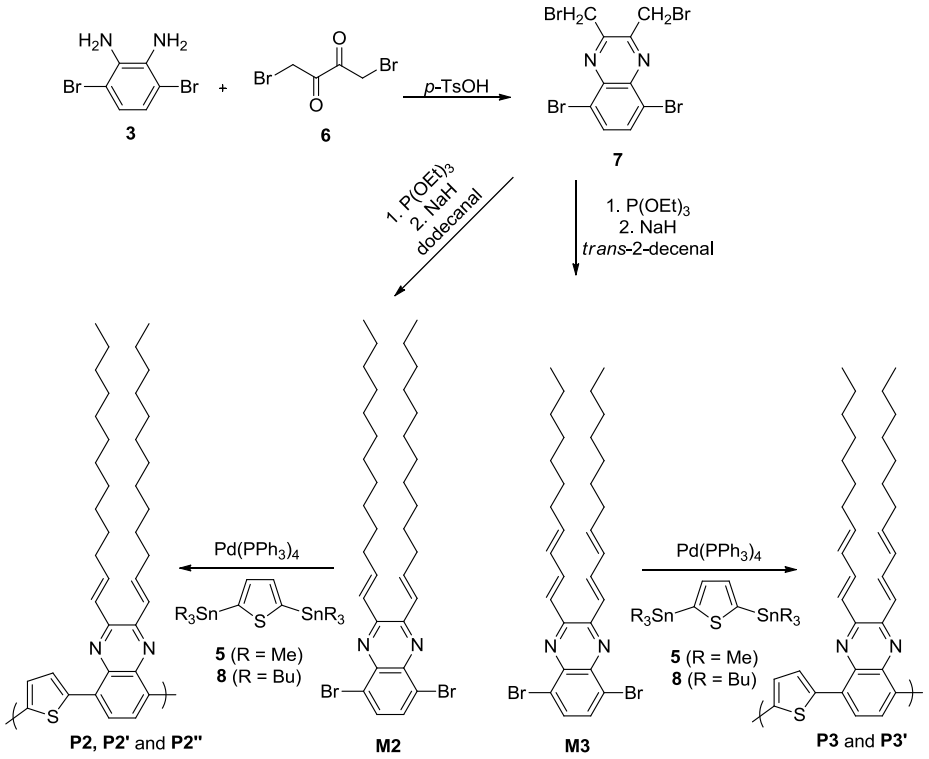

Scheme 6.2. Synthesis of monomers **M2** and **M3** and the corresponding poly(thienoquinoxaline)s **P2/P2'/ P2''** and **P3/P3'**, respectively.

Polymers **P2'** and **P3** were aditionally purified and fractionated by preparative GPC. A better fractionation of these polymers was thus possible, since these materials are extremely soluble in most organic solvents, which complicates efficient fractionation by Soxhlet extraction. The purified polymers are denoted as **P2'$_{GPC}$** and **P3$_{GPC}$**, respectively (Table 6.1). Polymer fractionation allowed to investigate the influence of the molecular weight on the solar cell performance.

The energy levels of the polymers, as determined by cyclic voltammetry, were in agreement with the values reported in literature for polymer **TQ1**, having a similar structure to polymers **P1**-**P3**.[9b] Regardless of the side chains, all polymers showed electrochemical band gaps close to 2.0 eV. The optical band gap, determined from the onset (in film) of the polymer absorption spectra, is ~1.65 eV for **P2'**/**P3** and slightly reduced for **P1**, *i.e.* 1.55 eV. The relatively large differences between the optical and

electrochemical band gaps are probably due to polymer aggregation, which complicates precise determination of the optical onset.

Table 6.2. Cyclic voltammetry data of polymers **P1-P3**.

Polymer	E^{ox}_{onset} (V)	E^{red}_{onset} (V)	HOMO (eV)	LUMO (eV)	E_g^{EC} (eV)	E_g^{OP} (eV)[a]
P1	0.43	-1.62	-5.36	-3.31	2.05	1.55
P2'	0.42	-1.48	-5.35	-3.45	1.90	1.65
P3	0.40	-1.67	-5.33	-3.26	2.07	1.66
TQ1[b]	0.47	-1.75	-5.70	-3.30	2.40	1.70

[a] In film; [b] from ref 9b.

Both in solution and in thin film polymers **P1**-**P3** displayed similar absorption spectra which were characterized by a low energy band, covering the 450-700 nm range, and a structured absorption band in the high energy part of the spectrum, between 250 and 400 nm. In thin film, the absorption maxima of these materials were red-shifted by ~50 nm (Figure 6.2). **P1** showed a high tendency to aggregate which facilitates polymer chain interactions. In this case, the onset of the absorption in thin film was red-shifted by ~100 nm compared to the one in solution. For **P2'**, which was additionally fractionated by means of preparative GPC, a nice correlation between the absorption maxima, the band gap of the material, and the number average molecular weight of the polymer was noticed (Figure 6.3).

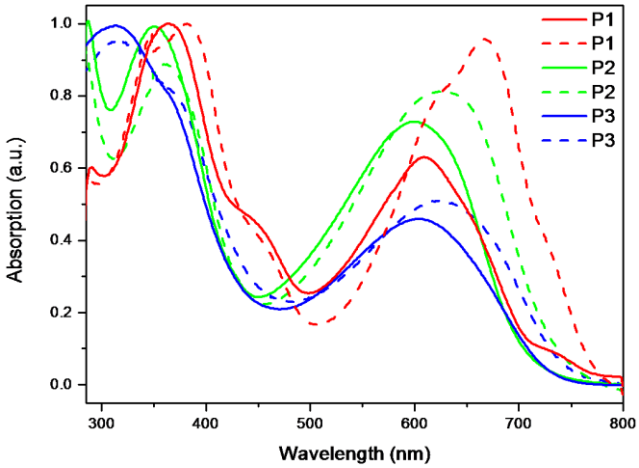

Figure 6.2. Absorption spectra of polymers **P1-P3** recorded from solution and from thin film.

6.2.2. Bulk Heterojunction Organic Solar Cells

Polymers **P1-P3** were used as (electron) donor materials in combination with a fullerene (electron) acceptor ($PC_{61}BM$ or $PC_{71}BM$) and their photovoltaic performance was evaluated in BHJ organic solar cells. Devices with a normal as well as an inverted configuration were fabricated. For the normal configuration, the BHJ solar cells had a layered structure of ITO/PEDOT:PSS/polymer:$PC_{61/71}BM$/Ca/Al. For the inverted configuration, the structure was ITO/TiO_x/polymer:$PC_{71}BM$/MoO_3/Ag. The output parameters were measured under air mass 1.5 global illumination conditions (AM 1.5G 100 mW cm^{-2}). A summary of all cells is given in Table 6.3 and some *J-V* curves are displayed in Figure 6.4.

Polymer:fullerene ratios from 1:1 to 1:3 were explored. In combination with $PC_{61}BM$ (1:3 w/w ratio), polymer **P1**, bearing aromatic side chains directly connected to the quinoxaline core, afforded 1.00% PCE. Polymers **P2** and **P3**, for which the alkyl side chains were connected by ethenyl and butadienyl linkers, showed relatively low PCEs (~ 0.16%). For **P3**, additional fractionation/purification of the polymer led to 0.45% PCE for $\mathbf{P3}_{\mathbf{GPC\_3}}$. The modest performances of these materials, and in particular for **P2** and **P3**, presumably arose from a bad active layer morphology (inhomogeneous films, as visualized by SEM).

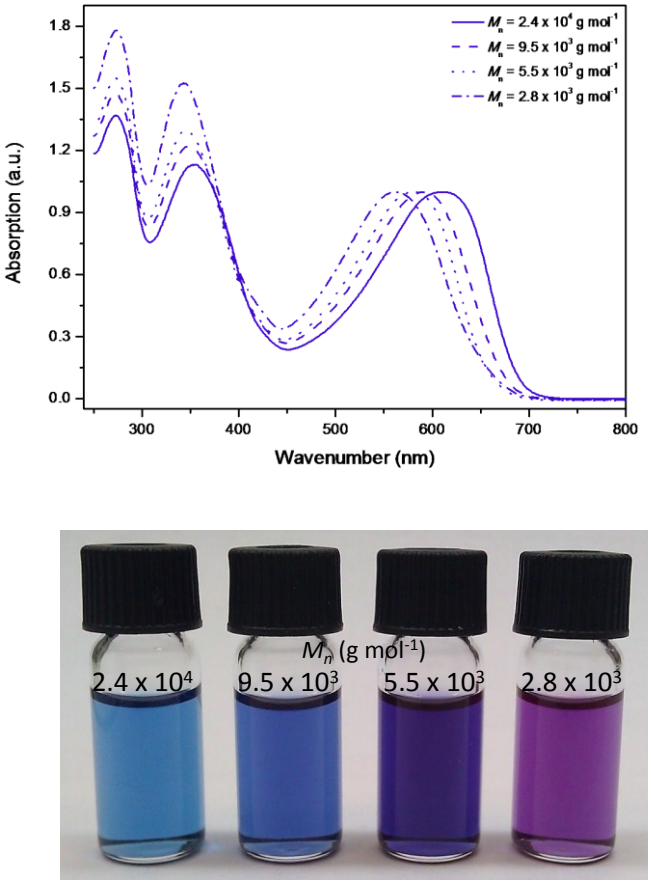

Figure 6.3. Absorption spectra recorded from $CHCl_3$ (top, normalized at the low energy band) and picture of the solutions of different **P2'** polymer fractions in THF (bottom).

In combination with $PC_{71}BM$ (1:3 (w/w) ratio), polymer **P2'**, having superior M_n values compared to **P2**, showed slightly improved output parameters (J_{sc} = 2.65 mA cm^{-2}, V_{oc} = 0.68 V, FF = 39%, PCE = 0.71%) when CB was used as the processing solvent. The addition of the processing additive 1,8-octanedithiol (ODT) led to a considerable reduction of the PCE, most probably due to an alteration of the morphology and/or the presence of residual ODT in the bulk, which can act as "hole trap". The charge transport was almost absent in solar cells for which the composite layer was prepared from chloroform solutions, suggesting a very bad morphology of the active layer. For **P2'$_{GPC\_1}$**, which had again slightly higher M_n values compared to **P2**, a PCE close to 1.00% was achieved using an inverted configuration. For **P2'$_{GPC\_1}$**, further increase of the M_n (2.6 x 10^4 g mol^{-1}) considerably improved the J_{sc} (3.16 mA cm^{-2}) and the FF

(57%), affording the highest PCE (1.44%) obtained for this polymer. Superior values for the J_{sc} are presumably due to a better morphology of the bulk and higher (hole) mobility of the high M_n polymer fraction.

Table 6.3. Solar cell performances of the poly(thienoquinoxaline) donor polymers **P1-P3**.

Donor Polymer	Processing Solvent(s)	M_n (g mol^{-1})	Ratio	V_{oc} (V)	J_{sc} (mA cm^{-2})	FF	PCE (%)
P1[a]	CB[b] + ODCB[c,d]	5.0 x 10^3	1:3	0.68	3.39	0.44	1.00
P1[e]	CB	5.0 x 10^3	1:2	0.71	7.67	0.41	2.24
P2[a]	CB[b]	5.2 x 10^3	1:3	0.38	1.16	0.35	0.16
P2[c]	ODCB[c]	5.2 x 10^3	1:2	0.56	1.01	0.27	0.15
P2'[e]	$CHCl_3$	1.3 x 10^4	1:3	0.56	0.05	0.09	0.002
P2'[e]	CB[b]	1.3 x 10^4	1:3	0.68	2.65	0.39	0.71
P2'[e]	CB[b] + ODT[f]	1.3 x 10^4	1:3	0.80	0.73	0.36	0.21
P2'$_{GPC\_1}$[e,g]	CB[b]	1.6 x 10^4	1:3	0.75	2.38	0.54	0.97
P2'$_{GPC\_1}$[e,g]	CB[b]	1.6 x 10^4	1:2	0.82	3.13	0.51	1.31
P2'$_{GPC\_2}$[e]	CB[b]	2.6 x 10^4	1:2	0.80	3.16	0.57	1.44
P2'$_{GPC\_2}$[e]	CB[b]	2.6 x 10^4	1:1	0.80	2.64	0.56	1.19
P3[a]	CB[b] + ODCB[c,d]	8.8 x 10^3	1:3	0.60	0.92	0.31	0.17
P3$_{GPC_1}$[a]	CB[b]	1.3 x 10^4	1:3	0.57	1.34	0.29	0.22
P3$_{GPC_2}$[a]	CB[b] + ODCB[c,d]	1.6 x 10^4	1:3	0.63	1.04	0.28	0.18
P3$_{GPC_3}$[a]	CB[b]	1.5 x 10^4	1:3	0.66	2.33	0.29	0.45

[a] in combination with $PC_{61}BM$; [b] CB = chlorobenzene; [c] ODCB = *ortho*-dichlorobenzene; [d] CB:ODCB = 1:1 (v/v); [e] in combination with $PC_{71}BM$; [f] ODT = 1,8-octanedithiol; [g] inverted solar cell configuration.

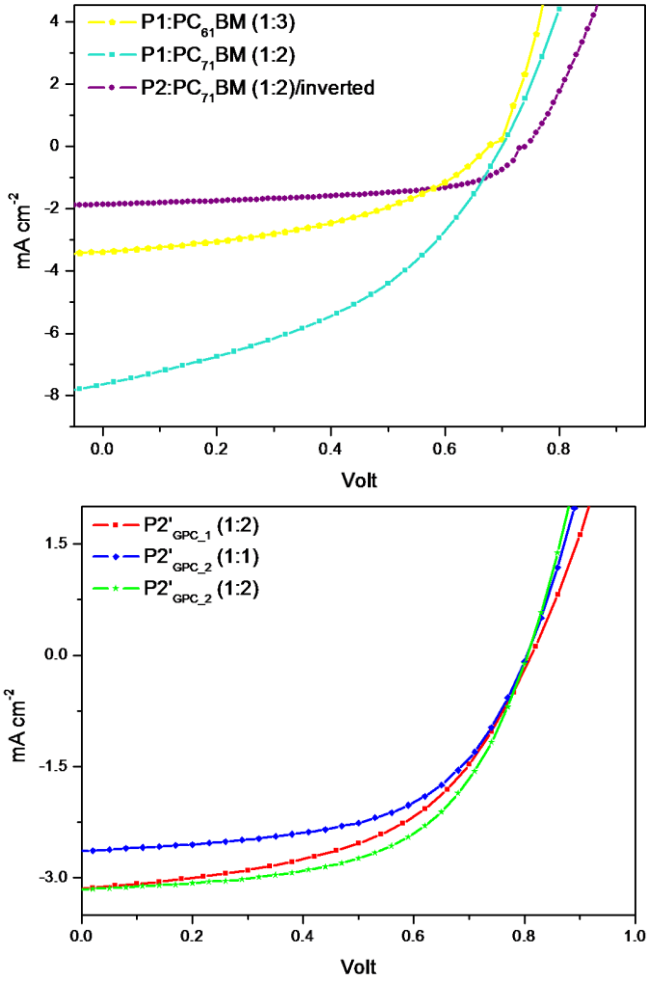

Figure 6.4. *J-V* curves for the series of BHJ solar cells fabricated with **P1** and **P2** (top) and with purified polymer **P2'** (bottom).

6.3. Conclusions

The synthesis of three poly(thienoquinoxaline) low band gap polymers **P1**-**P3** was achieved by Stille polycondensation reactions. For **P1**, the aromatic side chains were directly connected to the quinoxaline core, while for **P2** and **P3**, the alkyl side chains were connected by ethenyl and butadienyl linkers, respectively. For polymer **P2'**, synthesized in the presence of 2,5-bis(trimethylstannyl)thiophene, the M_n values of the material were considerably improved. The photovoltaic performance of the polymers **P1**-**P3**, used as (electron) donor materials in combination with $PC_{61/71}BM$ (electron)

acceptors, was low for **P2**/**P3** (~0.16%) and **P1** (~ 1.00% efficiency). Additional fractionation/purification of the polymers by preparative GPC allowed isolation of the higher M_n fractions, which showed superior charge transport, better organization features and hence afforded superior PCEs compared to the polymers isolated by simple Soxhlet extraction. For **P2'**, the optimal polymer:$PC_{71}BM$ ratio was 1:2 (w/w), the use of a 1:1 (w/w) ratio delivering lower current due to inefficient charge transfer. The highest efficiencies were obtained from **P1** (2.24%) and **P2'**$_{GPC\_2}$ (1.44%).

6.4. Experimental Section

Materials and Methods

NMR chemical shifts (δ, in ppm) were determined relative to the residual $CHCl_3$ absorption (7.26 ppm) or relative to one of the residual C_6H_5Cl absorption (7.14 ppm) of C_6D_5Cl. Gas chromatography-mass spectrometry (GC-MS) analyses were carried out applying Chrompack Cpsil5CB or Cpsil8CB capillary columns. Molecular weights and molecular weight distributions were determined relative to polystyrene standards (Polymer Labs) by gel permeation chromatography (GPC). Chromatograms were recorded on a Spectra Series P100 (Spectra Physics) equipped with two mixed-B columns (10 µm, 0.75 cm x 30 cm, Polymer Labs) and a refractive index detector (Shodex) at 40 °C. THF was most often used as the eluent at a flow rate of 1.0 mL min^{-1}. If chlorobenzene was used as the eluent, the temperature was raised to 80 °C. Preparative GPC was performed on JAIGEL *2H* and *2.5H* columns attached to a LC system equipped with a UV detector (path 0.5 mm) and a switch for recycling and collecting the eluent ($CHCl_3$: flow rate 3.5 mL min^{-1} and injection volume 1.0 mL) or on a JAI LC-92XX Next series equipped with JAIGEL *2H* and *3H* columns. Solution UV-Vis absorption measurements were performed with a scan rate of 600 nm min^{-1} in a continuous run from 1000 to 200 nm. Thin film electrochemical measurements were performed with an Eco Chemie Autolab PGSTAT 30 Potentiostat/Galvanostat using a conventional three-electrode cell under N_2 atmosphere (electrolyte: 0.1 mol L^{-1} $TBAPF_6$ in anhydrous CH_3CN). For the measurements, a $Ag/AgNO_3$ reference electrode (0.01 mol L^{-1} $AgNO_3$ and 0.1 mol L^{-1} $TBAPF_6$ in anhydrous CH_3CN), a platinum counter electrode and an indium tin oxide (ITO) coated glass substrate as working electrode were used. The polymers were deposited by drop-casting directly onto the ITO

substrates. Cyclic voltammograms were recorded at 50 mV s^{-1}. From the onset potentials of the oxidation and reduction the position of the energy levels could be estimated. All potentials were referenced using a known standard, ferrocene/ferrocenium, which in CH_3CN solution is estimated to have an oxidation potential of -4.98 eV *vs*. vacuum. Polymer bulk heterojunction solar cells were fabricated by spin coating a polymer:$PC_{61}BM$ or polymer:$PC_{71}BM$ (Solenne) blend in a 1:1, 1:2 or 1:3 w/w ratio, respectively, with or without 1,8-octanedithiol (24 mg mL^{-1}) (Sigma Aldrich) as an additive, sandwiched between a transparent anode and an evaporated metal cathode. For the normal solar cell architecture, the transparent anode was an ITO covered glass substrate which was coated with a 30 nm poly(3,4-ethylenedioxythiophene)/poly(styrenesulfonic acid) PEDOT/PSS (CLEVIOS P VP.AI 4083) layer applied by spin coating. The cathode, a bilayer of 50 nm Ca and 100 nm Al when $PC_{61}BM$ was used as acceptor or 20 nm Ca and 80 nm Al when $PC_{71}BM$ was used as acceptor, was thermally evaporated. For the inverted solar cell architecture, the transparent cathode was an ITO covered glass substrate which was coated with a 10 nm titanium oxide (TiO_x) layer applied by spin coating. The anode, a bilayer of 10 nm MoO_3 and 150 nm Ag, was thermally evaporated. The ITO glass substrate was cleaned by ultrasonification (sequentially) in soap solution, deionized water, acetone and isopropanol. For the bulk heterojunction devices the polymers and $PC_{61}BM$ (1:3 w/w ratio) or $PC_{71}BM$ (1:3 w/w ratio) were dissolved together in chlorobenzene, *ortho*-dichlorobenzene or a 1:1 (v/v) solvent mixture to give an overall 20, 30 or 40 mg mL^{-1} solution, respectively, which was stirred overnight at 80 °C inside a glovebox. Solar cell efficiencies were characterized under simulated 100 mW cm^{-2} AM 1.5 G irradiation from a Xe arc lamp with an AM 1.5 global filter.

Synthesis

Unless stated otherwise, all reagents and chemicals were obtained from commercial sources and used without further purification. 2,5-Bis(tributylstannyl)thiophene (97%) (**5**) was purchased from Sigma Aldrich and used without further purification.

2,5-Bis(trimethylstannyl)thiophene (**8**) was synthesized according to a literature procedure.[13] Material identity and purity were confirmed by GC-MS and ^{1}H NMR.

5,8-Dibromo-2,3-bis(5-(2-ethylhexyl)thiophen-2-yl)quinoxaline (M1), **5,8-dibromo-2,3-di((*E*)-tridec-1-en-1-yl)quinoxaline (M2)** and **5,8-dibromo-2,3-di((1*E*,3*E*)-**

undeca-1,3-dien-1-yl)quinoxaline (M3) were synthesized as previously reported.[11] Material identity and purity were confirmed by GC-MS and ^{1}H NMR.

Poly[2,3-bis(5-(2-ethylhexyl)thien-2-yl)quinoxaline-5,8-diyl-*alt*-thiophene-2,5-diyl] (P1): General procedure: **M1** (0.204 g, 0.301 mmol) and **5** (0.205 g, 0.310 mmol) were placed in a Schlenk tube which was brought under inert atmosphere. Toluene, degassed by bubbling through N_2 gas for 20 minutes, was added (10 mL) and the mixture was vigorously stirred for 10 minutes at r.t. $Pd(PPh_3)_4$ (3mol%) was then added and the mixture was allowed to react for 5 days at 100 ^oC. End-capping was performed in two stages by addition of 2-(tributylstannyl)thiophene (0.447 g, 1.20 mmol) and 2-bromothiophene (0.098 g, 0.60 mmol), respectively. The polymer was precipitated in methanol and purified by repetitive Soxhlet extraction with methanol, acetone, hexane and dichloromethane. The final polymer was extracted with chlorobenzene and was isolated as a dark green powder upon precipitation in methanol (0.110 g, 61%); ^{1}H NMR (300 MHz, C_6D_5Cl) δ 8.43-8.18 (br m, 2H), 7.73-7.51 (br m, 4H), 6.80-6.63 (br m, 2H), 2.98-2.86 (br m, 4H), 1.60-1.21 (br m, 18H), 0.98–0.76 (br m, 12H); UV-Vis ($CHCl_3$, nm) λ_{max} 263/366/608; UV-Vis (film, nm) λ_{max} 382/627/666; GPC (CB, PS standards) M_n = 5.0 x 10^3 g mol^{-1}, M_w = 9.5 x 10^3 g mol^{-1}, PDI = 1.9.

Poly[2,3-di((*E*)-tridec-1-en-1-yl)quinoxaline-5,8-diyl-*alt*-thiophene-2,5-diyl] (P2): According to the general procedure: **M2** (0.103 g, 0.160 mmol), **5** (0.108 g, 0.164 mmol), toluene (10 mL), $Pd(PPh_3)_4$ (3mol%), 2-(tributylstannyl)thiophene (0.238 g, 0.64 mmol), 2-bromothiophene (0.052 g, 0.32 mmol), dark blue powder (0.071 g, 78%); ^{1}H NMR (300 MHz, $CDCl_3$) δ 8.17-7.88 (br m, 6H), 7.04-6.67 (br m, 2H), 2.59-1.97 (br m, 4H), 1.50-0.96 (br m, 36H), 0.93–0.69 (br m, 6H); UV-Vis ($CHCl_3$, nm) λ_{max} 285/355/602; UV-Vis (film, nm) λ_{max} 285/363/628; GPC (THF, PS standards) M_n = 5.2 x 10^3 g mol^{-1}, M_w = 9.3 x 10^3 g mol^{-1}, PDI = 1.8.

Poly[2,3-di((*E*)-tridec-1-en-1-yl)quinoxaline-5,8-diyl-*alt*-thiophene-2,5-diyl] (P2'): According to the general procedure: **M2** (0.123 g, 0.19 mmol), **8** (0.077 g, 0.19 mmol), toluene (7 mL), $Pd(PPh_3)_4$ (3mol%), 2-(tributylstannyl)thiophene (0.283 g, 0.76 mmol), 2-bromothiophene (0.062 g, 0.38 mmol), dark blue powder (0.088 g, 81%); GPC (THF, PS standards) M_n = 1.3 x 10^4 g mol^{-1}, M_w = 3.4 x 10^4 g mol^{-1}, PDI = 2.6.

Poly[2,3-di((1*E*,3*E*)-undeca-1,3-dien-1-yl)quinoxaline-5,8-diyl-*alt*-thiophene-2,5-diyl] (P3): According to the general procedure: **M3** (0.094 g, 0.160 mmol), **5** (0.109 g,

0.164 mmol), toluene (6 mL), $Pd(PPh_3)_4$ (3mol%), 2-(tributylstannyl)thiophene (0.238 g, 0.64 mmol), 2-bromothiophene (0.052 g, 0.32 mmol), dark blue powder (0.075 g, 89%); UV-Vis ($CHCl_3$, nm) λ_{max} 313/604; UV-Vis (film, nm) λ_{max} 323/369/631; GPC (THF, PS standards) M_n = 8.8 x 10^3 g mol^{-1}, M_w = 2.6 x 10^3 g mol^{-1}, PDI = 2.9.

6.5. References

(1) Dou, L.; You, J.; Yang, J.; Chen, C.-C.; He, Y.; Murase, S.; Moriarty, T.; Emery, K.; Li, G.; Yang, Y. *Nat. Photon.* **2012**, *6*, 180.

(2) Zhou, H.; Yang, L.; You, W. *Macromolecules* **2012**, *45*, 607.

(3) Carsten, B.; He, F.; Son, H. J.; Xu, T.; Yu, L. *Chem. Rev.* **2011**, *111*, 1493.

(4) Zhou, H.; Yang, L.; Stoneking, S.; You, W. *ACS Appl. Mater. Interfaces* **2010**, *2*, 1377.

(5) Peet, J.; Kim, J. Y.; Coates, N. E.; Ma, W. L.; Moses, D.; Heeger, A. J.; Bazan, G. C. *Nat. Mater.* **2007**, *6*, 497.

(6) Price, S. C.; Stuart, A. C.; Yang, L.; Zhou, H.; You, W. *J. Am. Chem. Soc.* **2011**, *133*, 4625.

(7) (a) Falzon, M.-F.; Wienk, M. M.; Janssen, R. A. J. *J. Phys. Chem. C* **2011**, *115*, 3178; (b) Falzon, M.-F.; Zoombelt, A. P.; Wienk, M. M.; Janssen, R. A. J. *Phys. Chem. Chem. Phys.* **2011**, *13*, 8931.

(8) (a) Kitazawa, D.; Watanabe, N.; Yamamoto, S.; Tsukamoto, J. *Appl. Phys. Lett.* **2009**, *95*, 053701; (b) Li, H.; Tam, T. L.; Lam, Y. M.; Mhaisalkar, S. G.; Grimsdale, A. C. *Org. Lett.* **2010**, *13*, 46; (c) Zhang, J.; Cai, W.; Huang, F.; Wang, E.; Zhong, C.; Liu, S.; Wang, M.; Duan, C.; Yang, T.; Cao, Y. *Macromolecules* **2011**, *44*, 894; (d) He, Z.; Zhang, C.; Xu, X.; Zhang, L.; Huang, L.; Chen, J.; Wu, H.; Cao, Y. *Adv. Mater.* **2011**, *23*, 3086; (e) Cheng, Y.-J.; Wu, J.-S.; Shih, P.-I.; Chang, C.-Y.; Jwo, P.-C.; Kao, W.-S.; Hsu, C.-S. *Chem. Mater.* **2011**, *23*, 2361; (f) Zhang, X.; Shim, J. W.; Tiwari, S. P.; Zhang, Q.; Norton, J. E.; Wu, P.-T.; Barlow, S.; Jenekhe, S. A.; Kippelen, B.; Bredas, J.-L.; Marder, S. R. *J. Mater. Chem.* **2011**, *21*, 4971; (g) Lee, S. K.; Lee, W.-H.; Cho, J. M.; Park, S. J.; Park, J.-U.; Shin, W. S.; Lee, J.-C.; Kang, I.-N.; Moon, S.-J. *Macromolecules* **2011**, *44*, 5994; (h) Popere, B. C.; Della Pelle, A. M.; Thayumanavan, S. *Macromolecules* **2011**, *44*, 4767; (i) Huang, Y.; Zhang, M.; Ye, L.; Guo, X.; Han, C. C.; Li, Y.; Hou, J. *J. Mater. Chem.* **2012**, *22*, 5700.

(9) (a) Gadisa, A.; Mammo, W.; Andersson, L. M.; Admassie, S.; Zhang, F.; Andersson, M. R.; Inganäs, O. *Adv. Funct. Mater.* **2007**, *17*, 3836; (b) Wang, E.; Hou, L.; Wang, Z.; Hellström, S.; Zhang, F.; Inganäs, O.; Andersson, M. R. *Adv. Mater.* **2010**, *22*, 5240; (c) Zhang, Y.; Zou, J.; Yip, H.-L.; Chen, K.-S.; Zeigler,

D. F.; Sun, Y.; Jen, A. K. Y. *Chem. Mater.* **2011**, *23*, 2289; (d) Duan, R.; Ye, L.; Guo, X.; Huang, Y.; Wang, P.; Zhang, S.; Zhang, J.; Huo, L.; Hou, J. *Macromolecules* **2012**, *45*, 3032.

(10) (a) Huang, F.; Chen, K.-S.; Yip, H.-L.; Hau, S. K.; Acton, O.; Zhang, Y.; Luo, J.; Jen, A. K. Y. *J. Am. Chem. Soc.* **2009**, *131*, 13886; (b) Zhang, Z. G.; Zhang, S.; Min, J.; Cui, C.; Geng, H.; Shuai, Z.; Li, Y. *Macromolecules* **2012**; (c) Gu, Z.; Shen, P.; Tsang, S.-W.; Tao, Y.; Zhao, B.; Tang, P.; Nie, Y.; Fang, Y.; Tan, S. *Chem. Commun.* **2011**, *47*, 9381; (d) Gu, Z.; Tang, P.; Zhao, B.; Luo, H.; Guo, X.; Chen, H.; Yu, G.; Liu, X.; Shen, P.; Tan, S. *Macromolecules* **2012**, *45*, 2359.

(11) Marin, L.; Lutsen, L.; Vanderzande, D.; Maes, W. *Quinoxaline Derivatives with Broadened Absorption Patterns Toward Organic Photovoltaics, manuscript in progress*.

(12) Coffin, R. C.; Peet, J.; Rogers, J.; Bazan, G. C. *Nat. Chem.* **2009**, *1*, 657.

(13) Kilbinger, A. F. M.; Feast, W. J. *J. Mater. Chem.* **2000**, *10*, 1777.

Chapter 7

Quinoxaline-Based Low Band Gap Copolymers with Conjugated Side Chains for Organic Photovoltaics

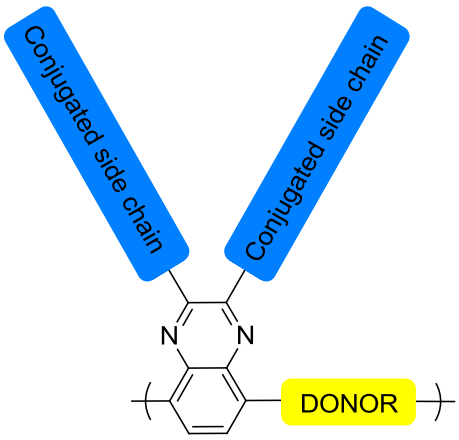

7.1. Introduction

Continuous efforts on the design and synthesis of new semiconducting polymers for organic solar cell applications and the development of new device architectures (*e.g.* tandem and inverted configurations) have steadily led to certified power conversion efficiencies (PCEs) currently exceeding the 10% threshold.[1,2] A major advantage of organic light harvesting materials is that they can be synthesized at relatively low production costs and allow fast processing from solution by roll to roll (R2R) printing of large area flexible substrates.[3] The development of low band gap conjugated polymers with absorption windows extended toward the near-IR region of the spectrum, where the photon flux is at its maximum, has played a crucial role in the recent progress that has been made in the field of organic photovoltaics (OPVs).[4]

At this moment, the record efficiency (for a tandem configuration) is held by poly[2,6′-4,8-bis(5-ethylhexylthienyl)benzo[1,2-*b*;3,4-*b*]dithiophene-*alt*-5-dibutyloctyl-3,6-bis(5-thiophen-2-yl)pyrrolo[3,4-*c*]pyrrole-1,4-dione] (**PBDTT-DPP**), a low band gap polymer in which benzo[1,2-*b*;3,4-*b*]dithiophene (BDT) donor units alternate with pyrrolo[3,4-*c*]pyrrole-1,4-dione acceptor units.[1] Numerous examples of conjugated polymers incorporating the planar BDT donor, in combination with a variety of acceptors, have proven to be efficient materials for OPV applications, with PCEs exceeding 6%.[5] One of the pioneering low band gap polymers, poly[2,6-(4,4-bis(2-ethylhexyl)-4*H*-cyclopenta[2,1-*b*;3,4-*b*′]dithiophene)-*alt*-4,7-(2,1,3-benzothiadiazole)] or **PCPDTBT**, for which a record efficiency of 5.5% was obtained in 2007, has also received considerable attention.[6] Efforts in replacing the electron poor 2,1,3-benzothiadiazole unit, while preserving the electron rich cyclopenta[2,1-*b*;3,4-*b*′]dithiophene (CPDT) moiety, have proven quite challenging for the development of highly efficient (electron) donor polymers.[7] Both BDT and CPDT were previously used in the synthesis of alternating copolymers in combination with a quinoxaline (Qx) acceptor bearing phenyl substituents or no side chains at all.[7b,8] Despite the low band gap character of these materials, the relatively low PCEs (0.2-1.2%) obtained in bulk heterojunction (BHJ) organic solar cells were mainly explained by inappropriate morphology of the active layer.

In this paper we present the synthesis of a series of two dimensionally conjugated donor-acceptor low band gap copolymers incorporating BDT/CPDT and

(bis(thieno))quinoxaline units along the polymer backbone. All quinoxaline monomers have aliphatic or heteroaromatic side chains which are separated by ethenyl and/or butadienyl spacers from the electron deficient quinoxaline core, which induces an additional vertical conjugation pathway for improved light harvesting.[9] Two polymers incorporate BDT and Qx units and are denoted as **PBDTQx1** and **PBDTQx2**. The third polymer is built from BDT and bis(thieno)quinoxaline (DTQx) units and is denoted as **PBDT-DTQx**. The fourth polymer is composed of an asymmetrically dialkyl-substituted CPDT and a Qx unit and is denoted as **PCPDT-Qx**. These polymers are evaluated as donor materials in BHJ solar cell devices.

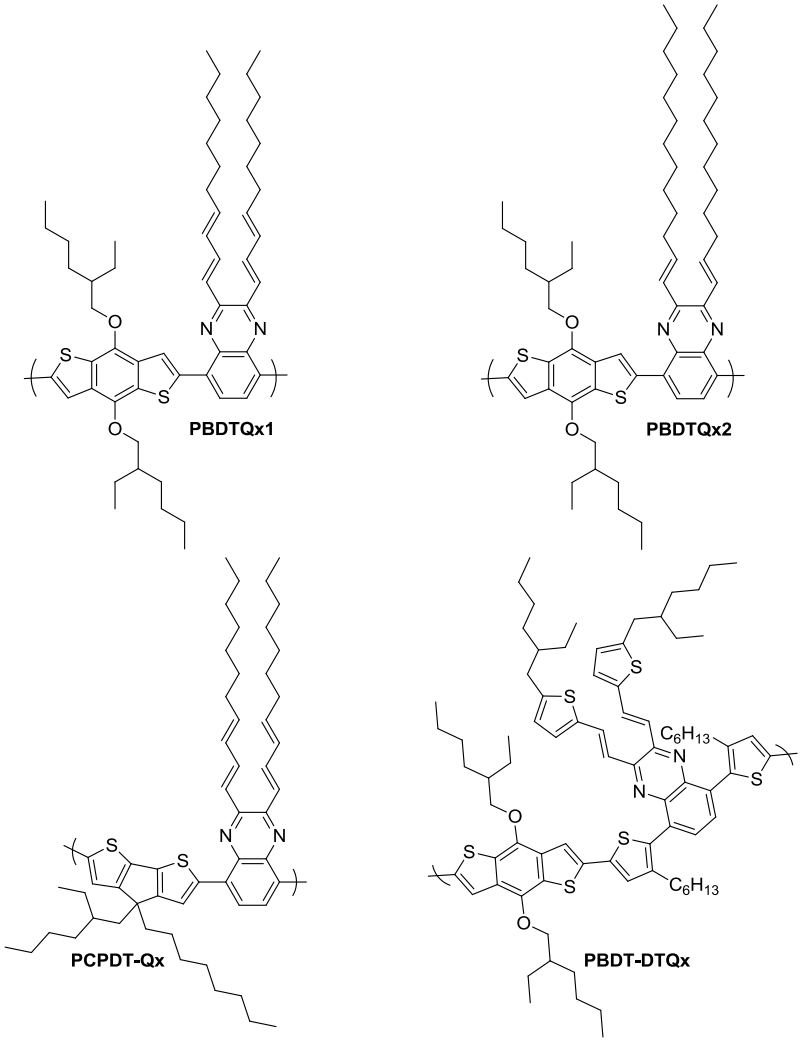

Figure 7.1. Structures of the **PBDTQx**, **PBDT-DTQx** and **PCPDT-Qx** polymers.

7.2. Results and Discussion

7.2.1. Synthesis and Characterization of the PBDTQx, PBDT-DTQx and PCPDT-Qx Polymers

The synthesis of the electron rich 4,8-bis((2-ethylhexyloxy)benzo[1,2-*b*:3,4-*b*]dithiophene-2,6-diyl)bis(trimethylstannyl) unit **D1** (Scheme 7.1) was performed according to a literature procedure, starting from thiophene-3-carboxylic acid (**1**).[5f] The latter was converted, in a first step, to the corresponding acyl chloride **2** and then to *N*,*N*-diethylthiophene-3-carboxamide (**3**). The cyclic benzo[1,2-*b*:3,4-*b*]dithiophene-4,8-dione derivative **4**, generated by treatment of the amide with *n*-butyllithium, was further reduced in the presence of Zn/NaOH to the corresponding diol. Addition of 2-ethylhexylbromide, in the presence of a catalytic amount of potassium iodide, followed by lithiation and stannylation by trimethyltin chloride, finally afforded monomer **D1** (Scheme 7.1).

The synthesis of the acceptor quinoxaline derivatives **A1**-**A3** was achieved following the synthetic protocols previously developed in our group.[9] 5,8-Dibromoquinoxalines **A1** and **A2** were obtained in four steps starting from 2,1,3-benzothiadiazole (**6**) (Scheme 7.2). Bromination, using a mixture of Br_2/HBr, followed by sulfur extrusion in the presence of $NaBH_4$ and condensation with 1,4-dibromobutane-2,3-dione (**9**) afforded 5,8-dibromo-2,3-bis(bromomethyl)quinoxaline (**10**). Treatment with triethyl phosphite, followed by proton abstraction and addition of the appropriate aldehyde, led to the formation of monomers **A1** and **A2**.

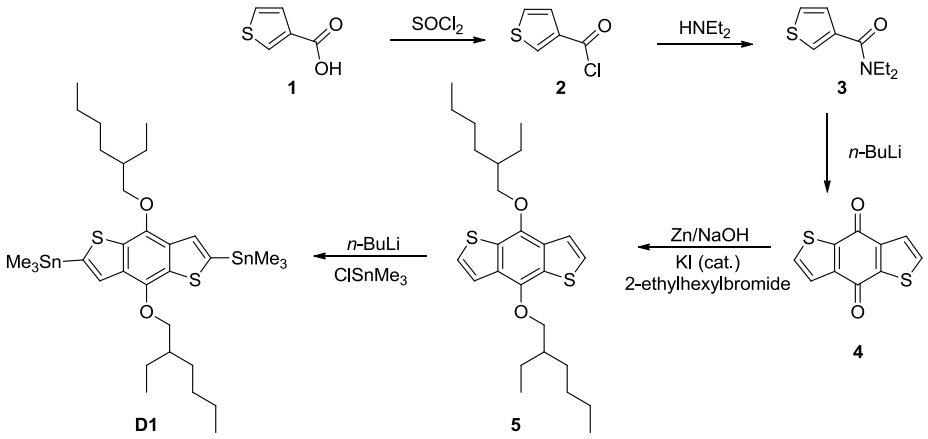

Scheme 7.1. Synthesis of the electron rich BDT monomer **D1**.

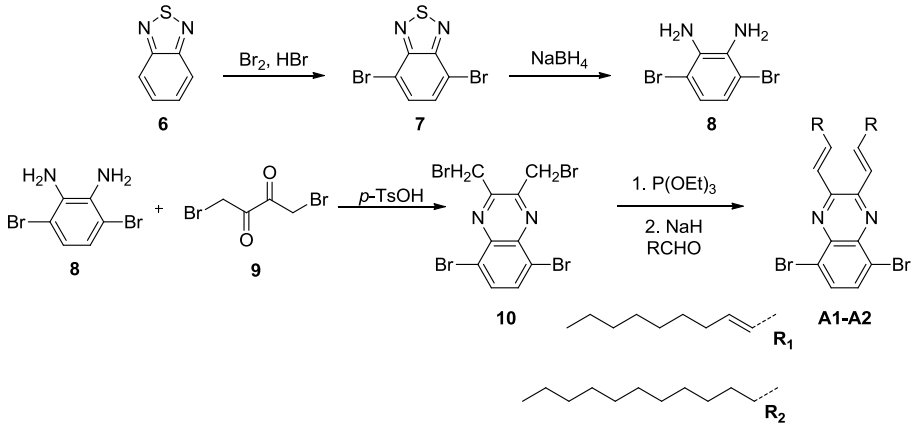

Scheme 7.2. Synthesis of the Qx electron acceptor monomers **A1-A2**.

The **PBDTQx** polymers were synthesized by Stille polycondensations between donor monomer **D1** and acceptor monomers **A1** and **A2**, using microwave irradiation (Scheme 7.3). One of the main advantages of microwave synthesisis that it allows faster screening and optimization of the conditions employed in the polymerization reactions, using little amounts of material. Additionally, compared to conventional heating, the reaction time is considerably reduced from several days to hours, which limits the degradation of the monomers and/or the catalyst. The polymerization, catalyzed by $Pd(PPh_3)_4$, was conducted for 1 hour at 140 ^oC under an argon atmosphere (~80 PSI), using toluene as a solvent. End-capping was performed in two stages, each lasting 15 minutes, by addition of 2-tributylstannylthiophene and 2-bromothiophene, respectively. Polymers **PBDTQx1-2** were isolated as dark blue powders upon precipitation in acetone. Purification/fractionation by means of preparative GPC (gel permeation chromatography) was performed for **PBDTQx2** prior to solar cell fabrication (these fractions are further on denoted as **PBDTQx2$_{GPC}$**).

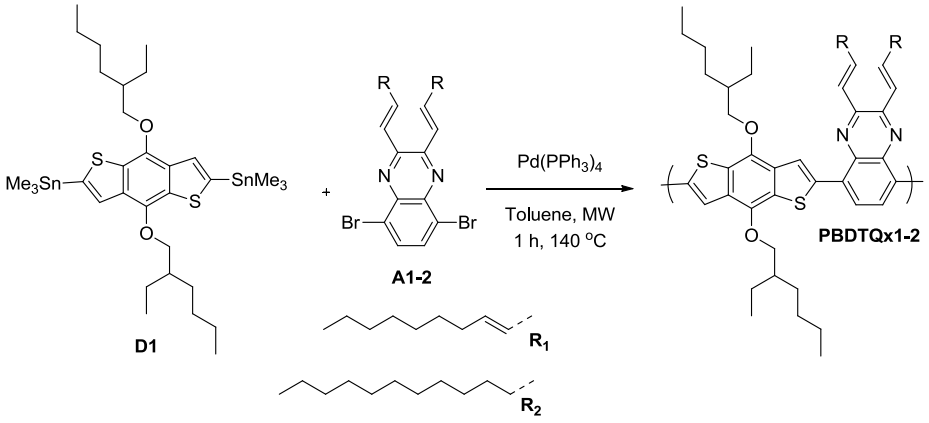

Scheme 7.3. Synthesis of the **PBDTQx** copolymers by Stille polycondensation reactions.

For the synthesis of Qx monomer **A3** (Scheme 7.4), the introduction of extra thiophene groups was achieved by Suzuki cross coupling between 2-bromo-3-hexylthiophene (**11**) and the commercially available 2,1,3-benzothiadiazole-4,7-bis(boronic acid pinacol ester) (**12**). This was followed by sulfur extrusion in the presence of $LiAlH_4$ and condensation with 1,4-dibromobutane-2,3-dione (**9**) to afford 2,3-bis(bromomethyl)-5,8-bis(3-hexylthiophen-2-yl)quinoxaline (**14**). Introduction of the bromine atoms in positions 5 of the thiophene rings was done by bromination in the presence of *N*-bromosuccinimide (NBS). Generation of the bisphosphonate (upon application of triethyl phosphite) followed by proton abstraction and addition of 5-(2-ethylhexyl)thiophene-2-carbaldehyde (**16**), led to the formation of monomer **A3**. The **PBDT-DTQx** polymer (Scheme 7.4) was then synthesized by Stille polycondensation between donor monomer **D1** and acceptor monomer **A3**, using microwave irradiation (*vide supra*). The final polymer was isolated as a dark red powder upon precipitation in acetone.

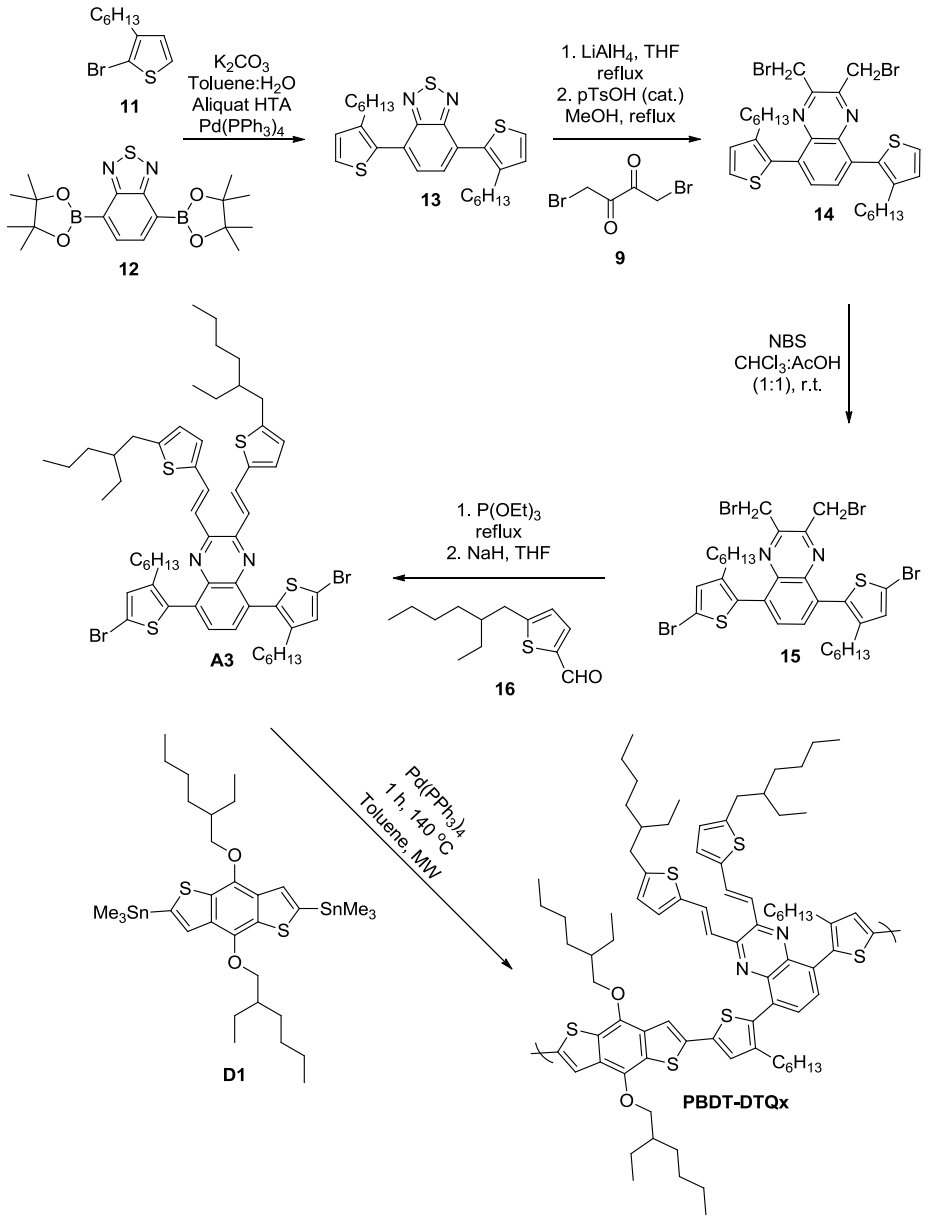

Scheme 7.4. Synthesis of the Qx electron acceptor monomer **A3** and of the corresponding **PBDT-DTQx** copolymer obtained by a Stille polycondensation reaction with the BDT electron donor unit **D1**.

The asymmetrically dialkyl-substituted CPDT monomer was prepared *via* a three-step synthetic protocol recently developed in our group (Scheme 7.5).[10,11] In the first step, Kumada coupling of 2-thienylmagnesium bromide (**17**) with 2,3-dibromothiophene (**18**) afforded 3-bromo-2,2'-bithiophene. Lithiation in position 3, followed by treatment with 5-ethylpentadecan-7-one (**20**) gave the dialkylated tertiary alcohol derivative **21**. Friedel-Crafts dehydration cyclization in sulfuric acid medium ultimately afforded the CPDT scaffold. The organostannyl derivative **D2** was obtained by lithiation and stannylation in the presence of trimethyltin chloride. The **PCPDT-Qx** polymer was synthesized from **D2** and quinoxaline derivative **A1** by Stille polycondensation (*vide supra*) (Scheme 7.5). The final polymer was isolated as a dark green powder upon precipitation in acetone.

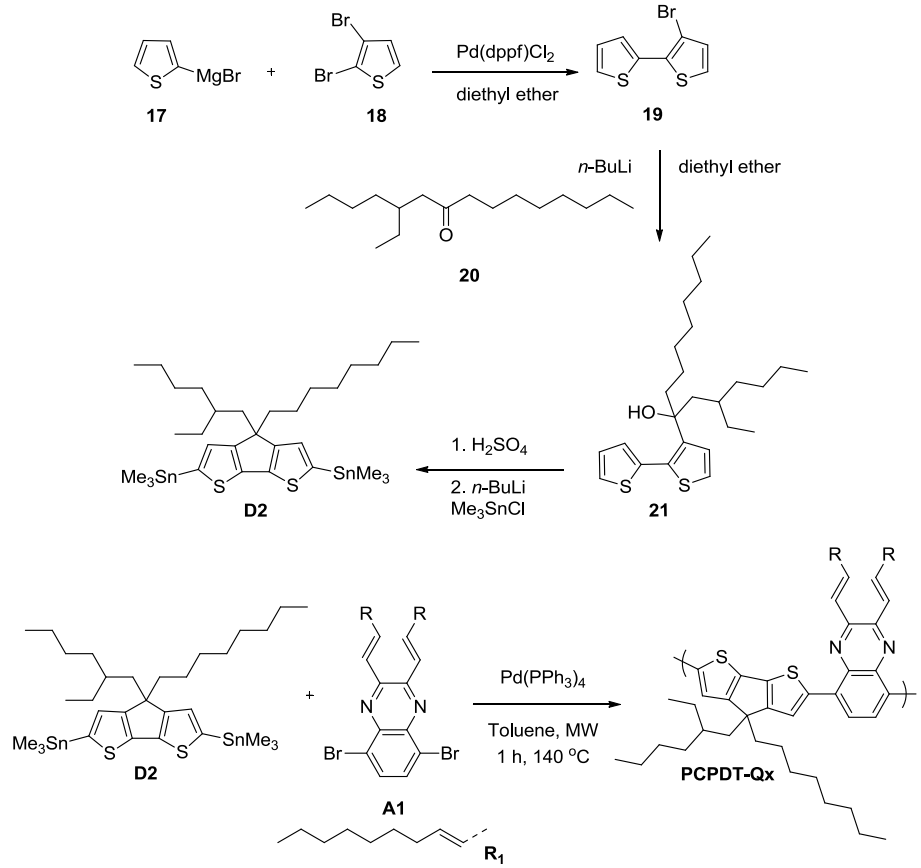

Scheme 7.5. Synthesis of the electron rich CPDT monomer **D2** and the **PCPDT-Qx** copolymer by a Stille polycondensation reaction with the Qx electron acceptor **A1**.

Polymer **PBDTQx2** was synthesized in 87% yield, while the other three polymers were obtained in modest yields ranging from 42 to 50%. Their molecular weights (and those of the polymer fractions isolated upon purification/fractionation by preparative GPC) were determined by GPC analysis in tetrahydrofuran (THF) at 40 ^{o}C (Table 7.1). The number average molecular weight (M_n) of the **PBDTQx** polymers was ~ 1.0 x 10^4 g mol^{-1}. The relatively low M_n values for **PCPDT-Qx** (4.8 x 10^3 g mol^{-1}) and in particular for **PBDT-DTQx** (3.8 x 10^3 g mol^{-1}) indicate the formation of oligomers rather than polymers. The poor results obtained for these polycondensation reactions could arise from a stoichiometric imbalance of the monomers and/or functionalities in the initial reaction mixture, related to the small scale (~50 mg) of the reactions.

Table 7.1. Analytical GPC data (THF) of the **PBDTQx1/2**, **PBDT-DTQx** and **PCPDT-Qx** copolymers.

Polymer	M_n (g mol^{-1})	M_w (g mol^{-1})	PDI
PBDTQx1[a]	1.0 x 10^4	5.5 x 10^4	5.5
PBDTQx2[a]	7.8 x 10^3	4.4 x 10^4	5.6
PBDTQx2$_{GPC_1}$	8.9 x 10^3	4.5 x 10^4	5.1
PBDTQx2$_{GPC_2}$	6.9 x 10^3	1.5 x 10^4	2.2
PBDTQx2$_{GPC_3}$	6.0 x 10^3	8.4 x 10^3	1.4
PBDT-DTQx[a]	3.8 x 10^3	1.1 x 10^4	2.8
PCPDT-Qx[a]	4.8 x 10^3	9.1 x 10^3	1.9

[a] Analysis of the polymer isolated upon precipitation in acetone.

The absorption spectra of the polymers were characterized by three distinct bands located between ~250-450 and 550-700 nm (Figure 7.2). For **PCPDT-Qx**, the low energy absorption band was located between ~500-850 nm, strongly red-shifted compared to the rest of the polymers. Taking into account the relatively low number average molecular weight of this polymer, it is envisaged that these properties can even be enhanced in materials with higher degrees of polymerization. Additional fractionation of **PBDTQx2**, by means of preparative GPC, allowed the isolation of three polymer fractions, denoted as **PBDTQx2$_{GPC}$**. A correlation between the

absorption maxima, the band gap of the material, and the number average molecular weight of the polymer was clearly noticed (Figure 7.2).

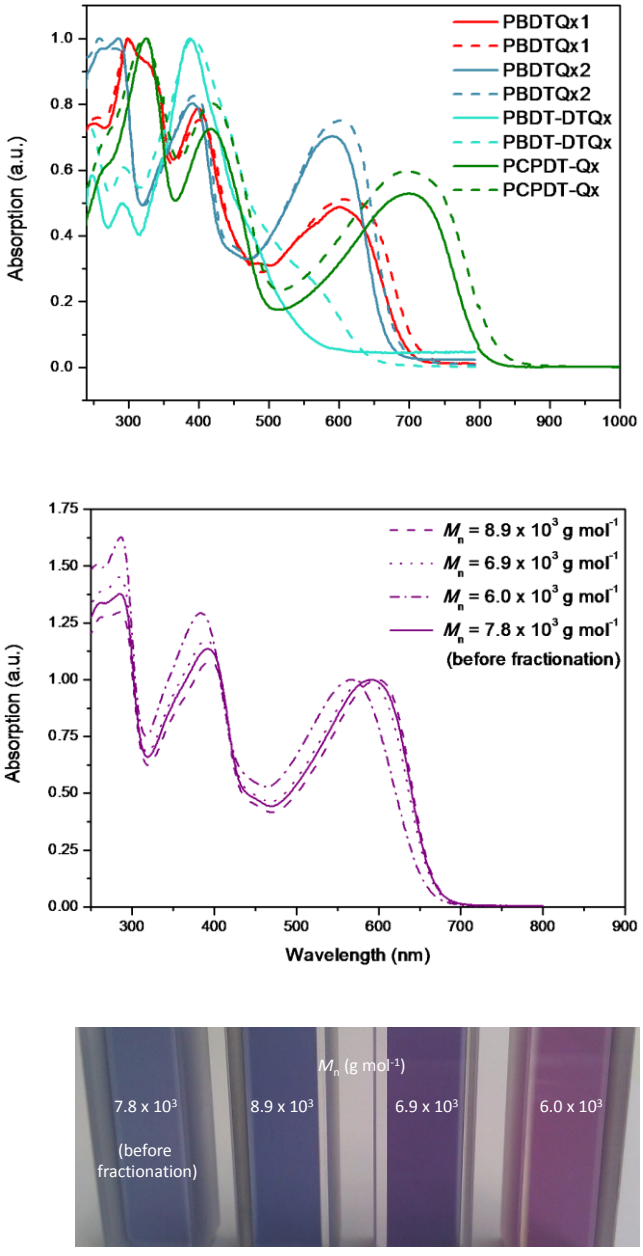

Figure 7.2. Normalized absorption spectra of the polymers recorded from solution ($CHCl_3$) and thin film (top), absorption spectra recorded from $CHCl_3$ (middle, normalized at the low energy band) and picture of the solutions of different **PBDTQx2** polymer fractions in $CHCl_3$ (bottom).

The energy levels of the synthesized polymers, as determined by cyclic voltammetry, are summarized in Table 7.2. Polymers **PBDTQx1**/**2** showed very similar electrochemical and optical (determined from the absorption onset in film) band gaps, close to ~2.0 and ~1.8 eV, respectively. For **PBDT-DTQx**, for which the degree of polymerization was low, these values were slightly higher. **PCPDT-Qx** had by far the lowest band gap values, *i.e.* 1.79 (electrochemical) and 1.51 eV (optical), the onset of the absorption (in solution as well as in thin film) being extended beyond 800 nm. In terms of energy levels and absorption pattern, the **PCPDT-Qx** low band gap polymer is very close to the parent **PCPDTBT** derivative.[6a]

Table 7.2. Cyclic voltammetry data of the **PBDTQx, PBDT-DTQx** and **PCPDT-Qx** polymers.

Polymer	E^{ox}_{onset} (V)	E^{red}_{onset} (V)	HOMO (eV)	LUMO (eV)	E_g^{EC} (eV)	E_g^{OP} (eV)[a]
PBDTQx1	0.46	-1.52	-5.39	-3.41	1.98	1.72
PBDTQx2	0.47	-1.59	-5.40	-3.34	2.06	1.80
PBDT-DTQx	0.52	-1.58	-5.45	-3.35	2.10	1.91
PCPDT-Qx	0.21	-1.58	-5.14	-3.93	1.79	1.51

[a] In film.

7.2.2. Bulk Heterojunction Solar Cells

PBDTQx2 was used as a donor material, in combination with $PC_{71}BM$, in the fabrication of BHJ organic solar cells. The devices had a layered structure ITO/PEDOT:PSS/polymer:$PC_{71}BM$/Ca/Al. The active layer was cast from a chlorobenzene (CB) solution which consisted of a 1:2 (w/w) ratio of **PBDTQx2**:$PC_{71}BM$. The output parameters were measured under air mass 1.5 global illumination conditions (AM 1.5G 100 mW cm^{-2}). Preliminary solar cell results obtained with the non-purified polymer afforded 0.76% PCE with a J_{sc} of 2.19 mA cm^{-2}, a V_{oc} of 0.77 V and a FF of 45%. Under the same conditions, the efficiency was improved to 1.06% when the purified polymer, *i.e.* **PBDTQx2**$_{GPC\_1}$ was used (Figure 7.3). The J_{sc} increased to 3.14 mA cm^{-2}, while the V_{oc} and FF remained virtually

unchanged. Compared to polymers of the same class which were already described in literature, for which efficiencies in the order of 0.20% were obtained, **PBDTQx2** clearly shows superior photovoltaic performances.[8a] Optimization of the processing solvent, the polymer:$PC_{71}BM$ ratio and the molecular weight distribution can further lead to increased PCEs.[12] These aspects are currently under investigation within our group.

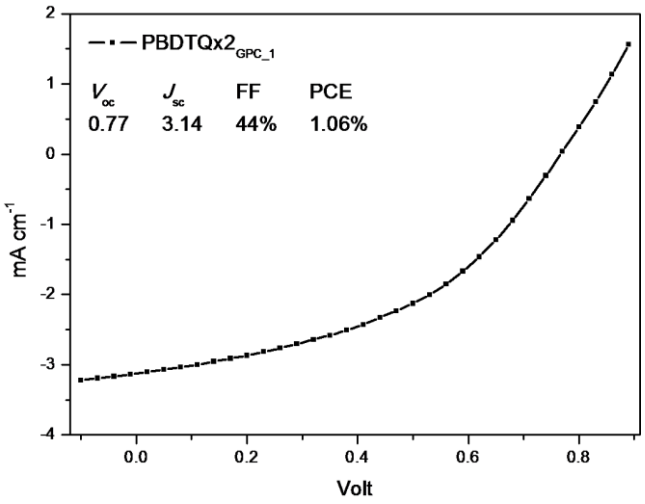

Figure 7.3. *J-V* curve for the best BHJ solar cell obtained with **PBDTQx2**$_{GPC\_1}$:$PC_{71}BM$.

The other three materials were not yet tested in BHJ solar cells due to the relatively low material amounts and/or low M_n values.

7.3. Conclusions

The synthesis of a series of low band gap light harvesting materials incorporating BDT or CPDT donors and (DT)Qx acceptors with conjugated alkyl or heteroaryl side chains was accomplished *via* Stille polycondensation reactions. The absorption spectra of these derivatives are characterized by three absorption bands, the onset (in thin film) being located in the near-IR region of the spectrum. Polymer **PBDTQx2** was used as a donor material in the fabrication of BHJ solar cells, in a blend with $PC_{71}BM$ as the acceptor. This combination afforded 1.06% PCE, a promising result which can further be improved by optimizing the polymer:$PC_{71}BM$ ratio, the processing parameters (*e.g.*

spin coating speed, solvent, the use of an additive, etc.) and the molecular weight (distribution). Optimization of the polycondensation reaction and extensive purification of the monomers is envisaged to reach higher degrees of polymerization for **PBDTQx1**, **PBDT-DTQx** and **PCPDT-Qx**. The photovoltaic performance of these donor materials will then also be evaluated in BHJ solar cells.

7.4. Experimental Section

Materials and Methods

NMR chemical shifts (δ, in ppm) were determined relative to the residual $CHCl_3$ absorption (7.26 ppm) of $CDCl_3$ or relative to one of the residual C_6H_5Cl absorptions (7.14 ppm) of C_6D_5Cl. Gas chromatography-mass spectrometry (GC-MS) analyses were carried out applying Chrompack Cpsil5CB or Cpsil8CB capillary columns. Molecular weights and molecular weight distributions were determined relative to polystyrene standards (Polymer Labs) by gel permeation chromatography (GPC). Chromatograms were recorded on a Spectra Series P100 (Spectra Physics) equipped with two mixed-B columns (10 µm, 0.75 cm x 30 cm, Polymer Labs) and a refractive index detector (Shodex) at 40 °C. THF was used as the eluent at a flow rate of 1.0 mL min^{-1}. Preparative GPC was performed on a JAI LC-92XX Next series equipped with JAIGEL *2H* and *3H* columns. Solution UV-Vis absorption measurements were performed with a scan rate of 600 nm min^{-1} in a continuous run from 1000 to 200 nm. Thin film electrochemical measurements were performed with an Eco Chemie Autolab PGSTAT 30 Potentiostat/Galvanostat using a conventional three-electrode cell under N_2 atmosphere (electrolyte: 0.1 mol L^{-1} $TBAPF_6$ in anhydrous CH_3CN). For the measurements, a $Ag/AgNO_3$ reference electrode (0.01 mol L^{-1} $AgNO_3$ and 0.1 mol L^{-1} $TBAPF_6$ in anhydrous CH_3CN), a platinum counter electrode and an indium tin oxide (ITO) coated glass substrate as working electrode were used. The polymers were deposited by drop-casting directly onto the ITO substrates. Cyclic voltammograms were recorded at 50 mV s^{-1}. From the onset potentials of the oxidation and reduction the position of the energy levels could be estimated. All potentials were referenced using a known standard, ferrocene/ferrocenium, which in CH_3CN solution is estimated to have an oxidation potential of -4.98 eV *vs*. vacuum. Polymer bulk heterojunction solar cells were fabricated by spin coating a polymer:$PC_{71}BM$ (Solenne) blend (1:2

w/w ratio) sandwiched between a transparent anode and an evaporated metal cathode. The transparent anode was an ITO covered glass substrate which was coated with a 30 nm poly(3,4-ethylenedioxythiophene)/poly(styrenesulfonic acid) PEDOT/PSS (CLEVIOS P VP.AI 4083) layer applied by spin coating. The cathode, a bilayer of 20 nm Ca and 80 nm Al, was thermally evaporated. The ITO glass substrate was cleaned by ultrasonification (sequentially) in soap solution, deionized water, acetone and isopropanol. For the bulk heterojunction devices the polymer and $PC_{71}BM$ (1:2 w/w ratio) were dissolved together in chlorobenzene, to give an overall 30 mg mL^{-1} solution, which was stirred overnight at 80 °C inside a glovebox. Solar cell efficiencies were characterized under simulated 100 mW cm^{-2} AM 1.5 G irradiation from a Xe arc lamp with an AM 1.5 global filter.

Synthesis

Unless stated otherwise, all reagents and chemicals were obtained from commercial sources and used without further purification.

4,8-Bis((2-ethylhexyloxy)benzo[1,2-*b*:3,4-*b*]dithiophene-2,6-diyl)bis(trimethylstannane) (**D1**) was synthesized according to a literature procedure.[5f] Material identity and purity were confirmed by GC-MS and ^{1}H NMR.

5,8-Dibromo-2,3-di((1*E*,3*E*)-undeca-1,3-dien-1-yl)quinoxaline (A1), **5,8-dibromo-2,3-di((*E*)-tridec-1-en-1-yl)quinoxaline (A2)** and **5,8-bis(5-bromo-3-hexylthien-2-yl)-2,3-bis((*E*)-2-(5-(2-ethylhexyl)thien-2-yl)vinyl)quinoxaline (A3)** were synthesized according to literature procedures.[9] Material identity and purity were confirmed by GC-MS and ^{1}H NMR.

4-(2'-Ethylhexyl)-4-octyl-4*H*-cyclopenta[2,1-*b*:3,4-*b*']dithiophene was synthesized according to a literature procedure.[10] Material identity and purity were confirmed by GC-MS and ^{1}H NMR.

(4-(2-Ethylhexyl)-4-octyl-4*H*-cyclopenta[2,1-*b*:3,4-*b*′]dithiophene-2,6-diyl)bis-(trimethylstannane) (D2) was synthesized according to a literature procedure.[13] ^{1}H NMR (400 MHz, $CDCl_3$) δ 6.97-6.90 (m, 2H), 1.90-1.76 (m, 4H), 1.25-1.08 (br m, 15H), 0.99-0.88 (m, 6H), 0.84 (t, J = 7.3 Hz, 3H), 0.73 (t, J = 6.5 Hz, 3H), 0.58 (t, J = 7.7 Hz, 3H), 0.37-0.34 (m, 18H).

Poly[4,8-bis(2-ethylhexyloxy)benzo[1,2-*b*:3,4-*b*]dithiophen-2-yl)-2,5-diyl-*alt*-2,3-di((1*E*,3*E*)-undeca-1,3-dien-1-yl)quinoxaline-5,8-diyl] (PBDTQx1): **General**

procedure: **D1** (0.053 g, 0.068 mmol) and **A1** (0.040 g, 0.068 mmol) were placed in a (10 mL) MW reaction vessel which was brought under inert atmosphere. Toluene (2.2 mL), degassed by bubbling through N_2 gas for 20 minutes, was added and the mixture was vigorously stirred for 10 minutes at r.t. The polymerization, catalyzed by $Pd(PPh_3)_4$ (3mol%), was conducted for 1 h at 140 ^oC under an argon atmosphere (~80 PSI). End-capping was performed in two stages, each lasting 15 minutes, by addition of 2-tributylstannylthiophene (0.101 g, 0.272 mmol) and 2-bromothiophene (0.022 g, 0.136 mmol), respectively. Polymer **P1** was precipitated in acetone and exhaustively washed with the same solvent, to afford a green fiber-like solid (0.029 g, 50%); ^1H NMR (300 MHz, C_6D_5Cl) δ 8.64-7.61 (br m, 6H), 6.61-6.22 (2 x br s, 6H), 4.69-4.44 (br m, 4H), 2.43-0.87 (br m, 56H); UV-Vis ($CHCl_3$, nm) λ_{max} 297/400/602; UV-Vis (film, nm) λ_{max} 298/402/625; GPC (THF, PS standards) M_n = 1.0 x 10^4 g mol^{-1}, M_w = 5.5 x 10^4 g mol^{-1}, PDI = 5.5.

Poly[4,8-bis(2-ethylhexyloxy)benzo[1,2-*b*:3,4-*b*]dithiophen-2-yl)-2,5-diyl-*alt*-2,3-di((*E*)-tridec-1-en-1-yl)quinoxaline-5,8-diyl] (PBDTQx2): According to the general procedure: **D1** (0.053 g, 0.068 mmol), **A2** (0.044 g, 0.068 mmol), toluene (2.2 mL), $Pd(PPh_3)_4$ (3 mol%), 2-tributylstannylthiophene (0.101 g, 0.272 mmol), 2-bromothiophene (0.022 g, 0.136 mmol), green solid (0.056 g, 87%); ^1H NMR (300 MHz, $CDCl_3$) δ 8.35-8.14 (br, 2H), 7.97-7.29 (br m, 4H), 7.12-6.86 (br m, 2H), 4.49-4.16 (br m, 4H), 2.85-2.34 (br m, 4H), 2.14-0.67 (br m, 72H); UV-Vis ($CHCl_3$, nm) λ_{max} 285/392/590; UV-Vis (film, nm) λ_{max} 279/288/395/603; GPC (THF, PS standards) M_n = 8.4 x 10^3 g mol^{-1}, M_w = 6.4 x 10^4 g mol^{-1}, PDI = 7.6.

Poly[4,8-bis(2-ethylhexyloxy)benzo[1,2-*b*:3,4-*b*]dithiophen-2-yl)-2,5-diyl-*alt*-2,3-bis((*E*)-2-(5-(2-ethylhexyl)thien-2-yl)vinyl)-5,8-bis(3-hexylthien-2-yl)quinoxaline-5,8-diyl] (PBDT-DTQx): According to the general procedure: **D1** (0.027 g, 0.035 mmol), **A3** (0.038 g, 0.035 mmol), toluene (1.5 mL), $Pd(PPh_3)_4$ (3 mol%), 2-tributylstannylthiophene (0.052 g, 0.140 mmol), 2-bromothiophene (0.011 g, 0.070 mmol), brown solid (0.020 g, 43%); ^1H NMR (300 MHz, $CDCl_3$) δ 8.26-8.17 (br m, 2H), 7.80-7.67 (br m, 2H), 7.64-7.58 (br m, 2H), 7.51-7.41 (br m, 2H), 7.40-7.34 (br m, 2H), 7.13-7.05 (br m, 2H), 6.74-6.66 (br m, 2H), 4.28-4.18 (br m, 4H), 2.82-2.66 (br m, 8H), 1.88-1.58 (br m, 4H), 1.47-1.34 (br m, 16H), 1.11-0.76 (br m, 30H); UV-Vis

($CHCl_3$, nm) λ_{max} 388; UV-Vis (film, nm) λ_{max} 391; GPC (THF, PS standards) M_n = 3.7 x 10^3 g mol^{-1}, M_w = 1.0 x 10^4 g mol^{-1}, PDI = 2.7.

Poly[4-(2-ethylhexyl)-4-octyl-4*H*-cyclopenta[2,1-*b*:3,4-*b'*]dithiophen-2,6-diyl-*alt*-2,3-di((1*E*,3*E*)-undeca-1,3-dien-1-yl)quinoxaline-5,8-diyl] (PCPDT-Qx): According to the general procedure: **D2** (0.082 g, 0.112 mmol), **A1** (0.066 g, 0.112 mmol), toluene (2.5 mL), $Pd(PPh_3)_4$ (3 mol%), 2-tributylstannylthiophene (0.167 g, 0.448 mmol), 2-bromothiophene (0.036 g, 0.224 mmol), green solid (0.040 g, 42%); ^{1}H NMR (300 MHz, $CDCl_3$) δ 8.14-7.32 (br m, 6H), 7.23-6.91 (br m, 2H), 6.59-6.12 (2 x br m, 4H), 2.42-2.14 (br, 4H), 2.13-1.85 (br m, 4H), 1.65-0.95 (br m, 41H), 0.93-0.58 (br m, 15H); UV-Vis ($CHCl_3$, nm) λ_{max} 327/417/699; UV-Vis (film, nm) λ_{max} 323/419/697; GPC (THF, PS standards) M_n = 4.8 x 10^3 g mol^{-1}, M_w = 9.1 x 10^3 g mol^{-1}, PDI = 1.9.

7.5. References

(1) Dou, L.; You, J.; Yang, J.; Chen, C.-C.; He, Y.; Murase, S.; Moriarty, T.; Emery, K.; Li, G.; Yang, Y. *Nat. Photon.* **2012**, *6*, 180.

(2) www.nrel.gov

(3) (a) Helgesen, M.; Sondergaard, R.; Krebs, F. C. *J. Mater. Chem.* **2010**, *20*, 36; (b) Espinosa, N.; Hosel, M.; Angmo, D.; Krebs, F. C. *Energy Environ. Sci.* **2012**, *5*, 5117.

(4) (a) Scharber, M. C.; Mühlbacher, D.; Koppe, M.; Denk, P.; Waldauf, C.; Heeger, A. J.; Brabec, C. J. *Adv. Mater.* **2006**, *18*, 789; (b) Heeger, A. J. *Chem. Soc. Rev.* **2010**, *39*, 2354; (c) Szarko, J. M.; Guo, J.; Rolczynski, B. S.; Chen, L. X. *J. Mater. Chem.* **2011**, *21*, 7849; (d) Beaujuge, P. M.; Fréchet, J. M. J. *J. Am. Chem. Soc.* **2011**, *133*, 20009.

(5) (a) Fu, Y.; Sun, M.; Wu, Y.; Bo, Z.; Ma, D. *J. Polym. Sci., Part A: Polym. Chem.* **2008**, *46*, 1349; (b) Piliego, C.; Holcombe, T. W.; Douglas, J. D.; Woo, C. H.; Beaujuge, P. M.; Fréchet, J. M. J. *J. Am. Chem. Soc.* **2010**, *132*, 7595; (c) Zou, Y.; Najari, A.; Berrouard, P.; Beaupré, S.; Réda Aïch, B.; Tao, Y.; Leclerc, M. *J. Am. Chem. Soc.* **2010**, *132*, 5330; (d) Zhang, Y.; Hau, S. K.; Yip, H.-L.; Sun, Y.; Acton, O.; Jen, A. K. Y. *Chem. Mater.* **2010**, *22*, 2696; (e) Zhang, G.; Fu, Y.; Zhang, Q.; Xie, Z. *Chem. Commun.* **2010**, *46*, 4997; (f) Huo, L.; Hou, J. *Polym. Chem.* **2011**, *2*, 2453; (g) Peng, Q.; Liu, X.; Su, D.; Fu, G.; Xu, J.; Dai, L. *Adv. Mater.* **2011**, *23*, 4554.

(6) (a) Peet, J.; Kim, J. Y.; Coates, N. E.; Ma, W. L.; Moses, D.; Heeger, A. J.; Bazan, G. C. *Nat. Mater.* **2007**, *6*, 497; (b) Kettle, J.; Horie, M.; Majewski, L. A.; Saunders, B. R.; Tuladhar, S.; Nelson, J.; Turner, M. L. *Sol. Energy Mater. Sol. Cells* **2011**, *95*, 2186; (c) Horie, M.; Kettle, J.; Yu, C.-Y.; Majewski, L. A.; Chang, S.-W.; Kirkpatrick, J.; Tuladhar, S. M.; Nelson, J.; Saunders, B. R.; Turner, M. L. *J. Mater. Chem.* **2012**, *22*, 381.

(7) (a) Moulé, A. J.; Tsami, A.; Bünnagel, T. W.; Forster, M.; Kronenberg, N. M.; Scharber, M.; Koppe, M.; Morana, M.; Brabec, C. J.; Meerholz, K.; Scherf, U. *Chem. Mater.* **2008**, *20*, 4045; (b) Bijleveld, J. C.; Shahid, M.; Gilot, J.; Wienk, M. M.; Janssen, R. A. J. *Adv. Funct. Mater.* **2009**, *19*, 3262; (c) Van Mierloo, S.; Hadipour, A.; Spijkman, M.-J.; Van den Brande, N.; Ruttens, B.; Kesters, J.;

D'Haen, J.; Van Assche, G.; de Leeuw, D. M.; Aernouts, T.; Manca, J.; Lutsen, L.; Vanderzande, D. J.; Maes, W. *Chem. Mater.* **2012**, *24*, 587.

(8) (a) Hou, J.; Park, M.-H.; Zhang, S.; Yao, Y.; Chen, L.-M.; Li, J.-H.; Yang, Y. *Macromolecules* **2008**, *41*, 6012; (b) Lee, P.-I.; Lien-Chung Hsu, S.; Lee, J. F.; Chuang, H.-Y.; Lin, P. *J. Polym. Sci., Part A: Polym. Chem.* **2011**, *49*, 662.

(9) Marin, L.; Lutsen, L.; Vanderzande, D.; Maes, W. *Quinoxaline Derivatives with Broadened Absorption Patterns Toward Organic Photovoltaics, manuscript in progress*.

(10) Van Mierloo, S.; Adriaensens, P. J.; Maes, W.; Lutsen, L.; Cleij, T. J.; Botek, E.; Champagne, B.; Vanderzande, D. J. *J. Org. Chem.* **2010**, *75*, 7202.

(11) The prime (') denotes that the monomer was prepared via the more recent three-step protocol.

(12) (a) Ma, W.; Kim, J. Y.; Lee, K.; Heeger, A. J. *Macromol. Rapid Commun.* **2007**, *28*, 1776; (b) Koppe, M.; Brabec, C. J.; Heiml, S.; Schausberger, A.; Duffy, W.; Heeney, M.; McCulloch, I. *Macromolecules* **2009**, *42*, 4661.

(13) Zhu, Z.; Waller, D.; Gaudiana, R.; Morana, M.; Mühlbacher, D.; Scharber, M.; Brabec, C. *Macromolecules* **2007**, *40*, 1981.

Summary

The steady development of new (photoactive) materials for organic solar cell applications has led to continuous improvements in the power conversion efficiencies (PCE) of these devices. Additionally, the use of new solar cell configurations (*e.g.* tandem devices) has allowed to obtain PCEs that nowadays exceed 10%. Having in mind the relatively low production costs, the development of stable materials and the potential advantages in terms of flexibility, transparency, aesthetics and low-light applications, this technology has a real potential of holding an important share of the future photovoltaics market.

The research work described in this PhD thesis was dedicated to the synthesis of two major (electron) donor and (electron) acceptor classes of materials, *i.e.* 4*H*-cyclopenta[2,1-*b*:3,4-*b'*]dithiophenes (CPDTs) and quinoxalines (Qxs), their integration in low band gap copolymers and evaluation of these derivatives as light harvesting materials for organic photovoltaics.

Being among the first low band gap polymers that have been developed for organic solar cells, affording PCEs superior to 5%, PCPDTBT has attracted considerable attention. The one-pot synthetic procedure giving access to the substituted CPDT building block has first been optimized and was then applied to combine CPDT donor units with a 2,1,3-benzothiadiazole acceptor by means of Suzuki polycondensation reactions. The photovoltaic performances of symmetrically substituted PCPDTBT-type polymers, carrying 2-ethyhexyl and dodecyl side chains, have been evaluated in solar cells with bilayer, bulk heterojunction and tandem configurations (**Chapter 1**). The efficiencies that have been obtained for the 2-ethyhexyl-substituted polymer were close to the reported literature values. The polymer decorated with dodecyl substituents, which was less soluble and therefore more difficult to process, afforded lower PCEs, probably due to a poor film morphology of the active layer blend. On the other hand, this material, being insoluble in chloroform, has allowed the preparation of a bilayer solar cell, for which the presence of a CT (charge transfer) ground state has been detected by the FTPS (Fourier-transform photocurrent spectroscopy) technique.

A series of PCPDTBT-type polymers bearing 2-ethylhexyl, octyl or dodecyl side chains, for which the CPDT building block was synthesized using the one-pot

procedure and/or a recently developed three step synthetic method, has been subjected to a thermally induced degradation study (**Chapter 4**). The evolution of the conjugated materials was monitored by UV-Vis/IR spectroscopy and a combined TG-TD-GC/MS technique. The synthesis of the monoalkylated CPDT derivative has afforded a deeper insight into the degradation pathway of this class of materials. Finally, the combined TG-TD-GC/MS technique revealed quasi-identical behavior for all polymers, regardless the synthetic history of the CPDT building block.

The synthesis of a new class of small molecules, *i.e.* 2*H*-cyclopenta[2,1-*b*:3,4-*b'*]dithiophene-2,6(4*H*)-diones, issued from the CPDT family, has been achieved by bromination of 4*H*-cyclopenta[2,1-*b*:3,4-*b'*]dithiophene derivatives in the presence of *N*-bromosuccinimide (NBS) (**Chapter 2**). It was proven that the amount of NBS and the solvent play a crucial role in the formation of these products, which were found to be thermodynamically favored (as demonstrated by theoretical calculations).

The conversion of 4*H*-cyclopenta[2,1-*b*:3,4-*b'*]dithiophen-4-one to the corresponding 5*H*-spiro(benzo[1,2-*b*:6,5-*b'*]dithiophene-4,4'-cyclopenta[2,1-*b*:3,4-*b'*]-dithiophen)-5-one was achieved by pinacol rearrangement in the presence of trivalent phosphorus reagents (**Chapter 3**). The proposed structure and the experimentally observed ^{13}C- and ^{1}H NMR chemical shifts were confirmed by X-ray crystallography and theoretical calculations. The good agreement between the experimental and theoretical data illustrated the power and accuracy of the calculation methods.

The synthesis and optical characterization of a series of two dimensionally (2D) conjugated 5,8-dibromoquinoxaline monomers and thiophene-Qx-thiophene triads, bearing alkyl, aryl or heteroaryl side chains separated by ethenyl and/or butadienyl spacers from the electron deficient quinoxaline core, have been performed (**Chapter 5**). At the monomer stage, the vertical conjugation created by the introduction of the conjugated side chains resulted in the extension of the absorption spectrum toward the visible range and the apparition of a second band as a result of the intramolecular charge transfer from the donor side chains to the electron acceptor Qx core. The synthesis of dibrominated triads, promising coupling units toward the synthesis of conjugated polymers, was achieved by careful design and optimization of the synthetic routes.

The synthesis of 2D-conjugated poly(thienoquinoxaline) derivatives was achieved by Stille polycondensation between 2,5-bis(trialkylstannyl)thiophenes and 5,8-

dibromoquinoxaline derivatives bearing ethenyl and/or butadienyl spacers between the solubilizing side chains and the quinoxaline core (**Chapter 6**). The purity of the organostannyl derivative was proven to be crucial for obtaining high degrees of polymerization. These donor polymers were then used, in combination with a fullerene acceptor, in the fabrication of bulk heterojunction solar cells. Additional fractionation of the polymers by means of preparative GPC showed a direct correlation between the number average molecular weight, the optical properties and the photovoltaic performance of the isolated fractions.

The combination of benzo[1,2-*b*:3,4-*b*]dithiophene (BDT) or 4*H*-cyclopenta[2,1-*b*:3,4-*b'*]dithiophene (CPDT) donors and quinoxaline or bis(thieno)quinoxaline acceptors by Stille polycondensation reactions afforded a series of low band gap polymers (**Chapter 7**). The lowest onset values, as determined from the absorption spectra, were noticed for PCPDT-Qx (~1.51 eV). Preliminary solar cell results using a PBDTQx2:$PC_{71}BM$ blend showed efficiencies of ~1.0%, superior to the ones reported in literature for similar polymers. Once again, fractionation by preparative GPC was shown beneficial.

Acknowledgements

At the end of my PhD I believe it is time to draw a line, to make a summary of this long, yet very intense period (especially the last couple of months). I am lucky to have always been surrounded by wonderful colleagues, friends and family, who were there to temper me, me and my emotions, that were oscillating between the Mount Everest and the Mariana Trench. Thank you all for helping me find the balance.

My first *dankwoord* goes to my promoter, Prof. Dr. Wouter Maes. Dear Wouter, I think I just might not have enough *dankwoorden* for you, for your help and support, for your interest in my work and for you optimistic way of thinking and being which helped me overcome the difficult moments that I have (often) encountered during my time in the lab. Thank you for always being around, or behind the computer, sending back articles and suggestions for things *still to be tried* in the lab. Thanks for taking the time to listen, whenever I had something on my mind. Thanks for correcting the thesis in a *supersonic* fashion and for always returning bicolor texts. I don't know if I would have made it without your guiding.

I would also like to thank my copromoters Prof. Dr. Dirk Vanderzande and Dr. Laurence Lutsen for giving me the opportunity to carry on a PhD at UHasselt and work on the SolarNtype project. Thank you for your constant interest in my work, especially in the PCPDTBT polymers which I always found hard to spell (and to prepare).

I would like to thank Prof. Dr. Jean Manca, Dr. Agnès Rivaton, Dr. Nikolay Radychev, Prof. Dr. Wim Dehaen, Prof. Dr. Peter Adriaensens and Prof. Dr. Thomas Junkers for accepting to be part of the jury and finding the time to read the thesis. Peter, thank you for your patience and time spent with the NMR experiments, which helped to elucidate and confirm the most unexpected products that I somehow managed to synthesize.

I would like to thank the permanent people in our group who took care of the good functioning of the equipment and for recording the NMR spectra (Koen), and the GPC measurements and administrative issues (Iris). I'm grateful to Huguette for the CV measurements and for the UV-Vis/IR *degradation* experiments of the PCPDTBT polymers. In the end, we managed to see the light at the end of the tunnel.

I would like to thank Prof. Dr. Robert Carleer for his interest and very useful remarks concerning the PCPDTBT polymers. Guy, thank you for carrying out the TGA and

Tenax experiments during a very busy period. Jan, thank you for all the GC-MS measurements and for the great job that you have done for the *Tenax columns* by counting and identifying the products down to permille values. It was always a pleasure chatting with you.

My colleagues have played a crucial role during my time in the lab or during the extracurricular activities. Joke, thanks for the climbing initiation (lessons) and for your company during the ski trips. I will never forget the extreme weather and road conditions that we had on our way to Austria. It's a pity you missed my acrobatic *salto* ☺☺☺… Wibren, thanks for the minute calculations that followed these trips and for lending your pump. Frederik, your *babbelen* (*in het Herkse dialect*) and storytellings were really funny, they served as intensive Dutch lessons and helped to considerably improve my *niveau*. Julija, thanks for your nice company at the various conferences (I must admit that the one in Spa was the best ☺ and the one in Blankenberge, when we walked on the beach during the foggy evening, was the scariest) and for being a quiet roommate. Inge, you were a nice desk and hood (the shiniest in the lab) neighbor. Thanks for entertaining me during the column purifications. Ans, good luck with your PhD and job applications and thanks for the long and funny talks, which most often took place in the *stinkkot* while drying your substrates (you're really skilled in this ☺). Tom, thanks for eating more chocolate than I do! It's really reassuring for me (I was almost convinced of my chocolate addiction). Jurgen, thanks for making top quality solar cells with very low amounts of material! In the end, the 3% of the PCPDTBT is a proof that the batch is still OK and it was not *cut in half*. Toon, the (lab/IMO) solar cell record efficiency man (together with Jurgen), thanks for your jokes and for creating a good *sfeer* in the lab… *Maar alléé*! Rafael, thanks for your interest in my colorful quinoxalines. David, thanks for the interesting discussions about electrochromic compounds (and not only) and for ordering the very useful *rotavap* connections. Hanne, thanks for the delicious cakes that you brought to the office. I wish you all the best with your baby and good luck with the birth which is planned few days from now. Süleyman, your presence in the lab was always pleasant and of great help, especially when I had runaway reactions or small fires. Thanks for the nice discussions, for listening to my complaints and for sharing the same principles. Good luck in the near future with the writing of your thesis. Pieter, it was an honor and a real pleasure working with you, going on small *catalyst trips* to IMO, running the polymerizations

and constantly keeping an eye on the *power* and on the color (with rough estimations of the M_n values). Thanks for all the *recyclings*, the nice pictures and graphs. This *samenwerking* weighed a lot on the outcome of my thesis. Thank you enormously! Kayte and Matthias, the GPC guys, thanks for all the measurements and the efforts you put in the analysis of the elugrams which were not always giving the expected results. Kayte, thanks for joining the operas and Matthias, thanks for belaying in Olympia. Sarah, what would my PhD be without you, without your encouragements and support? Thanks for your extremely positive way of being, for the jokes and the gossiping ☺, for working late in the lab (also weekends) and for doing as many (or even more) columns then I did. I will never forget the *CPDT rush*, the *brominations* (*en*, do you have the 432?), the agony of finding a non-leaking Schlenk or the precipitations (*en*, what color?). In the end, what matters is that we both made it … Thanks for everything! Thank you for your friendship and for the *PhD flowers* ☺!

The collaborations with different groups were essential for addressing the interdisciplinary character of this work.

Prof. Dr. Benoît Champagne and Dr. Yuexing Zhang, thank you for the theoretical calculations.

Dr. Koen Robeyns, thank you for the X-ray structure determination.

Prof. Dr. René Janssen and Dr. Xianwen Lou (TU/e), thank you for facilitating the polymer purifications and fractionations.

Prof. Dr. Martin Baumgarten and Dr. Timea Stelzig, you had an important contribution in the success of the Suzuki polymerizations. Martin, thank you for facilitating my two weeks stay in the MPIP, for the always very interesting discussions and your efforts to keep the project meetings on schedule (but not necessarily the evenings). Timi, thank you for making my visit in Mainz so pleasant, for the joyful conversations, for sharing the synthetic tips and tricks and for the numerous GPCs.

I would like to thank Tom Aernouts for managing to schedule the solar cell measurements before the end of the Polyspec project. Griet and Afshin, thanks for all the measurements and your help in the processing of the data.

Yasmine, thank you for working on the *final* quinoxaline monomer (that's what I was thinking at that moment) and for being so enthusiastic about the project. It was not an easy job … especially when (the first) reactions *refused* to work! I believe you will

hardly forget the huge and super fast columns that we ran together ☺. I wish you good luck with your master thesis and not only!

My Master promoter (Dr. Christophe Bucher) and teacher (Prof. Jean-Pierre Deprés) have *unveiled* my passion for chemistry (and columns ☺) and played a crucial role in my decision to carry out a PhD. Merci!

I would also like to thank the "Nierstraat Catering Service (NCS), specialized in catering for birthdays, weddings, graduation parties, divorces, funerals, etc. ☺☺☺" - Ema, Donato, Consuelo, Fortunato, Caro and Filippo (also, thanks for hiking in the rain, for the delicious cheese and for taking part in the mountain bike and kayak adventures ☺☺☺). Thank you for the nice parties and for preparing the best (Italian) food. Eva and Jimmy thanks for the BBQs and the hiking and kayak trips. Koen, thanks for original rain shelter. Balazs, thanks for sharing the sushi making expertise. Amparo, Tanya, Martin, Ambily, Pia, Ariel, Carlos, Diden and Pieter, it has always been a pleasure talking to you (during lunch time or whenever we met)! Wiebke and Niko, hiking together (in the rain/snow/sun) was so relaxing and joyful. Thanks for the lively discussions, for complaining as much as I did (mostly about the *Belgian weather*) and for always being around when I needed you. Wiebke, thanks for your nice concerts!

In the end, I would like to thank my parents, my sister and my niece for their love and support all along the years, for always being there (or here) when I needed you. Thank you for enduring me, especially the last couple of months (or years), when things (chemistry) were not always working as they should have. I love you all enormously!